Mechanism of action of dexrazoxane and its protection in cardiotoxicity induced by doxorubicin

BY

KAREENA LEANNE SCHNABL

A Thesis
Submitted to the Faculty of Graduate Studies
in Partial Fulfillment of the Requirements
for the Degree of

MASTER OF SCIENCE

Faculty of Pharmacy
University of Manitoba
Winnipeg, Manitoba

THE UNIVERSITY OF MANITOBA

FACULTY OF GRADUATE STUDIES

*****

COPYRIGHT PERMISSION PAGE

Mechanism of Action of Dexrazoxane and its Protection in Cardiotoxicity Induced by Doxorubicin

BY

Kareena Leanne Schnabl

A Thesis/Practicum submitted to the Faculty of Graduate Studies of The University of Manitoba in partial fulfillment of the requirements of the degree of

MASTER OF SCIENCE

Abstract

Doxorubicin is a very effective anticancer drug. Unfortunately, its clinical use continues to be limited by a potentially fatal, cumulative and dose-limiting cardiotoxicity, which is synergistic with the anticancer drug herceptin and mainly attributed to an iron-based oxidative stress on the heart. Dexrazoxane is a catalytic inhibitor of topoisomerase II and an iron chelator, which has recently been approved for use as a cardioprotective agent for doxorubicin-induced cardiomyopathy. The aim of the following study was to investigate the mechanistic basis for doxorubicin and 7.16.4 mouse antibody cardiotoxicity and the antineoplastic, resistance and cardioprotective mechanisms of dexrazoxane. A dexrazoxane-resistant human leukemia cell line (K562/DZ1) was further characterized. The K562/DZ1 cells were found to be 135-fold resistant to dexrazoxane, 80-fold resistant to levrazoxane and did not exhibit cross resistance to merbarone or vinblastine. Dexrazoxane did not antagonize the K562/DZ1 growth inhibitory effects of etoposide. We hypothesize that dexrazoxane resistance may involve a change in topoisomerase II function. Epifluorescence microscopy and fluorescence plate reader methods with the fluorescent probes JC-1, 2',7'-dichlorofluorescin, annexin V and propidium iodide were developed to study doxorubicin-induced mitochondrial damage, reactive oxygen species generation, apoptosis and necrosis of neonatal rat cardiomyocytes, respectively. Dexrazoxane reduced doxorubicin-induced mitochondrial damage as well as doxorubicin- and hydrogen peroxide-induced generation of reactive oxygen species. Doxorubicin induced cardiomyocyte apoptosis and necrosis within 48 h following 3 h exposure to 0.2, 0.3 and 1.0 μM doxorubicin. We propose that dexrazoxane

may reduce doxorubicin cardiotoxicity through the ability of its metal-chelating hydrolysis product, ADR-925, to either displace iron from its complexes with doxorubicin or chelate loosely bound or free iron, thereby reducing iron-based oxygen free radical damage to mitochondria and other cellular components. Future 7.16.4 mouse antibody cardiotoxicity studies should be undertaken using higher concentrations of antibody, as 7.16.4 did not inhibit cardiomyocyte growth or damage the plasma membrane in our studies.

Acknowledgements

My graduate student experience at the University of Manitoba was remarkable and I am fortunate to have had the opportunity to work with such a wonderful bunch of fun, enthusiastic and intelligent individuals.

I would especially like to thank my incredibly patient graduate supervisor, Dr. B. Hasinoff, for his guidance, support and enthusiasm. He was there for me during the moments of joy and frustration and has taught me all I need to know to become a successful academic. He encouraged me to work above and beyond my full potential and as a result I've accomplished more than I ever imagined possible. The advice and guidance from my advisory committee members, Dr. A. McIntosh and Dr. R. Bose, was also greatly appreciated. Everyone within the Faculty of Pharmacy offered their assistance during my program but I would especially like to thank Gu-Qi Wang, Patricia Schroeder, Dr. R. Marusak and Dr. N. Barnabe for going out of their way to teach me and help brainstorm ideas.

I would also like to thank my family and friends here and abroad for their advice and continuous support of my daily life situations and future ambitions. My parents, brother Brad, Rosemary, Patricia, Ganesh, Jun Zhi, Ashot, Daywin, Dean, Sebastian and Pauline especially brightened my days with their kind words, glowing smiles and endless laughter.

Finally, I would like to acknowledge the financial support from the Canadian Institutes of Health Research and the Manitoba Health Research Council.

Table of Contents

List of Abbreviations

ADP	adenosine diphosphate
ATP	adenosine triphosphate
DCF	2',7'-dichlorofluorescein
DCFH	2',7'-dichlorofluorescin
DCFH-DA	2,7,-dichlorofluorescin diacetate
DF-2	2% (v/v) fetal calf serum in DMEM/F-12
DF-10	10% (v/v) fetal calf serum in DMEM/F-12
DMEM/F-12	Dulbecco's modified Eagle medium/F-12
DMSO	dimethylsulfoxide
DOX	doxorubicin
DNAse	deoxyribonuclease
EDTA	ethylenediaminetetraacetic acid
EPR	electron paramagnetic resonance
FCS	fetal calf serum
FITC	fluorescein-isothiocyanate
GSH	glutathione
GSSH	glutathione disulphide
HBSS	Hank's buffered salt solution
HER2	human epidermal growth factor receptor protein 2
IgG	immunoglobulin G
JC-1	5,5',6,6', -tetrachloro-1,1',3,3'-tetraethyl benzimidazolylcarbocyanine iodide

K562	human leukemia cell line
K562/DZ1	dexrazoxane-resistant human leukemia cell line
LDH	lactate dehydrogenase
MTS	(3-(4,5-dimethyl-thiazol-2-yl)-5-(3-carboxymethoxyphenyl)-2-(4-sulfophenyl)-2H-tetrazolium)
MTT	(3-(4,5-dimethylthiazol-2-yl)-2.5-diphenyltetrazolium bromide)
NAD^+	nicotinimide adenine dinucleotide (oxidized form)
NADH	nicotinimide adenine dinucleotide (reduced form)
PBS	phosphate buffered saline
ROS	reactive oxygen species
SOD	superoxide dismutase

List of Figures

List of Tables

Chapter 1 Introduction

1.1 Chemotherapeutic targeting of DNA topoisomerase II

1.1.1 DNA topology and role of topoisomerases

The normal biological functioning of DNA only occurs if it is maintained in the proper topological state (Figure 1.1) [1]. In such essential biological processes as replication, transcription, chromosome condensation and segregation, recombination and DNA repair, free rotation of one DNA strand around the other and separation of the double helix are required (Figure 1.2) [2-9]. Separation and unwinding of the double helix is promoted by the torsional strain generated from naturally occurring negative DNA supercoiling but only to the extent of 5% of its duplex turns [1]. Furthermore, maintenance of the proper superhelical tension would require massive quantities of energy, since the vast amount of bulky eukaryotic DNA is attached to the nuclear matrix [8]. Consequently, eukaryotic cells have evolved a remarkable group of enzymes known as the topoisomerases to control DNA supercoiling with little expenditure of energy. The DNA topoisomerases unwind supercoiled DNA, separate DNA strands and catenate or decatenate intertwined DNA through breakage and reunion of DNA strands (Figure 1.2) [1, 2, 4, 6, 8-10]. In rapidly growing and dividing tumor cells, topoisomerase levels and activity are higher and maintenance of correct DNA conformation is essential with high transcription and replication rates [9]. Thus, topoisomerases have become a critical intracellular target for several chemotherapeutic drugs used in cancer treatment.

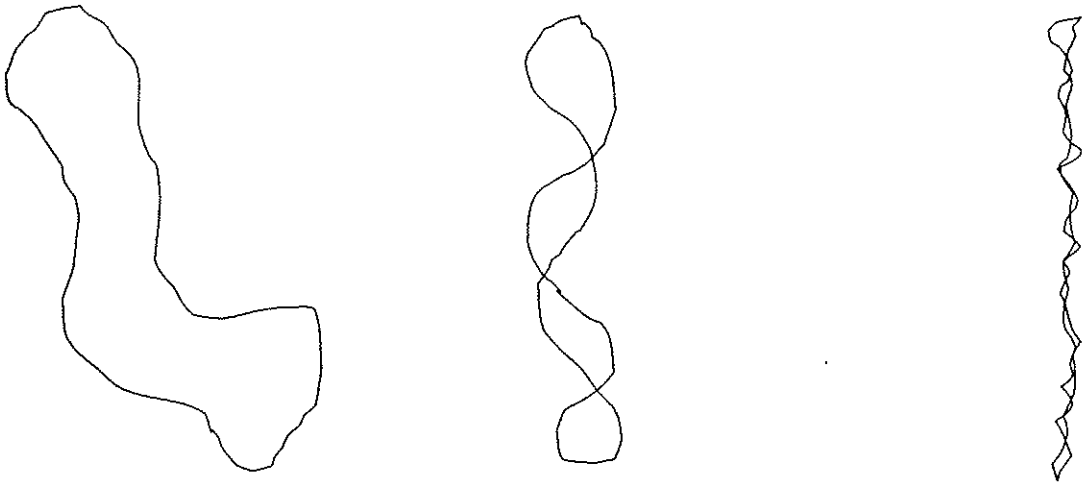

Figure 1.1 Topological requirements for DNA replication. Schematics of circular duplex DNA in various conformations (no supercoiling (left); tightly supercoiled (right)). Biological processes such as DNA replication require DNA to be in a relaxed, supercoiled conformation such as that portrayed in the middle diagram [1], pg 875.

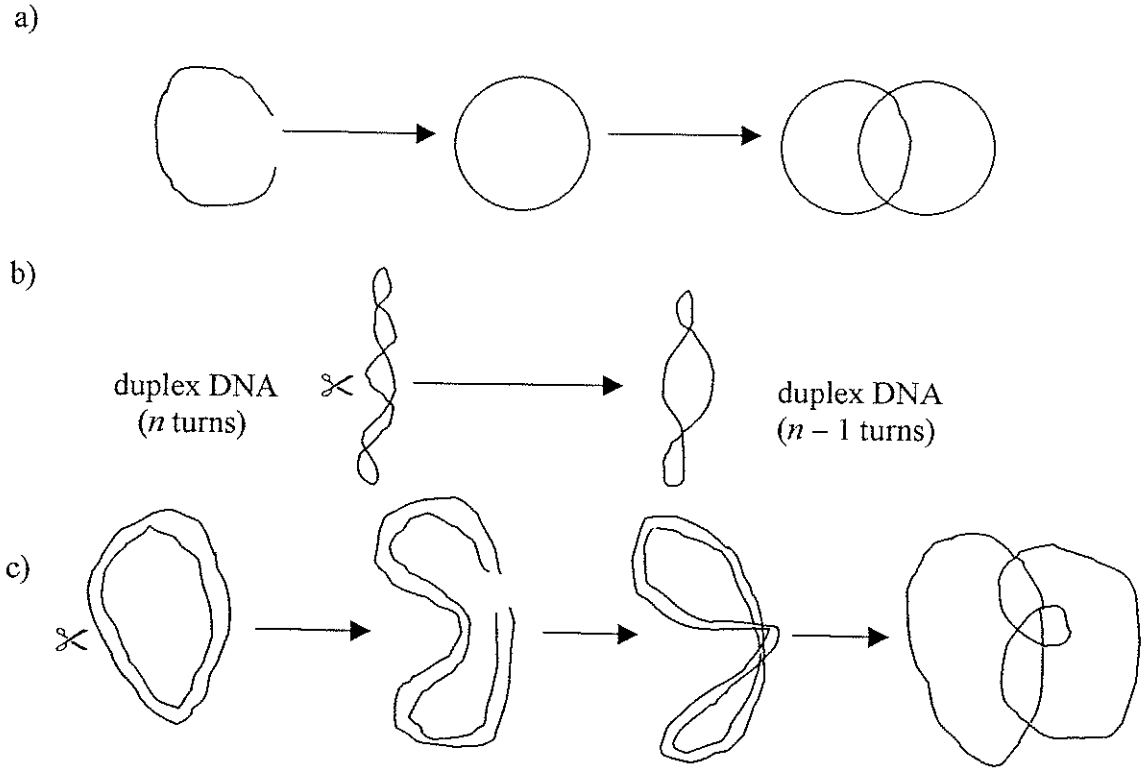

Figure 1.2 Maintenance of correct DNA topology by the topoisomerases. By cutting single or double stranded DNA, passing the strand through the gap and resealing the break, the topoisomerases can a) catenate or decatenate intertwined DNA, b) unwind duplex DNA or c) separate DNA strands [1], pg 879-881.

1.1.2 DNA topoisomerase II: Structure and catalytic activity

In mammalian cells, two forms of the topoisomerases have been described and their cDNA's cloned: DNA topoisomerase I and DNA topoisomerase II [3]. DNA topoisomerase II exists as two isoforms, α and β. Human topoisomerase IIα (hTOPIIα) catalyzes ATP-dependent strand-passing reactions and functions in DNA replication and chromosome condensation and segregation [7]. It is essential for cell growth and is a cell proliferation and tumor marker [4, 7, 9]. A schematic of the cell cycle is presented in Figure 1.3 [11]. Expression of hTOPIIα fluctuates during the cell cycle, peaks in late S/G2 phase and is the more sensitive isoform to anticancer drugs [4, 7, 9]. The function of hTOPIIβ remains unclear but it is expressed at a constant level throughout the cell cycle and may have a role in ribosomal RNA transcription [7, 9].

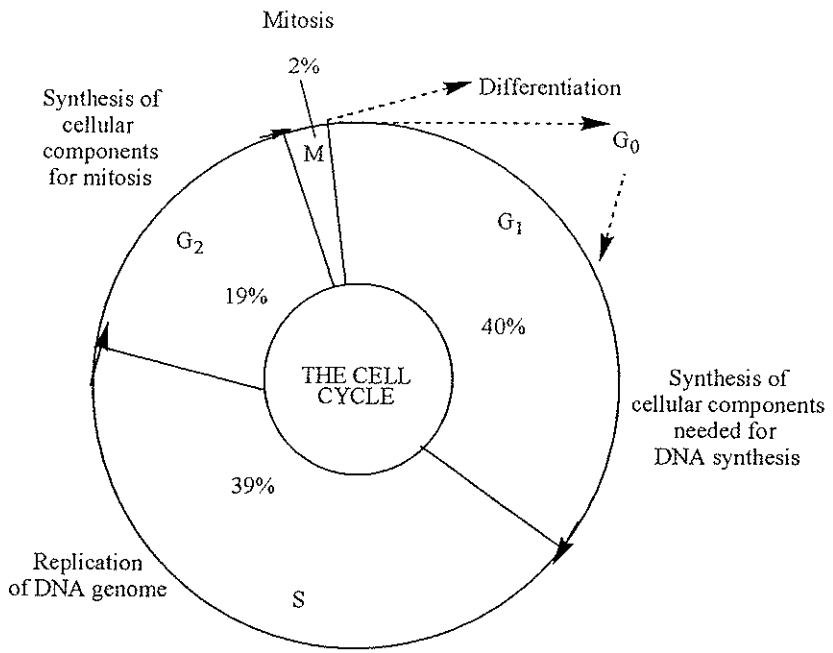

Figure 1.3 Depiction of the cell cycle phases that cells, normal and neoplastic, must traverse before and during cell division. The percentage given represents the approximate time spent in each phase by a typical malignant cell. Most anticancer drugs exert their action on cells traversing the cell cycle (cycling cells are more sensitive). However, some agents can kill both cycling and resting G_0 cells [11], pg 884.

Mammalian topoisomerase II enzymes are homodimeric and contain two major domains: the ATPase (N-terminal) and breakage/reunion (C-terminal) domains [7, 10]. The enzyme acts by introducing a transient double-stranded break into the DNA [4, 12, 17]. The DNA break is held together by the topoisomerase II dimer, which covalently binds to the 5'-end of each nicked strand at the two tyrosyl active sites on the enzyme, forming a bridge through which another DNA duplex can pass (Figure 1.4) [8]. After DNA strand passage, the transient DNA break religates rapidly [2, 4, 13]. The ATP-dependent catalytic cycle of topoisomerase II is illustrated in Figure 1.5 [10].

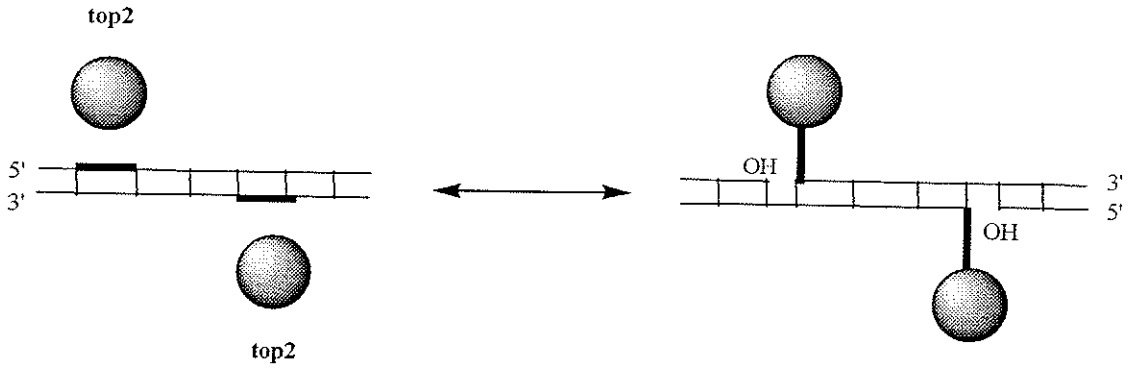

Figure 1.4 Topoisomerase II-DNA cleavable-complex formation [8], pg 186.

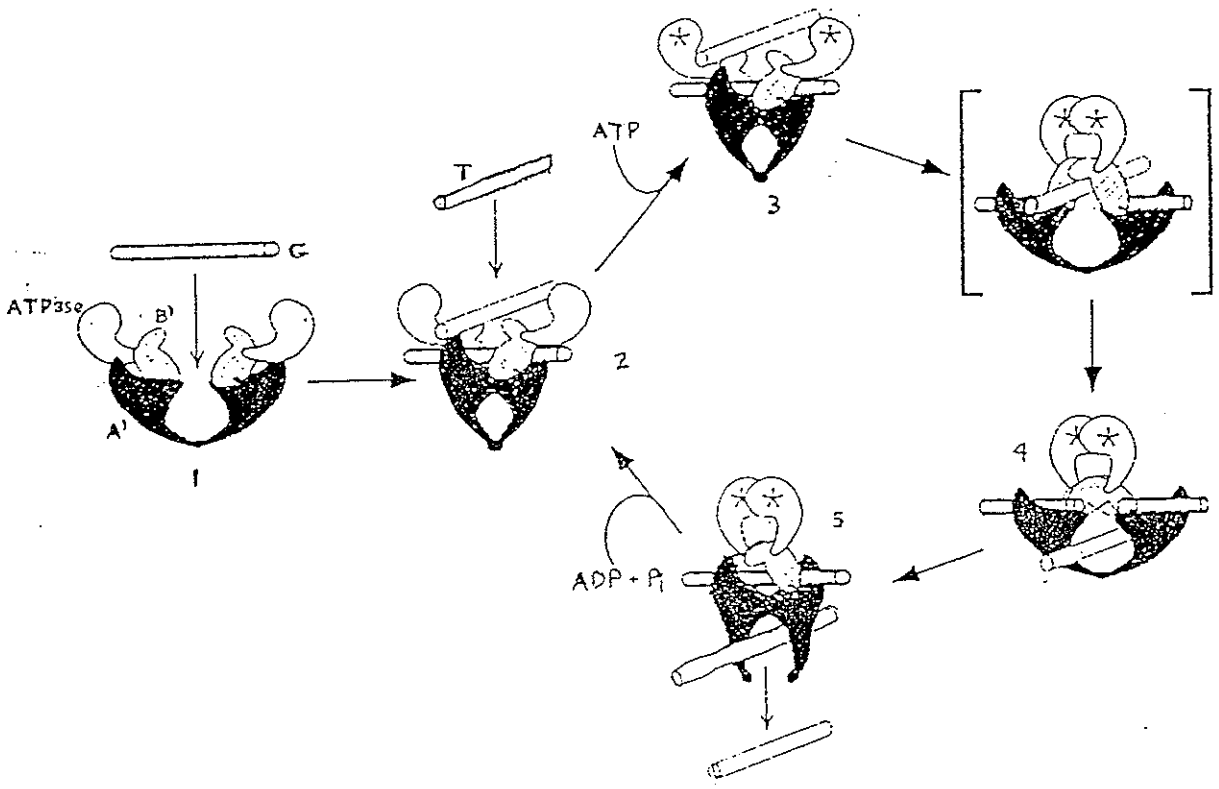

Figure 1.5 ATP-dependent catalytic cycle of topoisomerase II. The enzyme binds the DNA duplex G (gap segment) across the A' domains (Steps 1 and 2). A conformational change occurs in the enzyme promoting binding of a second DNA duplex T (transport segment) and ATP (Steps 2 and 3). ATP binding promotes dimerization of the ATPase domains, cleavage of the G duplex and transport of the T duplex through the dsDNA break in G (Steps 3 and 4). Following transport, the G duplex is religated, the T duplex escapes through the A' dimer interface and the enzyme is regenerated (Step 5) [10], pg 14. Reproduced with permission.

1.1.3 Cancer and topoisomerase II-targeting anticancer drugs

In tumor cells, topoisomerase II plays a very important role. In these rapidly growing and dividing cells high demands are put on maintaining the correct conformation of the DNA, as high transcription and replication rates are required [9]. Furthermore, the levels of topoisomerase II and its activity are higher than those found in normal tissue of the same origin [9]. Thus, topoisomerase II inhibitors became of interest to cancer biologists for their ability to more actively inhibit DNA and RNA synthesis and growth of tumor cells [4]. In fact, some of the most active and widely prescribed anticancer drugs currently in use for the treatment of human cancers target topoisomerase II [4, 7, 8, 13-16]. The group of drugs which target topoisomerase II are collectively called the topoisomerase II inhibitors and are further subdivided into topoisomerase II poisons or catalytic inhibitors of topoisomerase II depending on their mechanism of action. The following section will discuss the two classes of topoisomerase II inhibitors in more detail.

1.1.3.1 Cleavable complex-forming topoisomerase II poisons

Topoisomerase II plays a vital role in maintaining cell viability and consequently has become an important target for antiproliferative intervention [2]. It is the cellular target for some of the most active anticancer drugs used in the treatment of human malignancies. Among the topoisomerase II-targeted agents currently in clinical use are doxorubicin, etoposide, mitoxantrone and amsacrine [4, 7, 9, 15]. The chemical structures of these important topoisomerase II poisons are displayed in Figure 1.6. Whether these agents are DNA intercalators such as doxorubicin or nonintercalators such as etoposide (VP-16) both function directly by interfering with the cleavage/religation step of the

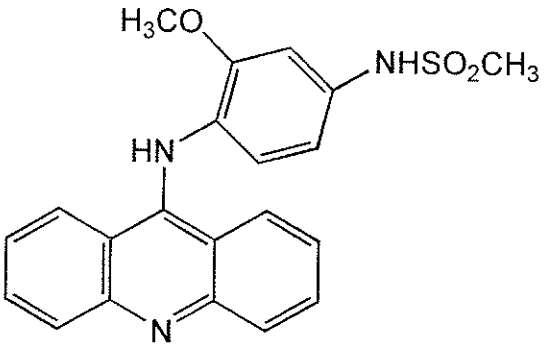

***m*-Amsacrine**

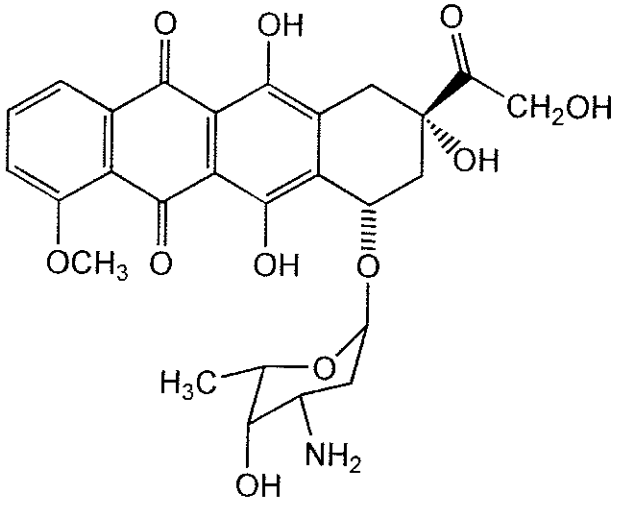

Doxorubicin

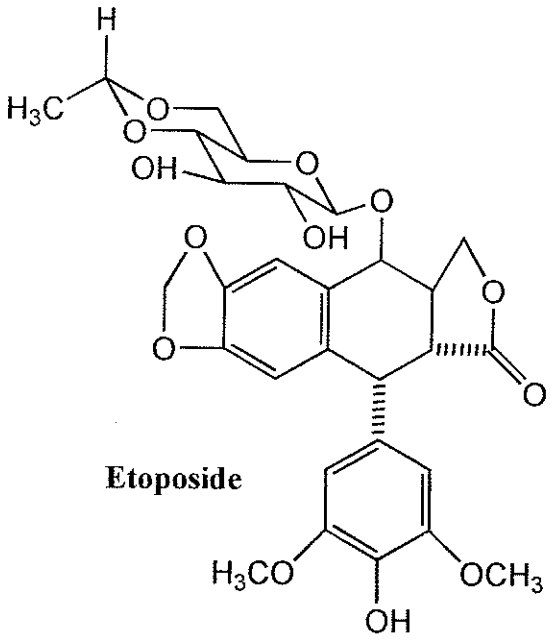

Etoposide

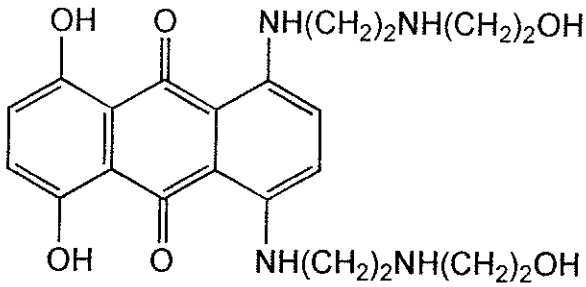

Mitoxantrone

Figure 1.6 Chemical structures of several topoisomerase II poisons.

catalytic cycle either through enhancement of the cleavage reaction or inhibition of religation (Figure 1.8) [2, 4, 8]. Although multiple mechanisms have been proposed for topoisomerase II poisoning [7], these drugs ultimately poison the enzyme and kill cells by stabilizing cleavable-complexes (Figures 1.9 and 1.10) [3, 4, 7, 9, 16]. The possible routes by which topoisomerase II-drug-DNA complexes form are shown in Figure 1.9 [4]. Stabilized topoisomerase II-DNA complexes may cause toxicity by interfering with replicational or transcriptional machinery moving along the DNA strand or by increasing levels of potentially lethal topoisomerase II-mediated DNA double strand breaks [3, 7-9, 16, 17]. The latter may result in chromosomal changes or illegitimate recombinations [9, 16, 17]. Recently, it has been claimed that p53 mediated apoptosis may be involved in the topoisomerase II-drug cell pathway [7, 9, 16].

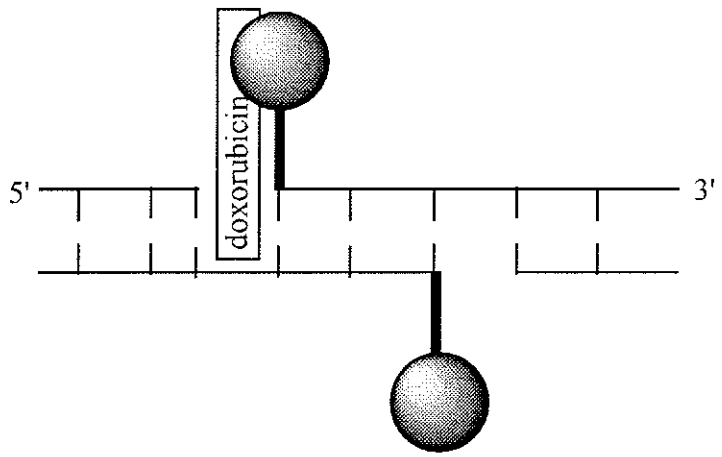

Figure 1.7 Topoisomerase II inhibition by the DNA intercalator doxorubicin. This figure was modified from [8], pg 190.

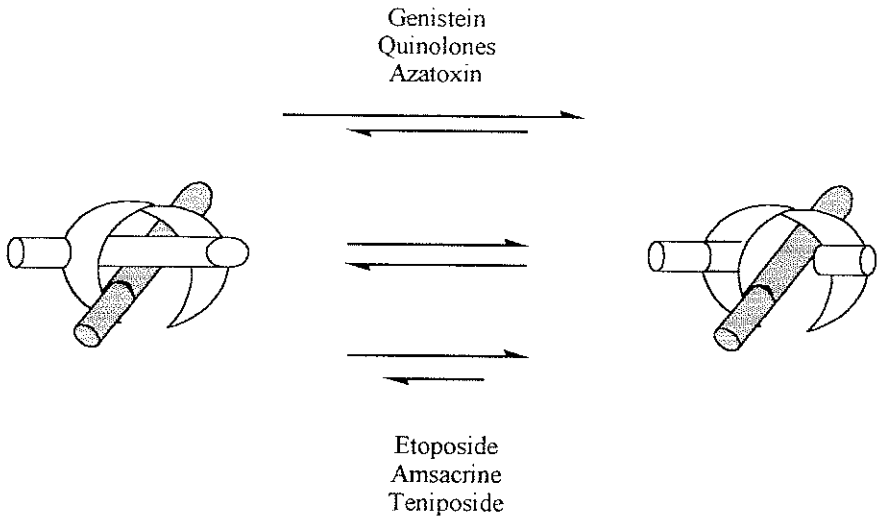

Figure 1.8 Effects of topoisomerase II poisons on the cleavage/religation equilibrium of topoisomerase II. Generally, cleavage-enhancing drugs either increase the rate of DNA cleavage by topoisomerase II (top) or decrease the rate of DNA religation (bottom).

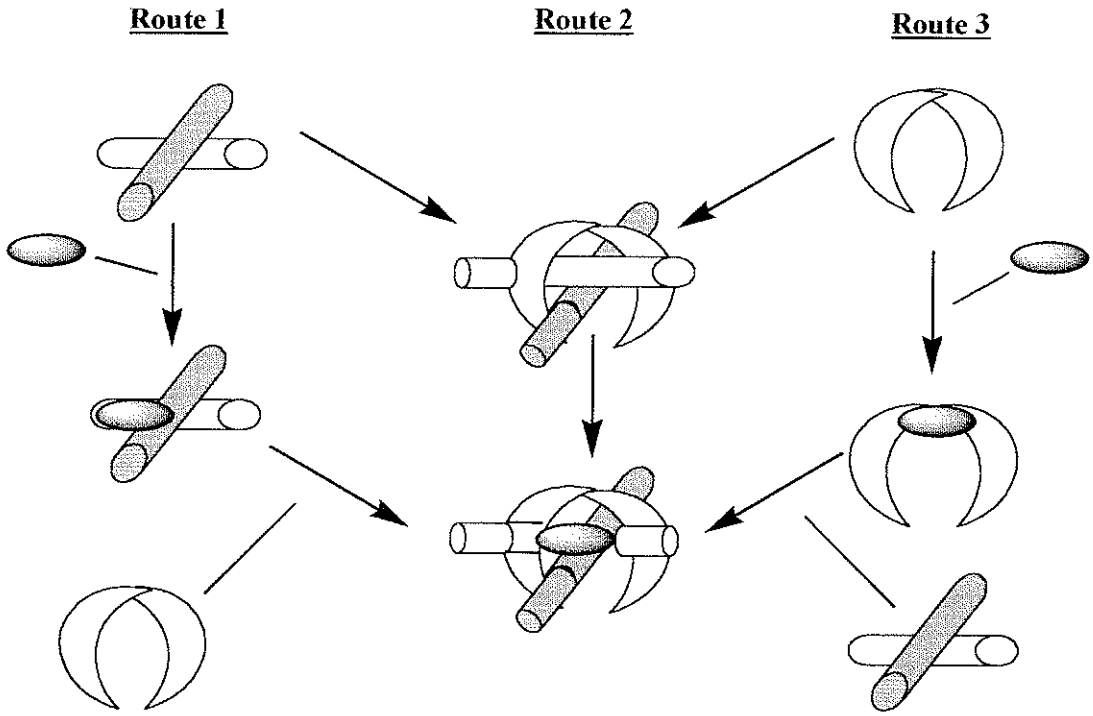

Figure 1.9 Possible routes for topoisomerase II-drug-DNA complex formation. Route 1 involves drug binding to DNA, followed by the enzyme binding to the drug-DNA complex. Route 2 consists of enzyme binding to the DNA, followed by the drug binding to the enzyme-DNA complex. Route 3 involves binding of drug to enzyme, followed by binding of the drug-enzyme complex to the DNA.

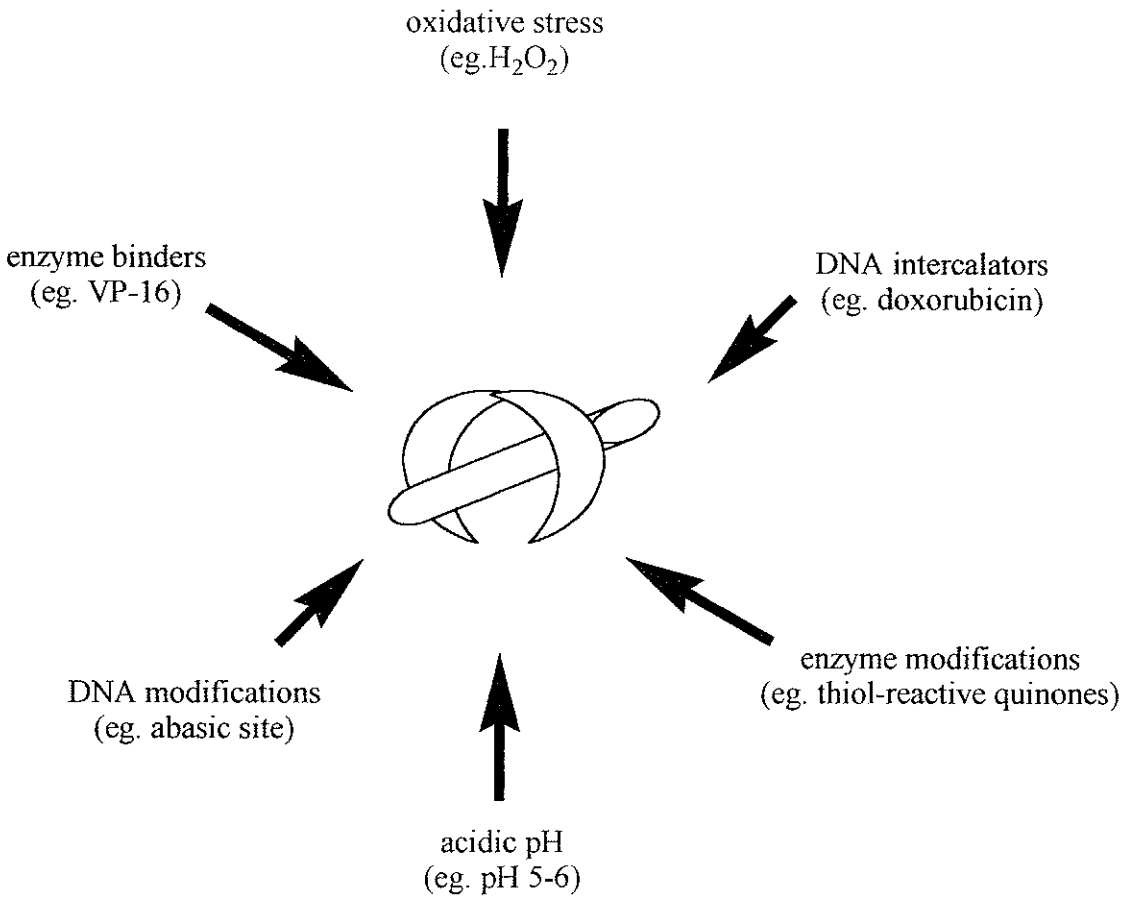

Figure 1.10 Multiple mechanisms for topoisomerase II poisoning.

Although stabilization of cleavable-complexes between topoisomerase II and DNA by topoisomerase II poisons may be a preceding event to cell death, cytotoxicity is not exclusively due to inhibition of topoisomerase II. Many of the topoisomerase II poisons themselves in addition to the cleavable-complexes they form are capable of initiating a series of events and cellular responses that damage DNA and lead to cell death (Figure 1.11) [8]. Moreover, the cellular effect of the topoisomerase II poison may also depend on various factors such as its concentration and intracellular distribution, the levels and activity of topoisomerase II and the presence of other physiological stresses (Figures 1.11, 1.12 and 1.13) [7, 8, 18]. At the plasma membrane level, it is also important to note that most topoisomerase II poisons are substrates for multi-drug resistance-associated proteins such as P-glycoprotein^{MDR}, which actively extrudes drugs from cells (Figure 1.14) [11]. Thus, cells over-expressing P-glycoprotein^{MDR} are resistant to most topoisomerase II inhibitors [3, 8, 18]. However, characterizing drug-resistant cell lines with topoisomerase II inhibitors has become a powerful tool for developing more efficacious chemotherapeutic regimens and novel anticancer drugs that overcome resistance while improving or maintaining antitumor activity [4].

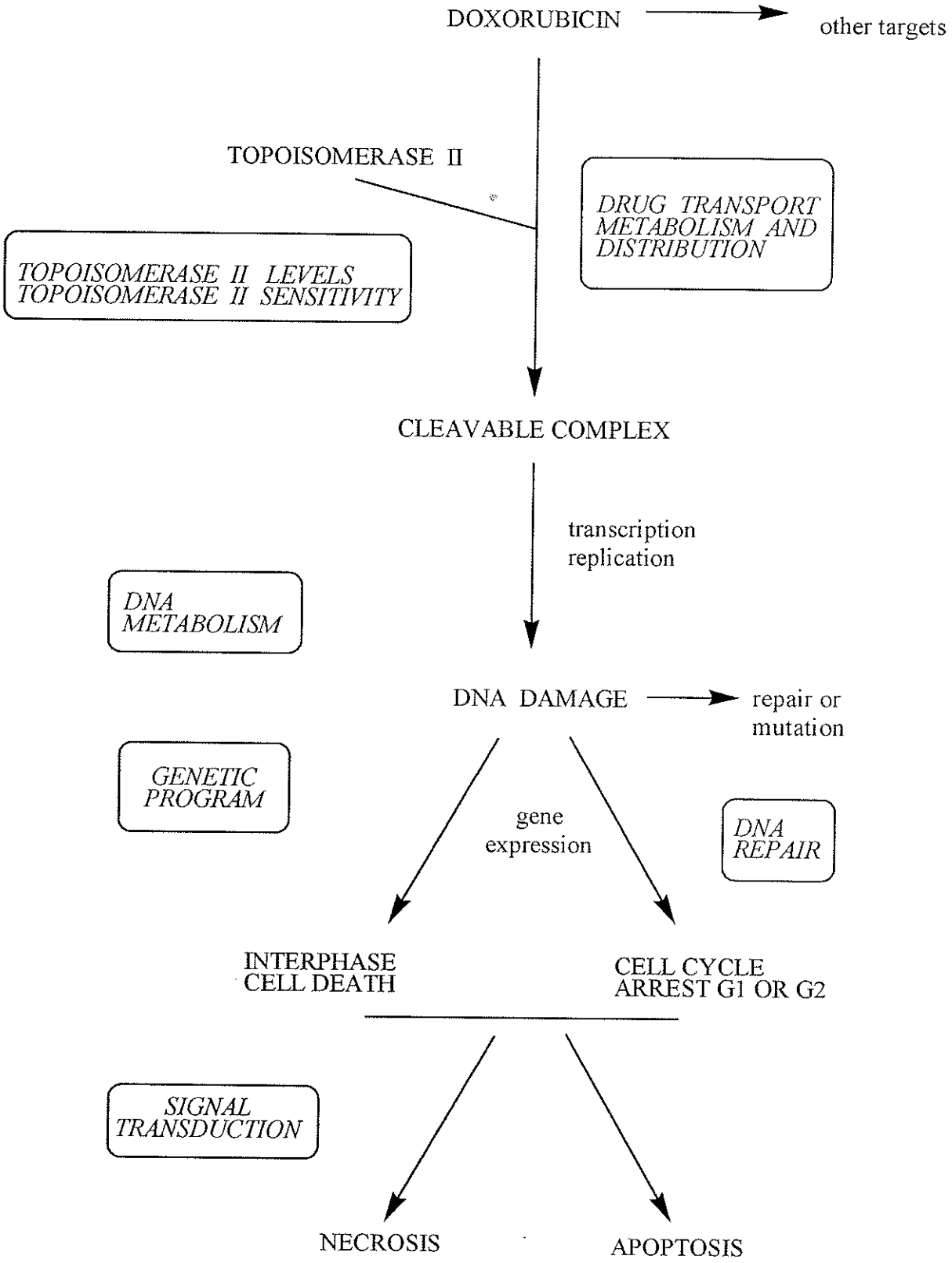

Figure 1.11 Determinants of sensitivity and resistance to topoisomerase II poisons[8], pg 191.

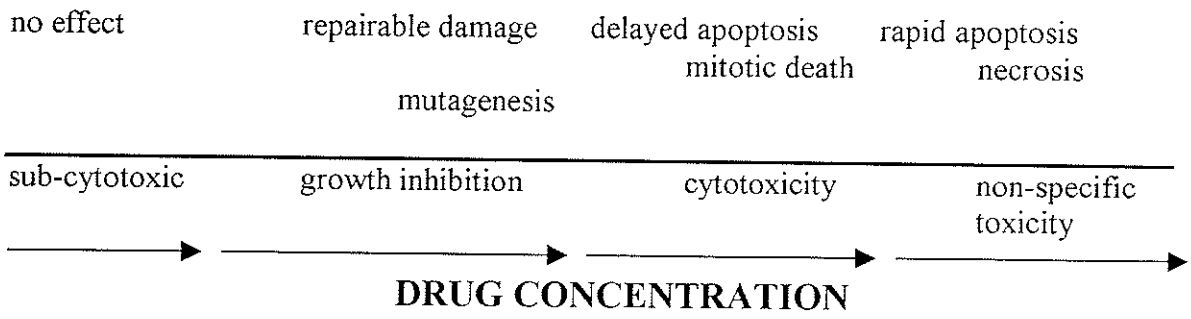

Figure 1.12 Cellular effects of topoisomerase II poisons on tumor cells as a function of drug concentration [18], pg 270.

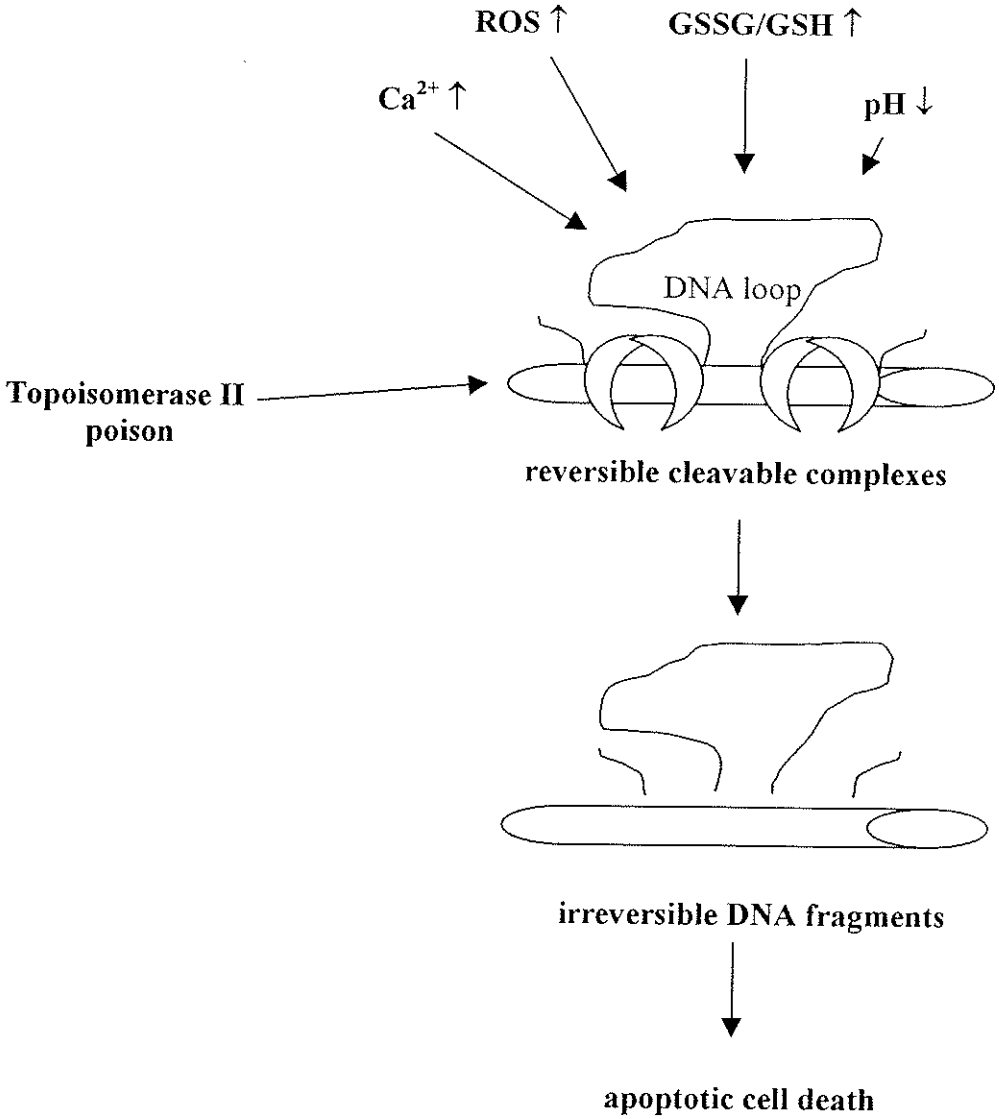

Figure 1.13 Topoisomerase II poisoning in cells under physiological stresses: role in apoptotic cell death [7], pg 68. GSSG/GSH: ratio of oxidized to reduced glutathione; ROS: reactive oxygen species

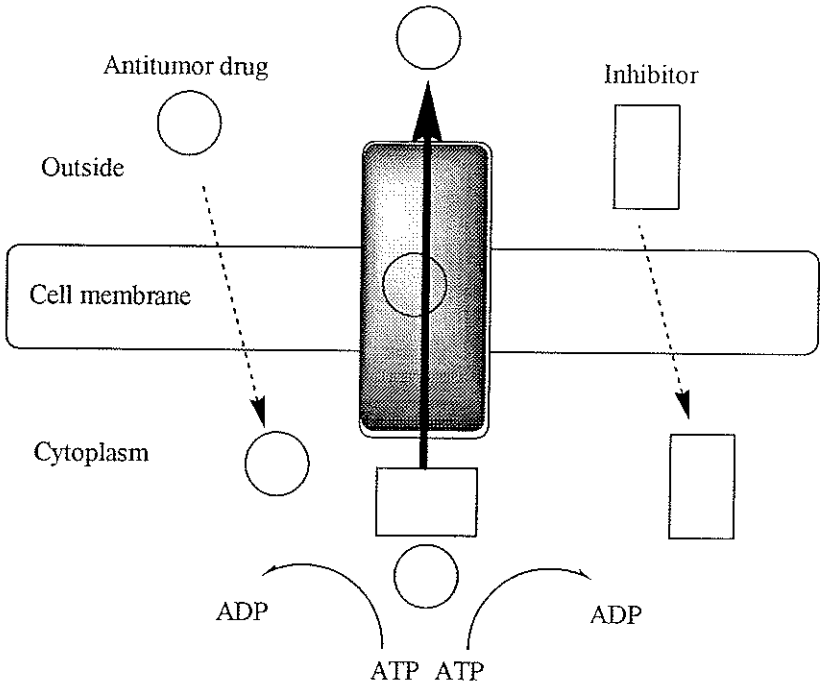

Figure 1.14 Schematic of the P-glycoprotein drug transport molecule responsible for multi-drug resistance in cancer cells. ATP is used to drive the efflux process [11], pg 885.

1.1.3.2 Catalytic inhibitors of topoisomerase II

A second class of drugs that affect the activity of topoisomerase II also appear to have clinical potential. In contrast to topoisomerase II poisons, these agents, known as the catalytic inhibitors, act by inhibiting the activity of the enzyme and display no ability to stimulate DNA cleavage (Figure 1.15) [13, 19]. Recently, catalytic inhibitors that display high activity against eukaryotic type II topoisomerases have been described. These are typified by drugs such as merbarone, fostriecin and the bisdioxopiperazines, whose chemical structures are shown in Figure 1.16. These drugs possess a variety of inhibitory mechanisms. The bisdioxopiperazines, for instance, block ATP hydrolysis, an action that traps the enzyme on DNA in its closed clamp form, preventing enzyme release and regeneration [19].

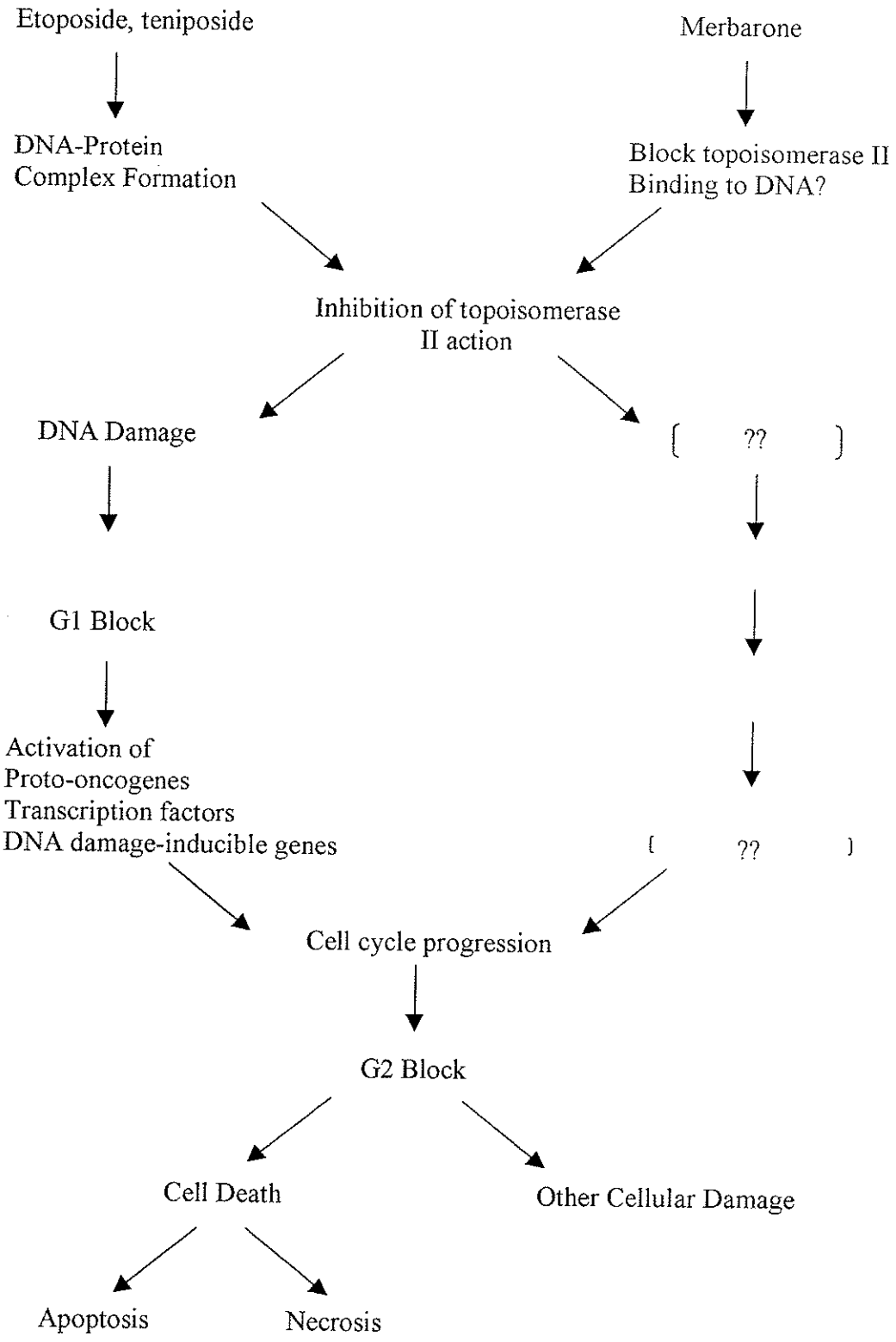

Figure 1.15 Cellular perturbations leading to cell death following treatment with topoisomerase II poisons (etoposide/teniposide) and the catalytic inhibitor merbarone [3], pg 516.

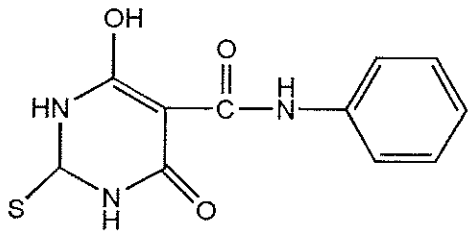

Merbarone

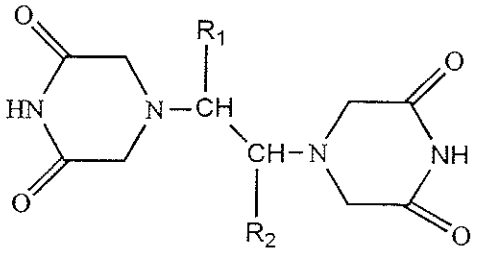

ICRF-154: R_1 = H, R_2 = H
ICRF-159: R_1 = CH_3, R_2 = H
ICRF-193: R_1 = CH_3, R_2 = CH_3

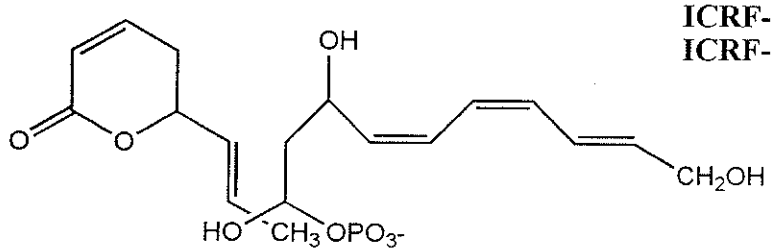

Fostriecin

Figure 1.16 Chemical structures of topoisomerase II catalytic inhibitors including merbarone, some bisdioxopiperazines (ICRF compounds) and fostriecin.

Many catalytic inhibitors have also been shown to antagonize the action of topoisomerase II poisons on topoisomerase II. This particular mode of topoisomerase II inhibition has evoked strong interest and resulted in the discovery of additional therapeutic value for these compounds. While some potential exists for the usage of bisdioxopiperazines in anticancer treatment regimens [20], this class of drugs has particularly sparked interest with their ability to overcome toxicities caused by cleavable-complex forming drugs such as doxorubicin and etoposide [20-25]. Although numerous studies suggest that the bisdioxopiperazine, dexrazoxane, reduces anthracycline cardiotoxicity through chelation of intracellular iron [26-30], its topoisomerase II

inhibitory mode of action may prove to be of equal importance in the clinical setting [20, 31].

On the other hand, interfering with the growth inhibitory effects of topoisomerase II poisons may be unfavorable, in terms of eradicating tumor cells [13]. However, there are a number of factors such as drug concentration and topoisomerase levels that can influence the outcome of administering a catalytic inhibitor with a topoisomerase II poison [5, 13]. For instance, low concentrations of a catalytic inhibitor may not occupy all available topoisomerase II sites thus promoting a synergistic effect on cell kill with a topoisomerase II poison [13]. In clinical practice, the attainable concentrations of drugs in the body fluid often promote an additive or synergistic effect on antitumor effects when topoisomerase II poisons and catalytic inhibitors are combined [13].

1.2 Anthracyclines in the treatment of cancer

1.2.1 Clinical use and toxicities

The anthracyclines are among the most utilized group of anticancer drugs developed (Figure 1.17) [32]. Doxorubicin is the most successful of the anthracyclines and is used to treat a wide range of hematological and solid tumor malignancies (Table 1.1) [15]. It is most commonly used as an adjuvant in the treatment of metastatic breast cancer [11, 15, 32] and has improved the life expectancy of countless patients since its discovery and introduction into investigational and approved chemotherapy regimens in the past 30 years [33, 34].

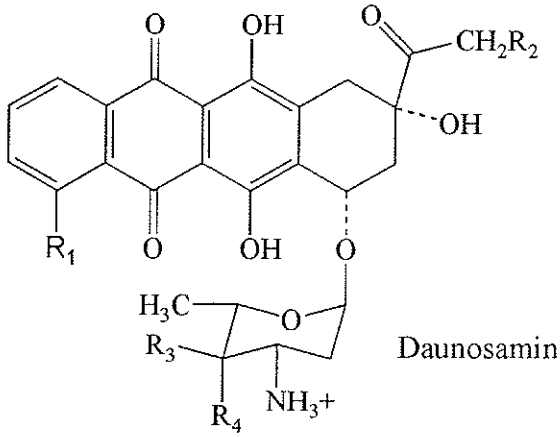

Anthracycline	R1	R2	R3	R4
Doxorubicin	-OCH3	-OH	-H	-OH
Daunorubicin	-OCH3	-H	-H	-OH
Epirubicin	-OCH3	-OH	-OH	-H
Idarubicin	-H	-H	-H	-OH

Figure 1.17 Chemical structures of the anthracyclines at physiological pH (7.4). All anthracyclines consist of an aglycone ring coupled to an amino sugar that carries a positive charge. The aglycone portion of the anthracyclines intercalates between adjacent DNA pairs while the positively charged sugar promotes attraction of the molecule to the negatively charged DNA and membrane phospholipids [47], pg 681.

Table 1.1 Clinical use of the anthracyclines in various malignancies.

Drug	Trade name	Major indications
Doxorubicin	Adriamycin	Lymphomas[a]
		Breast cancer[a]
		Sarcomas[a]
		Kaposi's sarcoma
		Leukemias
Daunorubicin	Cerubidine	Acute lymphocytic leukemia[a]
Idarubicin	Idamycin	Acute myelogenous leukemia

[a]Drug of choice for treatment of the disease.

Although a clinically effective anticancer drug, doxorubicin unfortunately is not without serious toxicities. In common to most anticancer drugs, myelosuppression is often an acute dose-limiting toxicity for cancer patients, who are often burdened with side effects such as mucositis, nausea and alopecia [11, 15, 32]. However, for doxorubicin and the other anthracyclines, their clinical use is particularly limited by acute and chronic dose-limiting toxicities to cardiac tissues [15, 27, 34-39]. The acute toxicity develops immediately after initiation of doxorubicin treatment and presents arrhythmias, tachycardia and hypotension [27, 34] while the chronic toxicity develops after completion of cumulative dose regimens, producing a potentially life-threatening dilative cardiomyopathy [34, 36, 39]. Anthracycline-induced cardiomyopathy is often irreversible and leads to congestive heart failure in approximately 30% of patients treated with cumulative doses above 600 mg/m^2 [35]. Consequently, the maximum recommended cumulative dose of doxorubicin for the 21-day schedule has been set at 550 mg/m^2, although many patients could greatly benefit from higher doses [15, 23, 32]. Late onset arrhythmia and sudden death often occur more than fifteen years after anthracycline treatment suggesting that more anthracycline-induced cardiotoxicity may appear in the future in patients who are presently asymptomatic [39].

1.2.2 Proposed mechanisms of drug action

Despite the extensive and long-standing clinical utilization of the anthracyclines, their mechanism of action is uncertain and is still a subject of considerable controversy. The sub-cellular basis for anthracycline-induced cardiomyopathy and its antitumor action were once thought to involve a common pathway. However, more recently it has become

possible to distinguish the importance of these mechanisms underlying their dual effects. The proposed pharmacological effects of the anthracyclines are listed in Table 1.2 [32].

Table 1.2 Pharmacological effects of the anthracyclines [32], pg 3.

Major mechanisms of action	
DNA intercalation	
Inhibition of topoisomerase II	
Production of hydroxyl free radicals	
Secondary mechanisms of action	
Inhibition of:	topoisomerase I
	mitochondrial oxidative phosphorylation
	DNA polymerases
	RNA polymerases and DNA repair enzymes
	DNA helicases
	metallothioneine synthesis
Membrane modulation	

1.2.2.1 Dissociation of cardiotoxic effects from antineoplastic effects

In regard to antitumor activity, the primary mode of action of the anthracyclines appears to be intercalation of the planar ring portion to the sugar-phosphate backbone of adjacent DNA base pairs of the DNA double helix [7, 8, 27, 32, 33]. This complexation provides an anchor to hold the amino sugar portion of the molecule in the minor groove, where its functional hydroxyl and amino groups face out such that they may interact with polymerases. DNA intercalation of the anthracyclines ultimately blocks DNA and RNA synthesis and inhibits DNA repair and expression of genes encoding cardiac muscle protein [27]. Intercalation also causes deformation of the DNA, stabilizing the topoisomerase II-DNA complex [32]. As discussed in section 1.1.3.1, stabilization of the cleavable-complex results in the formation of protein-linked double-strand DNA breaks [7, 16]. In tumor cells, these perturbations are believed to ultimately engage in a final common pathway of endonucleolytic DNA fragmentation known as apoptosis [7, 18, 26]. Although current studies have demonstrated that anthracyclines can induce

cardiomyocyte apoptosis [40, 41], the initiating events responsible for cardiac toxicity is not likely entirely due to DNA intercalation and topoisomerase II inhibition as cardiac myocytes are terminally differentiated, slow-dividing cells [42, 43].

Another important effect of anthracyclines is membrane binding, in particular to structures abundant in cardiolipin such as mitochondria [27, 44, 45]. Disruption of the mitochondrial membrane potential is also a well-established trigger of cardiomyocyte apoptosis [46].

Finally, the quinone-containing anthracyclines are able to redox cycle and promote the formation of free radicals [27, 29, 33, 36-39, 47] that are believed to play a central role in their cardiotoxicity. A major role in the development of cardiotoxicity has also been assigned to iron presumably because this metal and its complexes with anthracyclines can also catalyze free radical reactions that overwhelm the antioxidant defenses of cardiomyocytes [27, 36, 42, 45]. The heart is particularly sensitive to damage inflicted by free radicals because of its very low antioxidant enzyme activity and limited capability to utilize non protein thiols to protect against oxidative toxicity [27, 36, 37]. The role of iron-based free radical generation in anthracycline cardiotoxicity is supported by free radical scavenger and iron chelation experiments that modify anthracycline toxicity [27, 29, 36, 38, 45]. It is not clear whether iron-based free radical formation is essential to the tumor cell killing effect of anthracyclines.

1.2.2.2 Role of iron in anthracycline cardiotoxicity

The possible involvement of iron in anthracycline-induced cardiotoxicity first emerged in the mid 1970's, when a series of non polar derivatives of ethylenediamine-N,N'-tetraacetic acid (EDTA), including the bisdioxopiperazine, dexrazoxane (ICRF-

187), were demonstrated to prevent cardiac lesions and dysfunction induced by anthracyclines in both isolated heart models and whole animal studies (Figure 1.18) [23, 26, 28, 30]. Since then a role for iron has been maintained, as studies revealed the chemistry of the anthracyclines.

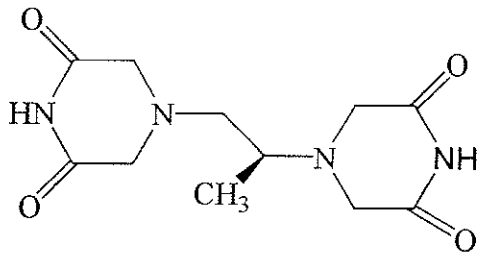

Dexrazoxane (ICRF-187)

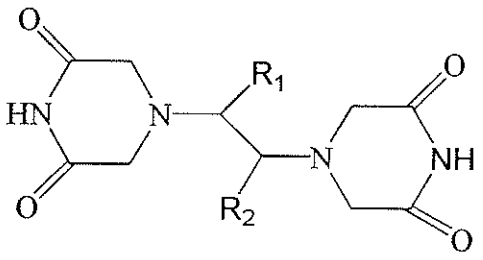

ICRF-154 $R_1 = R_2 = H$
ICRF-159 $R_1 = H$, $R_2 = CH_3$ (racemic)
ICRF-192 $R_1 = H$, $R_2 = C_2H_5$ (racemic)

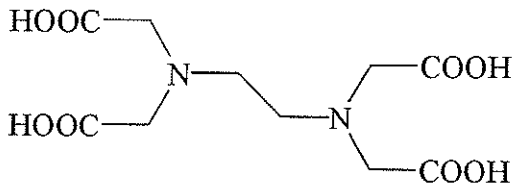

EDTA

Figure 1.18 Chemical structures of EDTA and several bisdioxopiperazines including dexrazoxane.

Electron paramagnetic resonance studies (EPR) have shown that reductases (E_{red} reduced form, E_{ox} oxidized form) such as NADPH cytochrome P450 can catalyze one electron addition to the quinone moiety of anthracyclines to form a semiquinone free radical ($DOX^{\bullet}$), particularly in myocardial cells with high levels of flavin-centered reductases (Equation 1) [27, 29, 36-39, 47, 48].

$$E_{red} + DOX \rightarrow E_{ox} + DOX^{\bullet} \quad (1)$$

This semiquinone free radical ($DOX^{\bullet}$) can readily regenerate the parent quinone and create superoxide anions ($O_2^{\bullet}$) through reduction of molecular oxygen (Equation 2).

$$DOX^{\bullet} + O_2 \rightarrow DOX + O_2^{\bullet} \quad (2)$$

As shown in Figure 1.19 [43], the superoxide anion can be metabolized to hydrogen peroxide (H_2O_2) by superoxide dismutase (SOD) and the H_2O_2 converted into water by catalase and glutathione peroxidase. However, because heart cells have relatively low levels of these antioxidant protective enzymes and doxorubicin suppresses glutathione peroxidase activity, their antioxidant systems are overwhelmed [27, 36, 37, 39, 42]. Thus, anthracyclines increase these reactive oxygen species above the physiological levels generated during normal aerobic metabolism and phagocytosis [36, 43]. Consequently, the myocardial cells are unable to eliminate superoxide anions, which reduce free ferric iron (Fe^{3+}) to ferrous iron (Fe^{2+}) (Equation 3) and hydrogen peroxide, which reacts with Fe^{2+} in the Fenton reaction to generate the highly reactive, hydroxyl radical ($OH^{\bullet}$)

(Equation 4). Anthracycline semiquinones can also release iron from the iron storage protein, ferritin, by relaying electrons between redox sites on its surface [35, 36].

$$O_2^{\bullet -} + Fe^{3+} \rightarrow O_2 + Fe^{2+} \quad (3)$$

$$Fe^{2+} + H_2O_2 \rightarrow + Fe^{3+} + OH^{\bullet} + OH^- \quad (4)$$

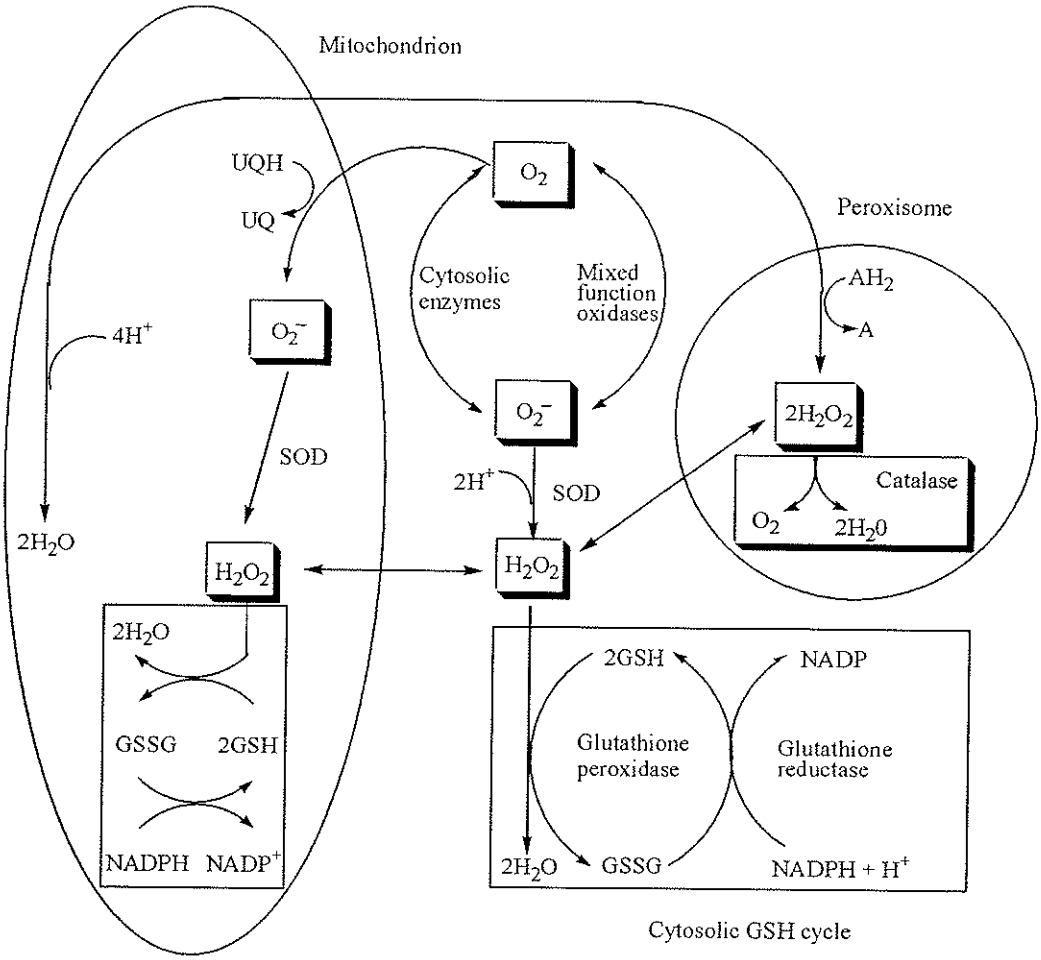

Figure 1.19 Cellular metabolism of oxygen and the accompanying antioxidant defense mechanisms [43], pg 15. UQ: ubiquinone; SOD: superoxide dismutase; GSSG: oxidized glutathione; GSH: reduced glutathione

Anthracyclines may also generate free radicals by a non-enzymatic mechanism involving the initial formation of a conjugate composed of Fe^{3+} with the hydroquinone positions C-11 and C-12 of the anthracycline (Figure 1.20) [26]. In the case of doxorubicin, the doxorubicin-iron (III) complex can undergo an internal redox reaction to doxorubicin-iron (II) by using an electron donated from glutathione (GSH) or the C-14 alcohol side chain hydroxyl group of the anthracycline itself (Figure 1.20, Equation 5) [36]. The doxorubicin-iron (II) complex can then reoxidize to the iron (III) complex by reducing oxygen to the superoxide anion (Equation 6).

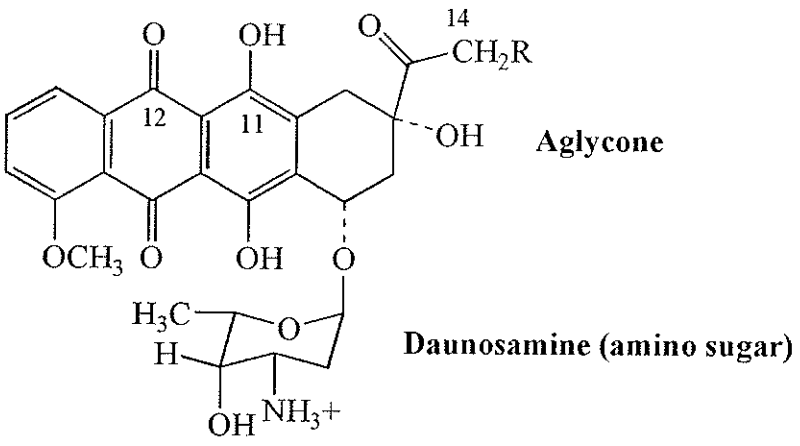

Doxorubicin R = OH
Daunorubicin R = H

Figure 1.20 Chemical structure of the anthracyclines [26], pg 2.

$$Fe^{3+}\text{-DOX} + e^{-} \rightarrow Fe^{2+}\text{-DOX} \quad (5)$$

$$Fe^{2+}\text{-DOX} + O_2 \rightarrow Fe^{3+}\text{-DOX} + O_2^{\bullet -} \quad (6)$$

As shown in Figure 1.19 [43], superoxide anion is dismutated into hydrogen peroxide by superoxide dismutase. The subsequent reaction of hydrogen peroxide with the doxorubicin-iron (II) complex produces the highly reactive hydroxyl radical (Equation 7).

$$Fe^{2+}\text{-DOX} + H_2O_2 \rightarrow Fe^{3+}\text{-DOX} + OH\bullet + OH^- \qquad (7)$$

The hydroxyl radical can eventually cause cardiac dysfunction by oxidizing lipids, proteins and DNA, in association with the redox activity of doxorubicin-iron complexes (Figure 1.21) [35, 36, 43].

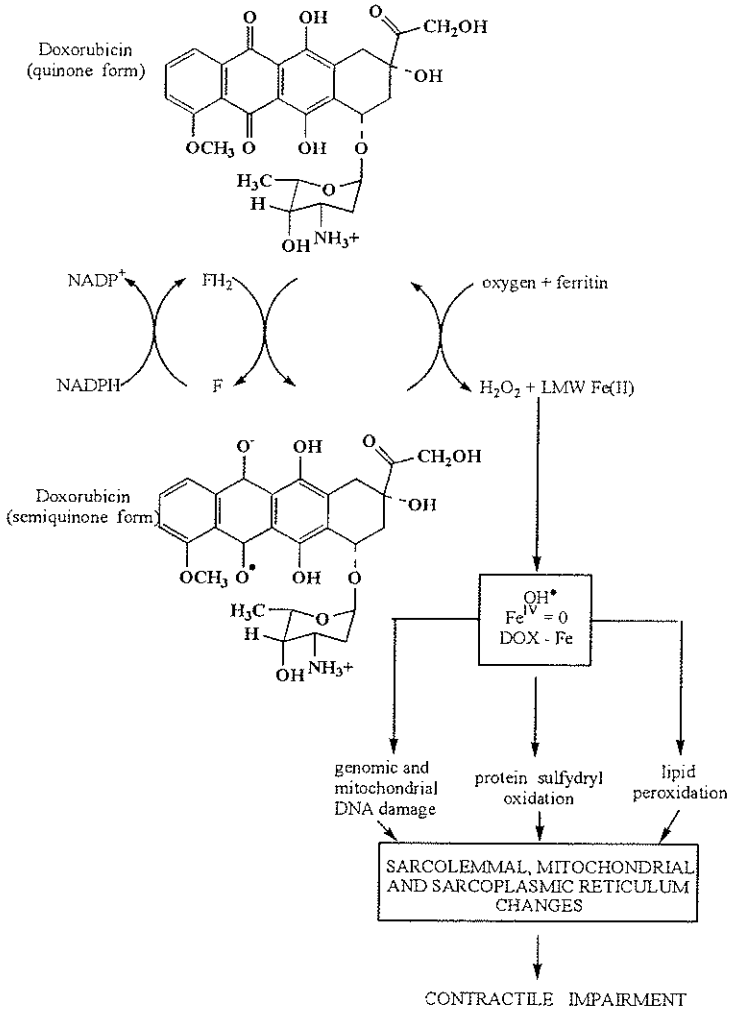

Figure 1.21 The iron and free radical hypothesis of cardiotoxicity. F/FH_2, oxidized/reduced flavoproteins (ex. NADH cytochrome P450 reductase); LWM, low molecular weight; Fe^{IV}=0, ferryl ion; DOX - Fe, doxorubicin-iron complex [36], pg 201.

1.3 Cytoprotective strategies for anthracycline cardiotoxicity

Since cardiac oxidative injury was identified to be the major limiting factor for clinical application of the anthracyclines in cancer chemotherapy, development of cytoprotective agents for anthracyclines has been prompted. The primary goal of the emerging class of cytoprotectant compounds has been to provide site-specific protection for normal tissues, without compromising antitumor efficacy [26, 28]. Table 1.3 lists some of the investigational and approved cytoprotectants for cancer chemotherapy toxicities [26].

Table 1.3 Cytoprotectants for cancer chemotherapy agents [26], pg 24.

Cytoprotective Agent	Status*	Effected Anticancer Agents	Tissues protected
Mesna	Approved	Cyclophosphamide	Urinary bladder
Glutathione	Investigational	Cisplatin	Kidney/peripheral nerves
Amifostine	Approved	Cisplatin	Kidney
Uridine	Investigational	Fluorouracil	Bone marrow
Razoxane (ICRF-159)	Investigational	Doxorubicin Daunorubicin	Heart Heart
N-acetylcysteine	Investigational	Doxorubicin	Heart
Dexrazoxane (ICRF-187)	Approved	Doxorubicin	Heart

* Regulatory status in 1996 in the United States.

Cytoprotective agents for anthracycline cardiotoxicity are not rescue agents but prophylactically alter normal tissue toxicity often by interacting directly with critical sub-cellular toxicity targets [26]. Unlike anthracycline treatment, dose escalation or intensification is not the ultimate goal of cytoprotectant therapy but rather reducing or preventing normal tissue damage with proportionate improvements in patient well being

[26]. The use of cardioprotective agents is associated with a reduction in cardiotoxicity and facilitates the use of higher cumulative doses of anthracyclines [27].

1.3.1 Cardioprotective agents for doxorubicin cardiotoxicity

As outlined in sections 1.2.2.1 and 1.2.2.2, doxorubicin-induced cardiotoxicity is mediated through different mechanisms including membrane lipid peroxidation, free radical formation, mitochondrial damage and iron-dependent oxidative damage to biological macromolecules [45]. Thus, the basic pharmacological approach adopted was to interrupt the cycle of reactive oxygen species generation with free radical scavenging antioxidants and iron chelators [45]. Although antioxidants such as N-acetylcysteine and the lipophilic vitamin α-tocopherol were demonstrated to reduce doxorubicin-induced cardiotoxicity in some in vitro and small animal experiments, in vitro studies with iron and large animal trials were not so successful [26-28, 30, 36, 45]. Unfortunately, none of these compounds have been proven to be cardioprotective in patients receiving doxorubicin. In contrast, the water-soluble iron chelators deferoxamine and dexrazoxane (ICRF-187), have been shown to attenuate doxorubicin-induced cardiomyopathy successfully [26-28, 30, 36, 45]. The organic thiophosphate, amifostine (WR-2721) is currently being investigated as a potential cytoprotectant against anthracycline-induced cardiotoxicity [26, 28].

1.3.1.1 Dexrazoxane protection against anthracycline cardiotoxicity

An important development in the application of iron chelators in cancer therapy has been the demonstration of the protective effect of the bisdioxopiperazine dexrazoxane against doxorubicin-induced cardiac toxicity in women with advanced breast cancer and children with cancer [24-28, 30]. Although dexrazoxane was originally synthesized as a

possible antitumor agent, the discovery of its cardioprotective action without interference with antitumor effects when co-administered with doxorubicin opened a new therapeutic window [20, 27, 49]. Significantly higher cumulative doses of the anthracyclines could be administered and the integrity of the heart cells maintained with co-administration of dexrazoxane [27]. Dexrazoxane has recently been FDA approved for use as a cardioprotective agent against doxorubicin-induced cardiotoxicity [39].

The chemistry, biochemistry and pharmacology of dexrazoxane have been thoroughly investigated [44, 49, 50]. The bisdioxopiperazine dexrazoxane is a nonpolar, water-soluble (+) enantiomer of the racemic drug razoxane (ICRF-159) (Figure 1.22). It readily diffuses across cell membranes and is hydrolyzed through enzymatic and non-enzymatic pathways to the charged double open ring form, ADR-925, via the one ring open intermediate forms B and C (Figure 1.23) [30]. ADR-925 structurally resembles EDTA (Figure 1.23) [30] and is in fact a strong chelator of metals such as Fe^{3+} and Cu^{2+}. ADR-925 and the one ring opened hydrolysis intermediates to a lesser extent are the cardioprotective forms of dexrazoxane and are able to chelate free or bound intracellular iron in the myocardium. Studies have demonstrated that these hydrolysis products can remove iron from transferrin (iron transport protein), ferritin and most importantly anthracycline-iron complexes [44]. Consequently, the formation of free radicals through redox cycling and iron-based oxygen free radical damage to the heart is reduced. The major pharmacokinetic properties of dexrazoxane are reviewed in Table 1.4 [30].

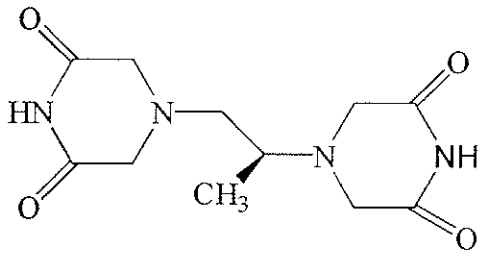

Dexrazoxane (ICRF-187)

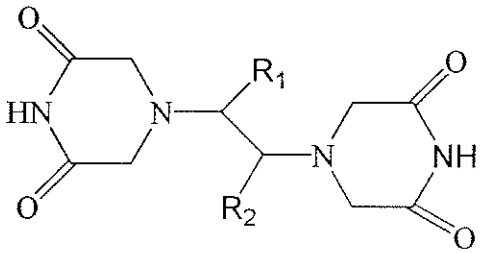

ICRF-154 $R_1 = R_2 = H$
ICRF-159 $R_1 = H$, $R_2 = CH_3$ (racemic)
ICRF-192 $R_1 = H$, $R_2 = C_2H_5$ (racemic)

Figure 1.22 Chemical structure of the bisdioxopiperazines.

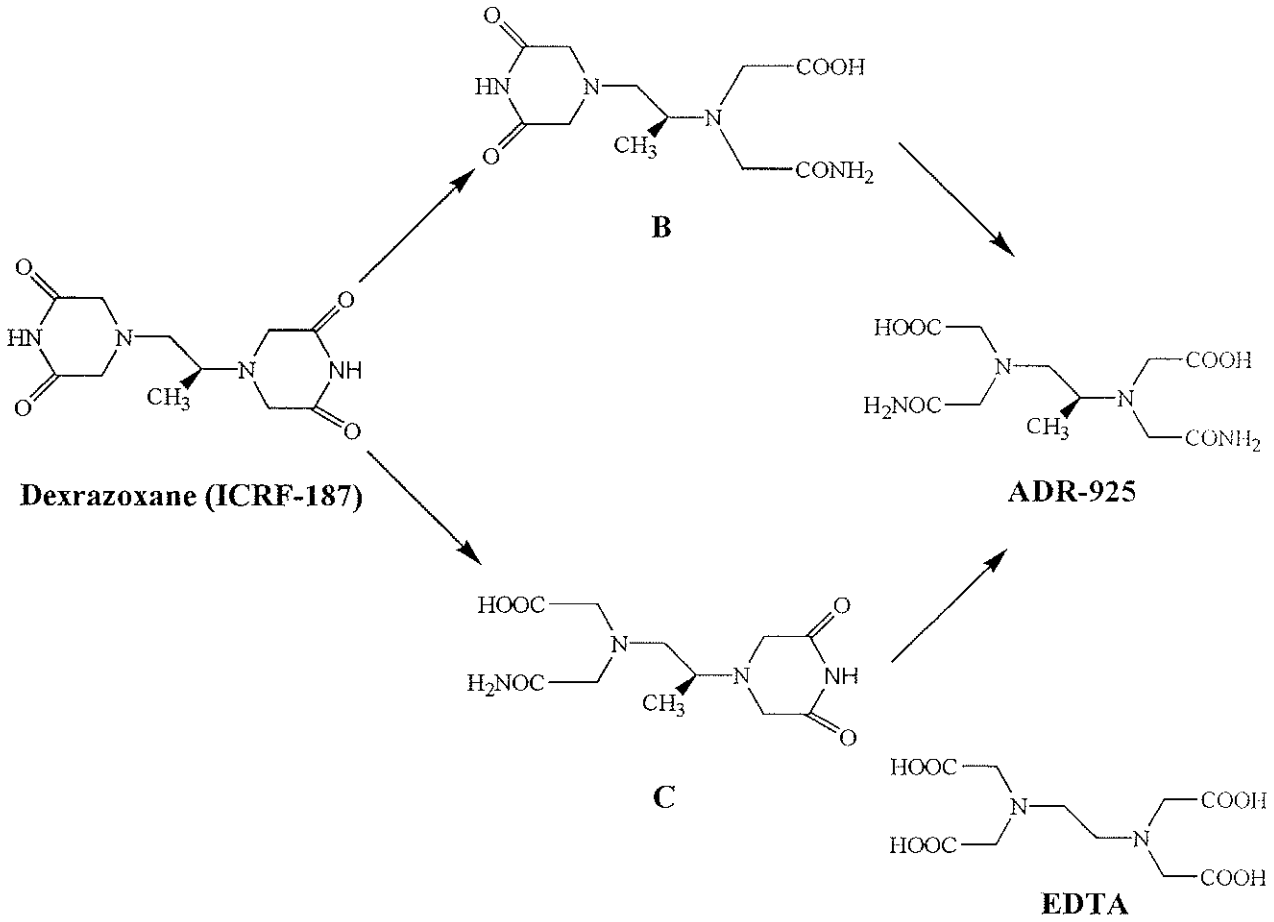

Figure 1.23 Reaction scheme for the hydrolysis of dexrazoxane. In the liver and kidney, the one ring opening hydrolysis is catalyzed by dihydropyrimidine amidohydrolase (DHPase). A base-catalyzed second ring opening hydrolysis follows this [30], pg 102.

Table 1.4 Pharmacokinetic properties of dexrazoxane in adult patients with cancer [30], pg 393.

Mean Cmax (500 mg/m^2)	36.5 μg/ml
$t_{1/2\alpha}$	~15 min
Vd_{ss}	~1.1L/kg
Binding to plasma proteins	<2%
Metabolism	Hydrolysis to active ring-opened products by dihydropyrimidine amidohydrolase
Elimination	Predominantly renal
Mean total body clearance	~0.29 L/h/kg
$t_{1/2\beta}$	2 to 4 h

Cmax = peak plasma concentration; $\mathbf{t_{1/2\alpha}}$ = distribution half-life; $\mathbf{t_{1/2\beta}}$ = elimination half-life; Vd_{ss} = volume of distribution at steady state

1.4 Herceptin in the treatment of cancer

1.4.1 General structure, pharmacokinetics, clinical use and cardiotoxicity

Herceptin (trastuzumab) is a recombinant DNA-derived humanized monoclonal antibody that binds with high affinity and specificity to the extracellular domain of the human epidermal growth factor receptor 2 protein (HER2) [51-54]. The antibody is of class IgG_1 and contains similar complementary-determining regions to the murine anti-p185, which binds to HER2 (Figure 1.24) [53-55]. At therapeutic doses in breast cancer patients, the mean half-life of herceptin is 5.8 days [53]. Herceptin serum concentrations reach steady state with mean trough and peak concentrations of 79 μg/ml and 123 μg/ml, respectively [53]. Herceptin has recently been approved by the Food and Drug Administration for the treatment of metastatic breast cancer [56]. In both *in vitro* assays and in animals, herceptin has been shown to inhibit proliferation of human tumor cells that overexpress HER2 [53]. Overexpression of HER2 occurs in approximately 25-30% of breast cancers [51, 54, 57-59]. Although superior antitumor efficacy was reported in clinical trials when herceptin was administered in combination with anthracyclines,

cardiac toxicity was an unexpected side effect of herceptin treatment [56, 57, 59]. A substantial number of women treated with herceptin developed ventricular dysfunction and congestive heart failure [56]. The incidence and severity of such cardiac dysfunction was highly dependent on prior or concurrent anthracycline exposure. The mechanism for herceptin-associated cardiotoxicity is unknown, although it may have a common pathophysiological basis with anthracycline-induced myocardial injury.

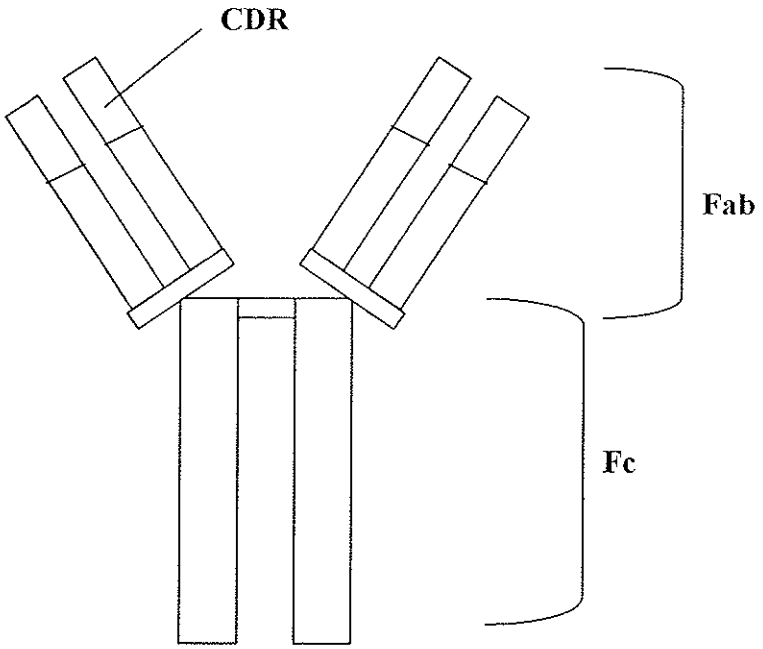

Figure 1.24 Schematic depiction of the general structure of an IgG molecule. CDR: complementarity-determining region

1.4.2 HER-2/*neu* signal transduction

The HER-2/*neu* gene encodes a transmembrane protein of 185-kd, which has intrinsic tyrosine kinase activity [51, 54, 58]. Point mutations at the transmembrane domain and gene overexpression are both believed to result in activation of HER2 protein [51]. This is likely due to the enhanced formation and stabilization of the receptor dimers,

allowing the protein to remain in an active state [51]. HER2 is a ligand-less member of the human epidermal growth factor family of receptor tyrosine kinases and is an important mediator of cell growth, differentiation and survival [52, 56]. In normal biological systems, HER2 functions as a co-receptor for a multitude of epidermal growth factor-like ligands that bind and activate other HER family members [52]. HER2 protein interacts directly or indirectly with many cellular proteins that may be important for the pathogenesis of human cancer [51].

1.4.3 Proposed mechanisms of drug action

A number of mechanisms have been proposed for herceptin action. The first mechanism of action is HER2 protein receptor downregulation [52]. When the herceptin antibody binds to HER2 protein receptors on the cell, it can cause receptors to be endocytosed into the cell. A few reports also suggest that herceptin has agonistic properties [52]. Because herceptin contains a human immunoglobulin G_1 (IgG_1) Fc region, it has been demonstrated to be capable of activating the human complement cascade [52]. Finally, herceptin has been proposed to take part in antibody-dependent cell-mediated cytotoxicity [52]. Through interaction of its Fc region with the surface of target cells, it can attract natural killer cells to the HER2 receptor complex cell for consumption.

1.5 Thesis research goal and study objectives

The ultimate goal of my thesis research was to investigate the mechanistic basis for doxorubicin and herceptin cardiotoxicity and the antineoplastic, resistance and cardioprotective mechanisms of dexrazoxane. In order to attain this goal, four major study objectives were devised.

The first study objective was to investigate dexrazoxane topoisomerase II inhibitory action and resistance through further characterization of a previously established dexrazoxane-resistant human leukemia cell line (K562/DZ1). In Chapter 2, cross resistance studies with the structurally similar catalytic topoisomerase II inhibitors, dexrazoxane, levrazoxane and merbarone and the structurally and mechanistically unrelated vinblastine were undertaken in K562 and K562/DZ1 cells with an MTS cytotoxicity assay. The resistance mechanism for dexrazoxane was further elucidated with the MTS assay by examining the cytotoxicity of dexrazoxane and etoposide together towards K562 and K562/DZ1 cell growth. Cross resistance studies are important as they provide anticancer drug mechanistic information for designing new treatment regimens and agents that overcome resistance while improving or maintaining antitumor effects.

The second study objective of this thesis was to develop and evaluate epifluorescence microscopy and fluorescence plate reader assays as alternative quantitative methods for studying cardiotoxic and cardioprotective agents in primary neonatal rat cardiomyocytes. The fluorescence assays developed may have significant physiological, pathophysiological and pharmacological implications in studying the normal and diseased heart. Once the procedures for probe loading, cell density, cell attachment and quantification of the fluorescence signal were optimized, these methods were employed to study the cardioprotective effects of dexrazoxane on doxorubicin-induced cardiomyocyte damage. Specifically, the effect of dexrazoxane on doxorubicin-induced mitochondrial damage (Chapter 3), reactive oxygen species generation (Chapter 4) and apoptosis and necrosis (Chapter 5) was examined with the fluorescent probes JC-1, 2',7'-dichlorofluorescin and annexin V/propidium iodide, respectively. Mechanistic

information on the cardioprotective effects of dexrazoxane may improve anthracycline cardiotoxicity treatment regimens or reveal new therapeutic avenues.

The final study objective was to begin some preliminary herceptin cardiotoxicity studies with the mouse 7.16.4 antibody. Specifically, the effect of 7.16.4 on cardiomyocyte growth and doxorubicin-induced lactate dehydrogenase release was investigated with a MTT cytotoxicity assay and a lactate dehydrogenase (LDH) release assay (Chapter 6). This study has set the stage for future investigation of 7.16.4 cardiotoxicity, as no prospective cardiotoxicity studies have been completed according to the currently available literature.

1.6 References

1. Voet D, Voet J: Biochmistry. Toronto, ON, John Wiley & Sons, 1996.

2. Bakshi RP, Galande S, Muniyappa K. 2001. Functional and regulatory characteristics of eukaryotic type II DNA topoisomerase. *Crit Rev Biochem Mol Biol* 36:1-37.

3. Beck WT, Kim R, Chen M. 1994. Novel actions of inhibitors of DNA topoisomerase II in drug-resistant tumor cells. *Cancer Chemother Pharmacol* 34:S14-8.

4. Burden DA, Osheroff N. 1998. Mechanism of action of eukaryotic topoisomerase II and drugs targeted to the enzyme. *Biochim Biophys Acta* 1400:139-54.

5. Fattman CL, Allan WP, Hasinoff BB, Yalowich JC. 1996. Collateral sensitivity to the bisdioxopiperazine dexrazoxane (ICRF-187) in etoposide (VP-16)-resistant human leukemia K562 cells. *Biochem Pharmacol* 52:635-42.

6. Kusumoto H, Rodgers QE, Boege F, Raimondi SC, Beck WT. 1996. Characterization of novel human leukemic cell lines selected for resistance to merbarone, a catalytic inhibitor of DNA topoisomerase II. *Cancer Res* 56:2573-83.

7. Li TK, Liu LF. 2001. Tumor cell death induced by topoisomerase-targeting drugs. *Annu Rev Pharmacol Toxicol* 41:53-77.

8. Pommier Y, Kerrigan D, Schwartz RE, Swack JA, McCurdy A. 1986. Altered DNA topoisomerase II activity in Chinese hamster cells resistant to topoisomerase II inhibitors. *Cancer Res* 46:3075-81.

9. Withoff S, De Jong S, De Vries EG, Mulder NH. 1996. Human DNA topoisomerase II: biochemistry and role in chemotherapy resistance (review). *Anticancer Res* 16:1867-80.

10. Berger JM. 1998. Structure of DNA topoisomerases. *Biochim Biophys Acta* 1400:3-18.

11. Katzung B: Basic and Clinical Pharmacology. San Francisco, CA, Appleton& Lange, 1998.

12. Hasinoff BB, Kuschak TI, Creighton AM, Fattman CL, Allan WP, Thampatty P, Yalowich JC. 1997. Characterization of a Chinese hamster ovary cell line with acquired resistance to the bisdioxopiperazine dexrazoxane (ICRF-187) catalytic inhibitor of topoisomerase II. *Biochem Pharmacol* 53:1843-53.

13.Andoh T, Ishida R. 1998. Catalytic inhibitors of DNA topoisomerase II. *Biochim Biophys Acta* 1400:155-71.

14.Dutcher JP, Novik Y, O'Boyle K, Marcoullis G, Secco C, Wiernik PH. 2000. 20th-century advances in drug therapy in oncology--Part. II. *J Clin Pharmacol* 40:1079-92.

15.Hande KR. 1998. Clinical applications of anticancer drugs targeted to topoisomerase II. *Biochim Biophys Acta* 1400:173-84.

16.Kaufmann SH. 1998. Cell death induced by topoisomerase-targeted drugs: more questions than answers. *Biochim Biophys Acta* 1400:195-211.

17.Baguley BC, Ferguson LR. 1998. Mutagenic properties of topoisomerase-targeted drugs. *Biochim Biophys Acta* 1400:213-22.

18.Larsen AK, Skladanowski A. 1998. Cellular resistance to topoisomerase-targeted drugs: from drug uptake to cell death. *Biochim Biophys Acta* 1400:257-74.

19.Fortune JM, Osheroff N. 1998. Merbarone inhibits the catalytic activity of human topoisomerase IIalpha by blocking DNA cleavage. *J Biol Chem* 273:17643-50.

20.Synold TW, Tetef ML, Doroshow JH. 1998. Antineoplastic activity of continuous exposure to dexrazoxane: potential new role as a novel topoisomerase II inhibitor. *Semin Oncol* 25:93-9.

21.Hasinoff BB, Abram ME, Barnabe N, Khelifa T, Allan WP, Yalowich JC. 2001. The catalytic DNA topoisomerase II inhibitor dexrazoxane (ICRF-187) induces differentiation and apoptosis in human leukemia K562 cells. *Mol Pharmacol* 59:453-61.

22.Hasinoff BB, Abram ME, Chee GL, Huebner E, Byard EH, Barnabe N, Ferrans VJ, Yu ZX, Yalowich JC. 2000. The catalytic DNA topoisomerase II inhibitor dexrazoxane (ICRF-187) induces endopolyploidy in Chinese hamster ovary cells. *J Pharmacol Exp Ther* 295:474-83.

23.Herman EH, Ferrans VJ. 1998. Preclinical animal models of cardiac protection from anthracycline- induced cardiotoxicity. *Semin Oncol* 25:15-21.

24.Lopez M, Vici P. 1998. European trials with dexrazoxane in amelioration of doxorubicin and epirubicin-induced cardiotoxicity. *Semin Oncol* 25:55-60.

25.Wexler LH. 1998. Ameliorating anthracycline cardiotoxicity in children with cancer: clinical trials with dexrazoxane. *Semin Oncol* 25:86-92.

26.Dorr RT. 1996. Cytoprotective agents for anthracyclines. *Semin Oncol* 23:23-34.

27.Hershko C, Pinson A, Link G. 1996. Prevention of anthracycline cardiotoxicity by iron chelation. *Acta Haematol* 95:87-92.

28.Links M, Lewis C. 1999. Chemoprotectants:A review of their clinical pharmacology and therapeutic efficacy. *Drugs* 57:293-308.

29.Malisza KL, Hasinoff BB. 1996. Inhibition of anthracycline semiquinone formation by ICRF-187 (dexrazoxane) in cells. *Free Radic Biol Med* 20:905-14.

30.Wiseman LR, Spencer CM. 1998. Dexrazoxane. A review of its use as a cardioprotective agent in patients receiving anthracycline-based chemotherapy. *Drugs* 56:385-403.

31.Sehested M, Jensen PB, Sorensen BS, Holm B, Friche E, Demant EJ. 1993. Antagonistic effect of the cardioprotector (+)-1,2-bis(3,5- dioxopiperazinyl-1-yl)propane (ICRF-187) on DNA breaks and cytotoxicity induced by the topoisomerase II directed drugs daunorubicin and etoposide (VP-16). *Biochem Pharmacol* 46:389-93.

32.Hortobagyi GN. 1997. Anthracyclines in the treatment of cancer. An overview. *Drugs* 54:1-7.

33.Gewirtz DA. 1999. A critical evaluation of the mechanisms of action proposed for the antitumor effects of the anthracycline antibiotics adriamycin and daunorubicin. *Biochem Pharmacol* 57:727-41.

34.Licata S, Saponiero A, Mordente A, Minotti G. 2000. Doxorubicin metabolism and toxicity in human myocardium: role of cytoplasmic deglycosidation and carbonyl reduction. *Chem Res Toxicol* 13:414-20.

35.Minotti G, Mancuso C, Frustaci A, Mordente A, Santini SA, Calafiore AM, Liberi G, Gentiloni N. 1996. Paradoxical inhibition of cardiac lipid peroxidation in cancer patients treated with doxorubicin. Pharmacologic and molecular reappraisal of anthracycline cardiotoxicity. *J Clin Invest* 98:650-61.

36.Minotti G, Cairo G, Monti E. 1999. Role of iron in anthracycline cardiotoxicity: new tunes for an old song? *Faseb J* 13:199-212.

37.Selvaratnam G, Philips RH, Mohamed AK. 1999. Cardiotoxicity of cytotoxic chemotherapy and its prevention. *Adverse Drug React Toxicol Rev* 18:61-105.

38.Singal PK, Iliskovic N, Li T, Kumar D. 1997. Adriamycin cardiomyopathy: pathophysiology and prevention. *Faseb J* 11:931-6.

39.Pai VB, Nahata MC. 2000. Cardiotoxicity of chemotherapeutic agents: incidence, treatment and prevention. *Drug Saf* 22:263-302.

40. Arola OJ, Saraste A, Pulkki K, Kallajoki M, Parvinen M, Voipio-Pulkki LM. 2000. Acute doxorubicin cardiotoxicity involves cardiomyocyte apoptosis. *Cancer Res* 60:1789-92.

41. Kumar D, Kirshenbaum L, Li T, Danelisen I, Singal P. 1999. Apoptosis in isolated adult cardiomyocytes exposed to adriamycin. *Ann N Y Acad Sci* 874:156-68.

42. Myers C. 1998. The role of iron in doxorubicin-induced cardiomyopathy. *Semin Oncol* 25:10-4.

43. Rubin E: Essential Pathology. Philadelphia, Lippincott Williams & Wilkins, 2001.

44. Hasinoff BB. 1998. Chemistry of dexrazoxane and analogues. *Semin Oncol* 25:3-9.

45. Saad S, Najjar T, Al-Rikabi A. 2001. The preventative role of deferoxamine against acute doxorubicin-induced cardiac, renal and hepatic toxicity in rats. *Pharmacological Research* 43:211-218.

46. Yaoita H, Ogawa K, Maehara K, Maruyama Y. 2000. Apoptosis in relevant clinical situations: contribution of apoptosis in myocardial infarction. *Cardiovasc Res* 45:630-41.

47. Malisza KL, Hasinoff BB. 1995. Production of hydroxyl radical by iron(III)-anthraquinone complexes through self-reduction and through reductive activation by the xanthine oxidase/hypoxanthine system. *Arch Biochem Biophys* 321:51-60.

48. Garner AP, Paine MJ, Rodriguez-Crespo I, Chinje EC, Ortiz De Montellano P, Stratford IJ, Tew DG, Wolf CR. 1999. Nitric oxide synthases catalyze the activation of redox cycling and bioreductive anticancer agents. *Cancer Res* 59:1929-34.

49. Hasinoff BB, Aoyama RG. 1999. Stereoselective metabolism of dexrazoxane (ICRF-187) and levrazoxane (ICRF-186). *Chirality* 11:286-90.

50. Hochster HS. 1998. Clinical pharmacology of dexrazoxane. *Semin Oncol* 25:37-42.

51. Hung MC, Lau YK. 1999. Basic science of HER-2/neu: a review. *Semin Oncol* 26:51-9.

52. Sliwkowski MX, Lofgren JA, Lewis GD, Hotaling TE, Fendly BM, Fox JA. 1999. Nonclinical studies addressing the mechanism of action of trastuzumab (Herceptin). *Semin Oncol* 26:60-70.

53. Goldenberg MM. 1999. Trastuzumab, a recombinant DNA-derived humanized monoclonal antibody, a novel agent for the treatment of metastatic breast cancer. *Clin Ther* 21:309-18.

54. Schaller G, Bangemann N, Becker C, Buhler H, Opri F, Weitzel HK. 1999. Therapy of metastatic breast cancer with humanized antibodies against the HER2 receptor protein. *J Cancer Res Clin Oncol* 125:520-4.

55. Weiner LM. 1999. An overview of monoclonal antibody therapy of cancer. *Semin Oncol* 26:41-50.

56. Feldman AM, Lorell BH, Reis SE. 2000. Trastuzumab in the treatment of metastatic breast cancer : anticancer therapy versus cardiotoxicity. *Circulation* 102:272-4.

57. Ewer MS, Gibbs HR, Swafford J, Benjamin RS. 1999. Cardiotoxicity in patients receiving transtuzumab (Herceptin): primary toxicity, synergistic or sequential stress, or surveillance artifact? *Semin Oncol* 26:96-101.

58. Reese DM, Slamon DJ. 1997. HER-2/neu signal transduction in human breast and ovarian cancer. *Stem Cells* 15:1-8.

59. Shak S. 1999. Overview of the trastuzumab (Herceptin) anti-HER2 monoclonal antibody clinical program in HER2 overexpressing metastatic breast cancer. Herceptin Multinational Investigator Study Group. *Semin Oncol* 26:71-7.

Chapter 2 Further characterization of the dexrazoxane-resistant K562 human leukemia cell line (K562/DZ1)

2.1 Introduction

Topoisomerase II is a DNA-binding enzyme that relieves torsional strain during replication and transcription and ensures efficient recombination and daughter DNA strand separation during mitosis [1-4]. A number of clinically effective anticancer agents including etoposide and doxorubicin target topoisomerase II (Figure 2.1) [5]. These drugs induce DNA strand breaks and poison the enzyme by stabilizing topoisomerase II-DNA cleavable-complexes [3, 5]. Acquired drug resistance to topoisomerase II poisons has been correlated with decreased formation of these complexes, altered enzyme levels, reduced drug accumulation and altered topoisomerase II function [2, 4, 6, 7].

A second class of drugs that affect the activity of topoisomerase II also appear to have clinical potential. In contrast to the complex-stabilizing topoisomerase II poisons, drugs such as the bisdioxopiperazines and merbarone are catalytic inhibitors of topoisomerase II that do not stabilize cleavable-complexes [1, 8-10]. Although the cytotoxicity of and resistance to topoisomerase II poisons are thought to be mediated through stabilization of cleavable-complexes, the mechanisms of cytotoxicity and resistance to catalytic inhibitors are not well understood [2, 4, 5, 7]. The formation and cytotoxicity of cleavable-complexes is reviewed in Section 1.1.3.1.

Our laboratory has isolated and begun to characterize a mutant human K562 leukemia cell line (K562/DZ1) with acquired resistance to the catalytic inhibitor dexrazoxane. The bisdioxopiperazines dexrazoxane (ICRF-187) and levrazoxane (ICRF-186) are enantiomers (Figure 2.2) that are believed to interfere with the ATP hydrolysis step of the topoisomerase II catalytic cycle and trap the enzyme in its closed clamp form

[1, 10-12]. Characterization and sequencing of topoisomerase IIα from three different dexrazoxane-resistant cell lines [9, 13, 14] has identified functional mutations at the clamp part of the dimer interface of the enzyme [14] and at the ATP binding site [13], suggesting that dexrazoxane may bind in the interface region. Moreover, recent functional point mutations near the ATP binding site and dimer interface of K562/DZ1 topoisomerase II have been identified in Dr. Jack Yalowich's laboratory (University of Pittsburgh, PA). Merbarone structurally resembles the bisdioxopiperazines (Figure 2.2), specifically blocks topoisomerase II-mediated cleavage of its DNA substrate and has been the subject of phase II clinical cancer trials [10]. Both the bisdioxopiperazines and merbarone have been shown to attenuate the DNA-cleavage enhancing properties of various topoisomerase II poisons including etoposide and doxorubicin [1, 15]. Preliminary cross resistance studies with etoposide and doxorubicin in our established K562/DZ1 cell line have shown moderate cross resistance [16].

A vast number of anticancer drugs that are structurally or functionally unrelated cytotoxic drugs may also confer cross resistance. This phenotypic expression has been termed multi-drug resistance and is thought to occur mainly by resistance mechanisms that affect drug transportation or drug detoxification [17-19]. Multi-drug resistant cell lines often exhibit increased expression of the transmembrane P-glycoprotein, an efflux pump that extrudes drugs from cells [18, 19]. The Vinca alkaloids such as vincristine and vinblastine are structurally and functionally distinct from the topoisomerase II inhibitors (Figure 2.3) [17]. However, in common to the topoisomerase II poisons, etoposide and doxorubicin, they are good substrates for P-glycoprotein (Figure 2.3) [18, 19].

In the following study, the established dexrazoxane-resistant K562/DZ1 human leukemia cell line was further characterized. Using a colorimetric, MTS cytotoxicity assay, growth inhibition experiments were conducted on K562 and K562/DZ1 cell lines to examine the degree of cross resistance conferred by dexrazoxane, levrazoxane, merbarone and vinblastine. To further elucidate the mechanism of resistance exhibited by the K562/DZ1 cells, dexrazoxane cytotoxicity was also evaluated in the presence of the cleavable complex-forming topoisomerase II poison etoposide.

2.2 Materials

Dexrazoxane hydrochloride (Zinecard®, ICRF-187) was a gift from Pharmacia & Upjohn (Columbus, OH) and levrazoxane (ICRF-186) was a gift from Adria-SP Inc. (Columbus, Ohio). Merbarone was received from Smith-Kline and Beecham Pharmaceuticals (Philadelphia, PA). Etoposide (VP-16, cat No. E-1383), vinblastine sulfate (cat No. V-1377), DMSO used to dissolve drugs (99.5 % cat No. D-5879) and HEPES (cell culture grade, cat No. H-9136) were obtained from Sigma Chemical Co. (St. Louis, MO). Sodium bicarbonate ($NaHCO_3$, cat No. BP328-079) was obtained from Fisher Scientific (Fairlawn, NJ). Dulbecco's phosphate buffered saline (PBS, cat No. D-5652), Dulbecco's modified Eagle medium (DMEM, cat No. 12800-017), penicillin-streptomycin (cat No. 25200-072) and fetal calf serum (FCS, cat No. 26140-079) were obtained from Gibco-BRL, Life Technologies Inc. (Burlington, ON). MTS, Cell Titer 96® AQ_{ueous} One Solution Reagent (cat No. G3580) was obtained from Promega Corp. (Madison, WI) and stored at -20°C shielded from light. Dr. Jack Yalowich (University of Pittsburgh, PA) donated the K562 cells and Mr. Michael Abram developed the K562/DZ1 cell line in our laboratory. Cell culture medium and buffers were made with

reverse osmosis distilled water and cells were grown in a 37°C incubator in an atmosphere of 5% (v/v) CO_2 in air.

2.3 Methods

2.3.1 Cell culture

2.3.1.1 Preparation of cell culture medium and buffer

The cell culture medium was prepared by dissolving one pack (10.0 g) of DMEM, 4.76 g of HEPES and 2.2 g of $NaHCO_3$ in 800 ml of H_2O. The pH of the solution was titrated to 7.2 ± .05 at room temperature with 1.0 M NaOH and a calibrated PHB-45 microprocessor pH meter. Penicillin-streptomycin (10 ml) was added aseptically to the medium followed by addition of enough H_2O to top the volume up to 900 ml. The medium was filter sterilized through a 0.2 μm Nalgene bottle top filter (Nalgene Company, Rochester, New York) and stored in the refrigerator for up to one month after 10% (v/v) fetal calf serum had been added. Before use, fetal calf serum was aseptically added in the laminar flow hood (Enviro Safety Cabinet, model ESC, Albuquerque, New Mexico) to the medium to give a final concentration of 10% (v/v).

Dulbecco's phosphate buffered saline was prepared by dissolving one pack (12 g) of PBS in 1000 ml of H_2O. The pH of the buffer was adjusted to 7.2 at room temperature with 1 M NaOH and a calibrated pH meter. Finally, the buffer was filter sterilized through a 0.2 μm bottle top filter and stored in the refrigerator at 4°C.

2.3.1.2 Culturing of K562 and K562/DZ1 cells

K562 and K562/DZ1 cell lines were grown as suspension cultures in 25 cm^2 T-flasks (cat No. 83.1813.503, Sarstedt Inc., St. Leonard, PQ) in DMEM (pH 7.2) containing 20 mM HEPES, 100 units/ml penicillin, 100 μg/ml streptomycin and 10%

(v/v) fetal calf serum. Cells were grown in the incubator in an atmosphere of 5% (v/v) CO_2 in air at 37°C. Exponentially growing cultures of K562 and K562/DZ1 cells approaching confluence (~$1x10^6$ cells/ml) were diluted to lower starting densities (>25,000 cells/ml) in fresh DMEM. A model Z_f Coulter counter (Coulter Electronics, Hialeah, FL) was used to determine cell densities (cells/ml) of aseptically removed 1-ml aliquots from confluent cultures. These cell densities were required for subsequent cell seeding.

2.3.1.3 Seeding cells for single drugging experiments

K562 and K562/DZ1 cells were seeded with a multi-channel pipette on separate 96-well, sterile tissue culture plates (flat bottom with lid, cat No. 831835, Sarstedt Inc., Newton, NC) at a density of 1800 cells/well and 2300 cells/well, respectively, in 50 µl of DMEM (for DMEM soluble drugs) or 88.5 µl of DMEM (for DMSO soluble drugs). The seeding cell densities chosen ensured that the cultures would reach confluence after 72 h based upon the 18 h and 21 h doubling times of K562 and K562/DZ1 cells, respectively [16]. During the seeding process, the cell suspensions were rocked gently in a sterile boat to prevent cell settlement. Cross contamination of the cell lines was prevented by using separate media stocks, plates and pipette tips.

2.3.1.4 Seeding cells for double drugging experiments

K562 and K562/DZ1 cells were seeded with sterile 5-ml pipettes into sterile 15-ml centrifuge tubes at a density of 100,000 cells per tube in 4.9 ml of DMEM. The cell density chosen accounted for 10% cell loss during centrifugations and ensured sufficient cell numbers for counting with the Coulter counter. During the seeding process, the cell

suspensions were swirled to keep the cells suspended. Cross contamination of the cell lines was prevented by using separate media stocks and pipettes.

2.3.2 Drug preparation and delivery

All drugs were thawed out in a dessicator at room temperature for 20 min prior to being weighed out with the microbalance (Micro Gram-Atic Balance, Fisher Scientific Company). Dexrazoxane and levrazoxane were dissolved in cell culture medium (DMEM) and filter sterilized through a 0.2 μm sterile cellulose acetate syringe filter. Merbarone, vinblastine and etoposide were dissolved in dimethylsulfoxide (DMSO) and were added to cell cultures such that the DMSO concentration did not exceed 0.5% (v/v). A DMSO control was included to ensure that DMSO itself did not significantly affect cell growth.

After the appropriate quantity of drug was weighed and solubilized, drug stock solutions were prepared. The ranges of drug concentrations used in the single drugging experiments were estimated based upon the approximate IC_{50}'s of the tested drugs in Chinese Hamster Ovary parental and dexrazoxane-resistant cell lines [9]. Six replicates were performed at each concentration. For single drug experiments, the DMEM soluble drugs (dexrazoxane, levrazoxane) were delivered at 40 μl/well while the DMSO soluble drugs (merbarone, vinblastine) were delivered at 0.5 μl/well, or ~0.5% (v/v) as previously described. After addition of the drug solutions, the final volume of each well was 90 μl. Into all outer wells was placed 100 μl of PBS for spectrophotometer blanking. Each plate was wrapped with Saran wrap to reduce evaporation and placed in the incubator at 37°C in an atmosphere of 5% (v/v) CO_2 in air for 72 h.

For double drug experiments, K562 cells were treated with 0, 9, 43, 86 and 430 μM dexrazoxane (99 μl) and K562/DZ1 cells were treated with 0, 9 and 86 μM dexrazoxane (99 μl) for 20 min at 37°C in an atmosphere of 5% (v/v) CO_2 in air. Halfway through the incubation period, the cells were briefly removed from the incubator and vortexed to keep the cells in suspension. After the 20 min incubation, the K562 cells were exposed to 0, 5 and 10 μM etoposide (1 μl) and the K562/DZ1 cells were exposed to 0, 5, 10, 20, 50 and 100 μM etoposide (1 μl) for 1 h. At 20-min intervals during the incubation, the cells were vortexed to keep them suspended. After the 1 h incubation, the cells were washed three times with DMEM. A wash involved centrifuging the cells for 6 min at 250 g, drawing off the supernatant, resuspending the cells in 5 ml of DMEM and incubating the cells for 20 min at 37°C in an atmosphere of 5% (v/v) CO_2 in air. After the third wash, 4-ml aliquots were removed from each centrifuge tube for cell counting with the Coulter counter. Once cell counts and densities (cells/ml) were determined, the original centrifuge tubes were diluted with DMEM to give a K562 cell density of 18,000 cells/ml and a K562/DZ1 cell density of 23,000 cells/ml. K562 and K562/DZ1 cells were seeded in sterile, 96-well microtitre plates at a cell density of 1800 cells/well and 2300 cells/well, respectively, in 90 μl of DMEM. All outer wells were filled with 100 μl of PBS and plates were wrapped in saran wrap for a 72 h incubation at 37°C with 5% (v/v) CO_2 in air.

2.3.3 Determination of growth inhibition with the MTS assay

The MTS or CellTiter 96® Aq_{ueous} One Solution assay is a colorimetric method used to determine the number of viable cells in proliferation or cytotoxicity assays. The one solution reagent contains the yellow tetrazolium dye, MTS, and the electron-coupling

reagent, phenazine methosulfate. Upon addition of this solution to cells in culture medium, the MTS is reduced to a blue colored soluble formazan product (Figure 2.4) by mitochondrial cytosolic reducing species such as NADH [20]. The amount of formazan product produced is directly proportional to the number of metabolically active cells in culture by measuring the absorbance at 490 nm.

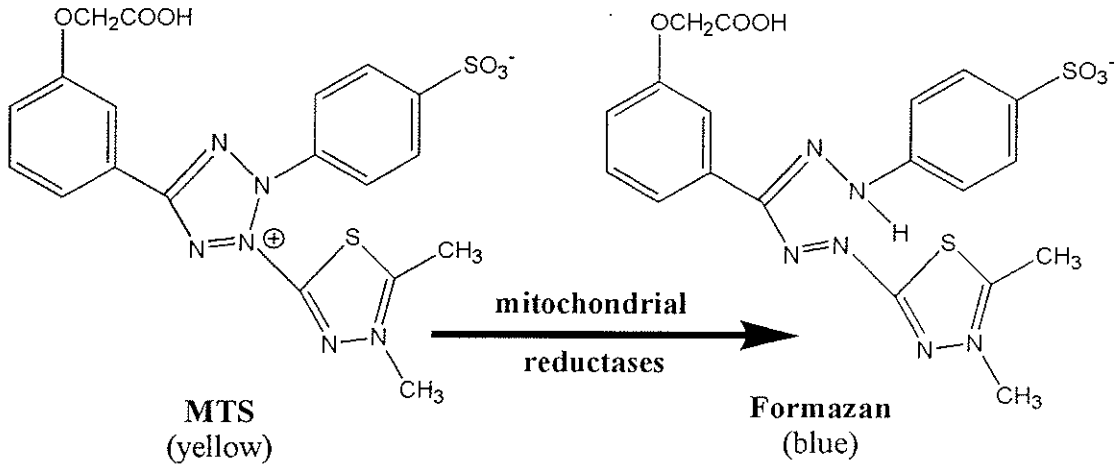

Figure 2.4 Chemical structure of MTS tetrazolium and its formazan product.

Before use, the MTS One Solution Reagent was thawed for 15 min in a 37°C water bath and aseptically transferred into a sterile boat. After 72 h of growth, 10 µl of MTS reagent was delivered with a multi-channel pipette to the appropriate wells to give a final volume of 100 µl/well. The plates were incubated for 3 h at 37°C in an atmosphere of 5% (v/v) CO_2 in air. A Thermomax 96-well plate reader (Molecular Devices, Menlo Park, CA) was used to measure absorbances at 490 nm. The absorbances were corrected by subtracting the absorbance at 650 nm from the absorbance at 490 nm to minimize non-specific, scattered light.

2.3.4 Determination of IC_{50}'s and resistance factors with dose-response curves

Data from the cytotoxicity experiments was transferred into SigmaPlot (Jandel Scientific, San Rafael, CA) for the determination of the 50% median inhibitory drug concentrations (IC_{50}'s). Prior to plotting the dose-response curves, outlying absorbances were removed using the transform file entitled *!outlier.xfm*. A non-linear, least squares fit of the absorbance-concentration data was completed in SigmaPlot using the following three- or four-parameter logistic equation (Equation 1),

$$Abs_{490/650} = (a - d) / (1 + ([D] / IC_{50})^{b}) + d \qquad (1)$$

where $Abs_{490/650}$ is the absorbance at 490 nm minus the absorbance at 650 nm, [D] is the drug concentration, IC_{50} is the median inhibitory drug concentration, b is the Hill-type exponential factor, a is the estimated maximal absorbance and d is the estimated background absorbance at the highest drug concentration. When the background absorbance was close to zero, d was set to zero to give a three-parameter logistic equation. The b value and the IC_{50} were first approximated with a two-parameter fit by substituting in values for a and d. Using the same a and d values with the computed b and IC_{50} values from the two-parameter fit equation, more accurate values of b and the IC_{50} were determined.

The resistance factor was calculated by taking the ratio of the IC_{50} for K562/DZ1 cells over the IC_{50} of K562 cells.

2.4 Results

2.4.1 Growth inhibitory effects of dexrazoxane, levrazoxane, merbarone and vinblastine on K562 and K562/DZ1 cells

The cytotoxicity profiles determined by MTS analysis for K562 and K562/DZ1 cells exposed to dexrazoxane, levrazoxane, merbarone and vinblastine for 72 h are illustrated in Figures 2.5, 2.6, 2.7 and 2.8. The K562 dose-response curves for

dexrazoxane and levrazoxane were biphasic while the K562/DZ1 dose-response curves were monophasic (Figures 2.5 and 2.6). The first phase was used in the determination of the dexrazoxane and levrazoxane IC_{50} values, as at high concentrations of these drugs their chelating metabolites also inhibit cell growth. The growth inhibition curves for both cell lines were monophasic for merbarone and vinblastine (Figures 2.7 and 2.8). The amount of growth inhibition due to DMSO alone at 0.5% (v/v) was less than 10% (data not shown). The IC_{50}'s and relative resistance factors for each drug tested are displayed in Table 2.1. When compared with the parental K562 cell line, K562/DZ1 cells were 135-fold resistant to dexrazoxane and 80-fold resistant to levrazoxane. K562/DZ1 cells did not exhibit cross resistance to merbarone or vinblastine.

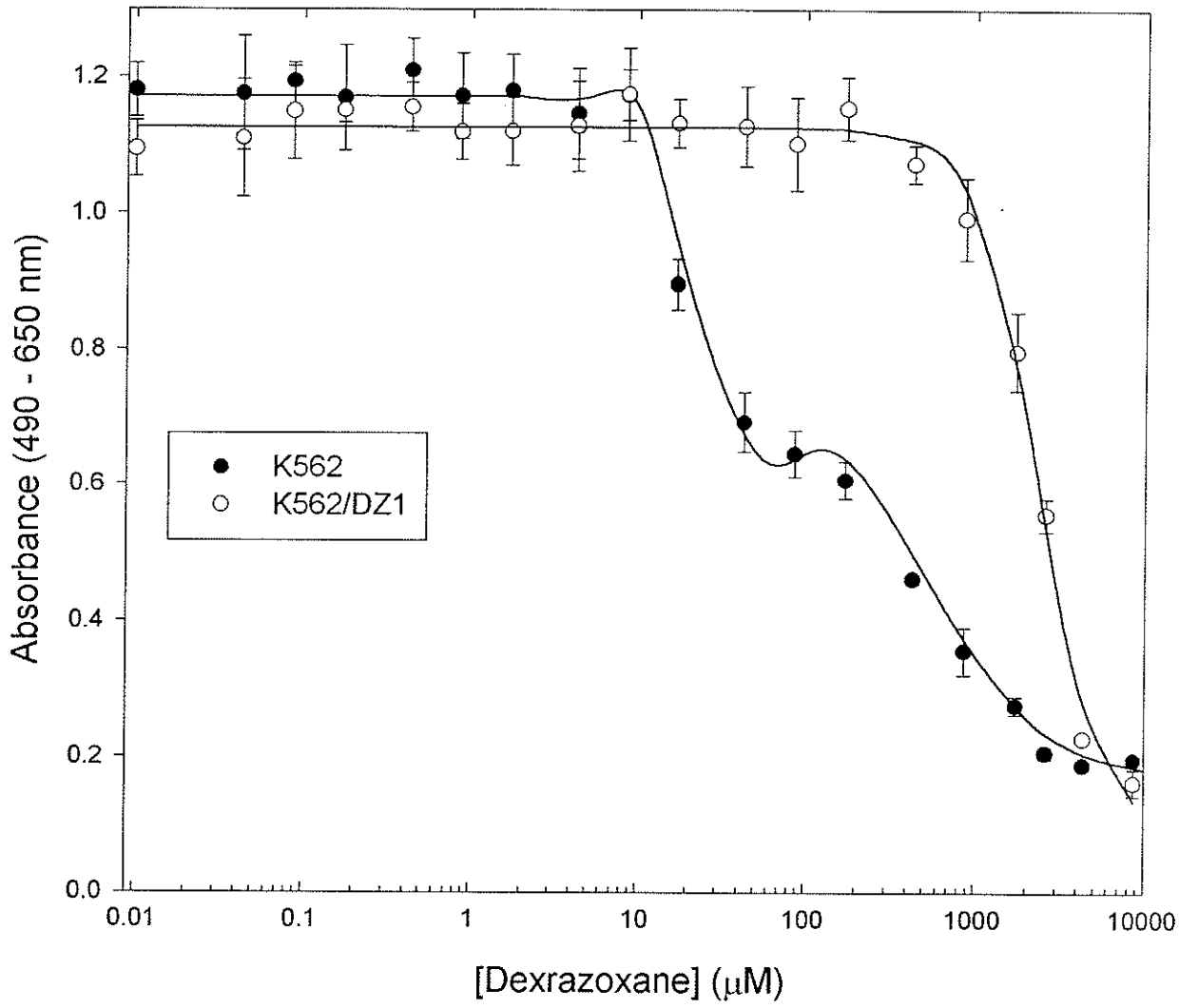

Figure 2.5 K562 and K562/DZ1 cell growth inhibition by dexrazoxane, as measured by MTS cytotoxicity assay. K562 and K562/DZ1 cells were seeded at a density of 1800 cells/well and 2300 cells/well, respectively, in 50 μl of DMEM. Dexrazoxane concentrations (0-8650 μM) were delivered to the cells at 40 μl/well for 72 h at 37°C in an atmosphere of 5% (v/v) CO_2 in air. Absorbances at 490-650 nm were determined after the cells were incubated for 3 h with 10 μl of MTS reagent. The final volume in each well was 100 μl. Data were fit to a four-parameter logistic equation and the curves display the results of the non-linear least squares regression analysis. Six replicates were performed at each concentration. The error bars represent standard errors and the lowest concentration plotted (0.01 μM) is the zero value. For the K562 cytotoxicity profile, data from the first phase (up until 86 μM) were used in the determination of the dexrazoxane IC_{50} value.

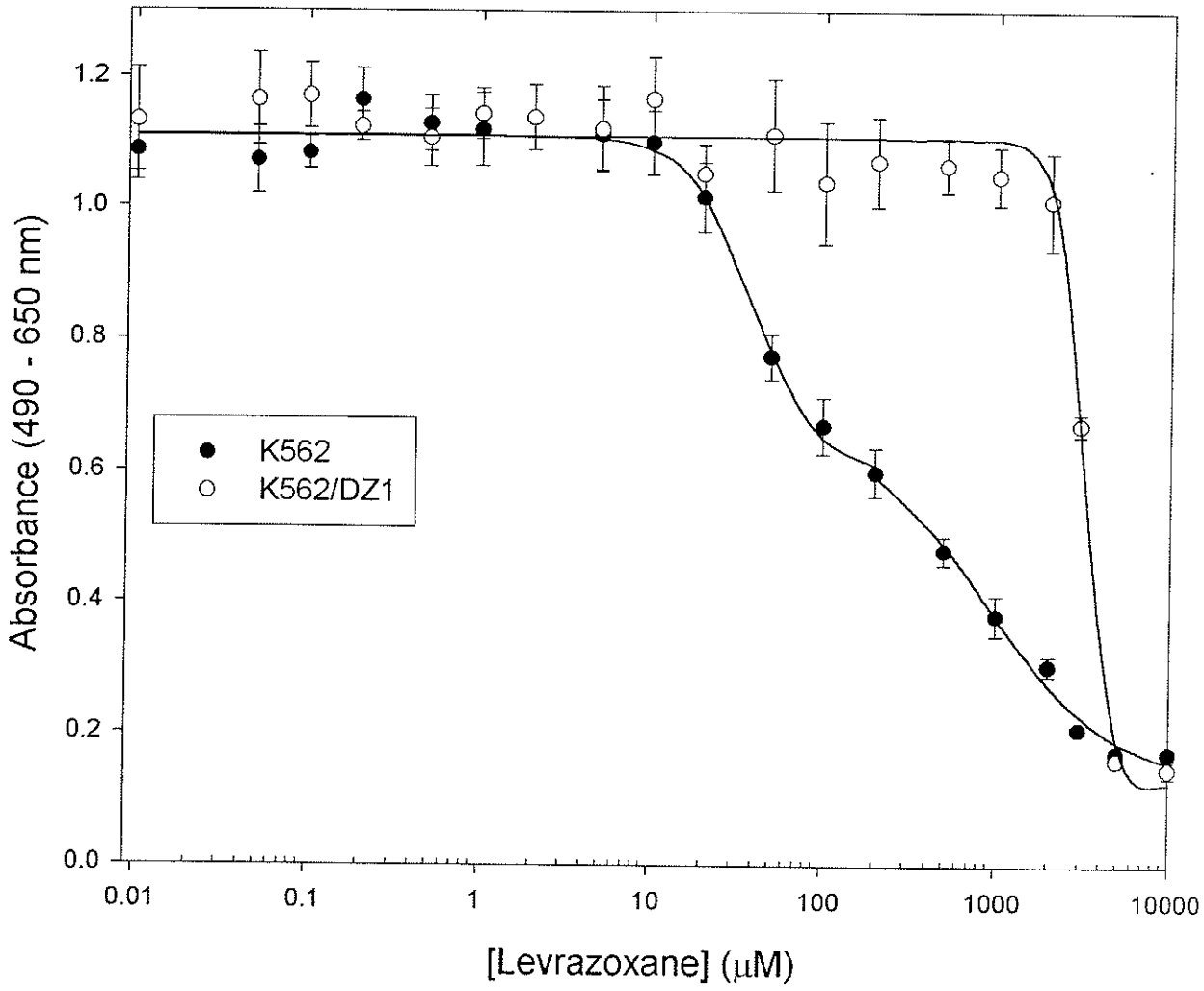

Figure 2.6 K562 and K562/DZ1 cell growth inhibition by levrazoxane, as measured by MTS cytotoxicity assay. K562 and K562/DZ1 cells were seeded at a density of 1800 cells/well and 2300 cells/well, respectively, in 50 μl of DMEM. Levrazoxane concentrations (0-10,000 μM) were delivered to the cells at 40 μl/well for 72 h at 37°C in an atmosphere of 5% (v/v) CO_2 in air. Absorbances at 490-650 nm were determined after the cells were incubated for 3 h with 10 μl of MTS reagent. The final volume in each well was 100 μl. Data were fit to a four-parameter logistic equation and the curves display the results of the non-linear least squares regression analysis. Six replicates were performed at each concentration. The error bars represent standard errors and the lowest concentration plotted (0.01 μM) is the zero value. For the K562 cytotoxicity profile, data from the first phase (up until 100 μM) were used in the determination of the levrazoxane IC_{50} value.

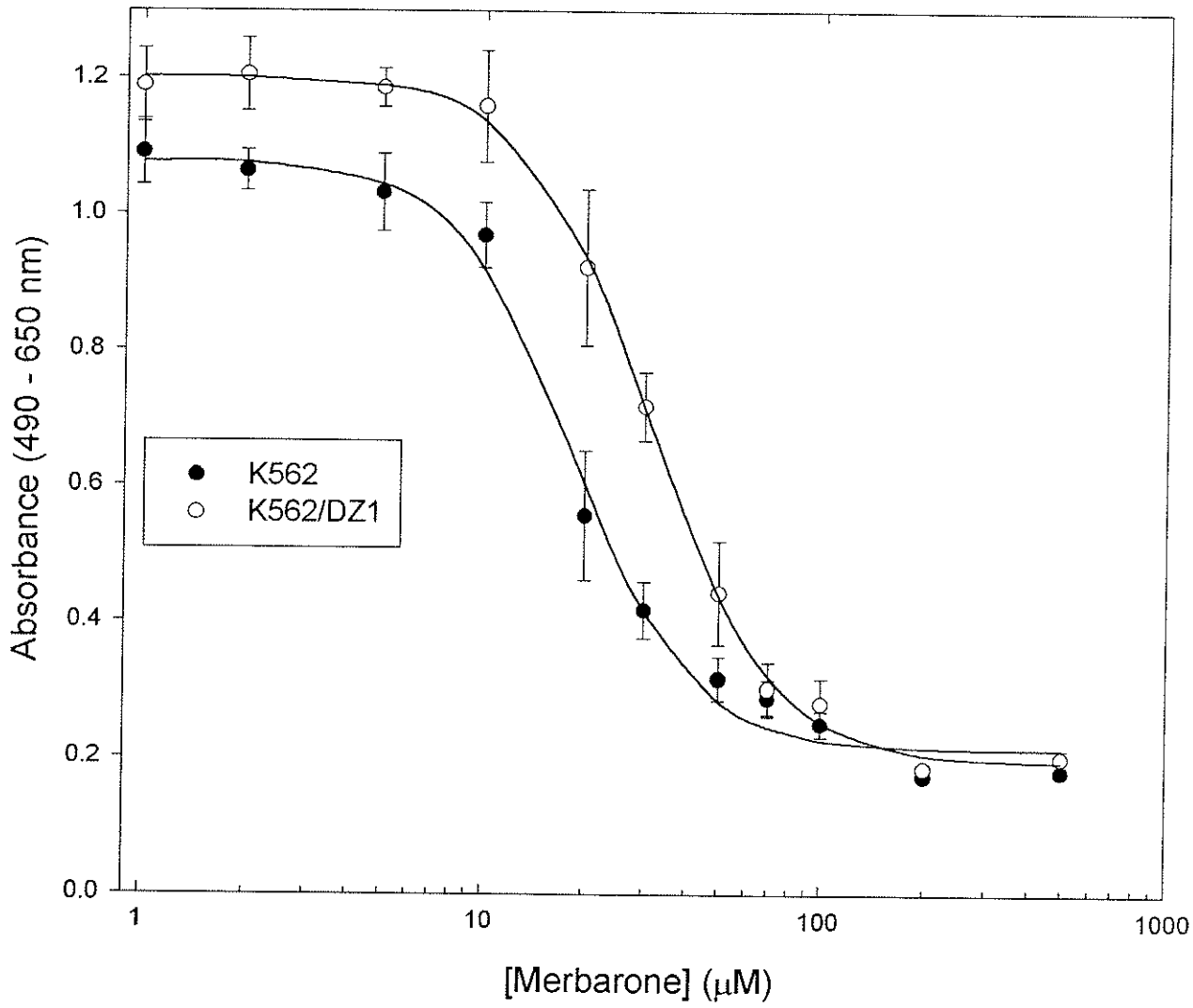

Figure 2.7 K562 and K562/DZ1 cell growth inhibition by merbarone, as measured by MTS cytotoxicity assay. K562 and K562/DZ1 cells were seeded at a density of 1800 cells/well and 2300 cells/well, respectively, in 88.5 μl of DMEM. Merbarone concentrations (0-500μM) were delivered to the cells at 0.5 μl/well for 72 h at 37°C in an atmosphere of 5% (v/v) CO_2 in air. Absorbances at 490-650 nm were determined after the cells were incubated for 3 h with 10 μl of MTS reagent. The final volume in the each well was 100 μl. Data were fit to a four-parameter logistic equation and the curves display the results of the non-linear least squares regression analysis. Six replicates were performed at each concentration and the error bars represent standard errors. The lowest concentration plotted (1 μM) is the zero value.

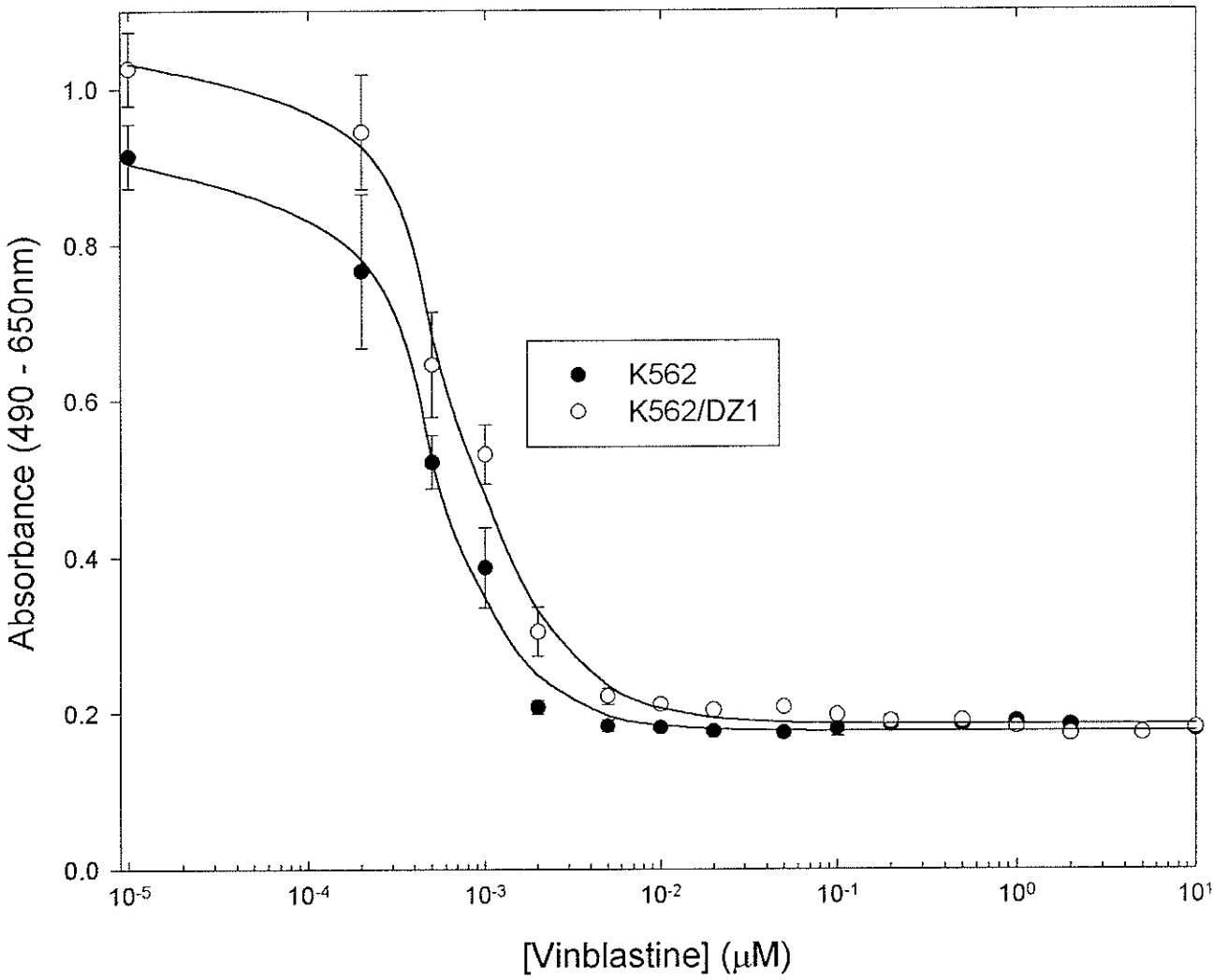

Figure 2.8 K562 and K562/DZ1 cell growth inhibition by vinblastine, as measured by MTS cytotoxicity assay. K562 and K562/DZ1 cells were seeded at a density of 1800 cells/well and 2300 cells/well, respectively, in 88.5 μl of DMEM. Vinblastine concentrations (0-10 μM) were delivered to the cells at 0.5 μl/well for 72 h at 37°C in an atmosphere of 5% (v/v) CO_2 in air. Absorbances at 490-650 nm were determined after the cells were incubated for 3 h with 10 μl of MTS reagent. The final volume of each well was 100 μl. Data were fit to a four-parameter logistic equation and the curves display the results of the non-linear least squares regression analysis. Six replicates were performed at each concentration and the error bars represent standard errors. The lowest concentration plotted (10^{-4} μM) is the zero value.

2.4.2 Combined growth inhibitory effects of dexrazoxane and etoposide on K562 and K562/DZ1 cells, as determined by MTS analysis

The cytotoxicity of 5 and 10 μM etoposide towards K562 cell growth in the presence of 9.0, 43, 86 and 430 μM dexrazoxane is illustrated in Figure 2.9. In the absence of dexrazoxane, etoposide displayed a dose-dependent inhibition of K562 cell growth. However, in the presence of dexrazoxane, etoposide cytotoxicity was antagonized. In Figure 2.10, the cytotoxicity of 5, 10, 20, 50 and 100 μM etoposide towards K562/DZ1 cell growth in the presence of 9.0 and 86 μM dexrazoxane is shown. Higher fixed concentrations of etoposide were used in the K562/DZ1 cytotoxicity experiment, as this cell line is moderately cross resistant to etoposide [16]. In contrast to the K562 cell line, dexrazoxane did not antagonize the growth inhibitory effects of etoposide in K562/DZ1 cells.

Table 2.1 Cytotoxicity of various topoisomerase II inhibitory agents and vinblastine towards K562 and K562/DZ1 cells as determined by MTS analysis

Drug	Cell line	IC_{50}[a] (μM)	S.E (μM)	Resistance factor[b]
Catalytic inhibitors of topoisomerase II				
Dexrazoxane (ICRF-187)	K562	17.0	1.0	-
	K562/DZ1	2288.0	142.9	134.6
Levrazoxane (ICRF-186)	K562	38.6	4.8	-
	K562/DZ1	3090.0	118.4	80.0
Merbarone	K562	18.4	1.5	-
	K562/DZ1	26.6	1.3	1.4
Non-topoisomerase II inhibitor (P-glycoprotein substrate)				
Vinblastine	K562	0.40	0.05	-
	K562/DZ1	0.55	0.07	1.37

[a] Cytotoxicity was measured by MTS analysis after 72 h exposure to the cytotoxic drug. The IC_{50} is the concentration of drug at which cell growth is 50% of the maximum observed inhibition. Median inhibitory concentrations ± standard errors for each drug were determined by fitting the absorbance-concentration data to a four-parameter logistic equation.

[b] The resistance factors were calculated by taking the ratio of the K562/DZ1 cell IC_{50} to the K562 cell IC_{50}.

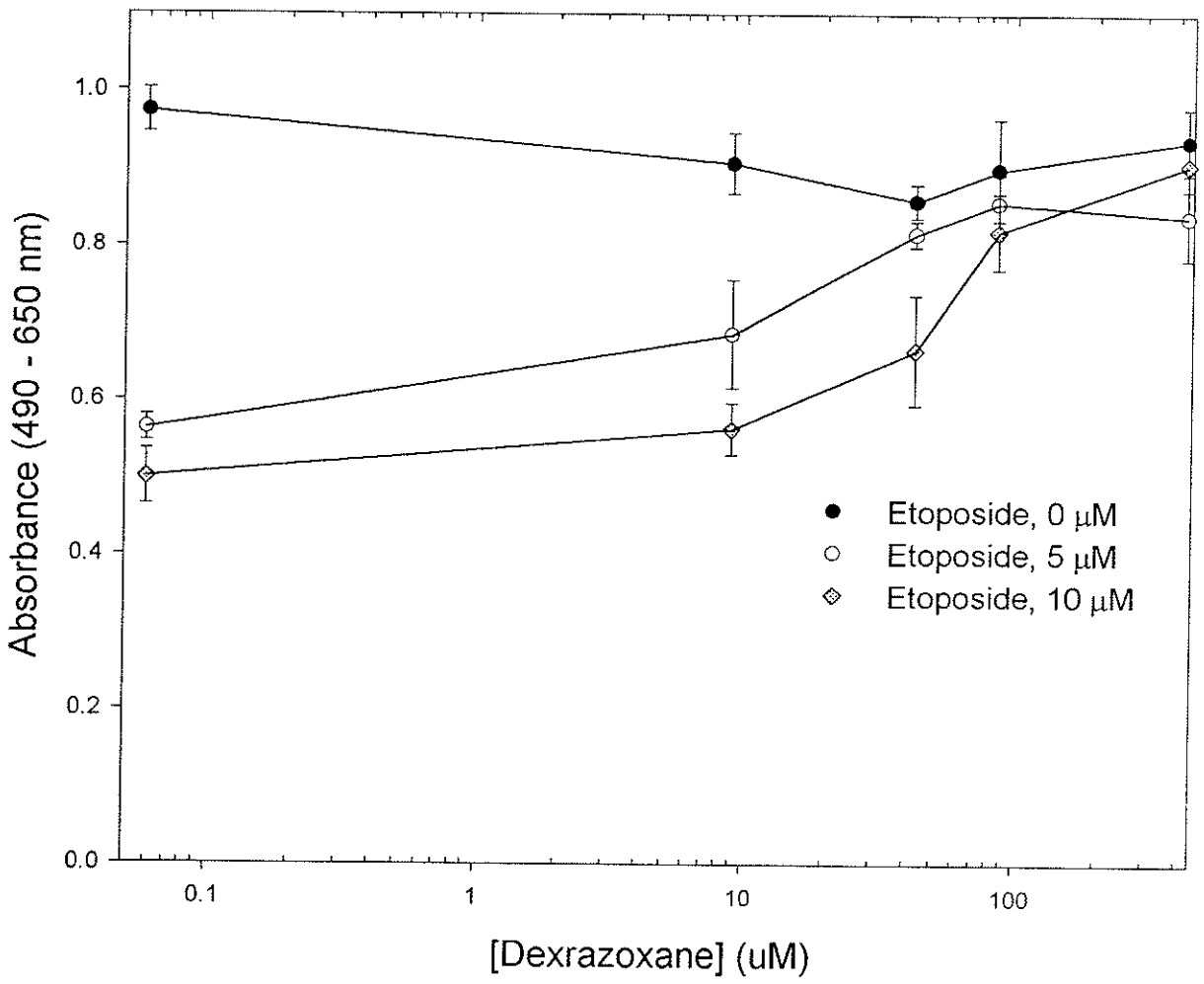

Figure 2.9 K562 cell growth inhibition by etoposide in the presence and absence of dexrazoxane, as measured by MTS cytotoxicity assay. K562 cells were seeded at a density of 100,000 cells/tube in 4.9 ml of DMEM. Cells were exposed to dexrazoxane concentrations (9.0, 43, 86 and 430 μM) at 99 μl/tube for 20 min at 37°C in an atmosphere of 5% (v/v) CO_2 in air. Following dexrazoxane treatment, cells were exposed to fixed concentrations of etoposide (5 and 10 μM) at 1 μl/tube for 1 h. After 1 h, the K562 cells were washed three times with DMEM, counted with the Coulter Counter and seeded onto sterile 96-well microtitre plates at a cell density of 1800 cells/well. K562 cells were incubated at 37°C and allowed to grow in an atmosphere of 5% (v/v) CO_2 for 72 h. Absorbances at 490-650 nm were determined after the cells were incubated with MTS for 3 h. Each data point is the average of six replicates with the errors displayed as standard errors. The lowest dexrazoxane concentrations plotted are the zero values.

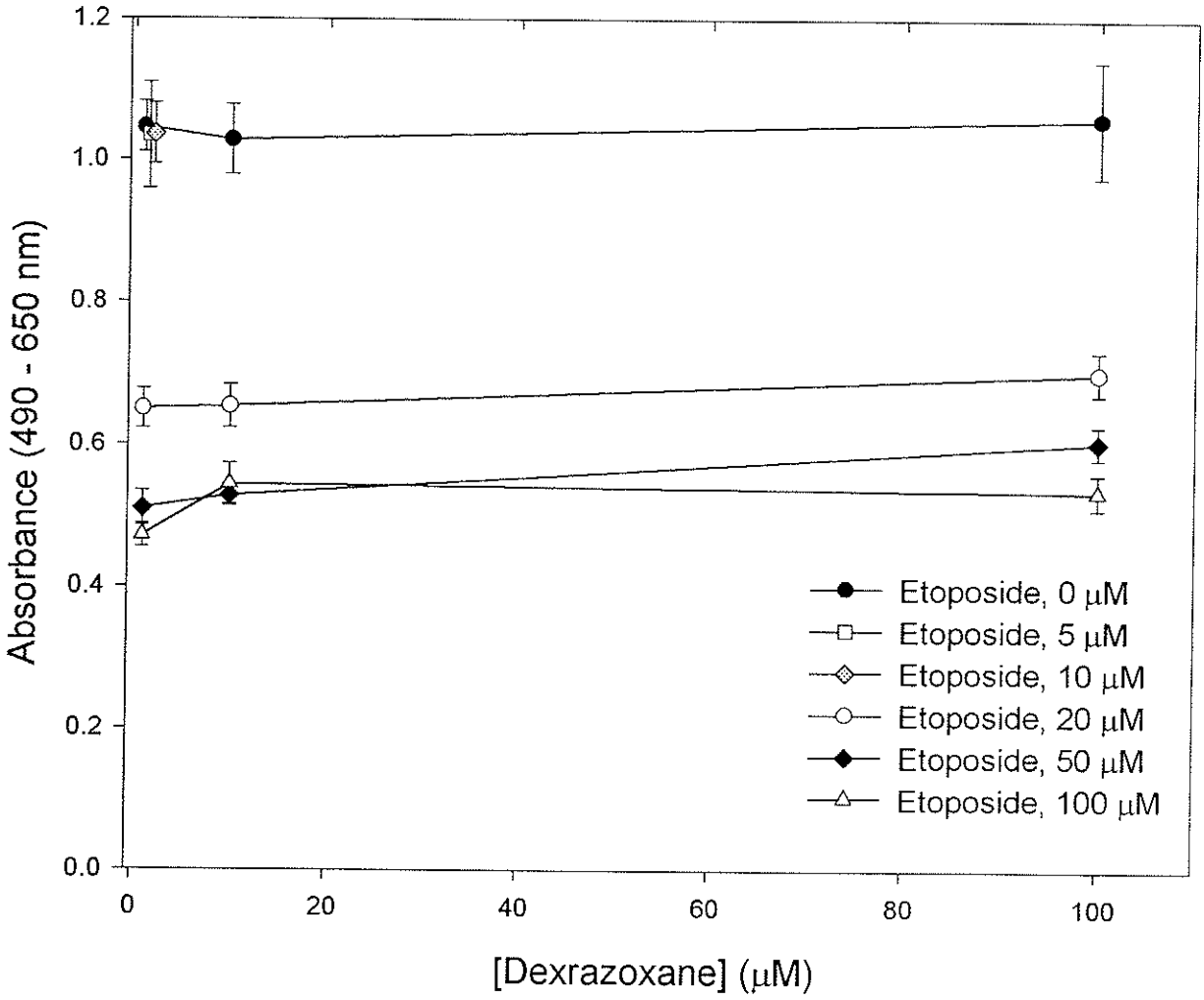

Figure 2.10 K562/DZ1 cell growth inhibition by etoposide in the presence and absence of dexrazoxane, as measured by MTS cytotoxicity assay. K562/DZ1 cells were seeded at a density of 100,000 cells/tube in 4.9 ml of DMEM. Cells were exposed to dexrazoxane concentrations (9.0 and 86 μM) at 99 μl/tube for 20 min at 37°C in an atmosphere of 5% (v/v) CO_2 in air. Following dexrazoxane treatment, cells were exposed to fixed concentrations of etoposide (5, 10, 20, 50 and 100 μM) at 1 μl/tube for 1 h. After 1 hr, the K562/DZ1 cells were washed three times with DMEM, counted with the Coulter Counter and seeded onto sterile 96-well microtitre plates at a cell density of 2300 cells/well. K562/DZ1 cells were incubated at 37°C and allowed to grow in an atmosphere of 5% (v/v) CO_2 for 72 h. Absorbances at 490-650 nm were determined after the cells were incubated with MTS for 3 h. Each data point is the average of six replicates with the errors displayed as standard errors. The zero values for experiments fixed with 5 and 10 μM etoposide are staggered to the right to make them visible.

2.5 Discussion

One way to attempt to understand the cytotoxic and resistance mechanisms of catalytic topoisomerase II inhibitors is to compare their cytotoxic profiles in a parental and resistant cell line. The dexrazoxane resistant K562/DZ1 cell line was selected by continually exposing K562 cells to 86 μM dexrazoxane [16]. K562 cells were exposed to 86 μM dexrazoxane for two weeks with daily media change, allowed to grow in the absence of dexrazoxane for one week and then secondarily treated with 86 μM dexrazoxane for four weeks with media change every other day [16]. In our study, we used the dexrazoxane-resistant human leukemia K562 cell line (K562/DZ1) to investigate the mechanisms of dexrazoxane resistance and differences in mechanisms of cytotoxicity among structurally similar catalytic topoisomerase II inhibitors. It has been demonstrated that the ability of the bisdioxopiperazines and merbarone to inhibit cell growth is correlated with their ability to inhibit the catalytic activity of topoisomerase II [10, 21]. This inhibition is presumed to be dependent upon the chemical structure and topoisomerase II inhibitory mechanism of the drug and has been shown to occur without promoting the formation or stabilization of the covalent topoisomerase II-DNA complex, unlike the topoisomerase II poisons such as etoposide and doxorubicin [9, 22, 23]. Using K562 and K562/DZ1 cells and a colorimetric MTS cytotoxicity assay, we examined the cytotoxicity profiles of the structurally similar catalytic topoisomerase II inhibitors, dexrazoxane, levrazoxane and merbarone.

The dexrazoxane and levrazoxane K562 cytotoxicity profiles generated by MTS analysis were biphasic and sigmoidal in nature (Figures 2.5 and 2.6). MTS cytotoxicity studies in CHO cells suggest that dexrazoxane induces cell cycle phase alterations and an

increase in cell size, which may influence mitochondrial number, function and consequently the level of MTS reduction to formazan [16]. Thus, the second phase of the MTS biphasic dose-response curve may be representative of a small cell population with high mitochondrial reductase activity. Such a population would be able to survive high dexrazoxane concentrations until divalent cations were chelated from the medium by dexrazoxane hydrolysis intermediates or ADR-925 [24, 25]. Dexrazoxane exhibited an IC_{50} value of 17.0 ± 1.0 μM in K562 cells and 2288 ± 143 μM in K562/DZ1 cells. Other dexrazoxane cytotoxicity studies in K562 and K562/DZ1 cells gave IC_{50} values of 20.3 ± 1.9 μM and 2568 ± 174 μM, which are comparable to the IC_{50} values that we attained [16]. Levrazoxane exhibited an IC_{50} value of 38.6 ± 4.8 μM in K562 cells and 3090 ± 118 μM in K562/DZ1 cells. It is not known precisely why levrazoxane was less cytotoxic or why the biphasic nature of the levrazoxane K562 dose-response curve was not as prominent as that of dexrazoxane (Figures 2.5 and 2.6, Table 2.1). However, it is known that levrazoxane is an enantiomer and the optical isomer of dexrazoxane and that it is hydrolyzed by dihydropyrimidine diamidohydrolase four times slower than dexrazoxane [26, 27], suggesting that there may be differences in their pharmacological action. Enantiomers, although structurally identical with many indistinguishable physical and chemical properties, show different behavior when they interact with other chiral substances [28]. By virtue of their inherent chirality, enzymes including topoisomerase II contain a number of asymmetric active sites that are highly specific both in binding chiral substrates and in catalyzing their reactions [29, 30]. Thus, the altered cytotoxicity profile of levrazoxane could be explained by its distinct interactions with chiral sites on topoisomerase II. Levrazoxane could have a different affinity from dexrazoxane for

binding sites on topoisomerase II or could alter the conformation of topoisomerase II in such a way that its catalytic activity is not as severely impaired as with dexrazoxane. The bisdioxopiperazines are believed to act by inhibiting the ATP hydrolysis step of the catalytic cycle of topoisomerase II and trapping the enzyme in its closed clamp form [1, 8, 10-12]. The K562/DZ1 cell line contains point mutations near the ATP binding site and dimer interface (Jack Yalowich, University of Pittsburgh, PA). Thus, levrazoxane may be orientated such that it has a weaker interaction with or restricted access to the topoisomerase II ATP binding site or dimer interface.

In contrast to the K562 growth inhibition curves, the K562/DZ1 growth inhibition curves for dexrazoxane and levrazoxane were monophasic and sigmoidal in nature (Figures 2.5 and 2.6). When compared to the K562 parental cell line, the K562/DZ1 cells were 135-fold resistant to dexrazoxane and 80-fold resistant to levrazoxane (Table 2.1). Previous dexrazoxane cross resistance studies with K562/DZ1 cells showed that the cell line was 126-fold resistant to dexrazoxane [16], which is comparable to the relative resistance value of 135-fold that we attained (Table 2.1). As previously discussed, point mutations near the ATP binding site and dimer interface of K562/DZ1 topoisomerase II have recently been identified in Jack Yalowich's lab (University of Pittsburgh, PA). Point mutations in enzymes can lead to conformational changes that alter their substrate specificity [29]. Moreover, cell lines resistant to topoisomerase II poisons or catalytic inhibitors have been shown to have altered topoisomerase II levels and/or decreased enzyme activity [7, 10, 14]. Therefore, bisdioxopiperazine resistance could be attributed to conformational changes in topoisomerase II that ultimately affect topoisomerase II levels, decrease topoisomerase II activity or reduce topoisomerase II affinity for

dexrazoxane and levrazoxane. Dexrazoxane and levrazoxane cross resistance could be a result of structurally altered K562/DZ1 topoisomerase II that limits or restricts their access to ATP binding or dimer interface sites on topoisomerase II. Although the topoisomerase II inhibitory effects would be attenuated or absent in such a situation, the cytotoxic effect of the bisdioxopiperazine metal-chelating hydrolysis intermediates and ADR-925 would still be present. Thus, the shift from the biphasic to the monophasic dose response curve could be indicative of a loss in topoisomerase II inhibitory action with sustained ADR-925 cytotoxic effects. It is interesting to note that the K562 and K562/DZ1 cytotoxicity profiles for ADR-925 closely resemble the K562/DZ1 cytotoxicity profiles for dexrazoxane and levrazoxane (Figure 2.5 and 2.6) [9, 16]. ADR-925 has been reported to have an IC_{50} value of 1229 ± 202 μM and 638 ± 52 μM in K562 and K562/DZ1 cells, respectively [16]. ADR-925 dose-response curves for K562 and K562/DZ1 cells have been shown to be monophasic and ADR-925 has been reported to be more cytotoxic towards K562/DZ1 cells than dexrazoxane or levrazoxane (Table 2.1) [16]. Such an observation would be expected since ADR-925 is not a topoisomerase II inhibitor and dexrazoxane and levrazoxane are hydrolyzed to other metabolites besides ADR-925 that chelate metals less efficiently [24, 26, 27, 31]. Moreover, the difference in cytotoxicity between dexrazoxane and levrazoxane could be due to differences in enzymatic hydrolysis rates and the relative amounts of hydrolysis products generated [27, 32].

Although merbarone cytotoxicity toward the K562 cell line was comparable to the bisdioxopiperazines (Table 2.1), the dose-response curve was monophasic and sigmoidal in nature (Figure 2.7). Merbarone is structurally similar to the bisdioxopiperazines but

has been shown in several studies to interfere with the catalytic cycle of topoisomerase II in a different manner than the bisdioxopiperazines [8, 10, 22]. Merbarone has been shown to induce apoptosis [8] and specifically block topoisomerase-II mediated DNA cleavage [10, 22]. In contrast to the bisdioxopiperazines, merbarone may be inhibiting cell growth of K562 cells exclusively through a topoisomerase II inhibitory mechanism. When compared to the K562 parental line, the K562/DZ1 cells did not exhibit cross resistance to merbarone (Table 2.1). Because the point mutations in the K562/DZ1 cell line are near the ATP binding site and dimer interface, the results of this study suggest that merbarone does not inhibit the catalytic activity of topoisomerase II through interaction with these sites but rather through a different mechanism. A merbarone study with human topoisomerase IIα has demonstrated that merbarone has no effect on enzyme-DNA binding or ATP hydrolysis but that it specifically blocks topoisomerase II-mediated cleavage of its DNA substrate [10]. Other studies in merbarone-resistant cell lines suggest that cross resistance to merbarone may be due to decreased levels of topoisomerase IIα, the more sensitive isoform to anticancer drugs [22]. In view of these considerations, the results of this study suggest that the cytotoxic and resistance mechanisms of bisdioxopiperazines and merbarone may differ based on their specific interactions with the catalytic cycle of topoisomerase II.

Previous cross resistance studies with the K562/DZ1 cell line in our lab suggest that the topoisomerase II poisons etoposide and doxorubicin are moderately cross resistant [16]. Acquired cross resistance to topoisomerase II poisons has been correlated with a decrease in topoisomerase II-DNA complexes related to a reduction in enzyme levels, a decrease in drug accumulation and/or a change in topoisomerase II function [2,

7, 18, 19, 33]. To distinguish between topoisomerase II-dependent and independent resistance mechanisms, we decided to perform a cross resistance study with vinblastine in our K562 and K562/DZ1 cell lines. Vinblastine is an anticancer drug that does not interfere with topoisomerase II [7, 17, 19]. However, like etoposide and doxorubicin, it confers varying degrees of cross resistance to multiple chemotherapy agents through a well-characterized multi-drug resistance mechanism, whereby a transmembrane pump extrudes the drug from cells, decreasing drug accumulation [7, 17, 19]. The transmembrane protein is called P-glycoprotein and it serves as a receptor for Vinca alkaloids with drug resistance being proportional to the amount of P-glycoprotein present in the cell membrane [7, 18, 19]. When compared to the parental K562 cell line, the K562/DZ1 cells were not cross resistant to vinblastine (Figure 2.8, Table 2.1). Thus, our K562/DZ1 cell line contains little if any P-glycoprotein and cross resistance to this cell line is most likely through a different mechanism.

To further elucidate the mechanism of dexrazoxane resistance exhibited by the K562/DZ1 cell line, we also studied the combined effect of dexrazoxane and etoposide in the parental and mutant K562 cell lines. In the absence of dexrazoxane, etoposide showed a dose-dependent growth inhibitory effect on K562 and K562/DZ1 cells, as measured by MTS analysis (Figures 2.9 and 2.10). As increasing concentrations of dexrazoxane were administered, the growth inhibitory effect of 5 and 10 μM etoposide in K562 cells was prevented (Figure 2.9). Etoposide is a topoisomerase II poison that kills cells by stabilizing cleavable-complexes [5, 17]. Several studies indicate that dexrazoxane can antagonize etoposide cytotoxicity by preventing the formation of DNA breaks induced by the cleavable-complex stabilizing drug [1, 15]. Dexrazoxane may prevent cleavable-

complex formation by interfering with ATP hydrolysis and trapping topoisomerase II on DNA in its closed clamp form [1, 13]. In the K562/DZ1 cell line, dexrazoxane could not antagonize the growth inhibitory effect of a wide range of etoposide concentrations (Figure 2.10). Because the K562/DZ1 cell line topoisomerase II contains point mutations near the ATP binding site and dimer interface, it is possible that dexrazoxane binding was limited or restricted at these sites. Consequently, ATP hydrolysis could take place and topoisomerase II-DNA complexes would be made available to etoposide for cleavable-complex formation and induction of DNA strand breaks. Thus, dexrazoxane cross resistance in the K562/DZ1 cell line may be attributed to a change in topoisomerase II function.

2.6 Conclusion

The present study contributes to the understanding of the cytotoxic and resistance mechanisms of several catalytic inhibitors of topoisomerase II. The cross resistance studies with dexrazoxane, levrazoxane and merbarone suggest that the orientation and structure of topoisomerase II inhibitors affect their cytotoxicity and mechanism for interfering with the catalytic cycle of topoisomerase II. Specifically, the bisdioxopiperazines (dexrazoxane and levrazoxane) and merbarone were revealed to interfere with topoisomerase II catalytic activity by different mechanisms. The ATP binding site and dimer interface of topoisomerase II were also identified to play a possible role in the cytotoxicity of the bisdioxopiperazines and their antagonism of etoposide cleavable-complex formation. Our cross resistance studies in the K562 and K562/DZ1 cell lines also suggest that dexrazoxane and levrazoxane may have a different resistance mechanism than merbarone. While merbarone has been proposed to decrease

topoisomerase IIα levels [10], we hypothesize that dexrazoxane and the other bisdioxopiperazines may change topoisomerase II function. Our K562/DZ1 cell line was a valuable tool for investigating topoisomerase II cytotoxic and resistance mechanisms. Future studies should attempt to further characterize this cell line with other catalytic topoisomerase II inhibitors.

2.7 References

1. Andoh, T., Ishida, R. 1998. Catalytic inhibitors of DNA topoisomerase II. *Biochim Biophys Acta* 1400:155-71.

2. Beck, W. T., Kim, R., Chen, M. 1994. Novel actions of inhibitors of DNA topoisomerase II in drug-resistant tumor cells. *Cancer Chemother Pharmacol* 34:S14-8.

3. Li, T. K., Liu, L. F. 2001. Tumor cell death induced by topoisomerase-targeting drugs. *Annu Rev Pharmacol Toxicol* 41:53-77

4. Withoff, S., De Jong, S., De Vries, E. G., Mulder, N. H. 1996. Human DNA topoisomerase II: biochemistry and role in chemotherapy resistance. *Anticancer Res* 16:1867-80.

5. Burden, D. A., Osheroff, N. 1998. Mechanism of action of eukaryotic topoisomerase II and drugs targeted to the enzyme. *Biochim Biophys Acta* 1400:139-54.

6. Fattman, C. L., Allan, W. P., Hasinoff, B. B., Yalowich, J. C. 1996. Collateral sensitivity to the bisdioxopiperazine dexrazoxane (ICRF-187) in etoposide (VP-16)-resistant human leukemia K562 cells. *Biochem Pharmacol* 52:635-42.

7. Pommier, Y., Leteurtre, F., Fesen, M. R., Fujimori, A., Bertrand, R., et al. 1994. Cellular determinants of sensitivity and resistance to DNA topoisomerase inhibitors. *Cancer Invest* 12:530-42

8. Khelifa, T., Beck, W. T. 1999. Merbarone, a catalytic inhibitor of DNA topoisomerase II, induces apoptosis in CEM cells through activation of ICE/CED-3-like protease. *Mol Pharmacol* 55:548-56.

9. Hasinoff, B. B., Kuschak, T. I., Creighton, A. M., Fattman, C. L., Allan, W. P., et al. 1997. Characterization of a Chinese hamster ovary cell line with acquired resistance to the bisdioxopiperazine dexrazoxane (ICRF-187) catalytic inhibitor of topoisomerase II. *Biochem Pharmacol* 53:1843-53.

10. Fortune, J. M., Osheroff, N. 1998. Merbarone inhibits the catalytic activity of human topoisomerase IIalpha by blocking DNA cleavage. *J Biol Chem* 273:17643-50.

11. Hasinoff, B. B., Abram, M. E., Chee, G. L., Huebner, E., Byard, E. H., et al. 2000. The catalytic DNA topoisomerase II inhibitor dexrazoxane (ICRF-187) induces endopolyploidy in Chinese hamster ovary cells. *J Pharmacol Exp Ther* 295:474-83.

12. Hasinoff, B. B., Abram, M. E., Barnabe, N., Khelifa, T., Allan, W. P., et al. 2001. The catalytic DNA topoisomerase II inhibitor dexrazoxane (ICRF-187) induces differentiation and apoptosis in human leukemia K562 cells. *Mol Pharmacol* 59:453-61.

13. Wessel, I., Jensen LH, Falk, J., Rose, A., Roerth, M., et al. 1999. Human small cell lung cancer NYH cells selected for resistance to the bisdioxopiperazine topoisomerase II inhibitor ICRF-187 demonstrate a functional R162Q mutation in the Walker A consensus ATP binding domain of the alpha isoform. *Cancer Res* 59:3442-3450

14. Yalowich, J., Thampatty, P., Allan, W., Chee, G., Hasinoff, B. 1998. Acquired resistance to ICRF-187 (dexrazoxane) in a CHO cell line is associated with a point mutation in DNA topoisomerase II alpha (topo II) and decreased drug-induced DNA-enzyme complexes. *Proc Am Assoc Cancer Res* 39:375

15. Sehested, M., Jensen, P. B., Sorensen, B. S., Holm, B., Friche, E., et al. 1993. Antagonistic effect of the cardioprotector (+)-1,2-bis(3,5- dioxopiperazinyl-1-yl)propane (ICRF-187) on DNA breaks and cytotoxicity induced by the topoisomerase II directed drugs daunorubicin and etoposide (VP-16). *Biochem Pharmacol* 46:389-93.

16. Abram, Michael. E. 2000. Characterization of growth, apoptosis, and differentiation of CHO and human erythroleukemic K562 cells exposed to dexrazoxane, and the selection of a dexrazoxane-resistant K562 cell line. M.Sc. Thesis by Michael Abram, pp. 332-333. Winnipeg: University of Manitoba

17. Dutcher, J., Novik, Y., O'Boyle, K., Marcoullis, G., Secco, C., et al. 2000. 20th-century advances in drug therapy in oncology--Part. II. *J Clin Pharmacol* 40:1079-92.

18. Loe, D. W., Deeley, R. G., Cole, S. P. 1996. Biology of the multidrug resistance-associated protein, MRP. *Eur J Cancer* 32A:945-57.

19. Lautier, D., Canitrot, Y., Deeley, R. G., Cole, S. P. 1996. Multidrug resistance mediated by the multidrug resistance protein (MRP) gene. *Biochem Pharmacol* 52:967-77.

20. Barltrop, J. 1991. 5-(3-carboxymethoxyphenyl)-2-(4,5-dimethylthiazolyl)-3-(4-sulfophenyl) tetrazolium, inner salt (MTS) and related analogs of 3-(4,5-dimethylthiazolyl)-2,5-diphenyltetrazolium bromide (MTT) reducing purple water-soluble formazans as cell viability indicators. *Bioorg. & Med. Chem. Lett.* 1:1573-1577

21. Hasinoff, B. B., Kuschak, T. I., Yalowich, J. C., Creighton, A. M. 1995. A QSAR study comparing the cytotoxicity and DNA topoisomerase II inhibitory effects of bisdioxopiperazine analogs of ICRF-187 (dexrazoxane). *Biochem Pharmacol* 50:953-8.

22. Kusumoto, H., Rodgers, Q. E., Boege, F., Raimondi, S. C., Beck, W. T. 1996. Characterization of novel human leukemic cell lines selected for resistance to merbarone, a catalytic inhibitor of DNA topoisomerase II. *Cancer Res* 56:2573-83.

23. Hasinoff, B. B., Kuschak, T. I., Fattman, C. L., Yalowich, J. C. 1998. The one-ring open hydrolysis intermediates of the cardioprotective agent dexrazoxane (ICRF-187) do not inhibit the growth of Chinese hamster ovary cells or the catalytic activity of DNA topoisomerase II. *Anticancer Drugs* 9:465-71.

24. Buss, J. L., Hasinoff, B. B. 1993. The one-ring open hydrolysis product intermediates of the cardioprotective agent ICRF-187 (dexrazoxane) displace iron from iron-anthracycline complexes. *Agents Actions* 40:86-95.

25. Hasinoff, B. B. 1998. Chemistry of dexrazoxane and analogues. *Semin Oncol* 25:3-9.

26. Hasinoff, B. B. 1993. Enzymatic ring-opening reactions of the chiral cardioprotective agent (+) (S)-ICRF-187 and its (-) (R)-enantiomer ICRF-186 by dihydropyrimidine amidohydrolase. *Drug Metab Dispos* 21:883-8.

27. Hasinoff, B. B., Venkataram, S., Singh, M., Kuschak, T. I. 1994. Metabolism of the cardioprotective agents dexrazoxane (ICRF-187) and levrazoxane (ICRF-186) by the isolated hepatocyte. *Xenobiotica* 24:977-87.

28. Solomons, T. W. G. 1992. *Organic Chemistry*. Toronto: John Wiley & Sons Inc.

29. Voet, D., Voet, J. 1995. *Biochemistry*. Toronto: John Wiley & Sons Inc.

30. Berger, J. M. 1998. Structure of DNA topoisomerases. *Biochim Biophys Acta* 1400:3-18.

31. Hasinoff, B. B. 1994. Stereoselective hydrolysis of ICRF-187 (dexrazoxane) and ICRF-186 by dihydropyrimidine amidohydrolase. *Chirality* 6:213-5

32. Hasinoff, B. B., Aoyama, R. G. 1999. Stereoselective metabolism of dexrazoxane (ICRF-187) and levrazoxane (ICRF-186). *Chirality* 11:286-90

33. Beck, W. T., Morgan, S. E., Mo, Y. Y., Bhat, U. G. 1999. Tumor cell resistance to DNA topoisomerase II inhibitors: new developments. *Drug Resist Updat* 2:382-389.

Chapter 3 Quantitative methods with JC-1 for measuring mitochondrial membrane potential in cardiac myocytes and dexrazoxane cardioprotection against doxorubicin-induced mitochondrial damage

3.1 Introduction

Doxorubicin is an anthracycline anticancer drug used in the treatment of a variety of leukemias and solid tumors [1]. However, its clinical use continues to be limited by a potentially fatal, cumulative and dose-dependent cardiotoxicity [2]. A considerable body of evidence suggests that this cardiotoxicity is mainly attributed to an iron-dependent, oxygen free radical-derived oxidative stress on the relatively unprotected cardiac muscle [3]. Dexrazoxane is clinically used for the prevention of doxorubicin-induced cardiomyopathy and is presumed to act by diffusing into the cell and hydrolyzing into its strong metal ion binding form, ADR-925 (Figure 3.1) [4]. ADR-925 is an analog of EDTA, which has been demonstrated to chelate free iron and displace Fe^{3+} from its complexes with doxorubicin, protecting cellular components from iron-based oxygen free radical damage [3, 5]. It is thought that iron bound to ADR-925 is less efficient at producing site-specific hydroxyl radical damage than iron bound to doxorubicin [6-8].

Of the cellular organelles proposed as possible primary sites of anthracycline toxicity, the mitochondrial membrane appears to be the most likely target (Figure 3.2) [2, 9]. The cationic and somewhat lipophilic nature of doxorubicin at physiological pH permits the drug to readily diffuse across cell membranes and accumulate in the more electronegative mitochondrial matrix (Figure 3.3) [10]. Doxorubicin also has a particularly high affinity for the negatively charged glycerophospholipid, cardiolipin, which is the major phospholipid component of the inner mitochondrial membrane (Figure 3.4) [1, 2].

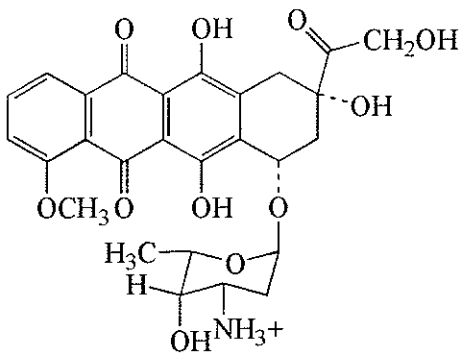

Doxorubicin

Figure 3.1 Chemical structure of doxorubicin at physiological pH (7.4).

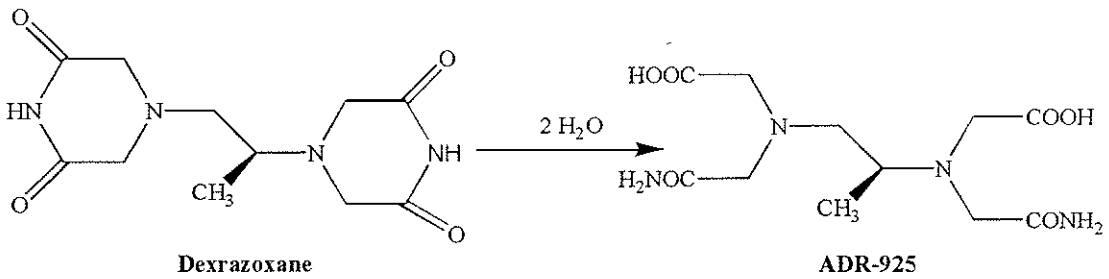

Dexrazoxane **ADR-925**

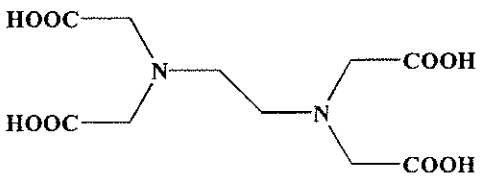

EDTA

Figure 3.2 Hydrolysis of dexrazoxane to ADR-925.

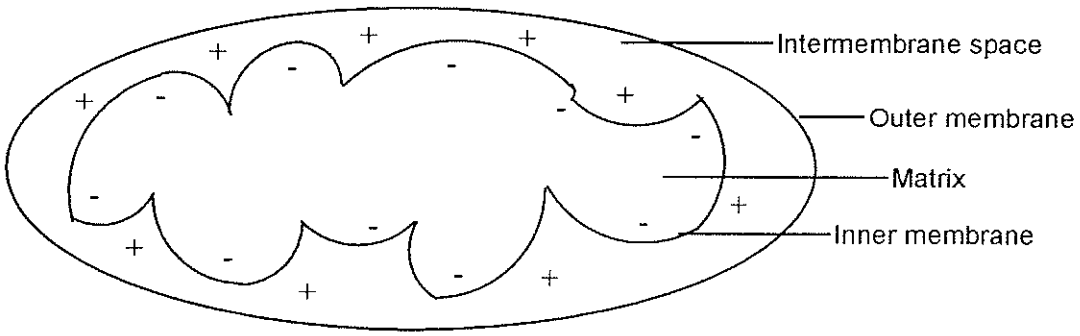

Figure 3.3 Diagram of a mitochondrion.

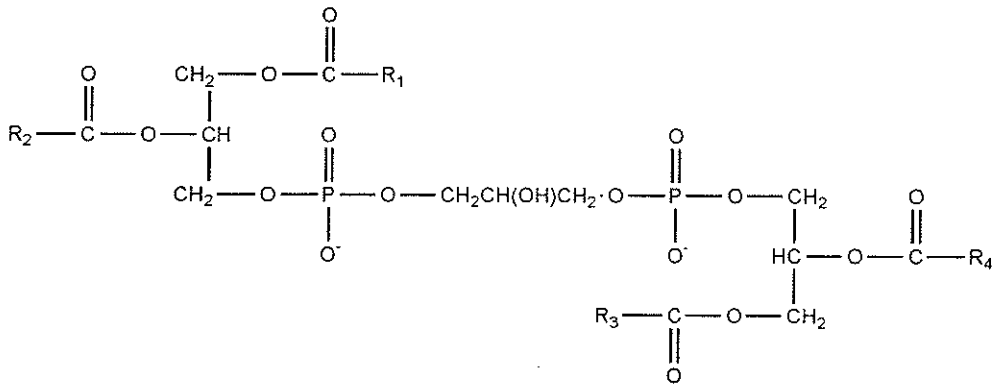

Figure 3.4 Chemical structure of the glycerophospholipid cardiolipin. The R groups are long-chain hydrocarbon tails of fatty acids.

Cardiolipin is rich in polyunsaturated fatty acids and is particularly susceptible to peroxidative injury by harmful radicals produced by redox cycling of anthracyclines and their complexes with iron [1]. These reactive oxygen species are believed to cause nuclear and mitochondrial DNA damage [9, 11], protein cross-linking [9, 12], lipid peroxidation [9, 12], inactivation of key enzymes in the mitochondrial respiratory chain [2, 9] and destruction of the mitochondrial membrane [2]. Lipid peroxidation is initiated by removal of an allylic hydrogen from an unsaturated fatty acid (LH) (Equation 1) [12], and propagates as follows:

$$LH + OH^{\bullet} \rightarrow L^{\bullet} + H_2O \quad (1)$$

$$L^{\bullet} + O_2 \rightarrow LOO^{\bullet} \quad (2)$$

$$LOO^{\bullet} + LH \rightarrow LOOH + L^{\bullet} \quad (3)$$

Morphologically, mitochondrial damage manifests as mitochondrial swelling and lysis, disruption of cristae and accumulation of dense calcium-containing intramitochondrial bodies [2]. Ultimately, the contraction of cultured myocytes is impaired by anthracycline treatment and is accompanied by a decrease in ATP synthesis [2]. Mitochondrial damage and ATP depletion are particularly detrimental to the heart since it is 50% mitochondria by weight and relies heavily on ATP for normal performance and survival [13].

Supply of cellular energy (ATP) by mitochondria depends on the maintenance of the chemiosmotic gradient across the inner mitochondrial membrane (Figure 3.5) [14]. This gradient, also known as the proton motive force (PMF), is generated by three respiratory enzyme complexes which use the free energy released during electron transport to translocate protons from the mitochondrial matrix into the intermembrane space [10]. The energy stored in PMF drives the phosphorylation of ADP by ATP

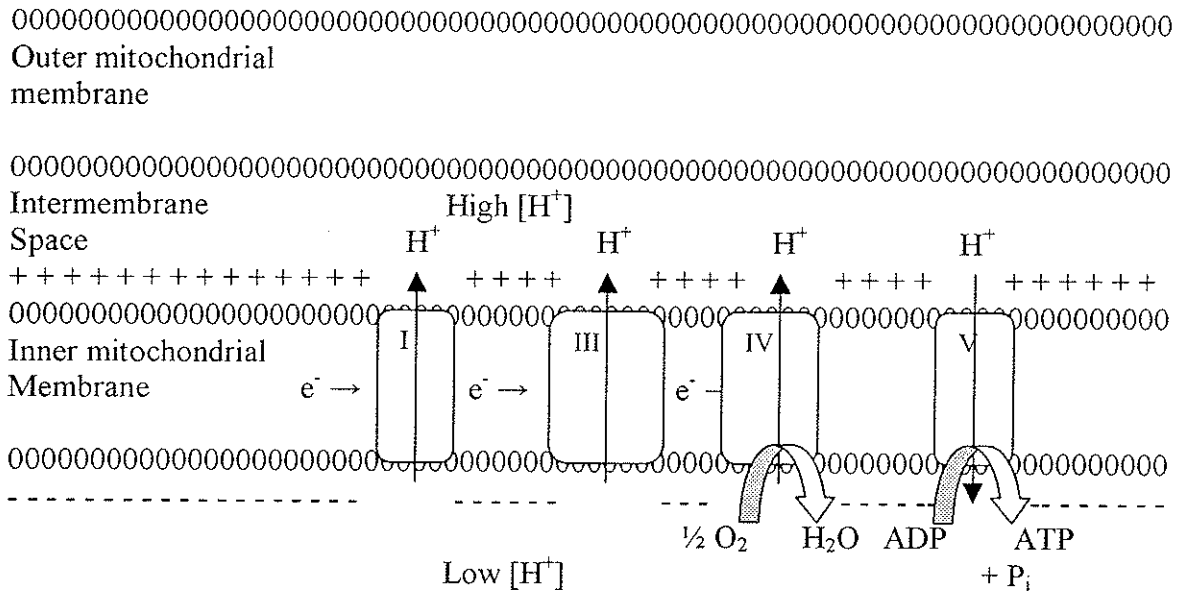

Figure 3.5 Coupling of electron transport and ATP synthesis by the generation of a proton electrochemical gradient across the inner mitochondrial membrane. H^+ are pumped out of the mitochondrion during electron transport and its exergonic return powers the synthesis of ATP [1], pg 583.

synthase and supports other mitochondrial activities such as calcium uptake, mitochondrial protein import and transport of metabolites [14]. The PMF has two components: the membrane potential, which arises from the net movement of positive charge across the inner membrane and the pH gradient [15]. Of these two components, the membrane potential contributes most of the energy stored in this gradient (-150 mV) [14]. Thus, maintenance of the mitochondrial membrane potential is essential for the normal performance and survival of high-energy demanding cells, such as the beating cardiomyocyte.

Cardiomyopathies are one of the prominent clinical manifestations of mitochondrial diseases and are associated with a compromised mitochondrial membrane potential [14, 16]. Moreover, the collapse of the mitochondrial membrane potential has been implicated in the molecular mechanism associated with reperfusion injury to the

heart, various drug toxicities and cardiomyocyte apoptosis [17-19]. Therefore, the development of reliable methods for evaluating the mitochondrial membrane potential in cardiomyocytes is of considerable importance to biomedical research.

In the past few years, many indicators for monitoring the mitochondrial membrane potential have been characterized with increasing emphasis towards fluorescent probes. Potentiometric optical probes enable researchers to perform membrane potential measurements in organelles and in cells that are too small to allow the use of microelectrodes [20]. Moreover, in conjunction with imaging techniques, these probes can be employed to map variations in membrane potential among cell populations [20]. Mitochondrion-selective agents can be used to probe mitochondrial activity, localization and abundance, as well as to monitor the effects of some pharmacological agents that alter mitochondrial function [20]. Recently, a number of fluorescent probes have been described to insert preferentially into actively respiring (hyperpolarized) mitochondria [16, 20-23]. According to the Nernst equation, (Equation 4) cationic, lipophilic compounds should become more concentrated in the more electronegative mitochondria than in the cytoplasm [14, 15, 24].

Electrical potential difference = Concentration difference
across the membrane across the membrane

$$E_A - E_B = \frac{RT}{zF} \ln \frac{[X]_B}{[X]_A} \qquad (4)$$

where R is the ideal gas constant, T is the absolute temperature, z is the charge number of the ion, F is the Faraday number and [X] is the concentration of the cationic compound in B, the mitochondrial matrix and A, the intermembrane space.

Based on this principal, lipophilic fluorescent cations, including rhodamines, rosamines and carbocyanine derivatives have been widely used in combination with fluorimetric,

microscopic or flow cytometric methods [14]. Although probes such as rhodamine-123 (Rh123) and chloro-methyl-X-rosamine are excellent for the study of transient and short-term phenomena, they suffer from a number of drawbacks [16]. For instance, uniform and identical loading of the probe is not guaranteed, Rh123 displays a lower sensitivity and 3,3'-dihexyloxocarbocyanine iodide ($DiOC_6$) responds to changes in plasma membrane potential [16].

JC-1 is a new cationic ratiometric dye, which displays potential-dependent accumulation in the mitochondrial membrane (Figure 3.6) [15, 25]. The monomeric form

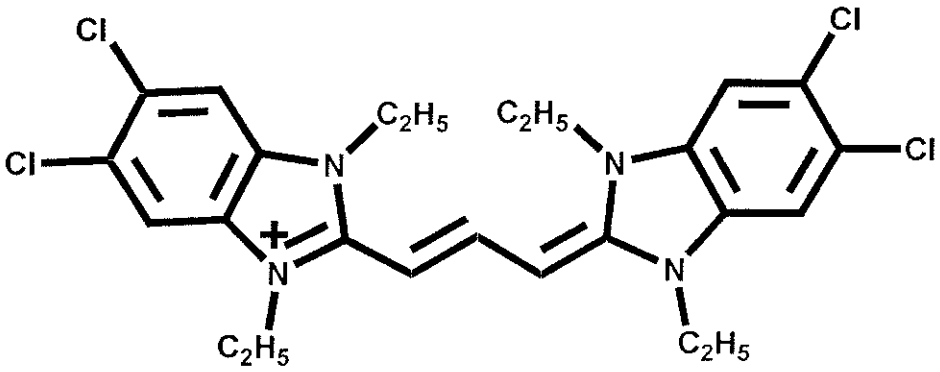

Figure 3.6 Chemical structure of the cationic, mitochondrial membrane potential sensor, JC-1.

of the dye fluoresces green (~ 525 nm) and forms concentration-dependent red fluorescing "J-aggregates" (~ 590 nm) as it accumulates in actively respiring (hyperpolarized) mitochondria [20, 25]. Thus, mitochondrial depolarization can be measured as a decrease in the red/green fluorescence intensity ratio [20]. The ratio of red to green is dependent only on the membrane potential and not on other factors such as mitochondrial size, shape and density that may influence single-component fluorescence

signals [20]. JC-1 is also more specific for the mitochondrial membrane potential and more consistent in its response to depolarization than the previous cationic dyes mentioned [20].

In this study, the dual emission properties of JC-1 were used to develop two quantitative methods for measuring mitochondrial membrane potential in neonatal rat cardiac myocytes. Using epifluorescence microscopy and the fluorescence plate reader, the experimental procedures for probe loading, cell density and quantitation of fluorescence signals were optimized. Finally, these methods were employed to examine the cardioprotective effect of dexrazoxane on doxorubicin-induced depolarization of and damage to the mitochondrial membrane.

3.2 Materials and Methods

3.2.1 Materials

Dexrazoxane hydrochloride (Zinecard®, ICRF-187) was a gift from Pharmacia & Upjohn (Columbus, OH). Doxorubicin hydrochloride was a gift from Adria-SP Inc. (Adriamycin, Columbus, OH). JC-1 was purchased from Molecular Probes (cat No.T-3168, Eugene, Oregon). Valinomycin (cat No.V-0627), nigericin (cat No. N-7143), trypan blue dye (cat. No. T-6146) and HEPES (cell culture grade, cat. No. H-9136) were obtained from Sigma Chemical Co. (St. Louis, MO). Sodium bicarbonate ($NaHCO_3$, cat. No. BP328-079), pre-cleaned microscope slides (cat No. 12-550A), preferred glass cover slips (cat. No. 12-545-85) and magnesium sulfate ($MgSO_4$) were obtained from Fisher Scientific (Fairlawn, NJ). Dulbecco's phosphate buffered saline (PBS, cat No. D-5652), Dulbecco's modified Eagle medium/F12 (DMEM/F-12, cat No. 12500-062), penicillin-streptomycin (cat No. 25200-072), fetal calf serum (FCS, cat No. 26140-079), horse

serum (cat No. 16050-122) and Hank's buffered salt solution (HBSS, without Ca^{2+} or Mg^{2+}, cat No. H-4891) were ordered from Gibco-BRL Life Technologies Inc. (Burlington, ON). Plating medium (7.5% (v/v) horse serum, 7.5% (v/v) FCS) and cell culturing medium (DF-10, 10% (v/v) FCS) were prepared in DMEM-F12. Na_2EDTA was obtained from BDH Chemicals Ltd. (Toronto, ON). D-glucose was supplied by Anala R (Toronto, ON) while calcium chloride ($CaCl_2$) was obtained from Anachemia (Montreal, QB). Black, microtitre assay plates (96-well, sterile, cat No. 3603) were supplied by Corning Incorporated (Corning, NY) while 6-well tissue culture plates (cat No. 83.1839) and 0.2 μm acetate syringe filters (cat No. 83.1826.001) were ordered from Sarstedt Inc. (St. Leonard, PQ). Falcon 3025 tissue culture plates and 0.4 μm cell strainers were obtained from Becton Dickensson (Lincoln Park, NJ). Deoxyribonuclease I (DNAse, cat No. 2139), trypsin (cat No. 3703) and collagenase (cat No. 4176) were obtained from Worthington Biochemical Corporation (Lakewood, NJ). Cell culture media and buffers were prepared in reverse osmosis distilled water and cardiomyocyte cultures were grown in a 37°C incubator in an atmosphere of 5% (v/v) CO_2 in air. Microscopy studies were carried out with a Zeiss epifluorescence microscope (Roper Scientific, Trenton, NJ) equipped with a high resolution, cooled color digital (CCD) camera, a camera coupler (Diagnostic Instruments Inc., Sterling Hts., MI) and a JC-1 XF2010 dichroic filter (Omega Optical, Brattleboro, Vermount). Images were acquired with Photometrics Cool Snap acquisition software (Version 1.2, Roper Scientific, Trenton, NJ) and were analyzed with Paintshop Pro imaging software (Version 6.00, Jasc Software Inc., Eden Prairies, MN).

3.2.2 Cell Culture

3.2.2.1 Preparation of media, buffers and enzyme solutions

Cell culture medium was prepared by dissolving one pack (10 g) of DMEM/F12, 11.915 g of HEPES and 2.438 g of $NaHCO_3$ in 990 ml of H_2O. The pH of the solution was adjusted to 7.4 ± .05 at room temperature with 1 M NaOH with a calibrated PHB-45 microprocessor pH meter. Penicillin-streptomycin (10 ml) was added and the medium was filter sterilized through a 0.2 μm bottle top filter (Nalgene Company, Rochester, New York) before storage at 4°C. The plating medium (7.5% (v/v) FCS/7.5% (v/v) horse serum in DMEM-F12) and culture medium (DF-10, 10% (v/v) FCS in DMEM-F12) were prepared on the day of isolation under sterile conditions in the laminar flow hood (Enviro Safety Cabinet, Model ESC, Albuquerque, New Mexico). Upon addition of serum, the media were stored for up to two weeks in the refrigerator.

Dulbecco's phosphate buffered saline containing glucose (PBS/glucose) was prepared by dissolving one pack (12 g) of PBS and 10 g of D-glucose in 1000 ml of H_2O. Hank's buffered salt solution (HBSS) supplemented with 1.3 mM Ca^{2+} and 0.8 mM Mg^{2+} was prepared by dissolving one bottle (9.5 g) of HBSS, 0.14 g of anhydrous $CaCl_2$ and 0.098 g of anhydrous $MgSO_4$ in 1000 ml of H_2O. The pH of both buffers was adjusted to 7.4 at room temperature with 1 M NaOH with a calibrated pH meter. Finally, the solutions were filter sterilized through a 0.2 μm bottle top filter and stored at 4°C for up to one month.

The 1% (w/v) DNAse solution was prepared by dissolving 0.025 g of DNAse in 2.5 ml of PBS/glucose. The 2% (w/v) collagenase and 2% (w/v) trypsin solutions were prepared by dissolving 0.1 g of collagenase and trypsin in 5 ml of PBS/glucose,

respectively. All enzyme solutions were filter sterilized through a 0.2 μm acetate syringe filter and aliquoted into sterile, 1.5 ml microcentrifuge tubes for storage in the -20°C freezer. Enzyme solutions were used for up to one month before making up fresh stocks, as the freezing and thawing process reduces the activity of the enzymes over time.

3.2.2.2 Isolation of neonatal rat cardiac myocytes

Primary cultures of neonatal rat cardiac myocytes were obtained by ethically approved University of Manitoba Animal Care Committee Standards and were used as the cell model for studying doxorubicin cardiotoxicity. Neonatal rat cardiac myocytes are capable of growing and dividing and possess similar properties to abnormally growing and dividing heart cells during heart failure [26]. Thus, the neonatal rat cardiac myocyte model seemed the most appropriate for our studies, which assessed chronic doxorubicin cardiotoxicity. A typical photomicrograph of viable, well-attached neonatal rat cardiac myocytes used in our studies is shown in Figure 3.7.

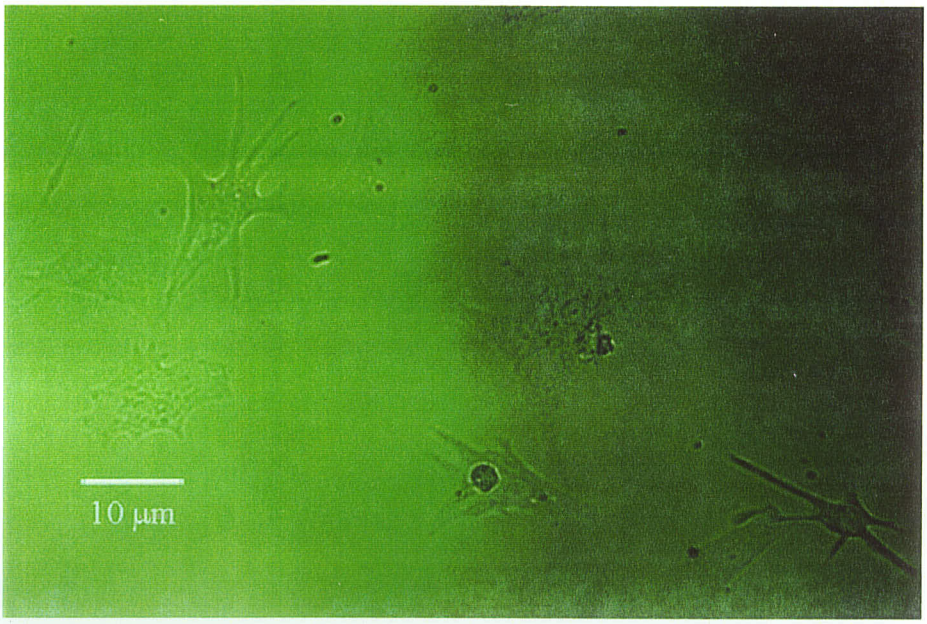

Figure 3.7 Photomicrograph of healthy neonatal rat cardiomyocytes used in our doxorubicin cardiotoxicity studies. The cardiomyocytes are well-attached with extensive pseudopodia. This bright field image was viewed with a 16X objective.

Before beginning the isolation, the sterile tissue-digesting jacketed flask was connected to a circulating water bath set at 36°C. All surgical tools were soaked in 70% (v/v) ethanol in H_20 for 30 min and media and buffers were equilibrated to their appropriate temperatures. For all isolations, hearts were excised from 12-15 Sprague-Dawley rat pups of 2-3-days-old.

Each rat was picked up gently and placed on a sterilized surface for cervical dislocation with sterilized forceps. Rats were briefly placed in 70% (v/v) ethanol in H_20 and flipped on their back for a midline sternotomy with sterilized surgical scissors. To excise the hearts, the chest cavity was cut open and pressure was applied from above and below the cavity to pop out the ventricle. Upon removal, hearts were immediately placed in 40 ml of ice-cold PBS/glucose. After washing the hearts twice with 40 ml of ice-cold PBS/glucose, the hearts were minced with sterilized shears in 5 ml of ice-cold PBS/glucose then washed twice with ice-cold PBS/glucose to remove any remaining red blood cells and debris.

To begin the dissociation, minced hearts were washed once with 15 ml of pre-warmed (37°C) PBS/glucose. The hearts were then transferred with a sterile, cut-opened end pipette tip in 3-4 ml of warm PBS/glucose to a sterile, tissue-digesting jacketed flask pre-equilibrated to 36°C.To maintain suspension clarity and prevent cell clumping, 80 µl of 1% (w/v) DNAse was added to the digesting solution. Then, 100 µl of 2% (w/v) collagenase and 200 µl of 2% (w/v) trypsin were added to the flask to digest the collagen and other proteins. Following addition of enzymes, the contents of the digestion flask were gently stirred with a stirrer set at low speed (2-3) for 8½ minutes. After the first digestion, the supernatant was discarded and replaced with 3 ml of warm PBS/glucose.

The same amounts of enzymes were added, and contents of the digestion flask were gently stirred for 8½ minutes. After the second digestion, the supernatant was transferred into 30 ml of ice-cold plating medium and replaced with 3 ml of warm PBS/glucose. The same amounts of enzymes were added and after 8½ minutes of gentle stirring (digestion 3), digestion flask contents were mixed gently up and down 10-15 times with a sterile, large, cut-opened end pipette tip. Digestions 4-6 were performed identical to digestion 3 except the size of the cut-opened pipette tip was reduced in diameter for each successive digestion. Less 1% (w/v) DNAse was required for the later digestions and was only added when the digestion solution was too viscous. On the final digestion, the supernatant was replaced with 2 ml of warm PBS/glucose and 100 µl of both 2% (w/v) collagenase and 2% (w/v) trypsin was added to the flask. After stirring the digested solution for 8½ minutes, the supernatant was placed into the tube of ice-cold plating medium and centrifuged for 5 min at 140 g. The supernatant was discarded and replaced with fresh ice-cold plating medium. The cells were resuspended with a sterile 25-ml pipette and passed through a 0.4 µm cell strainer into two separate sterile 50-ml conical tubes. Both tubes were centrifuged for 5 min at 140 g and the supernatant was drawn off leaving ~12 ml to resusupend the cells in. The resuspended cells were transferred to a Falcon 3025 tissue plate with a sterile 25-ml pipette and incubated for 48 min at 37°C in an atmosphere of 5% (v/v) CO_2 in air. Such conditions favored fibroblast attachment, leaving the cardiac myocytes in suspension. The suspension of cardiac myocytes and plate washes with warm plating medium were collected in a 50 ml conical tube and centrifuged for 5 min at 140 g. The supernatant was drawn off leaving ~10 ml to resuspend the cells in. The cells were resuspended with a sterile 10-ml pipette.

3.2.2.3 Determination of cell viability and cell density

Cell viability was assessed using a colorimetric, trypan blue dye exclusion method. Trypan blue is a cell impermeable dye that can be used to differentiate live from dead cells [20]. Its uptake by cells depends upon the integrity of the cell membrane. Viable cells with an intact plasma membrane exclude the dye and appear white while leaky cells take up the dye and stain blue.

Trypan blue dye (0.6% (w/v)) was prepared by dissolving 0.6 g of trypan blue dye in H_2O containing 150 mM NaCl and 1 mM Na_2EDTA. A 100 µl sample of the primary cardiac myocyte suspension was diluted 1:1 with trypan blue dye and a minimum of 250 cells were counted with the hemocytometer. The percentage of viable cells was determined by dividing the number of viable cells (white) over the total number of cells counted (white and blue) and multiplying by 100. The cell density in cells/ml was determined by multiplying the number of viable cells by 10^4 and then by the dilution factor (2).

3.2.2.4 Seeding cells

Epifluorescence microscopy experiments

The primary culture of cardiac myocytes was resuspended with a sterile 10-ml pipette before seeding. Cells were seeded on sterile 6-well plates containing sterile glass cover slips at a density of 200,000 cells per well in 2 ml of plating medium. A sterile 2-ml pipette was used to seed the plates and the cell suspension was rocked gently throughout the seeding process to prevent cell settlement. The cardiac myocytes were very sensitive to damage and were handled with utmost care to prevent significant drops in cell viability. The cell density chosen for seeding allowed for optimum cell viability

with ~40% coverage of cover slips for imaging of well-spaced cardiac myocytes. Following seeding, the plates were placed in the 37°C incubator in an atmosphere of 5% (v/v) CO_2 in air. Cells were left undisturbed for at least 48 h.

Fluorescence plate reader experiments

The primary culture of cardiac myocytes was resuspended with a sterile 10-ml pipette before seeding. Cells were seeded on sterile 96-well black microtitre plates at a density of 160,000 cells per well in 200 µl of plating medium. Black microtitre plates were used to minimize fluorescent signal cross talk between wells. Sterile 2-ml pipettes (Trial #1) or 200-1000 µl sterile, cut-opened end pipette tips (Trial #2 and #3) were used to seed the plates. Small opening pipettes or pipette tips were used to maintain high cell viability throughout the seeding process. The cell suspension was placed in a sterile boat and gently rocked throughout seeding to prevent cell settlement. The cell density chosen for seeding allowed for optimum cell viability and 95% confluence of the culture by the day of the experiments. All outer wells that did not contain cells were filled with 200 µl of Hank's buffer (with Ca^{2+} and Mg^{2+}) for fluorescence plate reader blanking and to reduce evaporation of media from inner wells. The plates were also wrapped in Saran wrap to further reduce evaporation from wells and were placed in the 37°C incubator in an atmosphere of 5% (v/v) CO_2 in air. Cells were left undisturbed for at least 48 h.

3.2.2.5 Culturing cells

Forty-eight hours following seeding, the cells were transferred from plating medium (7.5% (v/v) horse serum/7.5% (v/v) FCS in DMEM-F12) into culturing medium (DF-10, 10% (v/v) FCS in DMEM-F12) and were grown in an atmosphere of 5% (v/v) CO_2 in air at 37°C. All experiments were performed on cultures 3-4 days following

isolation. On these days, approximately 80% of the cells had recovered from the isolation and were beating.

3.2.3 Drug preparation and delivery

All drugs were thawed out in a dessicator at room temperature for 20 min prior to weighing. Drugs were weighed out with a microbalance (Micro Gram-Atic Balance, Fisher Scientific Company) and double gloves, a mask and safety goggles were worn when valinomycin or nigericin were being handled. Doxorubicin was dissolved in H_2O to give a stock concentration of 1 mM. The doxorubicin stock solution was wrapped in aluminum foil and stored at 4°C for up to three weeks. Dexrazoxane was dissolved in cell culture medium (DF-10) on the day of the experiment and filter sterilized through a 0.2 μm sterile cellulose acetate syringe filter. A 86 μM dexrazoxane solution for washing was also prepared and incubated in an atmosphere of 5% (v/v) CO_2 in air at 37°C. Valinomycin and nigericin were dissolved in DMSO on the day of the experiment.

Before drug treatment, cell culture medium in all wells was replaced with fresh medium (DF-10) and allowed to equilibrate to 37°C for at least 20 min. For all experiments, drugs were delivered in the center of the well and plates were swirled three times clockwise and three times counterclockwise after the addition of drug. All drug incubations were done at 37°C in an atmosphere of 5% (v/v) CO_2 in air.

Valinomycin is a K^+-selective ionophore, which has been demonstrated to uncouple oxidative phosphorylation and was chosen as a control for mitochondrial membrane depolarization [27-29]. Nigericin is a K^+/H^+ ionophore that has been demonstrated to stimulate mitochondrial ATPase activity and it was chosen as a control for mitochondrial membrane hyperpolarization [29, 30]. The DMSO soluble drugs,

valinomycin and nigericin, were added to each well such that the final DMSO concentration was <0.05% (v/v). Cells were exposed to 1 μM valinomycin for 24 h or 0.5 μM nigericin for 1 h, stained with 6 μM JC-1 for 20 min and imaged with the epifluorescence microscope. A DMSO control was also included for both exposure times to ensure that DMSO itself did not significantly affect the mitochondrial membrane potential.

Peak plasma concentrations of doxorubicin approaching 2.3 μg/ml has been reported in the literature [49]. Doxorubicin has a distribution half-life of 0.6 h and an elimination half-life of 16.7 h [49]. Based upon these pharmacokinetic parameters, the approximate plasma concentration of doxorubicin attained in clinical settings is 1.0 – 2.0 μM. Thus, we chose to test a range of pharmacological doxorubicin concentrations (0 - 2.0 μM) including those clinically relevant values [31, 49]. A 2.0 μM doxorubicin control was included to ensure that the fluorescence of doxorubicin was negligible. Single drug experiments with doxorubicin were either short- term (1 h) or long-term (48 h). In the short-term study, cells were exposed to 0.3, 0.5 and 1.0 μM doxorubicin for 1 h followed by immediate staining with JC-1 and imaging with the epifluorescence microscope. In the long-term study, cells were exposed for 3 h to a range of pharmacological doxorubicin concentrations (0 - 2 μM). Following treatment, the cells were washed three times with culturing medium (DF-10) to remove the remaining drug and incubated for 48 h at 37°C before staining with JC-1 and measuring the fluorescence signal. The doxorubicin concentrations administered for the epifluorescence microscopy experiments were 0.1, 0.15, 0.2, 0.25, 0.3, 0.5, 1.0 and 2.0 μM. For the fluorescence plate reader experiments, doxorubicin concentrations of 0.2, 0.3, 0.5, 1.0 and 2.0 μM were delivered. Changes in

morphology, beating rate and cell density were monitored with the phase contrast, inverted microscope (Nikon Canada Instruments Inc., Mississauga, ON) over 48 h.

The maximum dose of dexrazoxane reported to have been administered to cancer patients is 500 mg/m^2 [32]. Peak plasma concentrations of 120 μM dexrazoxane have been reported with a distribution half life of 15 min and an elimination half life of 2 – 4 h [32]. Given that the half life of dexrazoxane at a pH of 7.4 is 9.3 h, we chose to use 86 μM dexrazoxane in our studies [33]. In the double drug experiments, cardiac myocytes were pre-exposed to 86 μM dexrazoxane for 3 h followed by treatment with doxorubicin for 3 h. The doxorubicin concentrations administered for the epifluorescence microscopy experiment with dexrazoxane were 0.15, 0.2, 0.25, 0.3 and 0.5 μM. In the fluorescence plate reader experiments, the doxorubicin concentrations administered with dexrazoxane were the same as used in the single-drugging experiment. A dexrazoxane control was also included to ensure dexrazoxane itself did not significantly affect the mitochondrial membrane potential. Following the 3 h exposure to doxorubicin, cells were washed three times with cell culture medium (DF-10) or 86 μM dexrazoxane in DF-10 (for dexrazoxane treated wells). A wash involved aspirating the medium, replacing it with fresh medium and incubating the plate for 20 min. After the cells were washed, they were placed in the 37°C incubator in an atmosphere of 5% (v/v) CO_2 in air for 48 h.

3.2.4 JC-1 assay for measuring mitochondrial membrane potential

The JC-1 assay is a concentration-dependent assay that is used to monitor changes in the mitochondrial membrane potential. JC-1 is a fluorescent, cationic dye that exhibits potential-dependent accumulation in mitochondria, as indicated by a fluorescence emission shift from green (~525 nm) to red (~ 590 nm) [20]. The potential-sensitive color

shift is due to concentration-dependent formation of red fluorescing "J-aggregates" [20]. JC-1 is selectively taken up by actively respiring, (hyperpolarized) mitochondria where it forms red fluorescing "J-aggregates". Upon collapse of the mitochondrial membrane potential JC-1 is only weakly taken up and the dye monomers fluoresce green. Mitochondrial depolarization in a variety of cell types including myocytes has been measured with the ratiometric dye JC-1 by measuring the decrease in the average red/green fluorescence intensity ratio [20].

3.2.4.1 Development of the JC-1 staining protocol for cardiomyocyte mitochondria

The JC-1 staining protocol for cardiomyocyte mitochondria was developed using previous JC-1 loading conditions as the platform [14-17, 19, 25, 34-37]. Because precipitation and photobleaching of JC-1 at room temperature in the light was a problem, staining was done at 37°C in the dark. Loading concentrations of JC-1 ranging from 1 – 15 μM were tested in serum-containing medium (DF-10) at fixed times (10 and 20 min) in the 37°C incubator. Twenty minutes was identified to be the appropriate time for JC-1 loading. At low concentrations the fluorescence signal was too dim while precipitation of the dye remained a problem at high concentrations. Regardless of JC-1 concentration a blurry background limited the detail of the images. To overcome blurred images and precipitation problems, JC-1 staining solutions were prepared in serum free medium (DMEM F-12) and centrifuged to remove the precipitate. Depending on how well the ordered JC-1 stock was dried, loading concentrations had to be finely tuned. JC-1 concentrations of 6 – 8 μM at a loading time of at least 20 min were finally identified to be ideal for JC-1 staining of cardiomyocyte mitochondria. Details of the developed JC-1 staining protocol are discussed in the following sections.

3.2.4.2 Preparation of JC-1 stock solution

Solid JC-1 (MW = 652.23 g/mol) was thawed at room temperature for ~ 20 min in a light-shielded dessicator prior to weighing with the microbalance. To prepare a 1 mM stock of JC-1, 0.652 mg of JC-1 was dissolved in 1 ml of 99.5% dimethylsulfoxide (DMSO). The JC-1 solution was warmed up in the 37°C water bath to completely dissolve the dye and was wrapped in aluminum foil. To store in the -80°C freezer, the 1 mM JC-1 stock solution was aliquoted into microcentrifuge tubes (200 µl/tube) and wrapped in aluminum foil. A new JC-1 stock was thawed on each day, as dilute JC-1 solutions are not as stable during storage.

3.2.4.3 Preparation for staining

Before staining, the microcentrifuge, vortex, pipette tips, DMEM/F12 (no serum) and Hank's buffer (with Ca^{2+} and Mg^{2+}) were equilibrated in the 37°C incubator. The DMEM/F12 was divided into 1 ml aliquots in microcentrifuge tubes and the 1 mM JC-1 stock solution was diluted to 500 µM with 99.5% DMSO. To each of the microcentrifuge tubes containing 1 ml DMEM/F12 was added 12 – 16 µl of the 500 µM JC-1 solution to give a final concentration of 6 – 8 µM JC-1. Each microcentrifuge tube was vortexed and then centrifuged for 5 min at 16,000 g to separate out the fine JC-1 precipitate. The JC-1 supernatant was collected into a 50-ml conical tube (for the epifluorescence microscopy experiments) or boat (for the fluorescent plate reader experiments).

3.2.4.4 Loading cells with JC-1

Epifluorescence microscopy experiments

Because JC-1 is photosensitive and precipitates at room temperature, all staining was carried out in the 37°C incubator. Cell culture medium was removed from each well

with a pipette and replaced with 1.5 ml of JC-1 supernatant. The JC-1 supernatant (6 – 8 μM) was added very slowly over all regions of the glass cover slip. A different pipette tip was used for each well to prevent accumulation of trace JC-1 precipitate. Once the dye was added to the wells, the plate was swirled twice to the left and twice to the right and then incubated at 37°C for 20 min. After 20 min, 1.5 ml of warm Hank's buffer (with Ca^{2+} and Mg^{2+}) was added to each well. The plate was swirled a couple of times and then 2.4 ml of the diluted solution was removed. The cells were washed twice more by adding and removing 1.5 ml of Hank's buffer (with Ca^{2+} and Mg^{2+}).

Fluorescence plate reader experiments

All staining was carried out in the 37°C incubator. Cell culture medium was removed from each well with the multi-channel pipette and replaced with 150 μl of JC-1 supernatant (6 – 8 μM). Once the dye was added to the wells, the plate was swirled twice to the left and twice to the right and then incubated at 37°C for 20 min. After 20 min, 150 μl of Hank's buffer (with Ca^{2+} and Mg^{2+}) was added to each well. The plate was swirled a couple of times and then 240 μl of the diluted solution was removed. The cells were washed twice more by adding and removing 150 μl of Hank's buffer (with Ca^{2+} and Mg^{2+}).

3.2.5 Epifluorescence microscopy and the fluorescence plate reader as alternative methods for quantifying mitochondrial membrane potential with JC-1

Quantitative determination of the mitochondrial membrane potential typically employs "dual wavelength" or ratiometric dyes such as JC-1. The key advantage of ratiometric dyes is that the measured ratio is independent of the amount of dye in the cell. Using the ratio approach, variations in fluorescence due to factors such as uneven cell thickness, unequal dye distribution, dye leakage or photobleaching can be normalized.

Several studies have employed JC-1 for the measurement of mitochondrial membrane potential with microscopic and flow cytometric methods [16, 17, 19, 35, 37]. In order that our doxorubicin cardiotoxicity studies be clinically relevant, it was necessary that our cardiomyocyte preparation be attached and beating. Flow cytometry analysis measures fluorescence intensity in suspension cells and was not considered ideal for sensitive cardiomyocytes as handling and trypsinization would probably limit the quality of the preparation [38]. Laser scanning confocal microscopy provides high resolution images and is very sensitive, however, it is an expensive technology, to which few researchers have access [39]. Fluorescence microscopy has frequently been used in subjective analysis but higher precision and sensitivity is required to produce quantitative results [40]. Low concentrations of fluorescent molecules are often used when staining, and this gives rise to their sensitivity to photobleach when overexposed to light [20]. Epifluorescent microscopes equipped with cooled CCD cameras and light shutters allow researchers to minimize photobleaching by providing extremely high sensitivity [41]. The broad dynamic range of CCD camera systems allows dim objects and relatively bright objects to be viewed and measured within the same image [41]. Using a fixed exposure time, the fluorescence signals can be matched to the sensitivity of the CCD camera. Dichroic filters also minimize photobleaching by limiting the exposure of the specimen to light. Fluorescence plate readers equipped with fast light excitation and fast fluorescence capturing are also able to minimize photobleaching and provide highly sensitive measurements of fluorescence intensity [40]. While imaging and analysis with the epifluorescence microscope can be time-consuming, the fluorescence plate reader provides rapid measurement and analysis of fluorescence signals.

3.2.5.1 Preparation for epifluorescence microscope imaging

The mercury lamp was turned on 20 min prior to imaging to allow the lamp to stabilize. Cells were viewed on a Zeiss epifluorescence microscope (Roper Scientific, Trenton, NJ) at 16X objective and imaging was performed in the dark to minimize photobleaching. Fluorescence was detected using neofluor optics with a JC-1 dichroic filter set (XF2010, Omega Optical, Brattleboro, Vermont) and images were captured with a high resolution, cooled color digital (CCD) camera using Photometrics Cool Snap acquisition software (Version 1.2, Roper Scientific, Trenton, NJ). The focus and exposure time for all experiments was set at 0.25 and 2.0 s, respectively. Any camera dark noise was accounted for during camera calibration and was subtracted from the other images.

3.2.5.2 Mounting the cover slip onto the microscope slide

Dust and fingerprints were removed from microscope slides with a Kimwipe tissue. Microscope slides were placed on a Kimwipe tissue and small dabs of Vaseline were applied to each of four corners of a square. Into the center of the square was placed 30 µl of warm Hank's buffer (with Ca^{2+} and Mg^{2+}) to avoid drying and formation of precipitates of JC-1 on the cell surface. The cover slips were lifted up with a bent end syringe needle and the top edges were grasped with forceps. To wash off any salt films, the cover slips were briefly dipped in H_2O and touched to a Kimwipe tissue to absorb H_2O drops. The bottom sides of the cover slips (side with no attached myocytes) were dried by dragging them across a flat surface on a Kimwipe tissue. Cover slips were flipped over (myocyte side facing down), held at a 45° angle to the microscope slide and dropped onto the drop of Hank's buffer (with Ca^{2+} and Mg^{2+}).

3.2.5.3 Epifluorescence microscope imaging and analysis

Once the cover slip was mounted, the lights were turned off and the shutter on the epifluorescence microscope was closed. Using the microscope stage adjustment knobs, the top left-hand corner of the cover slip was brought directly beneath the 16X objective lens. The plane of focus was set on bright field mode to minimize photobleaching. Images were acquired by opening the shutter, switching to camera view and pressing the acquire button. After image acquisition, the shutter was closed and the view was switched back to the microscope view to minimize photobleaching. Using the microscope stage adjustment knobs, imaging was continued across the top, middle and bottom of the cover slip. For each treatment, approximately 12 images were taken. On average, each field contained approximately ten well-spaced myocytes.

Images of JC-1 stained mitochondria were analyzed using Paintshop Pro imaging software (Version 6.00, Jasc Software Inc., Eden Prairies, MN). Individual cells were zoomed in on with the magnifying glass tool, selected with the outline tool and cleaned up with the cut command. The small discrete elements that together constitute an image are called pixels. Using the histogram function, one can choose to view the red, green or blue plane of the image separately. Within each color plane, the histogram displays the number of pixels at various intensities (0 (dim) – 255 (bright)). For each imaged cell, the average red and green pixel intensities were reported from the histogram and used in subsequent calculation of the red/green pixel intensity ratio for each imaged cell. For each treatment, average red/green pixel intensity ratios were calculated for approximately 80 cells.

3.2.5.4 Fluorescence plate reader measurement and analysis

JC-1 stained cells were placed in a Fluorostar multi-well fluorescence plate reader (BMG Labtechnologies, Durham, NC) equipped with dual-emission optics and a current type photomultiplier tube. The temperature was maintained at 37°C and cells were excited from the bottom at 485 and 544 nm with a high-energy xenon flash lamp [16]. The excitation was medium band with a bandwidth of 10 nm. The cells were excited at two different wavelengths, as the monomer and the aggregated form of JC-1 absorb light maximally at these two different wavelengths. Excitation was followed by the collection of green fluorescence and red fluorescence bottom emissions at 520 and 590 nm, respectively [25]. The fluorescence from each well was captured, digitized and stored on the computer using Fluo 32 software (Version 4.20). Measurements were taken at a rate of 10 flashes per cycle (~120 s) and the data were exported to Microsoft Excel spreadsheet software for analysis. The average of the first row (Hank's buffer with Ca^{2+} and Mg^{2+}) was used as a background and this value was subtracted from all other fluorescence intensities.

3.2.6 Statistical analysis

Where indicated, levels of statistical significance were determined with SigmaStat statistical software (Version 2.0, Jandel Scientific, San Rafael, CA) using the Student's *t*-test. A P value below 0.05 was considered significant.

3.3 Results

3.3.1 Cell viability, cell yield and time-dependence for recovery of viable cells

As determined using the trypan blue exclusion method, cells were greater than 80% viable for all experiments performed. If cell viability was less than 80%, than only trace mitochondrial membrane depolarization was observed with doxorubicin treatment

(data not shown). On average, digestion of 12-15 hearts yielded 35 million cardiac myocytes. Approximately 80% of the cells recovered from isolation and were beating strongly on the days that experiments started (days 3 and 4 following isolation). Cells allowed to recover for longer periods of time after isolation had more actively respiring mitochondria, as measured by epifluorescence microscopy, and this was indicated as an increase in the average red/green pixel intensity ratio of JC-1 stained cardiomyocyte mitochondria (Figure 3.8). The information gained in this experiment was subsequently used to set ideal drug treatment and analysis times.

3.3.2 Morphology, beating rate and cell density changes observed with the microscope over 48 h in healthy and doxorubicin-treated cardiomyocytes

Prior to drug treatment, cardiac myocytes were well attached with extensive pseudopodia. Generally, the cells adhered more strongly to the plastic 96-well plates than to the glass cover slips and were most dense in the center of the well. Regions of higher density tended to beat faster than regions of low density, although all areas beat in phase. The beating rate was used as an indicator of cell viability. Cells that received no drug maintained the initial morphology throughout the experiment and continued to beat in phase, although the beating rate decreased slightly over time with nutrient depletion.

Several hours following doxorubicin treatment, an increase in the beating rate was observed and followed by a sudden drop in the beating rate and an appearance of arrhythmias after 24 h. Some cells began to round up and became more loosely attached in wells treated with 1.0 – 2.0 μM doxorubicin. After forty-eight hours, the cells started to break away from each other. At low concentrations of doxorubicin, cells were also rounded up and loosely attached and the occasional cell was beating very slowly and irregularly. Cell loss was observed in wells treated with 0.5 μM doxorubicin or greater,

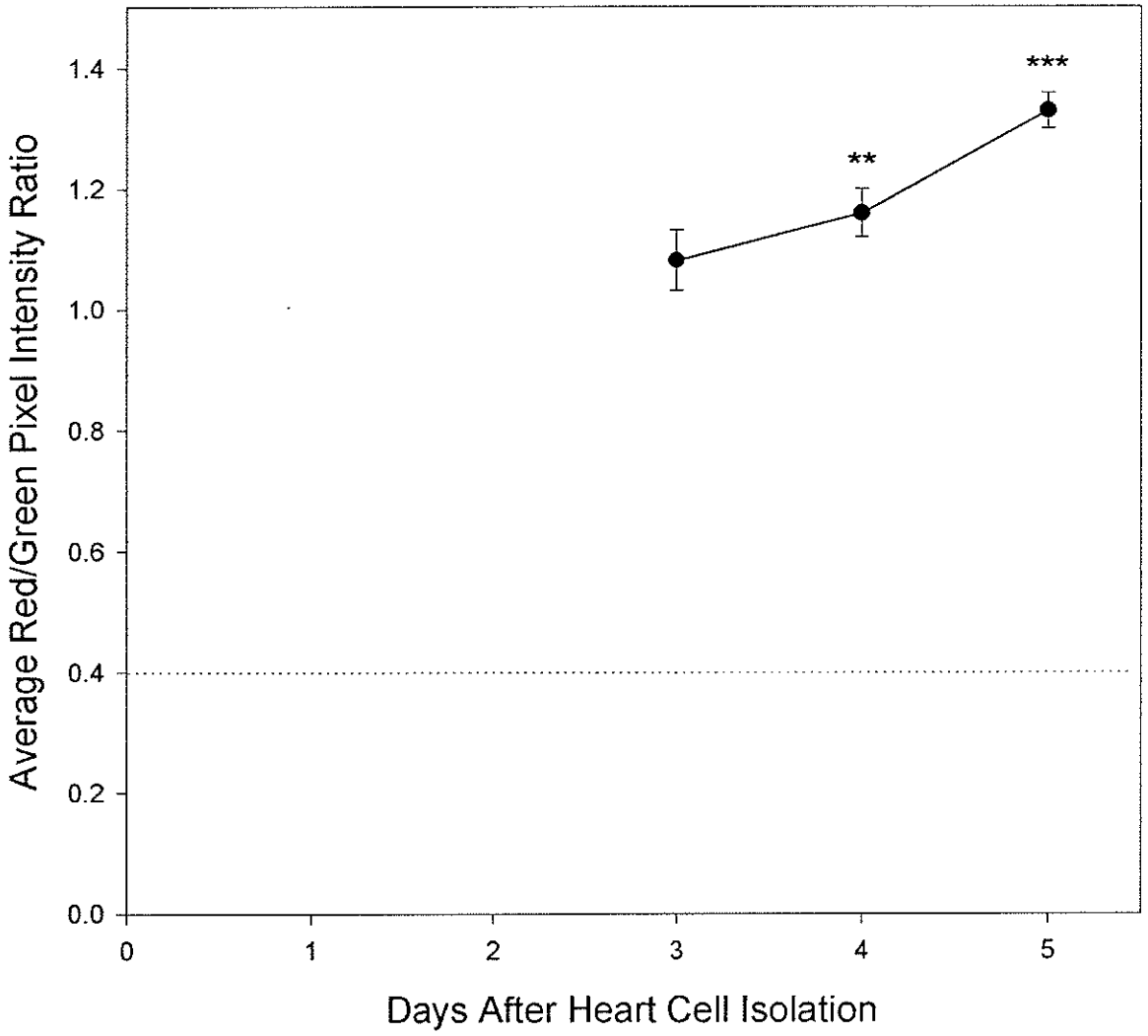

Figure 3.8 Time-dependent recovery of cardiomyocytes with actively respiring mitochondria. Cardiomyocytes were seeded at a density of 200,000 cells/well in 6-well tissue culture plates containing glass cover slips. The cells were incubated for at least 48 h at 37°C in an atmosphere of 5% (v/v) CO_2 in air. After 48 h, the cells were attached, beating and were transferred into culturing medium (DF-10, 10% FCS in DMEM-F12). Three, four and five days following isolation cardiomyocyte mitochondria were stained with 8 μM JC-1 for 20 min, wet-mounted onto a microscope slide and imaged with an epifluorescent microscope . The cells were all from the same primary culture, which was determined to be 80% viable. Approximately 20 cells were imaged for each time point and the error bars represent standard errors. The dotted line is the lowest average red/green pixel intensity ratio that could be attained when cardiomyocytes were exposed continuously to 1 μM valinomycin for 24 h. An increase in the average red/green pixel intensity ratio is indicative of mitochondrial membrane hyperpolarization. ** $P \leq 0.01$ compared to day 5, *** $P \leq 0.001$ compared to day 3

and no beating was apparent in wells treated with 1.0 – 2.0 μM doxorubicin. The majority of cells in the latter doxorubicin concentration range were rounded up and loosely attached.

3.3.3 Dose-dependent collapse of the mitochondrial membrane potential of doxorubicin-treated cardiomyocytes

The effect of doxorubicin on the mitochondrial membrane potential of neonatal rat cardiac myocytes was assessed by epifluorescence microscopy and the fluorescence plate reader following staining of the cardiomyocyte mitochondria with JC-1. Exposure of neonatal rat cardiac myocytes to a range of pharmacological concentrations of doxorubicin for 1 h showed a dose-dependent depolarization of the mitochondrial membrane. As displayed in Figure 3.9, a dose-dependent decrease in the average red/green pixel intensity ratio of JC-1 stained mitochondria was observed in cardiomyocytes imaged immediately following a 1 h exposure to 0.3, 0.5 and 1.0 μM doxorubicin. Cardiomyocytes grown for 48 h at 37°C in an atmosphere of 5% (v/v) CO_2 in air following 3 h exposure to 0.1, 0.15, 0.2, 0.25 0.3, 0.5, 1.0, 1.5 and 2.0 μM doxorubicin also displayed a dose-dependent decrease in the average red/green pixel intensity ratio (Figure 3.10). In both epifluorescence microscopy experiments, the average red/green pixel intensity ratio started to level off at doxorubicin concentrations greater than 0.5 μM (Figures 3.9 and 3.10). Doxorubicin fluorescence was negligible when cardiomyocytes treated with 1.0 μM doxorubicin were viewed with the epifluorescence microscope.

In the fluorescence plate reader experiments, cardiomyocytes grown for 48 h at 37°C in an atmosphere of 5% (v/v) CO_2 in air following 3 h exposure to 0.2, 0.3, 0.5, 1.0 and 2.0 μM doxorubicin displayed a dose-dependent decrease in the average red/green

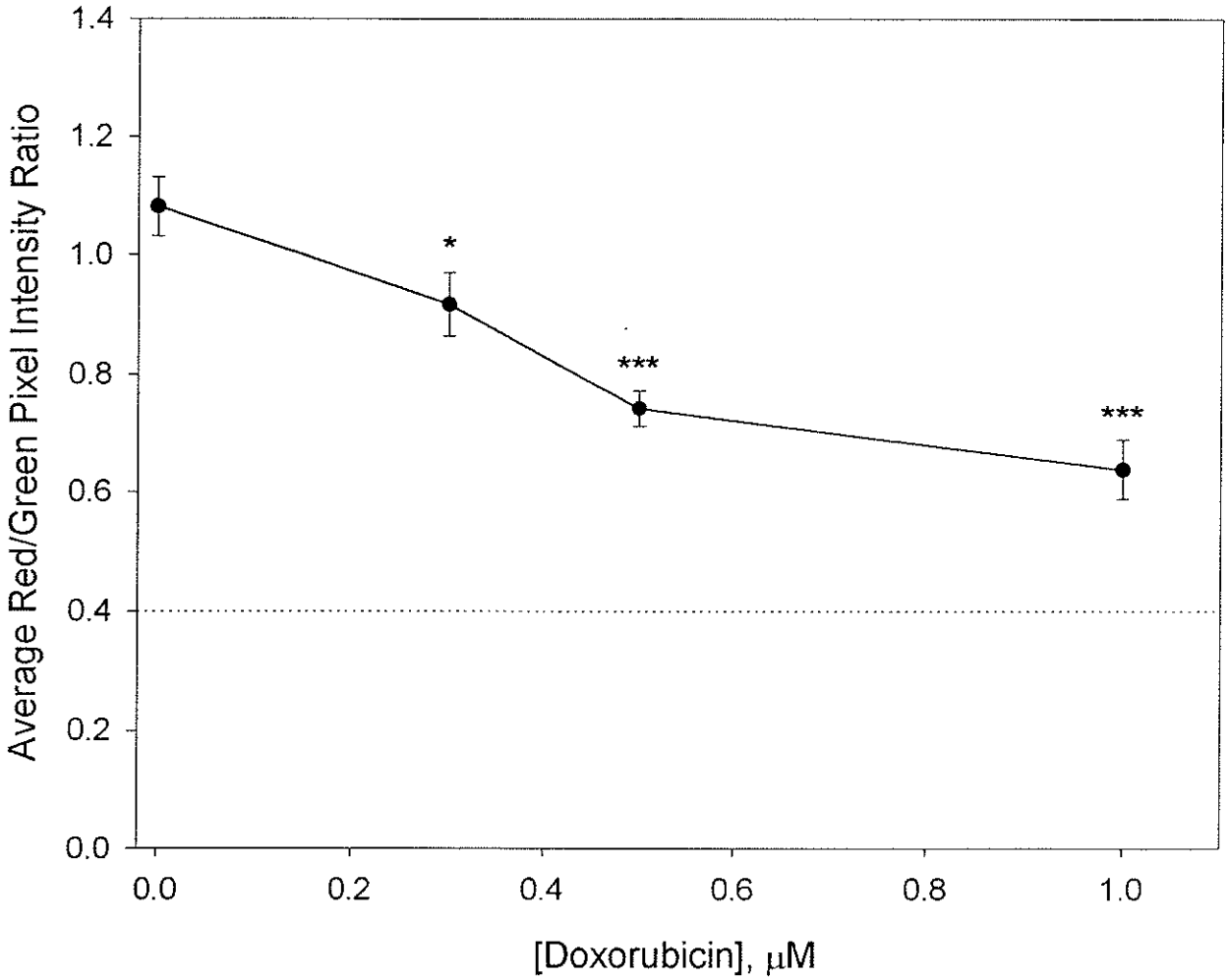

Figure 3.9 Dose-dependent collapse of the mitochondrial membrane potential of doxorubicin-treated cardiomyocytes, as measured by epifluorescence microscopy with the JC-1 assay. Cardiomyocytes were seeded at a density of 200,000 cells/well in 6-well tissue culture plates containing glass cover slips. The cells were incubated for at least 48 h at 37°C in an atmosphere of 5% (v/v) CO_2 in air. After 48 h, the cells were attached, beating and were transferred into culturing medium (DF-10, 10% FCS in DMEM-F12). Three days following isolation, the cells were exposed to 0.3, 0.5 and 1.0 μM doxorubicin for 1 h at 37°C in an atmosphere of 5% (v/v) CO_2 in air. After treatment, the cells were washed three times with DF-10, stained with 8 μM JC-1 for 20 min and imaged with an epifluorescent microscope. The cells were all from the same primary culture, which was determined to be 80% viable. Approximately 20 cells were imaged for each time point and the error bars represent standard errors. The dotted line is the lowest average red/green pixel intensity ratio that could be attained when cardiomyocytes were exposed continuously to 1 μM valinomycin for 24 h. A decrease in the average red/green pixel intensity ratio is indicative of mitochondrial membrane depolarization. * $P \leq 0.05$, *** $P \leq 0.001$ compared to the untreated cardiomyocyte preparation

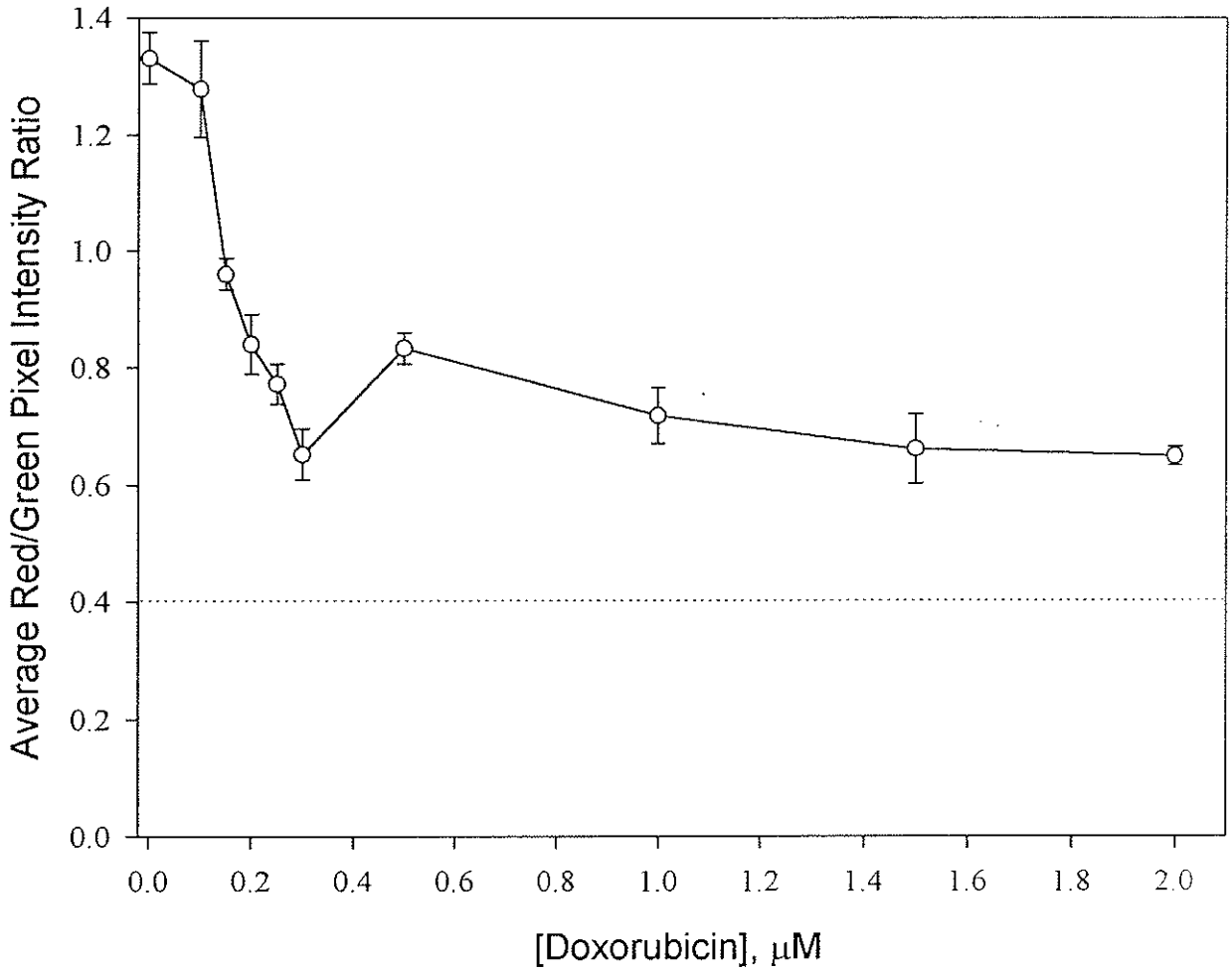

Figure 3.10 Dose-dependent collapse of the mitochondrial membrane potential of doxorubicin-treated cardiomyocytes, as measured by epifluorescence microscopy with the JC-1 assay. Cardiomyocytes were seeded at a density of 200,000 cells/well in 6-well tissue culture plates containing glass cover slips. The cells were incubated for at least 48 h at 37°C in an atmosphere of 5% (v/v) CO_2. After 48 h, the cells were attached, beating and were transferred into culturing medium (DF-10, 10% FCS in DMEM-F12). Three days following isolation, the cells were exposed to 0.1, 0.15, 0.2, 0.25, 0.3, 0.5, 1.0, 1.5 and 2.0 μM doxorubicin for 3 h at 37°C in an atmosphere of 5% (v/v) CO_2 in air. After treatment, the cells were washed three times with DF-10 and allowed to grow for 48 h at 37°C in an atmosphere of 5% (v/v) CO_2 in air. After 48 h, the cardiomyocyte mitochondria were stained with 6 μM JC-1 for 20 min and imaged with an epifluorescent microscope. The cells used in this experiment came from four different cardiomyocyte primary cultures that were between 86 and 99% viable. For each preparation approximately 80 cells were imaged per treatment and the error bars represent standard errors. All data points are an average of at least four trials except 0.1 and 1.5 μM doxorubicin, which were one and two trials, respecitively. The dotted line is the lowest average red/green pixel intensity ratio that could be attained when cardiomyocytes were exposed continuously to 1 μM valinomycin for 24 h. A decrease in the average red/green pixel intensity ratio is indicative of mitochondrial membrane depolarization. All data points $P \leq 0.001$ compared to the untreated cardiomyocyte preparation except 0.1 μM doxorubicin

fluorescence intensity ratio (Figures 3.11 and 3.12). Individual trials (Figure 3.11) and the average (Figure 3.12) were plotted, as growth of the different cardiomyocyte preparations in 96-well plates was variable. In Figures 3.11A and 3.12, the average red/green fluorescence intensity ratio decreased in a dose-dependent manner and leveled off at doxorubicin concentrations greater than 0.5 μM. The average red/green fluorescence intensity ratio also leveled off at high doses of doxorubicin in Figures 3.11B and 3.11C. However, in contrast to Figures 3.11A and 3.12 the decrease in the ratio was not as drastic and started to increase at doses greater than 0.3 μM doxorubicin. Doxorubicin fluorescence was negligible when cardiomyocytes were treated with 2.0 μM doxorubicin.

3.3.4 Effect of valinomycin and nigericin on the mitochondrial membrane potential of neonatal rat cardiomyocytes

In order to confirm depolarization of the mitochondrial membrane by doxorubicin and to assess the degree of membrane potential disruption, the effect of valinomycin on the mitochondrial membrane potential of cardiac myocytes was examined by epifluorescence microscopy. Valinomycin (1 μM) collapsed the mitochondrial membrane potential of neonatal rat cardiac myocytes after 24 h, as the majority of JC-1 stained cardiomyocyte mitochondria stained green (Figure 3.13). The average red/green pixel intensity ratio of valinomycin-treated cardiac myocytes was also significantly lower than the ratio measured for cardiac myocytes treated with 0.3 μM doxorubicin (Figure 3.14).

The effect of nigericin on the mitochondrial membrane potential of cardiac myocytes was also assessed by epifluorescence microscopy to define the upper limit of the average red/green pixel intensity ratio and confirm the hyperpolarized state of the mitochondria in the primary cardiomyocyte culture. As shown in Figure 3.14, the average red/green pixel intensity ratio of cardiac myocytes treated with 0.5 μM nigericin for 1 h

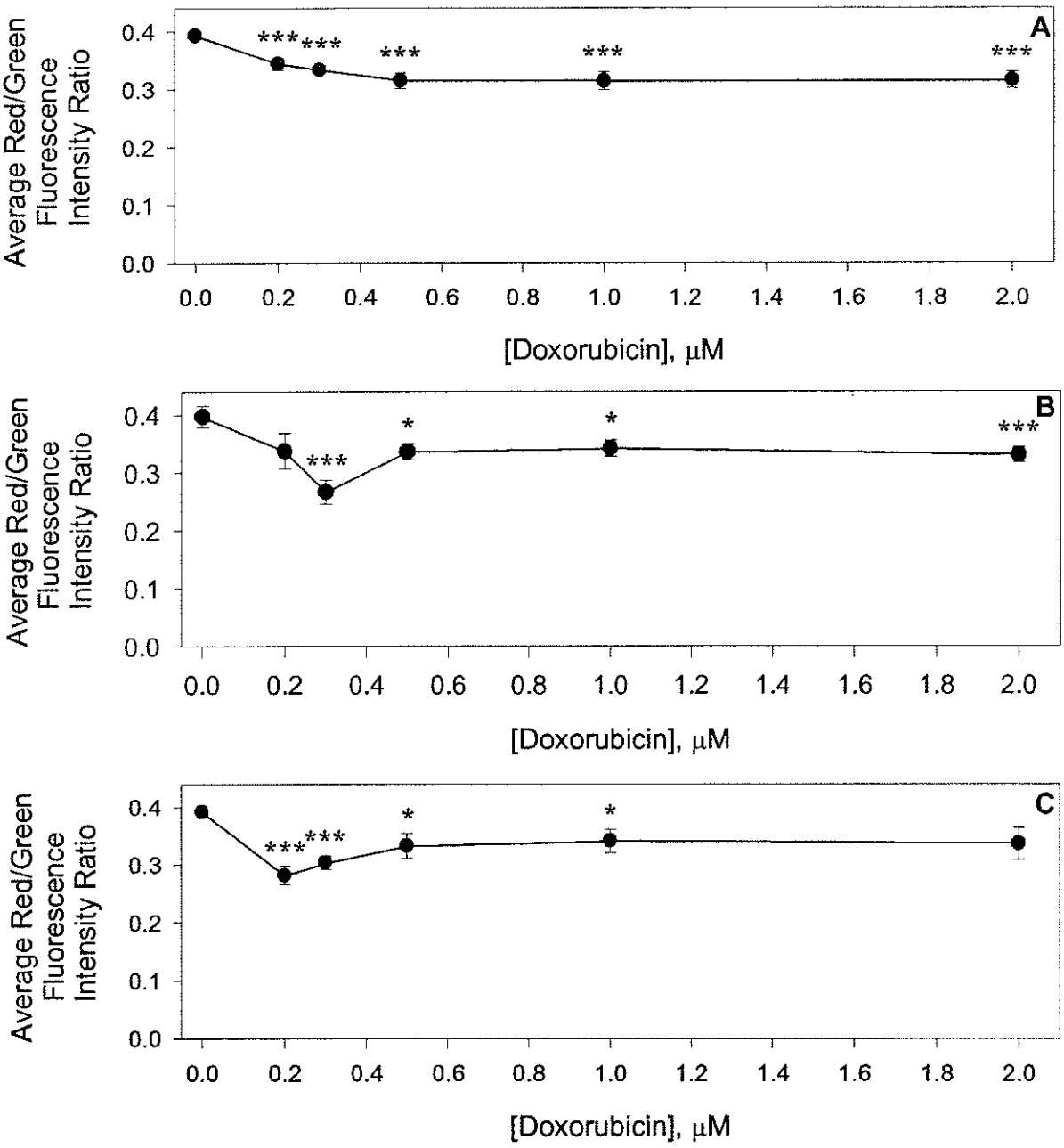

Figure 3.11 Dose-dependent collapse of the mitochondrial membrane potential of doxorubicin-treated cardiomyocytes, as measured by the fluorescence plate reader using the JC-1 assay. Cardiomyocytes were seeded at a density of 160,000 cells/well in 96-well tissue culture plates. The cells were incubated for at least 48 h at 37°C in an atmosphere of 5% (v/v) CO_2 in air. After 48 h, the cells were attached, beating and were transferred into culturing medium (DF-10, 10% FCS in DMEM-F12). Three days following isolation, the cells were exposed to 0.2, 0.3, 0.5. 1.0 and 2.0 μM doxorubicin for 3 h at 37°C in an atmosphere of 5% (v/v) CO_2 in air. After treatment, the cells were washed three times with DF-10 and allowed to grow for 48 h at 37°C in an atmosphere of 5% (v/v) CO_2 in air. After 48 h, the cardiomyocyte mitochondria were stained with 6 μM JC-1 for 20 min and the fluorescence signals were measured using the fluorescence plate reader. Cells were excited at 485/544 nm and green and red fluorescence emissions were collected at 520 and 590 nm, respectively. The cells used in this experiment came from three different cardiomyocyte primary cultures (A, B and C) that were between 93 and 97% viable. Each data point is the average of six replicates with the errors displayed as standard errors. The data in A was normalized to the zero value average of B and C. * $P \leq 0.05$, *** $P \leq 0.001$ compared to the untreated cardiomyocyte preparation

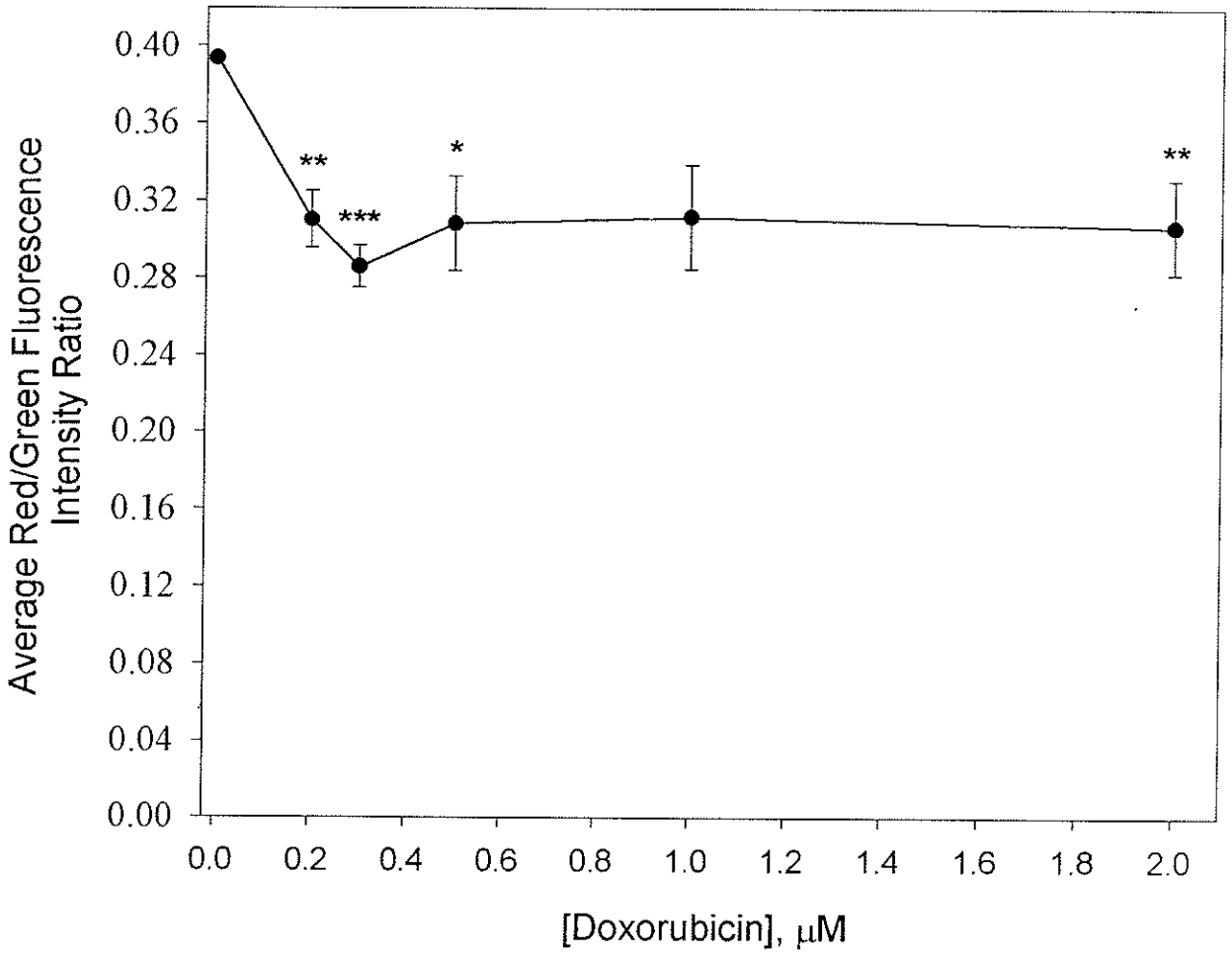

Figure 3.12 Dose-dependent collapse of the mitochondrial membrane potential of doxorubicin-treated cardiomyocytes, as measured by the fluorescence plate reader with the JC-1 assay. Cardiomyocytes were seeded at a density of 160,000 cells/well in 96-well tissue culture plates. The cells were incubated for at least 48 h at 37°C in an atmosphere of 5% (v/v) CO_2 in air. After 48 h, the cells were attached, beating and were transferred into culturing medium (DF-10, 10% FCS in DMEM-F12). Three days following isolation, the cells were exposed to 0.2, 0.3, 0.5. 1.0 and 2.0 μM doxorubicin for 3 h at 37°C in an atmosphere of 5% (v/v) CO_2 in air. After treatment, the cells were washed three times with DF-10 and allowed to grow for 48 h at 37°C in an atmosphere of 5% (v/v) CO_2 in air. After 48 h, the cardiomyocyte mitochondria were stained with 6 μM JC-1 for 20 min and the fluorescence signals were measured using the fluorescence plate reader. Cells were excited from the bottom at 485/544 nm and green and red fluorescence emissions were collected at 520 and 590 nm. The cells used in this experiment came from three different cardiomyocyte primary cultures that were between 93 and 97% viable. The data represents the average of the three trials combined in Figures 3.11 A, B and C. Each data point is the average of six replicates with the errors displayed as standard errors. * $P \leq 0.05$, ** $P \leq 0.01$, *** $P \leq 0.001$ compared to the untreated cardiomyocyte preparation

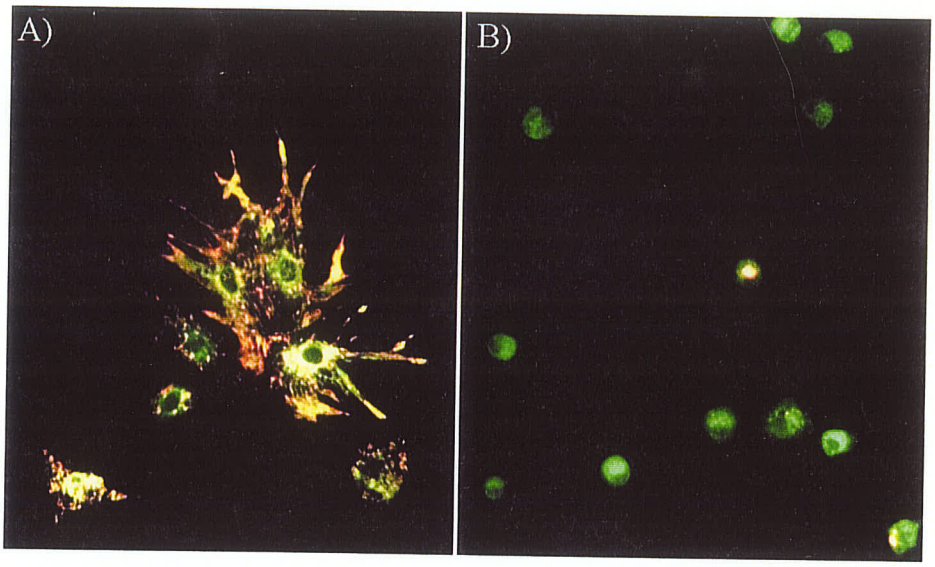

Figure 3.13 Epifluorescence photomicrographs of JC-1 stained cardiomyocyte mitochondria imaged with the 16 X objective following 24 h treatment with or without 1 μM valinomycin. A) control (0.025% (v/v) DMSO with no added valinomycin) and B) 1 μM valinomycin. The cardiomyocyte mitochondria that were not exposed to valinomycin stained mostly red. After 24 h exposure to 1 μM valinomycin, the majority of cardiomyocyte mitochondria stained greened with the occassional spot of red. The density of mitochondria also decreased following valinomycin treatment.

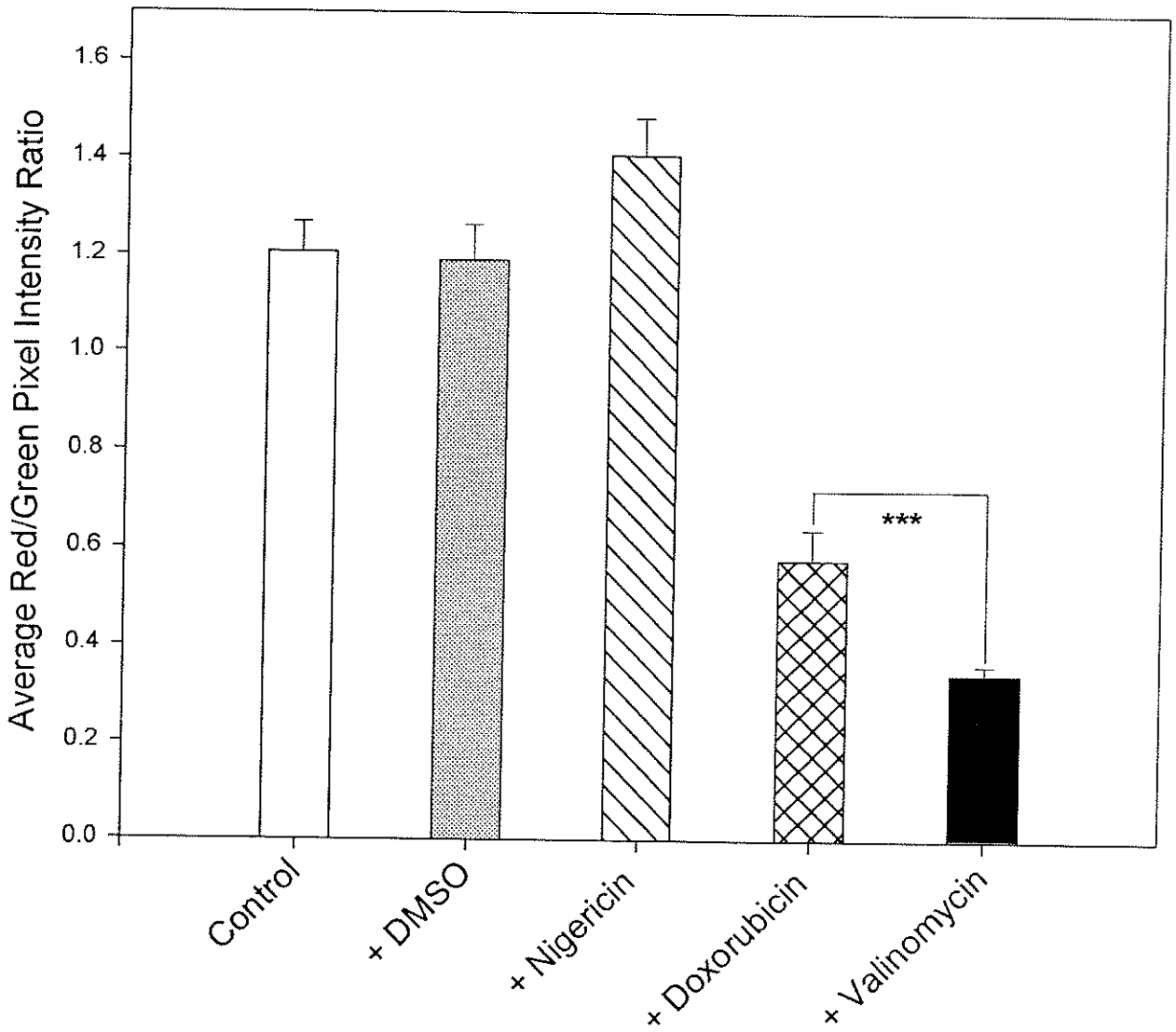

Figure 3.14 Membrane potential changes induced in nigericin-, valinomycin- and doxorubicin-treated cardiomyocyte mitochondria. Cardiomyocytes were seeded at a density of 200,000 cells/ml on 6-well tissue culture plates containing glass cover slips. Three days following isolation, cardiomyocytes were exposed to 0.3 μM doxorubicin for 3 h at 37°C in an atmosphere of 5% (v/v) CO_2 in air. After 3 h, the cells were washed three times with culturing medium (DF-10) and were grown for 48 h at 37°C in an atmosphere of 5% (v/v) CO_2 in air. Four and five days following isolation, cardiomyocytes were incubated with 1 μM valinomycin for 24 h or 0.5 μM nigericin for 1 h, respectively. On day 5, cardiomyocyte mitochondria from all treatments were stained with 6 μM JC-1 for 20 min and imaged with an epifluorescent microscope. The cells used in this experiment came from two myocyte preparations that were greater than 90% viable. Approximately 60 cells were analyzed for each treatment and the error bars represent standard errors. A decrease in the average red/green pixel intensity ratio is indicative of mitochondrial membrane depolarization while an increase signifies mitochondrial membrane hyperpolarization. *** $P \leq 0.001$ compared to one another, the control, DMSO and nigericin

was not significantly higher than the ratio obtained for cardiac myocytes receiving no drug treatment. Nigericin cytotoxicity was apparent and limited the time frame for observing mitochondrial membrane hyperpolarization.

3.3.5 Effect of dexrazoxane on the mitochondrial membrane potential of doxorubicin-treated cardiac myocytes

The effect of dexrazoxane on the mitochondrial membrane potential of doxorubicin-treated cardiac myocytes was investigated by epifluorescence microscopy and the fluorescence plate reader following staining of the mitochondria with JC-1. In the epifluorescence microscopy experiment, the decrease in the average red/green pixel intensity ratio induced in cardiac myocytes grown for 48 h following 3 h exposure to 0.15, 0.2, 0.25, 0.3 and 0.5 μM doxorubicin was prevented by a 3 h pre-exposure to 86 μM dexrazoxane (Figure 3.15). The cardioprotective effect of dexrazoxane was significant when cells were exposed to doxorubicin concentrations 0.2 – 0.5 μM, as cells exposed to dexrazoxane and doxorubicin possessed average red/green pixel intensity ratios that were not different from the dexrazoxane treatment alone. Dexrazoxane did not affect the mitochondrial membrane potential of cardiac myocytes when administered alone and gave an average red/green pixel intensity ratio that was comparable to cardiac myocytes that received no drug treatment.

In the fluorescence plate reader experiments, the effect of 3 h pre-exposure to 86 μM dexrazoxane on the mitochondrial membrane potential of cardiac myocytes incubated for 48 h following 3 h exposure to 0.2, 0.3, 0.5, 1.0 and 2.0 μM doxorubicin was variable with different cell preparations. In Figure 3.16A, dexrazoxane prevention of the doxorubicin-induced drop in the average red/green pixel intensity ratio was present in cardiac myocytes exposed to 0.3 – 2.0 μM doxorubicin. Dexrazoxane did significantly

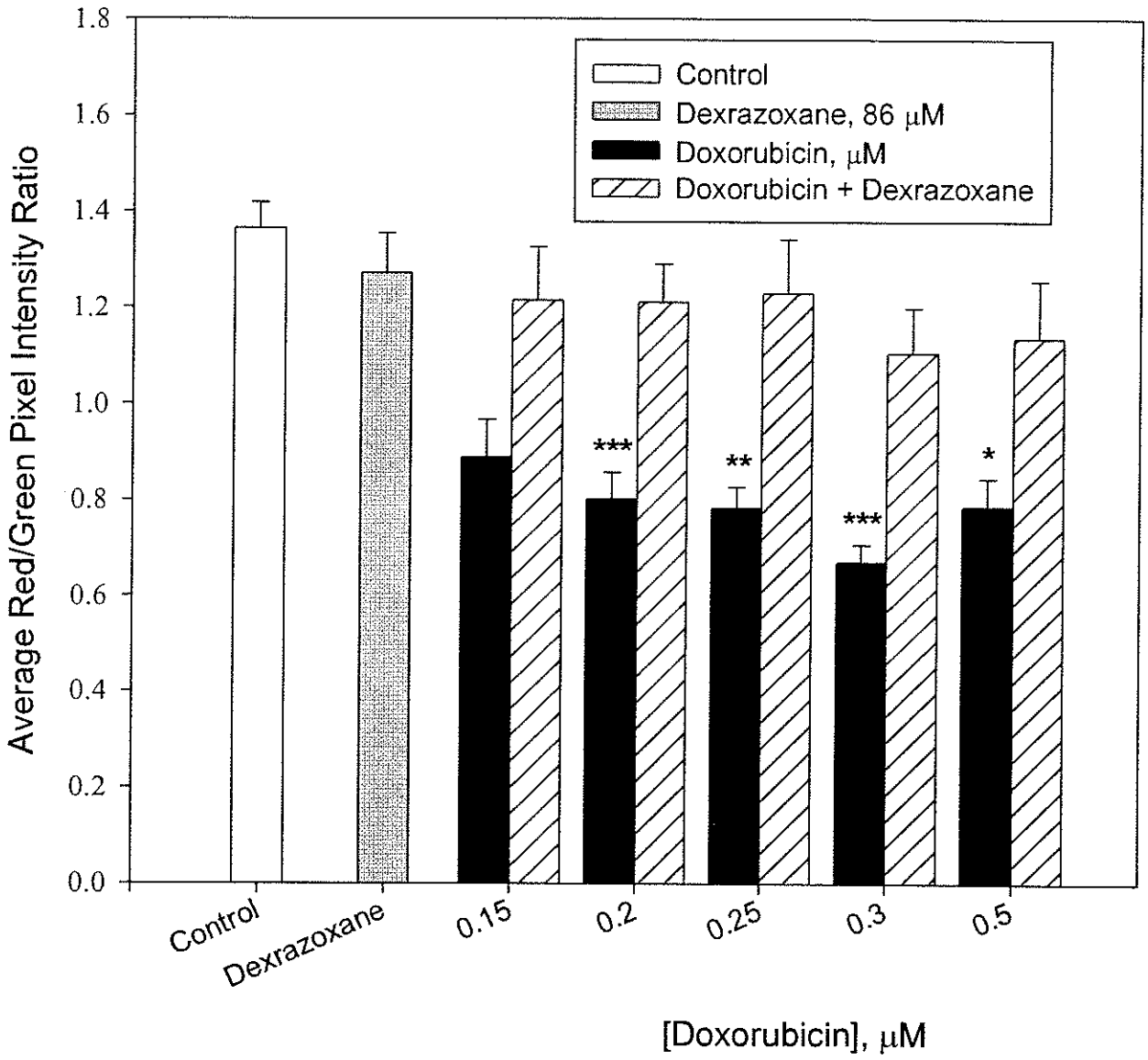

Figure 3.15 Dexrazoxane reduction of doxorubicin-induced mitochondrial membrane depolarization, as measured by epifluorescence microscopy with the JC-1 assay. Cardiomyocytes were pre-exposed to 86 μM dexrazoxane for 3 h followed by treatment with 0.15, 0.2, 0.25, 0.3 and 0.5 μM doxorubicin for 3 h. After drug treatment, the cells were washed three times with culture medium (with or without 86 μM dexrazoxane) and were incubated at 37°C for 48 h. Cardiomyocyte mitochondria were stained with 6 μM JC-1 for 20 min and images were taken with the epifluorescent microscope. The cells used in this experiment came from at least four different cardiomyocyte preparations that were between 86% and 99% viable. For each preparation approximately 80 cells were analyzed per treatment. The error bars represent standard errors of at least four replicated experiments. A decrease in the average red/green pixel intensity ratio is indicative of mitochondrial membrane depolarization. * $P \leq 0.05$, ** $P \leq 0.01$, *** $P \leq 0.005$ compared to the doxorubicin + dexrazoxane treatment

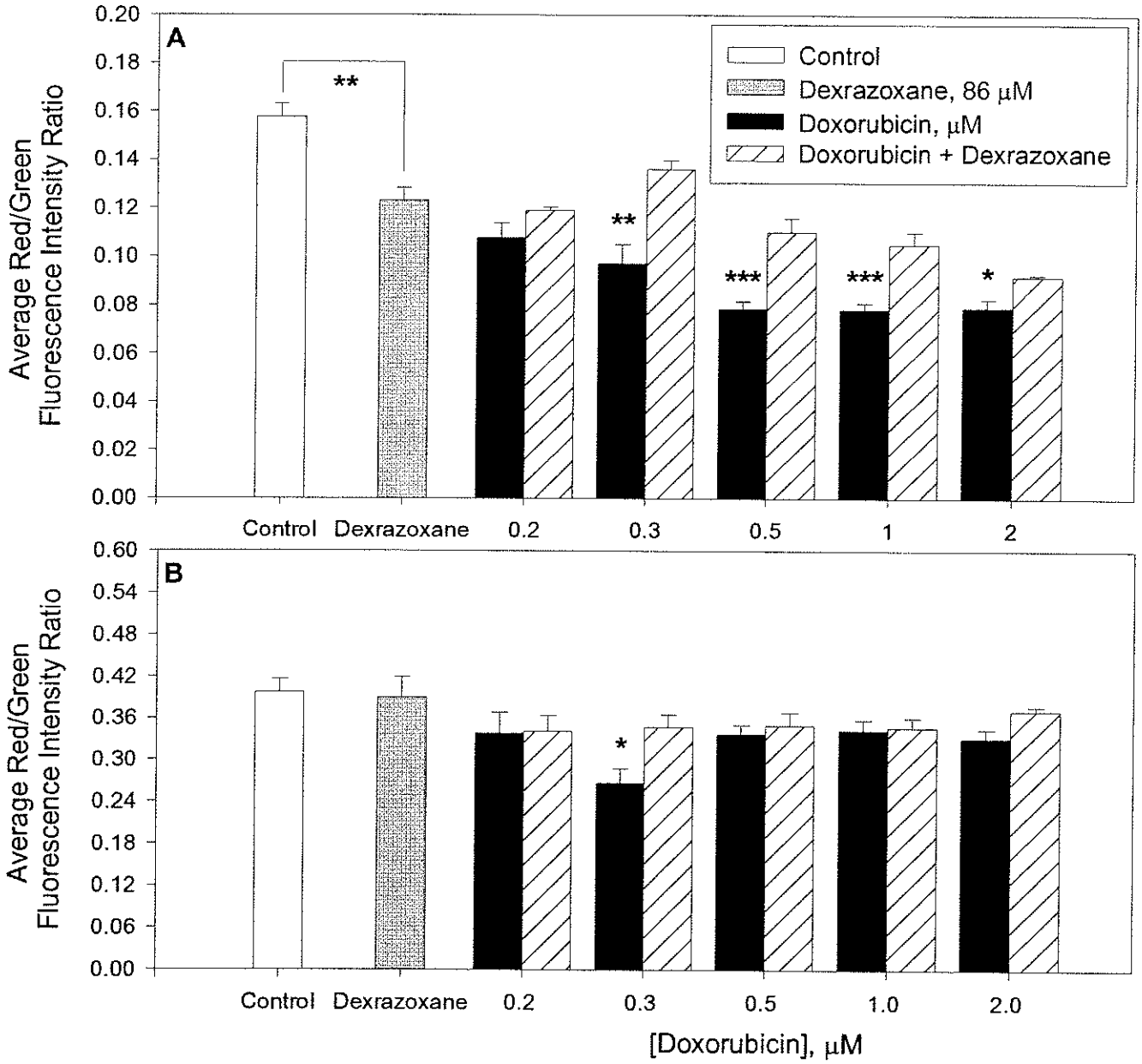

Figure 3.16 Dexrazoxane reduction of doxorubicin-induced mitochondrial membrane depolarization, as measured by the fluorescence plate reader with the JC-1 assay. Cardiomyocytes were seeded at a density of 160,000 cells/well in 200 μl of plating medium. Three days following isolation, the cardiomyocytes were pre-exposed to 86 μM dexrazoxane for 3 h followed by treatment with 0.2, 0.3, 0.5, 1.0 and 2.0 μM doxorubicin for 3 h. After drug treatment, the cells were washed three times with culture medium (with or without 86 μM dexrazoxane) and were allowed to grow at 37°C in an atmosphere of 5% (v/v) CO_2 for 48 h. Cardiomyocyte mitochondria were stained with 6 μM JC-1 for 20 min and the fluorescence was measured with the fluorescence plate reader. Cells were excited at 485/544 nm and green and red fluorescence emissions were collected at 520 and 590 nm, respectively. The cells used in this experiment came from two different cardiomyocyte preparations that were 91% and 93% viable (A and B). Each data point is the average of six replicates with the errors displayed as standard errors. A decrease in the average red/green fluorescence intensity ratio is indicative of mitochondrial membrane depolarization. * $P \leq 0.05$, ** $P \leq 0.01$ *** $P \leq 0.001$ compared to doxorubicin + dexrazoxane treatment

decrease the red/green pixel intensity ratio but all doxorubicin + dexrazoxane ratios were no different from the dexrazoxane alone ratio. However, in Figures 3.16B and 3.17, the doxorubicin-induced drop in the average red/green pixel intensity ratio of cardiac myocytes pre-exposed to dexrazoxane was only prevented at a doxorubicin concentration of 0.3 μM. In contrast to Figure 3.16A, dexrazoxane did not significantly reduce the average red/green pixel intensity ratio when administered alone. However, in combination with doxorubicin, dexrazoxane maintained this ratio and prevented the doxorubicin-induced drop in the average red/green pixel intensity ratio.

3.3.6 Mitochondrial changes associated with doxorubicin treatment and dexrazoxane reduction of mitochondrial damage

To provide biochemical and morphological evidence for doxorubicin-induced mitochondrial damage and protection by dexrazoxane with JC-1 staining, we conducted epifluorescence microscopic examinations on doxorubicin-treated cardiac myocytes with or without continuous exposure to 86 μM dexrazoxane. As depicted in Figure 3.18A, healthy cardiomyocytes contained a high density of elongated, mostly red-stained mitochondria. However, after the cells were grown for 48 h following 3 h exposure to 0.3 and 2.0 μM doxorubicin typical signs of mitochondrial damage were observed. The mitochondrial density was much lower and most of the mitochondria were rounded up, swollen and mostly green-stained (Figure 3.18B and D). In cardiac myocytes exposed to 2.0 μM doxorubicin, the few mitochondria present were compacted together (Figure 3.18D). Doxorubicin-treated mitochondria pre-exposed to 86 μM dexrazoxane for 3 h more closely resembled the healthy control mitochondria morphology (Figure 3.18C). Although a few rounded up, swollen, green mitochondria were identified, the majority of the mitochondria were elongated and red-stained. The density of mitochondria observed

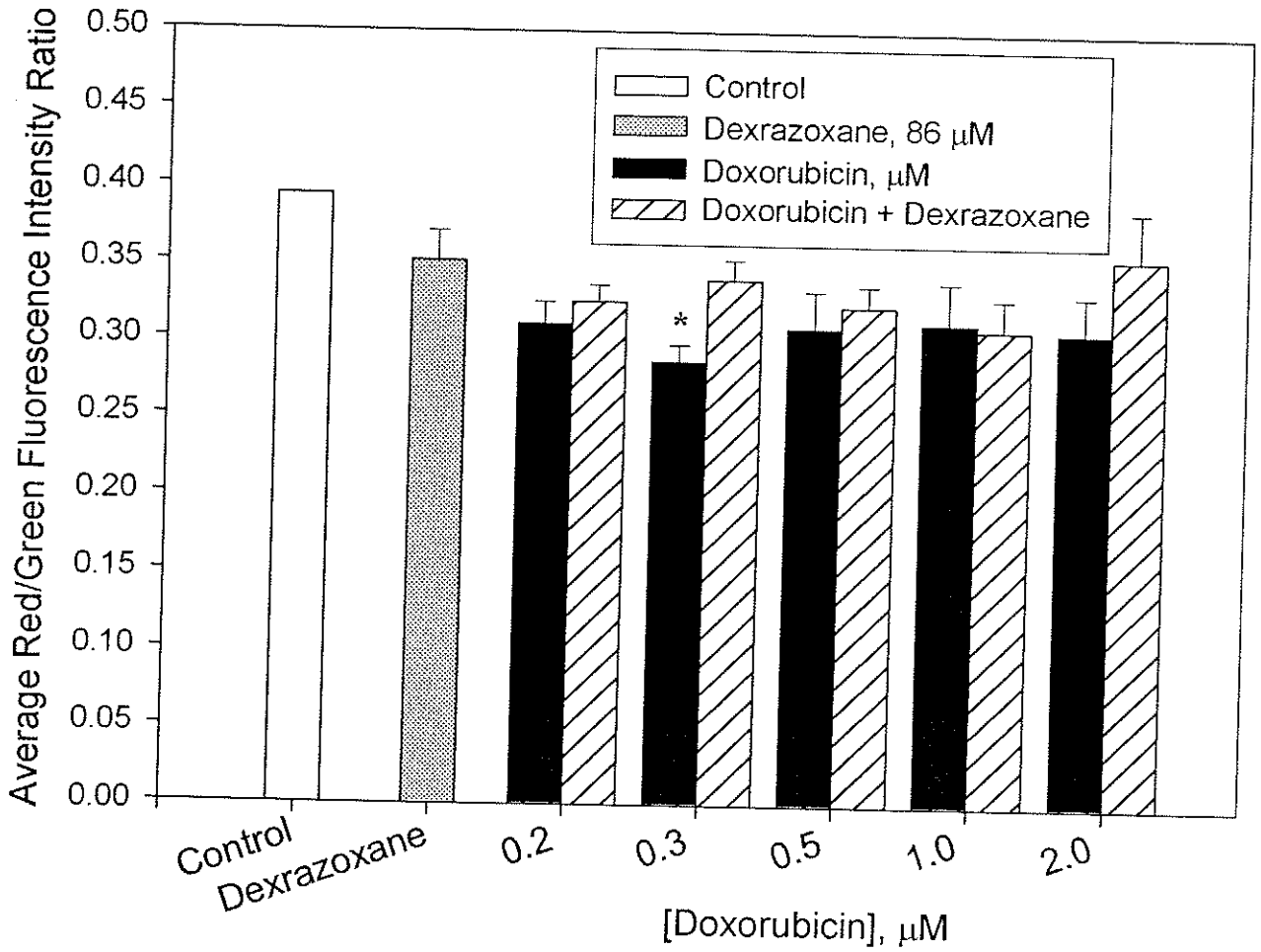

Figure 3.17 Dexrazoxane reduction of doxorubicin-induced mitochondrial membrane depolarization, as measured by the fluorescence plate reader with the JC-1 assay. Cardiomyocytes were seeded at a density of 160,000 cells/well in 200 μl of plating medium. Three days following isolation, the cardiomyocytes were pre-exposed to 86 μM dexrazoxane for 3 h followed by treatment with 0.2, 0.3, 0.5, 1.0 and 2.0 μM doxorubicin for 3 h. After drug treatment, the cells were washed three times with culture medium (with or without 86 μM dexrazoxane) and were allowed to grow at 37°C in an atmosphere of 5% (v/v) CO_2 in air for 48 h. Cardiomyocyte mitochondria were stained with 6 μM JC-1 for 20 min and the fluorescence was measured with the fluorescence plate reader. Cells were excited at 485/544 nm and green and red fluorescence emissions were collected at 520 and 590 nm, respectively. The cells used in this experiment came from two different cardiomyocyte preparations that were 91% and 93% viable. The data is an average of trials A and B in Figure 3.16 with the errors displayed as standard deviations. After statistical analysis, the data was normalized to the control value in Figure 3.16B. A decrease in the average red/green fluorescence intensity ratio is indicative of mitochondrial membrane depolarization. * $P \leq 0.05$ compared to doxorubicin + dexrazoxane treatment

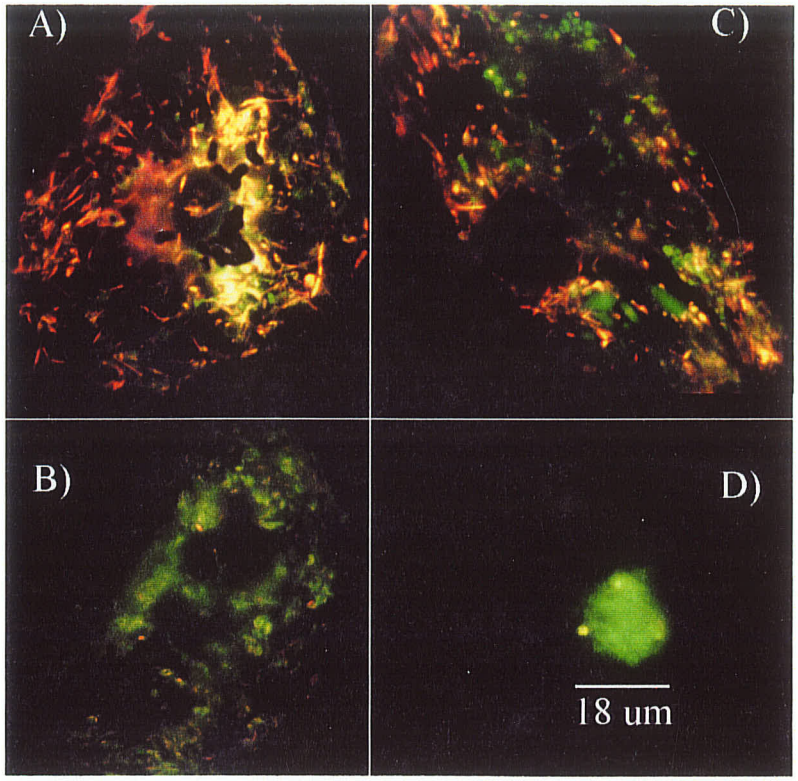

Figure 3.18 Epifluorescence photomicrographs of JC-1 stained cardiomyocyte mitochondria imaged under oil immersion with a 100X objective following doxorubicin treatment in the presence and absence of 86 μM dexrazoxane. Cardiomyocyte mitochondria were stained with 6 μM JC-1 for 20 min, washed three times with Ca^{2+}/Mg^{2+}-containing Hank's buffer and imaged with the epifluorescence microscope. Actively respiring mitochondria stained red while damaged mitochondria stained green. **A)** Untreated cardiomyocyte mitochondria stained mostly red and contained the highest density of elongated mitochondria. **B)** Cells were exposed to 0.3 μM doxorubicin for 3 h, washed three times with culturing medium (DF-10) and allowed to grow for 48 h at 37°C in an atmosphere of 5% (v/v) CO_2. Cardiomyocyte mitochondria stained mostly green, some mitochondria started to round up and the density of mitochondria was lower than the untreated cardiomyocyte preparation. **C)** Cardiomyocyte mitochondria were pre-exposed to 86 μM dexrazoxane for 3 h and then treated with 0.3 μM doxorubicin as discussed in B). Cardiomyocyte mitochondria stained mostly red with a few rounded up green mitochondria. The density of mitochondria was comparable to the untreated cardiomyocyte mitochondria in A). **D)** Cells were exposed to 2.0 μM doxorubicin for 3 h, washed three times with culturing medium (DF-10) and allowed to grow for 48 h at 37°C in an atmosphere of 5% (v/v) CO_2. Cardiomyocyte mitochondria stained green and were rounded up and swollen. The few mitochondria present were compacted together.

appeared to more closely resemble the density of healthy mitochondria that received no drug treatment.

3.4 Discussion

Although mitochondria have been identified to be likely targets for doxorubicin cardiotoxicity, the underlying mechanisms associated with mitochondrial dysfunction and cardiomyocyte death remain unclear [2, 9]. Dexrazoxane is clinically used for the prevention of doxorubicin-induced cardiomyopathy but it is not known whether it confers protection at the level of the mitochondrion. In our study, doxorubicin was shown to collapse the mitochondrial membrane potential and damage the mitochondrial membrane. Using a neonatal rat cardiomyocyte model, we developed an epifluorescence microscopy and fluorescence plate reader method with JC-1 to investigate the cardioprotective effects of dexrazoxane on doxorubicin-induced mitochondrial damage.

The neonatal rat cardiomyocyte model was an excellent model for our cardiotoxicity studies with doxorubicin. As mentioned in Section 3.3.2.2, we chose to use this model because neonatal rat cardiac myocytes possess similar properties to abnormally proliferating heart cells during heart failure [26]. Neonatal rat cardiac myocytes maintain their ability to grow and divide days after isolation [42]. Moreover, the changes in beating rate observed over 48 h with the microscope following 3 h doxorubicin treatment closely resembled the clinical scenario of cancer patients treated with doxorubicin. In doxorubicin-treated cancer patients, tachycardia is an acute effect and early symptom of congestive heart failure, which is often accompanied by arrythmias [31, 43]. In our microscope studies, an increase in beating rate was observed a few hours following doxorubicin treatment. After 24 h, the beating rate suddenly dropped and was

accompanied by arrythmias. Most heart cells stopped beating after 48 h. Thus, the neonatal rat cardiomyocyte model was a very effective model for studying chronic doxorubicin cardiotoxicity and could be applied to pathophysiological and pharmacological heart failure studies.

The changes in heart cell morphology noted during microscopic observation of doxorubicin-treated cells were typical signs of cell damage. After 24 h, the cells exposed to doxorubicin started to round up and become more loosely attached. Apoptotic cells are typically rounded up and studies have shown that doxorubicin can induce cardiomyocyte apoptosis [17, 18, 34, 44, 45]. The cardiac myocytes started to break away from each other after 48 h of doxorubicin treatment. Based on the observation that dense regions of cardiomyocytes beat faster, cardiomyocytes likely need to be in close proximity to each other to function normally and survive. Electrical coupling between cardiac muscle cells is mediated by specialized sites of plasma membrane termed "gap junctions", which link cytoplasmic compartments of neighboring cells and allow direct transfer of small ions and molecules [46]. Gap junctions provide low resistance electrical pathways between cardiac cells, necessary for rapid impulse propagation and thus, coordinate contraction of the myocardium [46]. Several lipophilic compounds have been shown to inhibit gap junctional communication in cultured rat cardiomyocytes [46]. Hence, doxorubicin could be interfering with gap junctional communication pathways essential for normal functioning and survival. The observed cell loss associated with exposure to high doses of doxorubicin is indicative of severe cell damage. It is possible that the pseudopodia required for cell attachment were damaged or that the cells lysed. Lactate dehydrogenase release studies with cardiomyocytes that measure cell membrane integrity have been

done in our lab. Our results have demonstrated that cardiomyocyte lysis is apparent after 48 h exposure to high concentrations of doxorubicin (>0.5 μM). The cell morphology studies with the microscope suggest that doxorubicin cardiomyocyte damage is progressive and dose-dependent.

In the epifluorescence microscopy experiments, mitochondrial membrane depolarization as indicated by a decrease in the red/green pixel intensity ratio, was induced by doxorubicin within 1 h (Figure 3.9). Cardiomyocytes allowed to grow for 48 h in the incubator following 3 h exposure to pharmacological concentrations of doxorubicin also had depolarized mitochondrial membranes (Figure 3.10). Moreover, the degree to which doxorubicin collapsed the mitochondrial membrane potential was dose-dependent and leveled off at doxorubicin concentrations greater than 0.5 μM (Figures 3.9 and 3.10). Doxorubicin fluorescence was not likely responsible for this phenomenon, as doxorubicin fluorescence was negligible in the microscope control experiment (data not shown). However, cell loss at higher concentrations of doxorubicin and the corresponding drop in green fluorescence signal may have been a contributing factor.

In the fluorescence plate reader experiments, depolarization of the mitochondrial membrane potential was also dose-dependent and leveled off at higher doxorubicin concentrations (Figures 3.11 and 3.12). However, the drop in the average red/green fluorescence intensity ratio was less drastic than in the epifluorescence microscopy experiments and in Figures 3.11B and C, the average red/green fluorescence intensity ratio began to rise at doxorubicin concentrations greater than 0.3 μM. The cardiomyocyte preparations were variable in their recovery after isolation and did not grow as well in the crowded 96-well plates as in the 6-well plates. The rise in the red/green fluorescence

intensity ratio could be partially attributed to doxorubicin fluorescence, as the red fluorescence signal generated by JC-1 stained cardiomyocytes was quite small. In contrast to the epifluorescence experiments, cell loss is less likely to have contributed to the rise in the red/green fluorescence intensity ratio, as the green fluorescence signals were similar for all treatments. It was also hypothesized that doxorubicin only partially disrupted the mitochondrial membrane potential and that the leveling off point in the graph was as low as the average red/green ratio could be dropped. To test this hypothesis, we examined the effect of valinomycin on the mitochondrial membrane potential of cardiac myocytes and compared it to that of doxorubicin. Valinomycin is a K^+-selective ionophore, which has been demonstrated in several studies to uncouple oxidative phosphorylation and completely abolish the mitochondrial membrane potential [27-29]. In our study, exposure of cardiac myocytes to 1 μM valinomycin, collapsed the mitochondrial membrane potential (Figure 3.13 and 3.14). Moreover, the average red/green pixel intensity ratio was significantly lower than that of doxorubicin (Figure 3.14). Thus, depolarization of the mitochondrial membrane potential by doxorubicin was not complete but partial.

It was also of interest to us to define the upper value for the average red/green pixel intensity ratio and confirm the hyperpolarization state of our primary culture of neonatal rat cardiomyocytes. In order to achieve our goal, we examined the effect of nigericin on the mitochondrial membrane potential of cardiac myocytes. Nigericin is a polyether ionophore that stimulates ATPase activity and hyperpolarizes the membrane potential [29, 30]. In our study, exposure of cardiac myocytes to 0.5 μM nigericin for 1 h did not significantly increase the average red/green pixel intensity ratio compared to the

control (Figure 3.14). The extreme toxicity of nigericin to the cardiac myocytes made it difficult to time the hyperpolarization event. The cells swelled and vacuolization occurred almost immediately following the hyperpolarization event. Although we were unable to define the upper red/green pixel intensity value, our study does suggest that the neonatal rat cardiomyocyte preparation was at least partially hyperpolarized with actively respiring mitochondria.

Once the appropriate controls were completed and the best doxorubicin concentration range for mitochondrial membrane depolarization was identified, we decided to examine the effects of dexrazoxane on the mitochondrial membrane potential of healthy cardiac myocytes and doxorubicin-treated cardiomyocytes. In the epifluorescence microscopy experiment, dexrazoxane did not affect the mitochondrial membrane potential of healthy cardiomyocytes (Figure 3.15). Moreover, the decrease in the average red/green pixel intensity ratio induced by doxorubicin was prevented by a 3 h pre-exposure to 86 μM dexrazoxane with continuous dexrazoxane exposure during the 48 h growth period (Figure 3.15). In fact, the protection was very efficient, as the average red/green pixel intensity ratio for cardiomyocytes treated with doxorubicin and dexrazoxane was not significantly different from the ratio obtained when dexrazoxane was administered alone (Figure 3.17). As mentioned in Chapter 1, doxorubicin, in its semiquinone free radical and iron-complexed forms is able to generate reactive oxygen species [3, 7, 8]. Its toxicity is quite specific for mitochondria, as the cationic and somewhat lipophilic nature of doxorubicin permits it to accumulate in the more electronegative mitochondria. Several studies also suggest that doxorubicin has a very high affinity for the glycerophospholipid, cardiolipin, which is very abundant in the inner

mitochondrial membrane [1, 2]. The heart is very sensitive to doxorubicin treatment because it is rich in mitochondria that are actively respiring to satisfy the high ATP demanding beating cardiomyocytes [13]. Thus, the antioxidant defense system in the heart is quickly overwhelmed by oxidative stress, as it contains very low antioxidant enzyme activity and a limited capacity to utilize non-protein thiols to protect against oxidative toxicity [2]. A number of studies indicate that these accumulated oxidants are capable of disrupting the mitochondrial membrane potential [17, 36, 37]. The final hydrolysis product of dexrazoxane, ADR-925, has been shown to chelate free iron and displace iron from its complexes with doxorubicin [3]. ADR-925 bound to iron is believed to be less efficient at producing site-specific hydroxyl radical damage [6-8]. Thus, it is proposed in this study that dexrazoxane protects the mitochondria from doxorubicin cardiotoxicity through the ability of its hydrolysis product, ADR-925, to prevent iron-based oxygen free radical damage.

In the fluorescence plate reader experiments, the results were variable depending upon the cardiomyocyte preparation. On average, dexrazoxane did not significantly alter the mitochondrial membrane potential (Figures 3.16B and 3.17), however, in one trial it depolarized the mitochondrial membrane potential (Figure 3.16A). The dose of dexrazoxane used in these experiments was 86 μM. Because we were working at the higher end of the therapeutic window, some cardiotoxicity could be expected [32]. It is also possible that the different cardiomyocyte preparations had varying abilities to metabolize dexrazoxane. Because the dexrazoxane hydrolysis products have different metal-chelating abilities, it could be inferred that their toxicites would also be different [47]. When the trials were averaged together dexrazoxane prevented doxorubicin-induced

depolarization when 0.3 μM doxorubicin was administered (Figure 3.17). However, when the experiments were analyzed separately, the protection appeared to be more promising. In Figure 3.16A, dexrazoxane prevented doxorubicin-induced depolarization when concentrations of 0.3 - 2.0 μM doxorubicin were administered. Moreover, cardioprotection was maintained even when high doses of doxorubicin were administered. Such an observation is very exciting, as the concentration of doxorubicin commonly administered in clinical situations is ~1.0 μM [31]. In Figure 3.16B, protection was observed when 0.3 μM doxorubicin was administered in combination with dexrazoxane to the cardiomyocytes. In this experiment, doxorubicin-induced mitochondrial membrane depolarization was not significant enough at concentrations of 0.2, 0.5, 1.0 and 2.0 μM to protect with dexrazoxane. Cardiomyocyte preparation variability could be a factor affecting the toxicity of doxorubicin.

In order to provide morphological evidence for doxorubicin mitochondrial damage and dexrazoxane protection, epifluorescence microscopy images were taken of JC-1 stained mitochondria that were exposed to doxorubicin in the presence or absence of dexrazoxane. Control cardiomyocytes contained a high density of elongated, mostly red stained mitochondria (Figure 3.18A). Healthy mitochondria are elongated [12] and red staining suggests that the mitochondria were actively respiring (hyperpolarized). Because the membrane potential of control mitochondria was intact, cationic JC-1 readily accumulated in the electronegative mitochondria and formed red fluorescing J-aggregates. However, when cardiomyocytes were exposed to 0.3 or 2.0 μM doxorubicin the density of mitochondria was noticeably less and the mitochondria were rounded-up, swollen and stained mostly green (Figure 3.18B and D). As the mitochondrial membrane

is damaged by doxorubicin and the membrane potential is disrupted, less JC-1 is taken up by mitochondria and green fluorescence of the dye monomers predominates. Thus, the doxorubicin-treated cardiomyocytes that contained green stained mitochondria were depolarized. As mentioned in Section 1.1, mitochondrial membrane depolarization disrupts the mitochondrial membrane potential and interferes with the generation of ATP [48]. Bioenergetic studies with doxorubicin in cardiac myocytes has shown that doxorubicin depletes ATP reserves and disturbs Ca^{2+} homeostasis through interference with the Na^{+}/Ca^{2+} exchanger and Ca^{2+}-ATPase [48]. Disturbances in ionic gradients disrupt organelle volume regulation and promote movement of water into mitochondria. Swelling of mitochondria is a typical morphological feature of mitochondrial damage [12]. Several morphological studies of damaged mitochondria have revealed decreases in mitochondrial mass, accompanied with mitochondrial swelling and a decrease in the length and diameter of the mitochondria [19, 35, 37]. The decrease in mitochondria density could be due to lysis of mitochondria. The few remaining mitochondria in cardiomyocytes exposed to 2.0 μM doxorubicin were compacted together (Figure 3.21 D). It is possible that the cardiomyocytes were apoptotic since cell shrinkage is a well-established feature of apoptosis [34]. Although extensive mitochondrial damage was displayed in cardiomyocytes treated with doxorubicin, doxorubicin-treated cardiomyocytes pre-exposed to dexrazoxane showed attenuated mitochondrial damage. Mitochondrial density was higher and most of the mitochondria were elongated and red stained similar to the healthy control cardiomyocyte mitochondria (Figure 3.21 C). Thus, from the epifluorescence mitochondrial imaging study with JC-1, it is evident that

dexrazoxane not only prevents doxorubicin-induced depolarization of the mitochondrial membrane but also protects the mitochondrial membrane from doxorubicin damage.

After completing the cardiomyocyte mitochondria JC-1 studies with doxorubicin and dexrazoxane using epifluorescence microscopy and the fluorescence plate reader, one can evaluate the methods for quantifying the mitochondrial membrane potential with JC-1. The epifluorescence microscopy method was very effective for the initial development of the mitochondrial membrane potential fluorescence assay. Staining procedures with JC-1 could be easily optimized based on microscopic observations. For example, if the mitochondria stained too dim, one could increase the concentration of JC-1 or the exposure time with JC-1 and clearly see the effect. If there was a precipitate or an intense background fluorescence signal interfering, it could be picked up immediately. The epifluorescence microscope fluorescence assay with JC-1 was also sensitive to relatively small changes in the mitochondrial membrane potential. For instance, in the dose-dependent depolarization experiment with doxorubicin a difference in the average red/green pixel intensity ratio could be deciphered when comparing doses only 0.05 μM apart (Figure 3.10). The average red/green pixel intensity ratios and trends were also quite consistent between the trials performed (data not shown). Moreover, the microscope was a good method for monitoring changes in cardiomyocyte and mitochondria morphology as well as beating rate and cell density. However, the epifluorescence microscopic method did have its drawbacks, particularly in quantifying the fluorescence signal. Cell loss could not be accounted for, photobleaching of JC-1 could have affected the fluorescence signal and bias was a factor in the tedious, time-consuming analysis of JC-1 stained cardiomyocytes with Paint Shop Pro. In contrast to epifluorescence

microscopy, bias was eliminated and JC-1 photobleaching was minimal in the fluorescence plate reader experiments. This method was very rapid and sensitive, as weak fluorescence signals could be amplified by the photomultiplier tube. However, because the cardiomyocyte preparations were so variable between experiments, the sensitivity of this method gave rise to non-reproducible results. Slight differences in cell density or cell viability significantly altered the measured fluorescence signal. Furthermore, cardiomyocyte recovery from isolation and growth was hampered in the crowded 96-well plates and unfortunately limited the reliability of the fluorescence plate reader method for our studies with cardiomyocytes.

3.5 Conclusions

Our studies with cultured neonatal rat cardiomyocytes identified and acknowledged the complexity of environmental factors encountered when working with mammalian cell cultures. The neonatal rat cardiomyocyte model used in our studies was clinically relevant and proved to be an excellent model for studying doxorubicin cardiotoxicity. This model could also be applied to pathophysiological or pharmacological heart failure studies. Two quantitative methods with JC-1 for measuring changes in the mitochondrial membrane potential were also developed that may have future implications in biomedical research. Epifluorescence microscopy proved to be an excellent method for developing fluorescence-based cytotoxicity assays and for monitoring morphological and activity changes in cells while the fluorescent plate reader was very fast and sensitive in its measurements of fluorescence signals. In conjunction, these two methods could be very powerful tools for the development and analysis of fluorescence-based cytotoxicity studies. Our doxorubicin cardiotoxicity studies indicate

that pharmacological concentrations of doxorubicin are able to partially disrupt the mitochondrial membrane potential of cardiomyocytes in a time and dose-dependent manner. Mitochondrial damage was shown to be an early event associated with doxorubicin treatment and was progressive and severe. Our study proposes that dexrazoxane prevents mitochondrial damage induced by doxorubicin possibly through the ability of its hydrolysis product, ADR-925, to prevent iron-based oxygen free radical damage.

3.6 References

1. Saad SY, Najjar TA, Al-Rikabi AC. 2001. The preventive role of deferoxamine against acute doxorubicin-induced cardiac, renal and hepatic toxicity in rats. *Pharmacol Res* 43:211-8.

2. Hershko C, Pinson A, Link G. 1996. Prevention of anthracycline cardiotoxicity by iron chelation. *Acta Haematol* 95:87-92.

3. Malisza KL, Hasinoff BB. 1996. Inhibition of anthracycline semiquinone formation by ICRF-187 (dexrazoxane) in cells. *Free Radic Biol Med* 20:905-14.

4. Buss J, Hasinoff B. 1997. Metal-ion promoted hydrolysis of the antioxidant cardioprotective agent dexrazoxane (ICRF-187) and its one-ring open hydrolysis products to its metal-chelating active form. *J. Inorg. Biochem.* 68:101-108.

5. Hasinoff BB. 1998. Chemistry of dexrazoxane and analogues. *Semin Oncol* 25:3-9.

6. Hasinoff BB. 1995. NADPH-cytochrome-P450 reductase promotes hydroxyl radical production by the iron complex of ADR-925, the hydrolysis product of ICRF-187 (dexrazoxane). *Free Radic Res* 22:319-25.

7. Malisza KL, Hasinoff BB. 1995. Doxorubicin reduces the iron(III) complexes of the hydrolysis products of the antioxidant cardioprotective agent dexrazoxane (ICRF-187) and produces hydroxyl radicals. *Arch Biochem Biophys* 316:680-8.

8. Malisza KL, Hasinoff BB. 1995. Production of hydroxyl radical by iron(III)-anthraquinone complexes through self-reduction and through reductive activation by the xanthine oxidase/hypoxanthine system. *Arch Biochem Biophys* 321:51-60.

9. Miura T, Muraoka S, Ogiso T. 1995. Adriamycin-Fe3+-induced mitochondrial protein damage with lipid peroxidation. *Biol Pharm Bull* 18:514-7.

10. Voet D, Voet J: Biochemistry. Toronto, Ontario, John Wiley & Sons Inc., 1995.

11. Lawrence JW, Claire DC, Weissig V, Rowe TC. 1996. Delayed cytotoxicity and cleavage of mitochondrial DNA in ciprofloxacin- treated mammalian cells. *Mol Pharmacol* 50:1178-88.

12. Rubin E: Essential Pathology. Philadelphia, PA, Lippencott Williams and Wilkins, 2001.

13. Myers C. 1998. The role of iron in doxorubicin-induced cardiomyopathy. *Semin Oncol* 25:10-4.

14. Mathur A, Hong Y, Kemp BK, Barrientos AA, Erusalimsky JD. 2000. Evaluation of fluorescent dyes for the detection of mitochondrial membrane potential changes in cultured cardiomyocytes. *Cardiovasc Res* 46:126-38.

15. Reers M, Smiley ST, Mottola-Hartshorn C, Chen A, Lin M, Chen LB. 1995. Mitochondrial membrane potential monitored by JC-1 dye. *Methods Enzymol* 260:406-17.

16. Nuydens R, Novalbos J, Dispersyn G, Weber C, Borgers M, Geerts H. 1999. A rapid method for the evaluation of compounds with mitochondria- protective properties. *J Neurosci Methods* 92:153-9.

17. Roberg K, Johansson U, Ollinger K. 1999. Lysosomal release of cathepsin D precedes relocation of cytochrome c and loss of mitochondrial transmembrane potential during apoptosis induced by oxidative stress. *Free Radic Biol Med* 27:1228-37.

18. Scheffler I. 2000. A century of mitochondrial research:achievements and perspectives. *Mitochondrion* 1:3-31.

19. Virag L, Salzman AL, Szabo C. 1998. Poly(ADP-ribose) synthetase activation mediates mitochondrial injury during oxidant-induced cell death. *J Immunol* 161:3753-9.

20. Haugland R: Handbook of Fluorescent Probes and Research Chemicals. Eugene, Oregon, Molecular Probes, 1996.

21. Bernardi P, Petronilli V, Di Lisa F, Forte M. 2001. A mitochondrial perspective on cell death. *Trends Biochem Sci* 26:112-7.

22. Keij JF, Bell-Prince C, Steinkamp JA. 2000. Staining of mitochondrial membranes with 10-nonyl acridine orange, MitoFluor Green, and MitoTracker Green is affected by mitochondrial membrane potential altering drugs. *Cytometry* 39:203-10.

23. Salvioli S, Ardizzoni A, Franceschi C, Cossarizza A. 1997. JC-1, but not DiOC6(3) or rhodamine 123, is a reliable fluorescent probe to assess delta psi changes in intact cells: implications for studies on mitochondrial functionality during apoptosis. *FEBS Lett* 411:77-82.

24. Berne R, Levy M: Principles of Physiology. Toronto, Ontario, Mosby-Year Book Inc., 1996.

25. Reers M; Smith TW, Chen LB. 1991. J-aggregate formation of a carbocyanine as a quantitative fluorescent indicator of membrane potential. *Biochemistry* 30:4480-6.

26. Anversa P, Kajstura J. 1998. Ventricular myocytes are not terminally differentiated in the adult mammalian heart. *Circ Res* 83:1-14.

27. Heerdt B, Houston M, Anthony G, Augenlicht L. 1998. Mitochondrial membrane potential in the coordination of p53-independent proliferation and apoptosis pathways in human colonic carcinoma cells. *Cancer Research* 58:2869-2875.

28. Heerdt B, Houston M, Anthony G, Augenlicht L. 1999. Initiation of growth arrest and apoptosis of MCF-7 mammary carcinoma cells by tributyrin, a triglyceride analogue of the short-chain fatty acid butyrate, is associated with mitochondrial activity. *Cancer Research* 59:1584-1591.

29. Heerdt B, Houston M, Mariadson J, Augenlicht L. 2000. Dissociation of staurosporine-induced apoptosis from G2-M arrest in SW620 human colonic carcinoma cells: Initiation of the apoptotic cascade is associated with elevation of the mitochondrial membrane potential. *Cancer Research* 60:6704-6713.

30. Varnes ME, Clay ME, Freeman K, Antunez AR, Oleinick NL. 1990. Enhancement of photodynamic cell killing (with chloroaluminum phthalocyanine) by treatment of V79 cells with the ionophore nigericin. *Cancer Res* 50:1620-5.

31. Singal PK, Iliskovic N, Li T, Kumar D. 1997. Adriamycin cardiomyopathy: pathophysiology and prevention. *Faseb J* 11:931-6.

32. Wiseman L, Spencer C. 1998. Dexrazoxane:A review of its use as a cardioprotective agent in patients receiving anthracycline-based chemotherapy. *Drugs* 56:385-403.

33. Hasinoff B. 1994. Pharmacodynamics of the hydrolysis-activation of the cardioprotective agent (+)-1,2-bis93,5-dioxopiperazinyl-l-yl)propane. *J. Pharm. Sci.* 83:64-67.

34. Cossarizza A, Franceschi C, Monti D, Salvioli S, Bellesia E, Rivabene R, Biondo L, Rainaldi G, Tinari A, Malorni W. 1995. Protective effect of N-acetylcysteine in tumor necrosis factor-alpha- induced apoptosis in U937 cells: the role of mitochondria. *Exp Cell Res* 220:232-40.

35. Mancini M, Sedghinasab M, Knowlton K, Tam A, Hockenbery D, Anderson BO. 1998. Flow cytometric measurement of mitochondrial mass and function: a novel method for assessing chemoresistance. *Ann Surg Oncol* 5:287-95.

36. Scanlon JM, Reynolds IJ. 1998. Effects of oxidants and glutamate receptor activation on mitochondrial membrane potential in rat forebrain neurons. *J Neurochem* 71:2392-400.

37. Shenker BJ, Guo TL, O I, Shapiro IM. 1999. Induction of apoptosis in human T-cells by methyl mercury: temporal relationship between mitochondrial dysfunction and loss of reductive reserve. *Toxicol Appl Pharmacol* 157:23-35.

38. Burchiel S, Lauer F, Gerule D, Mounho B, Salas V. 1999. Uses and future applications of flow cytometry in immunotoxicity testing. *Methods* 19:28-35.

39. Periasamy A. 2001. Fluorescence resonance energy transfer microscopy:a mini review. *J Biomed Opt* 6:287-291.

40. Wang H, Joseph J. 1999. Quantifying cellular oxidative stress by dichlorofluorescein assay using microplate reader. *Free Radical Biology and Medicine* 27:612-616.

41. www.roperscientific.com, Roper Scientific.

42. Tseng Y, Kopel R, Stabil J, McGonnigal B, Nguyen T, Gruppuso P, Padbury J. 2001. Cardiomyocyte development switches from hyperplasmic to hypertrophic growth between postnatal days 3 and 4 in rats. *FASEB J* 15:1921-1926.

43. Vinita B, Nahata M. 2000. Cardiotoxicity of chemotherapeutic agents:Incidence, treatment and prevention. *Drug Safety* 22:263-302.

44. Wang L, Ma W, Markovich R, Chen JW, Wang PH. 1998. Regulation of cardiomyocyte apoptotic signaling by insulin-like growth factor I. *Circ Res* 83:516-22.

45. Yue TL, Wang C, Gu JL, Ma XL, Kumar S, Lee JC, Feuerstein GZ, Thomas H, Maleeff B, Ohlstein EH. 2000. Inhibition of extracellular signal-regulated kinase enhances Ischemia/Reoxygenation-induced apoptosis in cultured cardiac myocytes and exaggerates reperfusion injury in isolated perfused heart. *Circ Res* 86:692-9.

46. Verrecchia F, Herve J. 1997. Reversible inhibition of gap junctional communication elicited by several classes of lipophilic compounds in cultured rat cardiomyocytes. *Can J Cardiol* 13:1093-1100.

47. Buss J, Hasinoff B. 1993. The one-ring open hydrolysis product intermediates of the cardioprotective agent ICRF-187 (dexrazoxane) displace iron from iron-anthracycline complexes. *Agents Actions* 40:86-95.

48. Zhou S, Heller L, Wallace K. 2001. Interference with calcium-dependent mitochondrial bioenergetics in cardiac myocytes isolated from doxorubicin-treated rats. *Toxicol Appl Pharmacol* 175:60-67.

49. Sparano J, Speyer J, Gradishar W. 1999. Phase I trial of escalating doses of paclitaxel plus doxorubicin and dexrazoxane in patients with advanced breast cancer. *J Clin Oncol* 17:880-886.

Chapter 4 An epifluorescent microscopic method with 2',7'-dichlorofluorescin for measuring oxidative stress in cardiac myocytes and dexrazoxane cardioprotection against doxorubicin-induced generation of reactive oxygen species

4.1 Introduction

The range of pathophysiological and physiological phenomena that implicate reactive oxygen species as mediators of injury or as second messengers continues to expand. Today, a role for oxidative stress has been associated with the regulation of vascular tone, chemical toxicity, apoptosis, aging, ischemia-reperfusion injury, inflammation, neuromuscular diseases, cancer, atherosclerosis and many other processes [1-10]. In order to understand the mechanisms underlying these processes involving reactive oxygen species and to implement treatment or prevention, an analytical method for quantifying and evaluating oxidative stress in living cell models is very important. Although there are various methods to assess oxidative damage of cells, such as measuring lipid peroxidation products and DNA adducts, few of them evaluate oxidative stress directly [9, 11]. The most frequently used method for directly quantifying reactive oxygen species generation is electron paramagnetic resonance spectroscopy [6, 10, 12]. However, this method requires excessively high levels of oxidants to generate measurable levels of reactive oxygen species and some reactive oxygen species are not free radicals such as hydrogen peroxide [6]. Other free radicals are extremely reactive (e.g., OH radicals) while others (superoxide) are very difficult to detect directly under physiological conditions. Moreover, electron paramagnetic resonance spectroscopy appears to be particularly troublesome for studying cardiomyocytes. As identified in Chapter 3, cardiomyocytes are very sensitive to their environment and loading them into a narrow electron paramagnetic resonance tube would likely damage the cells and drop

their cell viability even before experiments could be started. Furthermore, studies on cardiomyocytes are more clinically relevant when the cardiomyocyte preparations are adherent, beating and communicating with one another rather than drifting in suspension.

Recently, fluorescent, chemiluminescent and chromogenic probes have been used extensively to monitor oxidative activity in cells. One of the most popular approaches involves the use of chemically reduced non-fluorescent forms of highly fluorescent dyes such as fluorescein. Upon reaction with oxidizing species, these reduced compounds are oxidized back to the parent dye molecule, resulting in a dramatic increase in fluorescence intensity. A measurement of oxidation of 2',7'-dichlorofluorescin is a popular and well-established method for measuring cellular reactive oxygen species production [6, 7, 9-16]. The use of 2',7'-dichlorofluorescin (DCFH) for this purpose is shown in Figure 4.1. The lipophilic, diacetate ester of 2',7'-dichlorofluorescin (DCFH-DA) is added to cells where it rapidly diffuses across the cell membrane and is hydrolyzed by intracellular esterases to 2',7'-dichlorofluorescin (DCFH), which yields the highly green fluorescent 2',7'-dichlorofluorescein (DCF) upon oxidation. Oxidation of 2',7'-dichlorofluorescin has been achieved by reaction with hydrogen peroxide in the presence of peroxidase, cytochrome *c* or Fe^{2+} [9-13, 15]. Localization studies in isolated cardiomyocytes have shown that 2',7'-dichlorofluorescin and DCF localize mainly in mitochondria [16].

Many studies have used fluorescence microscopy to measure oxidative stress in cells using 2',7'-dichlorofluorescin [6, 7, 14]. However, this method has been limited due to photochemical oxidation of 2',7'-dichlorofluorescin to fluorescing DCF [9]. A method for reducing the time of light exposure when imaging cells under the microscope is

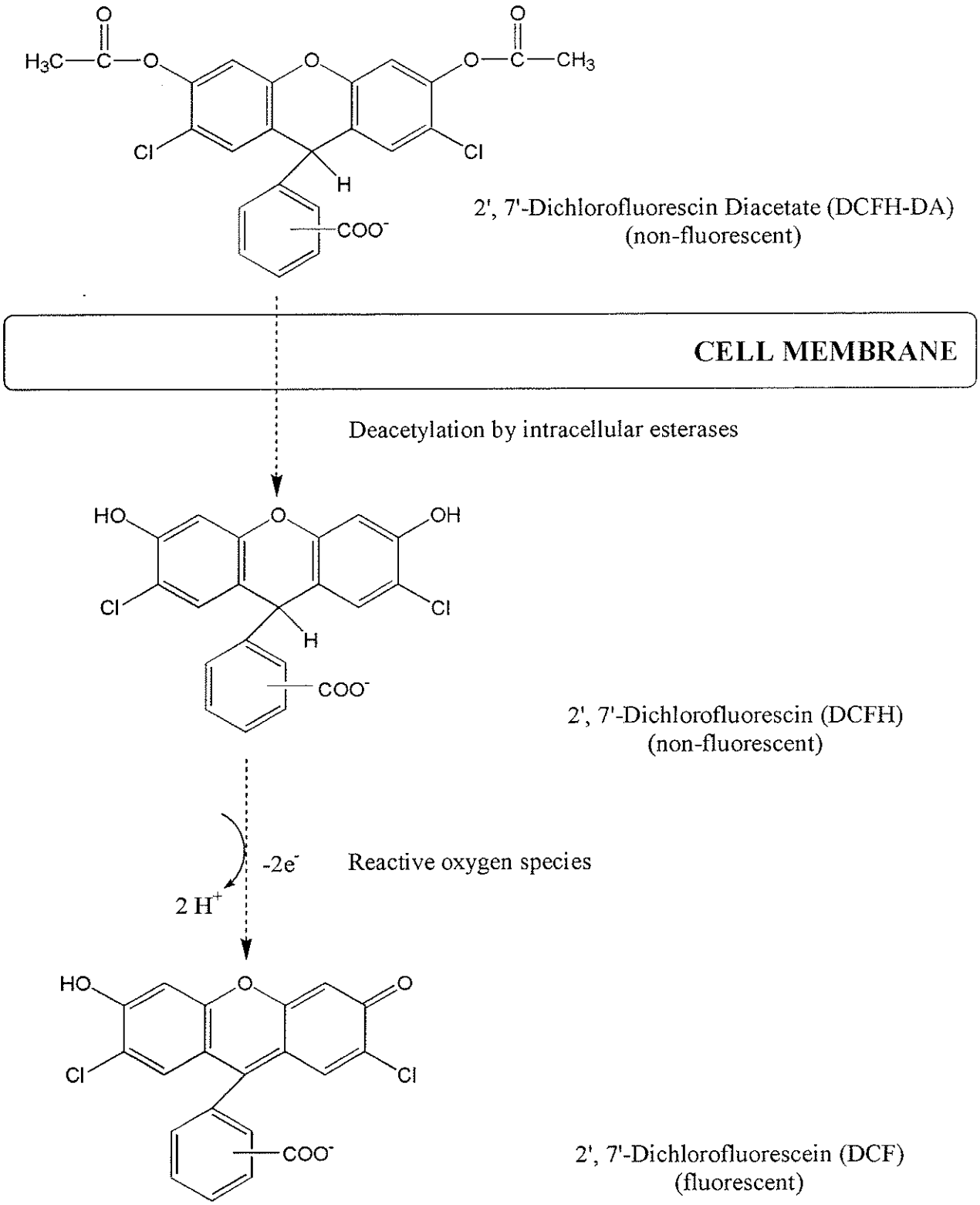

Figure 4.1 Proposed mechanism of entry of DCFH-DA into cells. After DCFH-DA crosses the cell membrane, it is deesterified to DCFH, which is oxidized to fluorescent DCF by reactive oxygen species [11], pg 228.

required. There is also need for a standard method for quantifying oxidative stress with the microscope [9]. The present study contributes to the development of an improved fluorescence microscopy method with 2',7'-dichlorofluorescin by revealing oxidative stress associated with doxorubicin exposure in isolated neonatal rat cardiac myocytes.

Doxorubicin is an anthracycline antibiotic with broad-spectrum activity and high potency against human malignant neoplasms. However, its use is limited due to a severe cardiotoxicity that promotes the rapid development of cardiomyopathy and heart failure. A considerable body of evidence suggests that this cardiotoxicity is mainly attributed to an iron-dependent, oxygen free radical-derived oxidative stress on the relatively unprotected cardiac muscle [17-20]. According to our study in Chapter 3, doxorubicin was able to disrupt the mitochondrial membrane potential and damage the mitochondrial membrane. A number of studies suggest that reactive oxygen species are also capable of damaging the mitochondrial membrane and disrupting the mitochondrial membrane potential [1, 8, 16, 21-24]. In the previous chapter, the iron-chelating drug, dexrazoxane was shown to prevent mitochondrial membrane potential disruption and mitochondrial damage induced by doxorubicin. In view of these considerations, it is reasonable to assume that dexrazoxane treatment may limit mitochondrial damage and the cardiotoxicity of doxorubicin by preventing the participation of intracellular iron with doxorubicin in free radical generation.

In this study, the oxidant-sensitive probe 2',7'-dichlorofluorescin was used to develop and evaluate an epifluorescence microscopy method for quantifying reactive oxygen species generation in neonatal rat cardiac myocytes. Once the procedures for probe loading, cell attachment and quantification of the fluorescence signal were

optimized, this method was employed to examine the effect of dexrazoxane on doxorubicin-induced generation of reactive oxygen species in neonatal rat cardiac myocytes.

4.2 Materials

Dexrazoxane hydrochloride (Zinecard®, ICRF-187) was a gift from Pharmacia & Upjohn (Columbus, OH) and doxorubicin hydrochloride was a gift from Adria-SP Inc. (Columbus, OH). Hydrogen peroxide (H_2O_2, 30 wt % in H_2O, cat No. 21,676-3) was obtained from Aldrich Chemical Company Inc. (Milwaukee, Wis). 2',7'-Dichlorofluorescin (cat No. D-6883), poly-l-lysine hydrochloride (cat No. P-2658), trypan blue dye (cat No. T-6146) and HEPES (cell culture grade, cat No. H-9136) were purchased from Sigma Chemical Co. (St. Louis, MO). Sodium bicarbonate ($NaHCO_3$, cat. No. BP328-079), pre-cleaned microscope slides (cat No. 12-550A), preferred glass cover slips (cat. No. 12-545-85) and magnesium sulfate ($MgSO_4$) were obtained from Fisher Scientific (Fairlawn, NJ). Dulbecco's phosphate buffered saline (PBS, cat No. D-5652), Dulbecco's modified Eagle medium/F12 (DMEM/F-12, cat No. 12500-062), penicillin-streptomycin (cat No. 25200-072), fetal calf serum (FCS, cat No. 26140-079), horse serum (cat No. 16050-122) and Hank's buffered salt solution (HBSS, without Ca^{2+} or Mg^{2+}, cat No. H-4891) were ordered from Gibco-BRL Life Technologies Inc. (Burlington, ON). D-glucose was supplied by Anala R (Toronto, ON) while calcium chloride ($CaCl_2$, cat No. AC-1946) was obtained from Anachemia Ltd. (Montreal, QB). Five molar HCl (cat No. LC15360-2) was purchased from LabChem Inc. (Pittsburgh, PA) and Microfine pH paper was obtained from (Micro Essential Laboratory, Brooklyn, NY). Six-well flat bottom tissue culture plates (cat No. 83.1839) and 0.2 μm acetate

syringe filters (cat No. 83.1826.001) were ordered from Sarstedt Inc. (St. Leonard, PQ). Falcon 3025 tissue culture plates and 40 μm cell strainers were obtained from Becton Dickensson (Lincoln Park, NJ). Deoxyribonuclease I (DNAse, cat No. 2139), trypsin (cat No. 3703) and collagenase (cat No. 4176) were obtained from Worthington Biochemical Corporation (Lakewood, NJ). Cell culture media and buffers were prepared in reverse osmosis distilled water and cardiomyocyte cultures were grown in a 37°C incubator in an atmosphere of 5% (v/v) CO_2 in air. Microscopy studies were carried out with a Zeiss epifluorescence microscope (Roper Scientific, Trenton, NJ) equipped with a high resolution, cooled color digital (CCD) camera, a camera coupler (Diagnostic Instruments Inc., Sterling Hts., Ml) and a fluorescein filter set (XF-115, Omega Optical, Brattleboro, Vermount). Images were acquired with Photometrics Cool Snap acquisition software (Version 1.2, Roper Scientific, Trenton, NJ) and were analyzed with Scion Image imaging software (Version 4.02, Scion Corporation, Frederick, Maryland).

4.3 Methods

4.3.1 Cell culture

4.3.1.1 Isolation of neonatal rat cardiomyocytes and determination of cell viability and cell density

As described in Section 3.3.2.2, a primary culture of neonatal rat cardiomyocytes was prepared and used as the model for doxorubicin cardiotoxicity studies. Cell viability and cell density was calculated as described in Section 3.3.2.3.

4.3.1.2 Treatment of glass cover slips with poly-l-lysine

Before the cells were seeded onto 6-well plates containing sterilized, preferred glass cover slips, the cover slips were treated with poly-l-lysine hydrochloride to improve cardiomyocyte attachment. The positively charged amino groups of lysine attract the

negatively charged cells to the glass surface. A structure of poly-l-lysine is shown in Figure 4.2. A 0.3 mg/ml poly-l-lysine hydrochloride solution was prepared in H_2O and filter sterilized through a 0.2 μm sterile cellulose acetate syringe filter. Each cover slip was coated with 400 μl of poly-l-lysine for 30 min at room temperature. After 30 min, the cover slips were washed three times with 2.0 ml of H_2O and allowed sufficient time to dry.

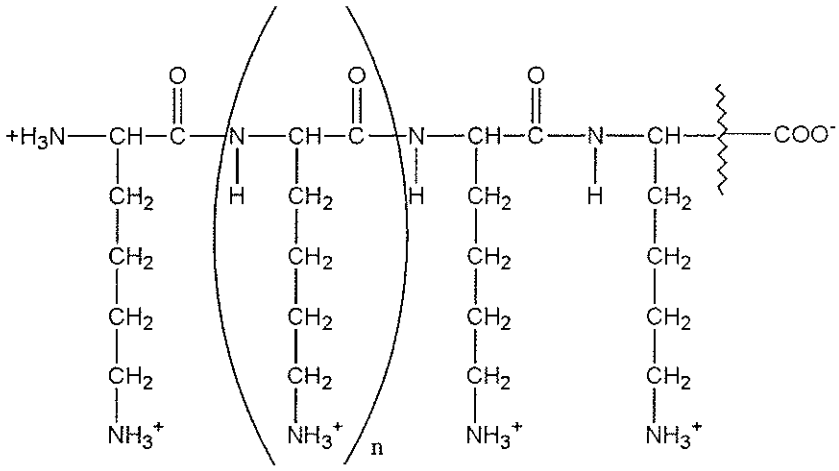

Figure 4.2 Chemical structure of poly-l-lysine.

4.3.1.3 Seeding cells

Cells were seeded in sterile 6-well plates containing poly-l-lysine treated glass cover slips at a density of 200,000 cells per well in 2 ml of plating medium. Details of the seeding process are outlined in Section 3.3.2.4.

4.3.1.4 Culturing cells

Forty-eight hours following seeding, cells were transferred from plating medium into culturing medium (DF-10) and were grown in an atmosphere of 5% (v/v) CO_2 in air at 37°C. All experiments were performed on cultures four days following isolation. On

these days, approximately 80% of the cells had recovered from the isolation and were beating.

4.3.2 Loading cells with 2', 7' –dichlorofluorescin

To study the effect of doxorubicin on intracellular oxidant production, cardiomyocytes were loaded with 2',7'-dichlorofluorescin. A 10 mM stock solution of 2',7'-dichlorofluorescin diacetate was prepared daily in 100% ethanol, wrapped in aluminum foil, kept on ice and diluted in Ca^{2+}/Mg^{2+}-containing Hank's buffer to 10 μM just before experiments. Before probe loading, the cells were transferred into Ca^{2+}/Mg^{2+} (1.3/0.8 mM)-containing Hank's buffer (pH 7.4) to equilibrate the cells to room temperature. Cells were loaded with the probe by incubating the cells at room temperature in the dark with 10 μM 2',7'-dichlorofluorescin diacetate. After 20 min of incubation, the cells were washed twice with Ca^{2+}/Mg^{2+}-containing Hank's buffer (pH 7.4) to remove the extracellular probe and were transferred into DMEM F-12 (serum free media) for hydrogen peroxide and drug treatment.

4.3.3 Drug delivery

A 30% (w/v) solution of hydrogen peroxide was serially diluted with H_2O to 50 μM immediately before experiments. As discussed in section 1.2.2.2, hydrogen peroxide can produce the highly reactive hydroxyl radical in the Fenton reaction with ferrous iron and was chosen to serve as a control for iron-based oxidative stress. Doxorubicin and dexrazoxane stocks were prepared as detailed in section 3.3.3. Controls for cell fluorescence and doxorubicin fluorescence at all three concentrations (10, 50 and 100 μM) were also included as was a dexrazoxane control to assure that dexrazoxane did not significantly alter intracellular oxidant production. Cardiac myocytes were pre-exposed to

86 μM dexrazoxane for 1 h followed by treatment with doxorubicin (10, 50 and 100 μM) or hydrogen peroxide (50 μM) for 20 min and 1 h, respectively. Incubations with hydrogen peroxide, doxorubicin and dexrazoxane were done at 37°C in an atmosphere of 5% (v/v) CO_2 in air. After hydrogen peroxide and drug treatment, the 2',7'-dichlorofluorescin-loaded cells were washed three times with Ca^{2+}/Mg^{2+}-containing Hank's buffer and imaged with the epifluorescence microscope.

4.3.4 Epifluorescence microscope imaging and analysis

Procedures for mounting cover slips and imaging were previously discussed in section 3.3.5. Before the cells were imaged, a camera calibration was completed. Any camera dark noise was accounted for during camera calibration and was subtracted off of the other images. Cells were observed at 16X objective with a Zeiss epifluorescence microscope equipped with a cooled color digital (CCD) camera. Bright field images were acquired first with an exposure time of 0.5 s. Excitation of 2',7'-dichlorofluorescin was achieved by selecting the appropriate band of light from the mercury lamp beam with the fluorescein filter set. Fluorescent images were acquired with an exposure time of 1 s. Imaging was done quickly in the dark and the shutter was kept closed between images to limit any photooxidation of 2',7'-dichlorofluorescin. For each treatment, approximately 9-10 images were taken. On average, each field contained 6 cells.

Images of DCF fluorescing cardiomyocytes were analyzed by redirected sampling using Scion Image imaging software (Version 4.02, Scion Corporation, Frederick, Maryland). The brightfield image with its corresponding fluorescent image was loaded into Scion Image. The images were loaded as a 3-color stack with red on top, green in the middle and blue on the bottom. The image with the best resolution was selected from the

stack. Individual cells on the bright field image were selected with the outline tool with the corresponding green DCF fluorescent image opened below it on the stack of windows. Selecting on the brightfield image allows for measurement on the fluorescent image. The mean DCF fluorescence intensity and area for each cell was determined by choosing "measure" from the analyze menu. All determined values were pasted into a Microsoft Excel spreadsheet and mean DCF fluorescence intensities, average cell areas and relative DCF fluorescence intensity per area values were calculated for approximately 60 outlined cells per treatment.

4.3.5 Statistical analysis

Where indicated, levels of statistical significance were determined with SigmaStat statistical software (Version 2.0, Jandel Scientific, San Rafael, CA) using the Student's *t*-test. A P value below 0.05 was considered significant.

4.4 Results

4.4.1 Effect of doxorubicin on myocyte area and 2',7'-dichlorofluorescin oxidation in cardiomyocytes

The effect of doxorubicin on myocyte area and 2',7'-dichlorofluorescin oxidation was assessed in 2',7'-dichlorofluorescin-loaded neonatal rat cardiomyocytes by epifluorescence microscopy. Following 20 min incubation of cardiomyocytes at 37°C with doxorubicin concentrations of 10, 50 and 100 μM, doxorubicin enhanced 2',7'-dichlorofluorescin oxidation to DCF in comparison to untreated cardiomyocytes, as indicated by a significant increase in mean DCF fluorescence intensity (Figures 4.3 and 4.4). A significant reduction in cell area upon exposure to 10 and 50 μM doxorubicin was also observed (Figure 4.5). Moreover, the relative DCF fluorescence intensity/cell area

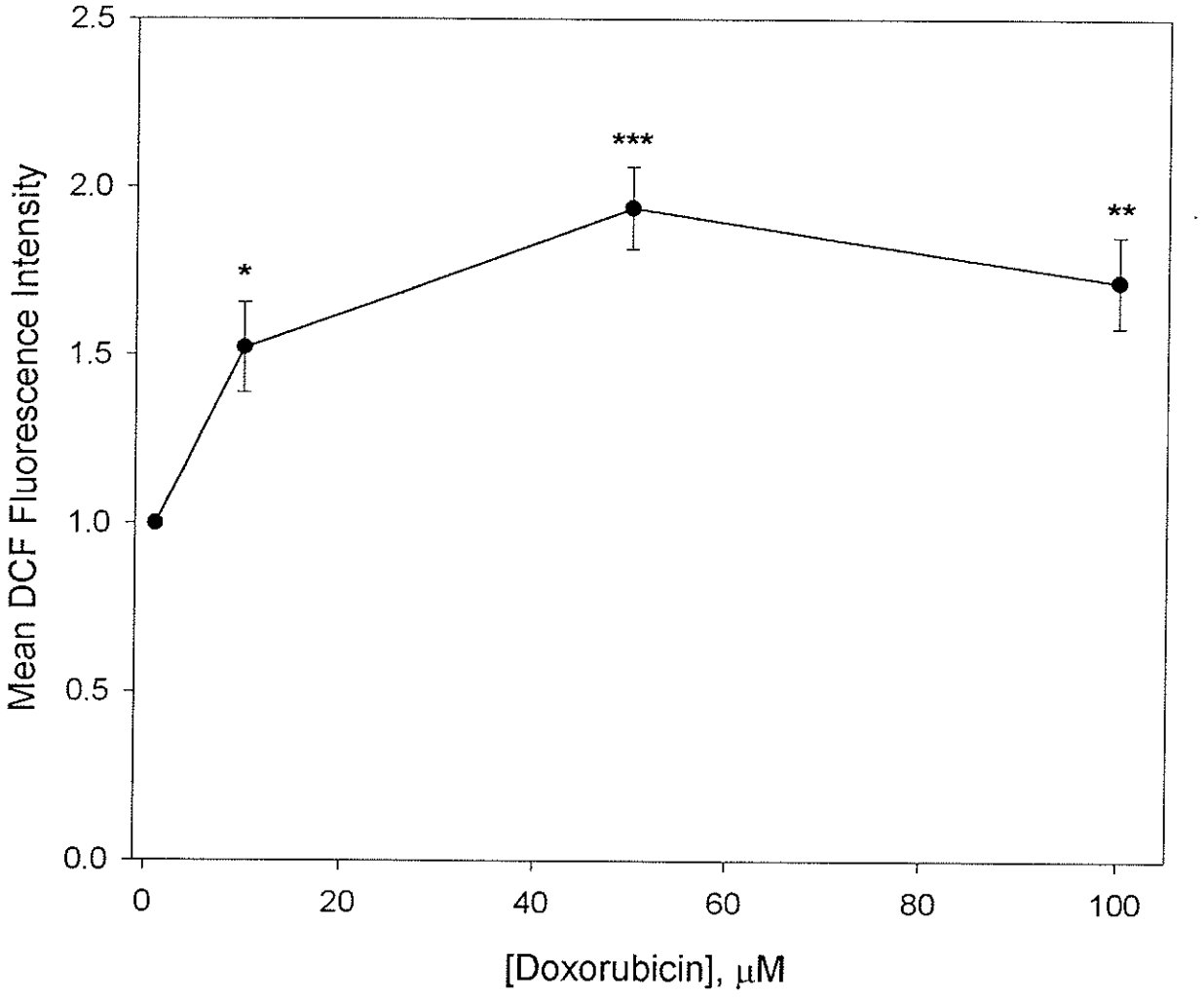

Figure 4.3 Effect of doxorubicin on oxidation of intracellular 2',7'-dichlorofluorescin to 2',7'-dichlorofluorescein (DCF) in neonatal rat cardiomyocytes. Cardiomyocytes were loaded with 10 μM 2',7'-dichlorofluorescin diacetate for 20 min at room temperature in the dark and exposed to 10, 50 and 100 μM doxorubicin for 20 min at 37°C in an atmosphere of 5% (v/v) CO_2 in air. Cells were washed three times with Ca^{2+}/Mg^{2+}-containing Hank's buffer and imaged with an epifluorescence microscope. Mean DCF fluorescence intensities were determined with Scion Image by redirected sampling. Cells used in this experiment came from five different cardiomyocyte preparations that were greater than 90% viable. Each data point is an average of at least five replicates with errors represented as standard errors. After statistical analysis, the data was normalized by dividing each value by the control value. * $P \leq 0.05$; ** $P \leq 0.01$; *** $P \leq 0.001$ compared to the untreated cardiomyocyte preparation

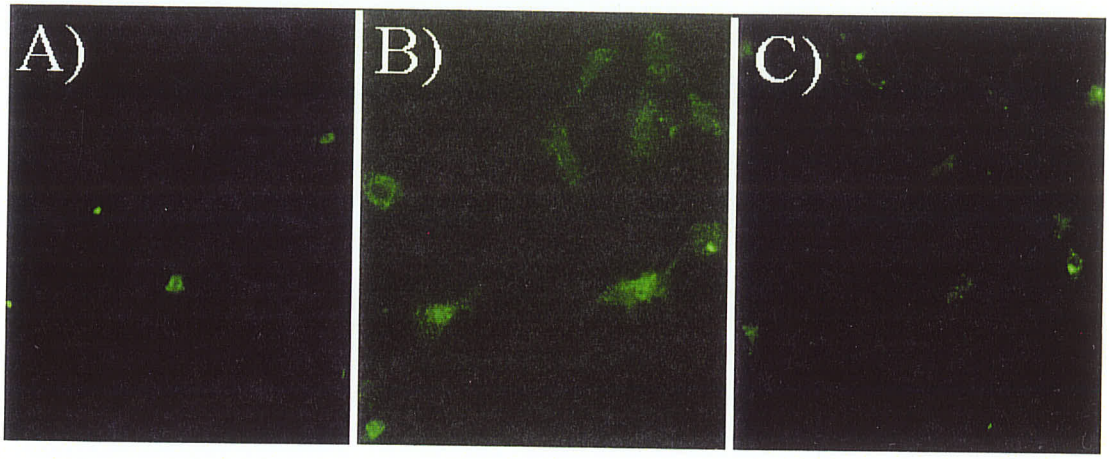

Figure 4.4 Epifluorescence photomicrographs of 2',7'-dichlorofluorescin-loaded cardiomyocytes imaged with a 16X objective following treatment with doxorubicin in the presence or absence of 86 μM dexrazoxane. Cardiomyocytes were loaded with 10 μM 2',7'-dichlorofluorescin diacetate for 20 min at room temperature in the dark and pre-exposed to 86 μM dexrazoxane for 1 hr at 37°C in an atmosphere of 5% (v/v) CO_2. After 1 hr, the cells were treated with 50 μM doxorubicin for 20 min at 37°C in an atmosphere of 5% (v/v) CO_2, washed three times with Ca^{2+}/Mg^{2+}-containing Hank's buffer and imaged with the epifluorescence microscope. In the presence of reactive oxygen species, 2',7'-dichlorofluorescin is oxidized to the green fluorescing 2',7'-dichlorofluorescein (DCF). A) control (with no added doxorubicin); B) 50 μM doxorubicin and C) 50 μM doxorubicin + 86 μM dexrazoxane. Dexrazoxane prevented doxorubicin induced oxidation of 2',7'-dichlorofluorescin to 2',7'-dichlorofluorescein (DCF).

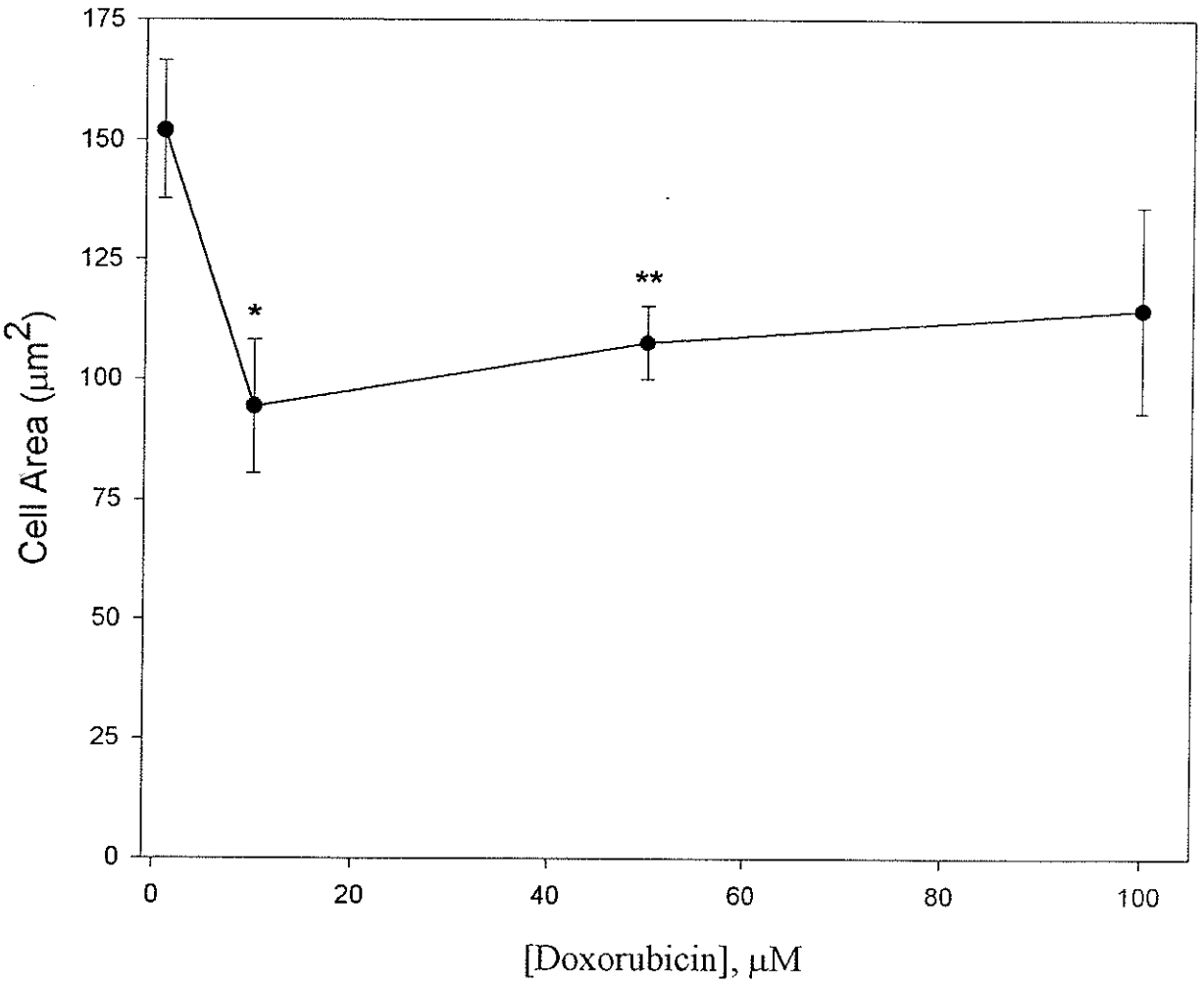

Figure 4.5 Effect of doxorubicin on neonatal rat cardiomyocyte area. Cardiomyocytes were loaded with 10 μM 2',7'-dichlorofluorescin diacetate for 20 min at room temperature in the dark and exposed to 10, 50 and 100 μM doxorubicin for 20 min at 37°C in an atmosphere of 5% (v/v) CO_2 in air. Cells were washed three times with Ca^{2+}/Mg^{2+}-containing Hank's buffer and imaged with the epifluorescence microscope. Cell areas in microscope units were determined with Scion Image using redirected sampling and converted into area units of μm^2 with the known area of a square on the hemocytometer at 16X objective. Cells used in this experiment came from five different cardiomyocyte preparations that were greater than 90% viable. Each data point is an average of at least five replicates with errors represented as standard errors. * $P \leq 0.05$; ** $P \leq 0.01$ compared to the untreated cardiomyocyte preparation

increased significantly in cardiac myocytes exposed to 10, 50 and 100 μM doxorubicin (Figure 4.6).

4.4.2 Effect of dexrazoxane on hydrogen peroxide and doxorubicin-induced 2',7'-dichlorofluorescin oxidation in cardiomyocytes

The effect of dexrazoxane on hydrogen peroxide and doxorubicin-induced 2',7'-dichlorofluorescin oxidation was assessed by epifluorescence microscopy in 2',7'-dichlorofluorescin-loaded neonatal rat cardiomyocytes. 2',7'-Dichlorofluorescin oxidation induced in cardiac myocytes exposed to 50 μM hydrogen peroxide for 1 h or 10, 50 and 100 μM doxorubicin for 20 min was prevented by a 1 h pre-exposure to 86 μM dexrazoxane (Figure 4.7). The epifluorescence photomicrographs of DCF fluorescing cardiomyocytes treated with doxorubicin in the presence or absence of dexrazoxane in Figure 4.4 also illustrates the inhibitory effect of dexrazoxane on 2',7'-dichlorofluorescin oxidation. In addition, the rise in the relative DCF fluorescence intensity/cell area value initiated by hydrogen peroxide and doxorubicin was also prevented by dexrazoxane (Figure 4.8). Moreover, the protection was very efficient, as cells exposed to dexrazoxane and either hydrogen peroxide or doxorubicin exhibited relative DCF fluorescence intensity/cell area values that were comparable to that of the dexrazoxane treatment alone. Dexrazoxane did not significantly affect intracellular production of reactive oxygen species or myocyte area and gave a mean DCF fluorescence intensity similar to cardiac myocytes that received no drug treatment (Figure 4.7).

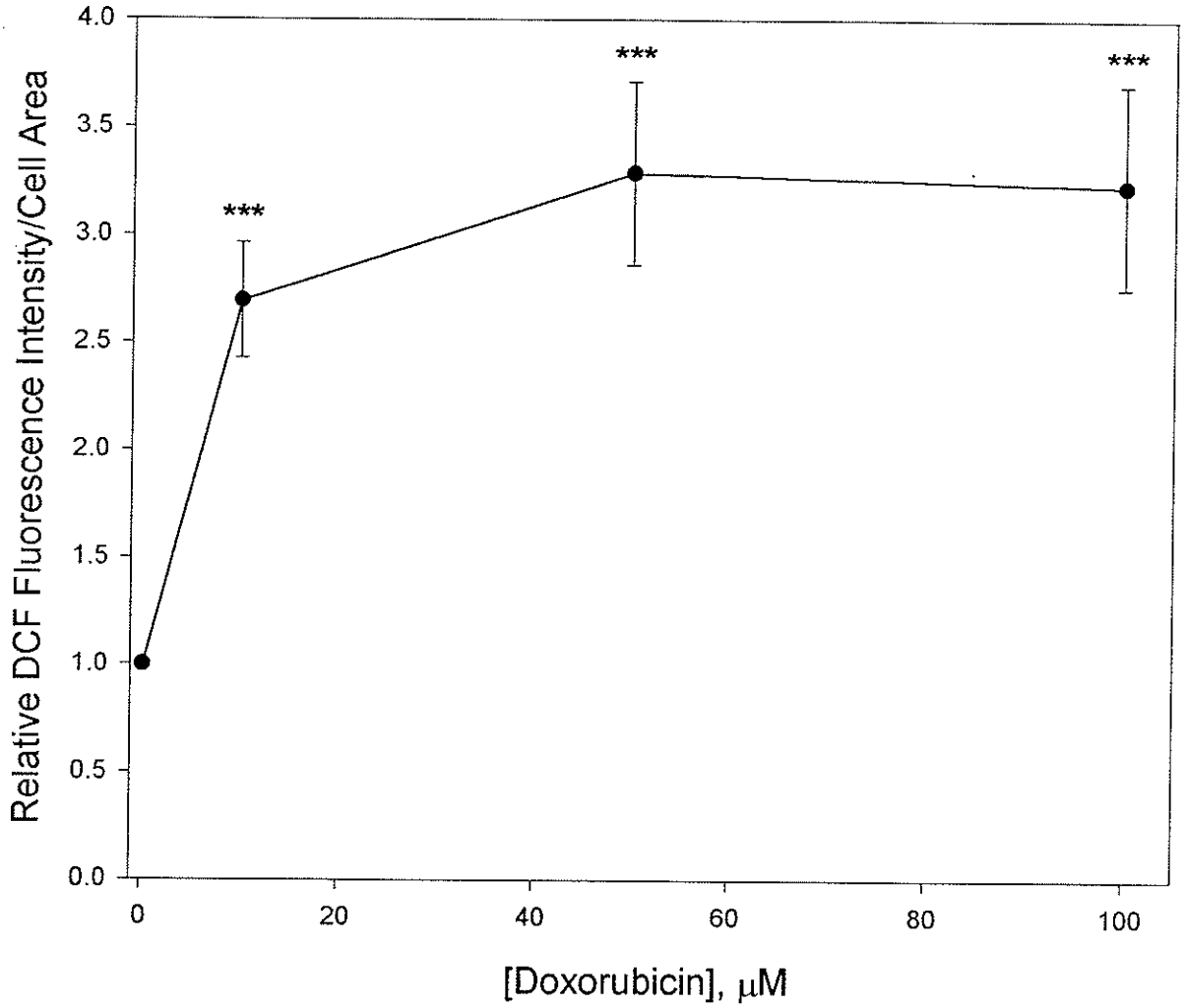

Figure 4.6 Effect of doxorubicin on the relative DCF fluorescence intensity/myocyte area value. Cardiomyocytes were loaded with 10 μM 2',7'-dichlorofluorescin diacetate for 20 min at room temperature in the dark and exposed to 10, 50 and 100 μM doxorubicin for 20 min at 37°C in an atmosphere of 5% (v/v) CO_2. Cells were washed three times with Ca^{2+}/Mg^{2+}-containing Hank's buffer and imaged with an epifluorescence microscope. Relative DCF fluorescence intensities and cell areas were determined with Scion Image by redirected sampling. Cells used in this experiment came from five different cardiomyocyte preparations that were greater than 90% viable. Each data point is an average of at least five replicates with errors represented as standard errors. After statistical analysis, the data was normalized by dividing each value by the control value. *** $P \leq 0.001$ compared to the untreated cardiomyocyte preparation

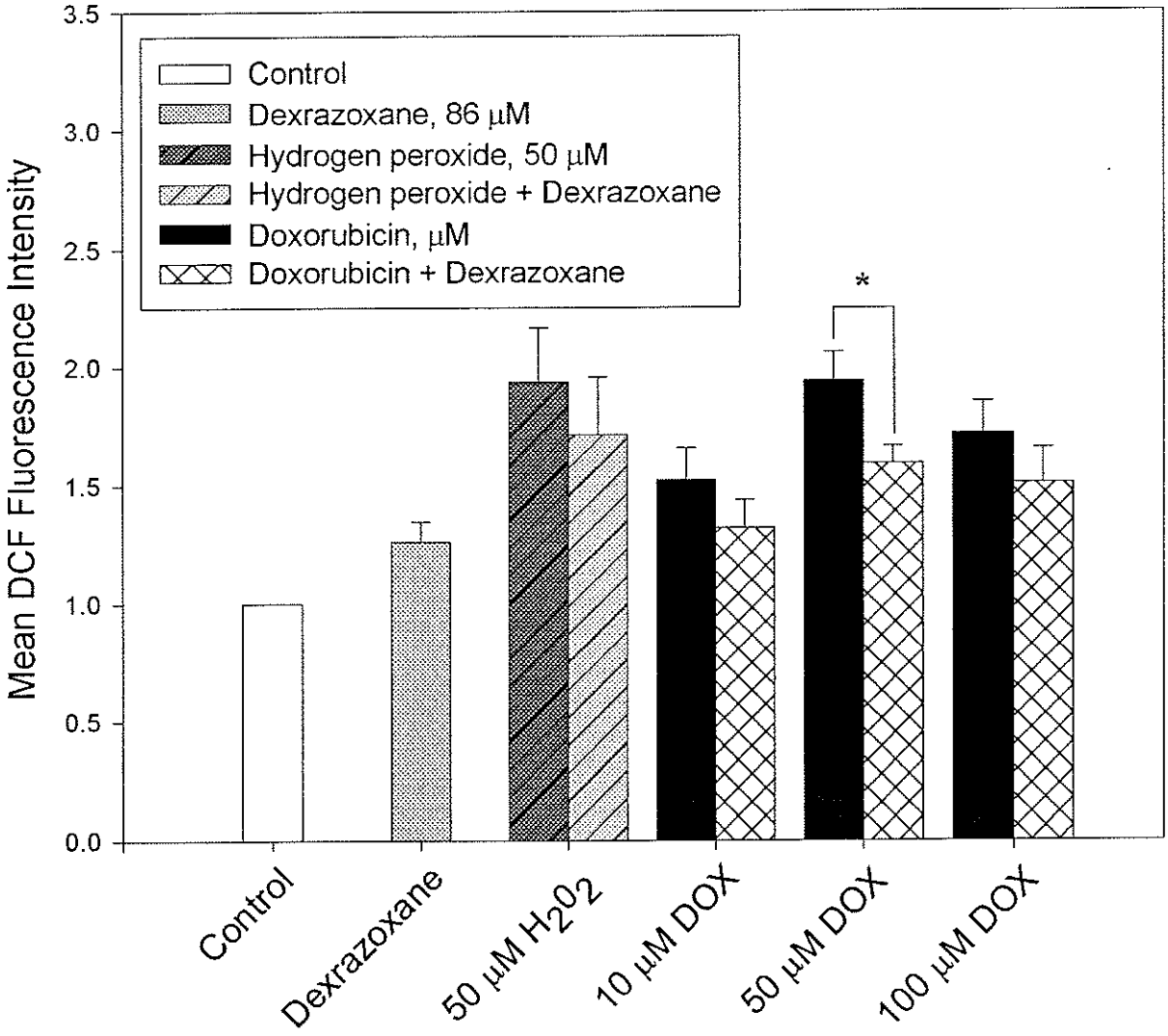

Figure 4.7 Effect of dexrazoxane on hydrogen peroxide and doxorubicin-induced 2',7'-dichlorofluorescin oxidation. Cardiomyocytes were loaded with 10 μM 2',7'-dichlorofluorescin diacetate for 20 min at room temperature in the dark and pre-exposed to 86 μM dexrazoxane for 1 h at 37°C in an atmosphere of 5% (v/v) CO_2 in air. After 1 h, the cells were treated with 50 μM hydrogen peroxide for 1 h or 10, 50 and 100 μM doxorubicin for 20 min at 37°C in an atmosphere of 5% (v/v) CO_2. Cells were washed three times with Ca^{2+}/Mg^{2+}-containing Hank's buffer and imaged with the epifluorescence microscope. Mean DCF fluorescence intensities were determined with Scion Image by redirected sampling. Cells used in this experiment came from five different cardiomyocyte preparations that were greater than 90% viable. Each data point is an average of at least five replicates with errors represented as standard errors. After statistical analysis, the data was normalized by dividing each value by the control value. * $P \leq 0.05$

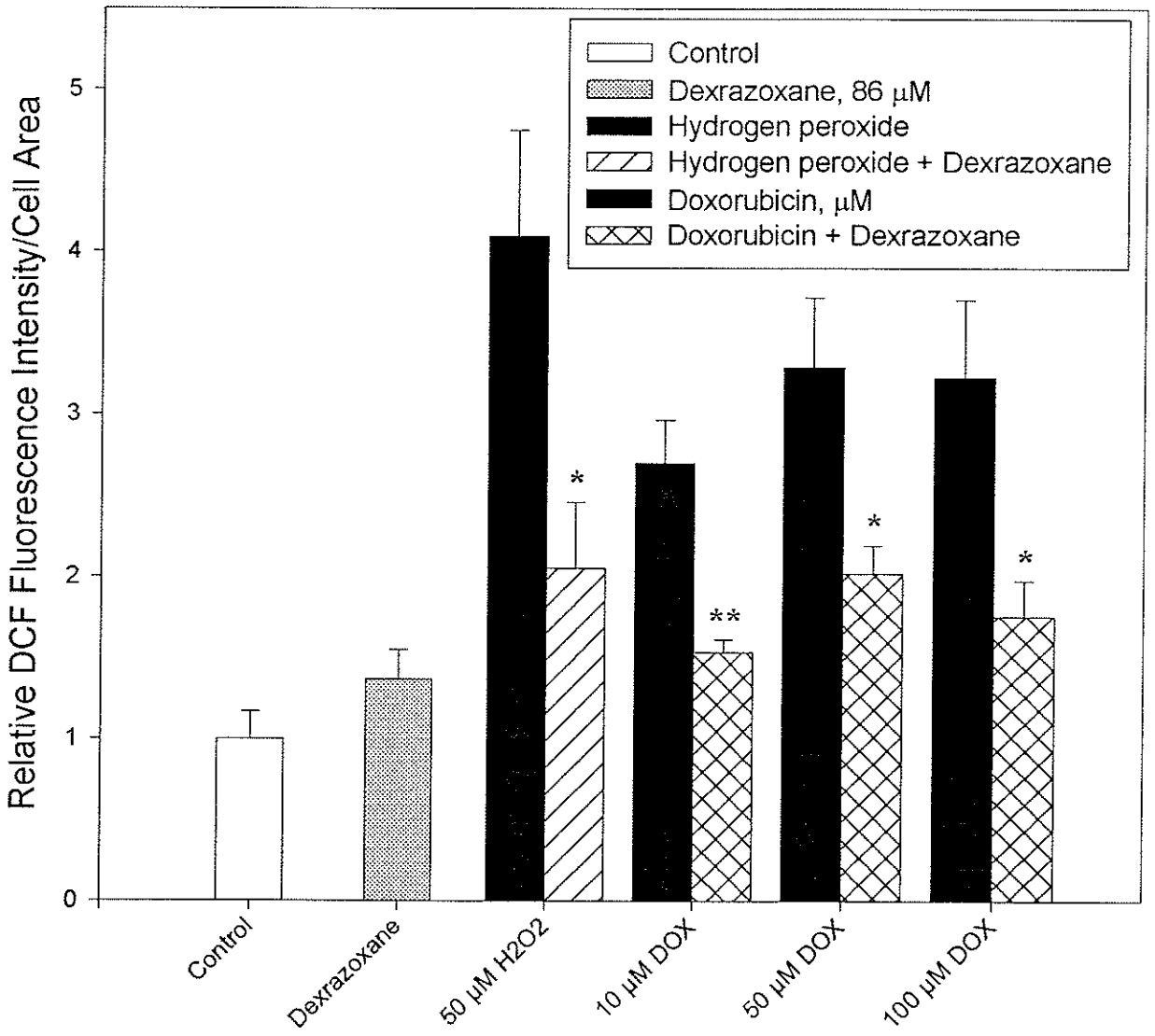

Figure 4.8 Effect of dexrazoxane on the hydrogen peroxide and doxorubicin relative DCF fluorescence intensity/cell area values. Cardiomyocytes were loaded with 10 μM 2',7'-dichlorofluorescin diacetate for 20 min at room temperature in the dark and pre-exposed to 86 μM dexrazoxane for 1 h at 37°C in an atmosphere of 5% (v/v) CO_2 in air. After 1 h, the cells were treated with 50 μM hydrogen peroxide for 1 h or 10, 50 and 100 μM doxorubicin for 20 min at 37°C in an atmosphere of 5% (v/v) CO_2. Cells were washed three times with Ca^{2+}/Mg^{2+}-containing Hank's buffer and imaged with the epifluorescence microscope. Relative DCF fluorescence intensities and cell areas were determined with Scion Image by redirected sampling. Cells used in this experiment came from five different cardiomyocyte preparations that were greater than 90% viable. Each data point is an average of at least five replicates with errors represented as standard errors. After statistical analysis, the data was normalized by dividing each value by the control value. * $P \leq 0.05$; ** $P \leq 0.01$ compared to the hydrogen peroxide or doxorubicin alone treatment

4.5 Discussion

Reactive oxygen species have been shown to be of major importance in heart ischemia-reperfusion injury, left ventricular hypertrophy, induction of preconditioning, cardiac arrhythmias and drug cardiotoxicity [16]. Therefore, development of techniques for quantifying oxidative stress in cardiac myocytes is extremely important. The present study contributes to the development and evaluation of an epifluorescent microscopic method with 2',7'-dichlorofluorescin by revealing oxidative stress associated with doxorubicin exposure in isolated neonatal rat cardiac myocytes. 2',7'-Dichlorofluorescin diacetate is a stable lipid-soluble compound that is readily taken up by myocytes, deacetylated by cytosolic enzymes into a non-fluorescent product (2',7'-dichlorofluorescin) and trapped within the cytosol. 2',7'-Dichlorofluorescin is then oxidized to the highly green fluorescent probe 2',7'-dichlorofluorescein (DCF). This transformation from the non-fluorescent to the fluorescent form is irreversible and has been reported to occur mainly in the mitochondria of cardiac myocytes [6, 16].

In our study, doxorubicin had a significant affect on myocyte area. Cardiomyocytes exposed to 10, 50 and 100 μM doxorubicin for 20 min at 37°C decreased in size (Figure 4.5). Cell shrinkage was significant when cardiomyocytes were exposed to 10 and 50 μM doxorubicin (Figure 4.5). The reduction in myocyte area associated with doxorubicin treatment could be indicative of cell death, as cell shrinkage is a well-established morphological feature of apoptosis [1, 7, 23]. In Chapter 3, our mitochondrial morphology studies (Figure 3.18D) suggested that the compacted mitochondria observed following treatment with 2.0 μM doxorubicin could be indicative of a decrease in cell size. Several other studies have identified the anthracyclines as

inducers of apoptosis [6, 7] and even more have demonstrated that apoptosis can be induced by oxidative stress [1, 7, 22-24]. However, in our study, cardiomyocyte area was not significantly decreased upon exposure to 100 μM doxorubicin (Figure 4.5). At this high concentration, some of the cells started to swell. Depending on the severity of damage cardiomyocytes may die by apoptosis or necrosis [1, 7]. Swelling is a morphological feature of necrotic cells [22]. Thus, it is possible that 100 μM doxorubicin induced both cardiomyocyte apoptotic and necrotic death.

Doxorubicin and hydrogen peroxide were able to oxidize 2',7'-dichlorofluorescin into the green fluorescing DCF (Figures 4.3, 4.4 and 4.7). These studies suggest that doxorubicin and hydrogen peroxide are capable of generating intracellular reactive oxygen species. The increase in 2'7'-dichlorofluorescein (DCF) fluorescence observed in this study is consistent with the suggested oxidative mechanism of doxorubicin cardiotoxicity. Several studies have demonstrated that doxorubicin can generate superoxide and hydroxyl radicals in both its semiquinone free radical and iron-complexed forms [18, 19]. The fact that catalase has been shown to greatly reduce hydroxyl radical formation by iron-doxorubicin complexes indicates that hydrogen peroxide is involved [18]. The inhibition of hydrogen peroxide and doxorubicin-induced generation of reactive oxygen species in cardiac myocytes by the iron chelator dexrazoxane indicates that iron plays an important role in the process (Figure 4.7) [20]. Iron acts as a cofactor in the formation of reactive oxygen species catalyzed by the quinone group of anthracyclines and thus dexrazoxane may bind iron and displace it from iron-doxorubicin complexes [7]. Iron also acts as a cofactor in the formation of hydroxyl radical by the Fenton reaction with hydrogen peroxide and dexrazoxane may be working at this level as well [7].

Studies have shown that dexrazoxane is able to chelate free iron and displace it from its complexes with doxorubicin [20]. Thus, we propose that dexrazoxane likely acts by diffusing into the cell, hydrolyzing to its active, rings-open, metal-ion chelating form and either displacing iron from the iron-doxorubicin complex, or chelating loosely bound or free iron, thereby reducing iron-based oxygen radical production.

The major criticism of the oxidative mechanism of doxorubicin action is that the majority of evidence favoring this hypothesis of doxorubicin cardiotoxicity has been obtained in sub-cellular fractions, often in combination with extremely high concentrations of doxorubicin not encountered in clinical practice [6]. In this study, doxorubicin concentrations as low as 10 μM were demonstrated to generate reactive oxygen species in neonatal rat cardiomyocytes within 20 min (Figure 4.3). Although clinically relevant concentrations are approximately 1 μM doxorubicin, patient exposure time to the drug is much longer and cumulative free radical generation and heart damage could be possible [7]. However, such acute events as systolic and diastolic dysfunction that often occur minutes after injection of anthracyclines could be caused, at least in part, by the rapid oxidative stress associated with doxorubicin treatment that was observed in this study [6].

It was a surprise to not observe a dose-dependent increase in reactive oxygen species generation in cardiac myocytes exposed to 50 and 100 μM doxorubicin (Figure 4.3). Because the emission spectra of doxorubicin and DCF overlap, it is possible that at high concentrations of doxorubicin, doxorubicin was quenching DCF fluorescence or vice versa [6]. If high concentrations of doxorubicin were quenching DCF or vice versa, then one would expect less doxorubicin to be available to participate in free radical

reactions. This effect would underestimate the true dichlorofluorescein production at high doxorubicin concentrations, whereas sensitivity of this approach to detect free radical formation at low drug concentrations would not be altered. Thus, the generation of reactive oxygen species by doxorubicin at the higher concentrations used in this study could be more significant than that observed. However, it becomes difficult to detect it by the fluorescence method due to the inner filter effect present at high doxorubicin concentrations.

Doxorubicin and hydrogen peroxide also caused a significant increase ($P \leq 0.001$) in the relative DCF fluorescence intensity/cell area value (Figures 4.6 and 4.8). We chose to display the data on a per area basis, as doxorubicin was not only generating reactive oxygen species and promoting cell shrinkage but inducing free radical damage over a small area. Dexrazoxane was able to prevent the rise in the relative DCF fluorescence intesity/cell area value induced by hydrogen peroxide. Thus, dexrazoxane was not only attenuating reactive oxygen species generation and preserving cell size but limiting oxidative damage to a smaller area on the cardiomyocyte.

4.6 Conclusions

Epifluorescence microscopy in conjunction with 2',7'-dichlorofluorescin was a very effective method for quantifying reactive oxygen species generation in cardiac myocytes. This technique could be applied to study oxidative stress in other pathophysiological and pharmacological studies in the heart. In this study, doxorubicin was demonstrated to be a generator of reactive oxygen species with hydrogen peroxide and iron playing an important role in the process. This study also served as an excellent model for acute doxorubicin cardiotoxicity and addressed a possible role for doxorubicin

in cardiomyocyte apoptosis. Future studies should focus on investigating doxorubicin-induced generation of reactive oxygen species in a chronic cardiotoxicity model. Finally, dexrazoxane was demonstrated to reduce doxorubicin-induced generation of reactive oxygen species attributed to potential oxidative damage of cardiac myocytes. It is possible that dexrazoxane exerts its cardioprotective effect through the ability of it hydrolysis product, ADR-925, to prevent iron-based oxygen free radical damage.

4.7 References

1. Bishopric N, Andreka P, Slepak T, Webster K. 2001. Molecular mechanisms of apoptosis in the cardiac myocyte. *Curr Opin Pharmacol* 1:141-150.

2. Kala SV, Hasinoff BB, Richardson JS. 1996. Brain samples from Alzheimer's patients have elevated levels of loosely bound iron. *Int J Neurosci* 86:263-9.

3. Markesbery WR. 1997. Oxidative stress hypothesis in Alzheimer's disease. *Free Radic Biol Med* 23:134-47.

4. McIntosh LJ, Trush MA, Troncoso JC. 1997. Increased susceptibility of Alzheimer's disease temporal cortex to oxygen free radical-mediated processes. *Free Radic Biol Med* 23:183-90.

5. Poli G, Parola M. 1997. Oxidative damage and fibrogenesis. *Free Radic Biol Med* 22:287-305.

6. Sarvazyan N. 1996. Visualization of doxorubicin-induced oxidative stress in isolated cardiac myocytes. *Am J Physiol* 271:H2079-85.

7. Sawyer DB, Fukazawa R, Arstall MA, Kelly RA. 1999. Daunorubicin-induced apoptosis in rat cardiac myocytes is inhibited by dexrazoxane. *Circ Res* 84:257-65.

8. Scanlon JM, Reynolds IJ. 1998. Effects of oxidants and glutamate receptor activation on mitochondrial membrane potential in rat forebrain neurons. *J Neurochem* 71:2392-400.

9. Wang H, Joseph JA. 1999. Quantifying cellular oxidative stress by dichlorofluorescein assay using microplate reader. *Free Radic Biol Med* 27:612-6.

10. Zhu H, Bannenberg GL, Moldeus P, Shertzer HG. 1994. Oxidation pathways for the intracellular probe 2',7'- dichlorofluorescein. *Arch Toxicol* 68:582-7.

11. LeBel CP, Ischiropoulos H, Bondy SC. 1992. Evaluation of the probe 2',7'-dichlorofluorescin as an indicator of reactive oxygen species formation and oxidative stress. *Chem Res Toxicol* 5:227-31.

12. Marchesi E, Rota C, Fann YC, Chignell CF, Mason RP. 1999. Photoreduction of the fluorescent dye 2'-7'-dichlorofluorescein: a spin trapping and direct electron spin resonance study with implications for oxidative stress measurements. *Free Radic Biol Med* 26:148-61.

13. Jakubowski W, Bartosz G. 2000. 2,7-dichlorofluorescin oxidation and reactive oxygen species: what does it measure? *Cell Biol Int* 24:757-60.

14. Konorev EA, Kennedy MC, Kalyanaraman B. 1999. Cell-permeable superoxide dismutase and glutathione peroxidase mimetics afford superior protection against doxorubicin-induced cardiotoxicity: the role of reactive oxygen and nitrogen intermediates. *Arch Biochem Biophys* 368:421-8.

15. Rota C, Chignell CF, Mason RP. 1999. Evidence for free radical formation during the oxidation of 2'-7'- dichlorofluorescin to the fluorescent dye 2'-7'-dichlorofluorescein by horseradish peroxidase: possible implications for oxidative stress measurements. *Free Radic Biol Med* 27:873-81.

16. Swift LM, Sarvazyan N. 2000. Localization of dichlorofluorescin in cardiac myocytes: implications for assessment of oxidative stress. *Am J Physiol Heart Circ Physiol* 278:H982-90.

17. Hershko C, Pinson A, Link G. 1996. Prevention of anthracycline cardiotoxicity by iron chelation. *Acta Haematol* 95:87-92.

18. Malisza KL, Hasinoff BB. 1995. Production of hydroxyl radical by iron(III)-anthraquinone complexes through self-reduction and through reductive activation by the xanthine oxidase/hypoxanthine system. *Arch Biochem Biophys* 321:51-60.

19. Malisza KL, Hasinoff BB. 1995. Doxorubicin reduces the iron(III) complexes of the hydrolysis products of the antioxidant cardioprotective agent dexrazoxane (ICRF-187) and produces hydroxyl radicals. *Arch Biochem Biophys* 316:680-8.

20. Malisza KL, Hasinoff BB. 1996. Inhibition of anthracycline semiquinone formation by ICRF-187 (dexrazoxane) in cells. *Free Radic Biol Med* 20:905-14.

21. Bernardi P, Petronilli V, Di Lisa F, Forte M. 2001. A mitochondrial perspective on cell death. *Trends Biochem Sci* 26:112-7.

22. Halestrap AP, Doran E, Gillespie JP, O'Toole A. 2000. Mitochondria and cell death. *Biochem Soc Trans* 28:170-7.

23. Roberg K, Johansson U, Ollinger K. 1999. Lysosomal release of cathepsin D precedes relocation of cytochrome c and loss of mitochondrial transmembrane potential during apoptosis induced by oxidative stress. *Free Radic Biol Med* 27:1228-37.

24. Virag L, Salzman AL, Szabo C. 1998. Poly(ADP-ribose) synthetase activation mediates mitochondrial injury during oxidant-induced cell death. *J Immunol* 161:3753-9.

Chapter 5 Doxorubicin-induced apoptosis and necrosis in neonatal rat cardiac myocytes and summary of doxorubicin cardiotoxicity studies

5.1 Introduction

5.1.1 Cardiomyocyte apoptosis and necrosis

Cardiomyocytes lose viability in response to stress stimuli such as hypoxia, ischemia, free radical stress, adrenergic overstimulation, work overload, toxin exposure and withdrawal of growth factors [1-4]. In response to these stimuli, cell death can develop within minutes or several hours. Cell death of very rapid onset is typically a consequence of tissue necrosis [3]. Such necrotic cell death is a consequence of acute disruption of cellular metabolism and can lead to severe ATP depletion, ion dysregulation, mitochondrial and cellular swelling, activation of degradative enzymes, plasma membrane failure, cell lysis and an inflammatory response [3]. Necrotic cell death rarely serves the needs of the organism and in highly aerobic tissues like the heart and brain that do not regenerate, necrosis leads to permanent functional deficit [3].

Apoptosis, on the other hand, is an active, precisely regulated, energy requiring process, which appears to be controlled by a genetic program [5]. It is often referred to as "programmed cell death" and only eliminates the damaged or superfluous cells without harming their healthy neighbors [1]. Controlled deletion of cells serves many useful functions in normal tissue development, in regulating proliferating cell populations and during stress to ensure the survival and integrity of the organism [1]. Cardiac myocytes, although terminally differentiated, contain the genes and signal transduction pathways necessary for programmed cell death and thus retain the ability to die by apoptosis [6]. In contrast to necrosis, apoptosis takes several hours or days to fully develop and metabolism is not as severely impaired [3]. Apoptosis is characterized by a series of

typical morphological events including cell shrinkage, fragmentation into membrane-bound apoptotic bodies and rapid phagocytosis by neighboring cells [7, 15]. Internucleosomal fragmentation of genomic DNA is also a hallmark of apoptosis [7]. In humans and other mammals, adult cardiac myocytes are thought to have a very limited capacity for self-renewal [4]. Thus, functional impairment can result if apoptosis is not balanced by cell replacement in the adult myocardium [8, 32].

5.1.2 Implications for studying apoptosis in cardiomyocytes

Over the last 10 years, there has been a steep increase in apoptosis research. It is acknowledged that apoptosis plays a crucial role in homeostasis and pathology. As such, apoptosis has been recognized as a key process in the cardiovascular system. It is an important contributor to the intact and complete development of the cardiovascular system and to the adaptation of the cardiovascular system to its continuously changing demands (i.e. stress, sports and illness) [6]. Moreover, increasing evidence shows that cardiomyocyte apoptosis occurs in various cardiovascular conditions. Apoptosis occurs concomitantly with necrosis in the infarcted and reperfused myocardium, in end stage heart failure and a broad spectrum of other cardiovascular diseases [1, 4, 6]. Recently, the role of apoptosis in myocardial diseases has attracted considerable attention as a potentially reversible cause of cardiac functional deterioration. Progress in the understanding of the cellular mechanisms of apoptosis in cardiac myocytes has opened new therapeutic avenues for prevention of myocyte loss. A major determinant for the success of this novel approach is the degree to which apoptosis contributes to total myocyte loss and to which extent this additional loss of contractile mass can be prevented to reduce functional deterioration and mortality in cardiac disease [8].

5.1.3 Detection and quantification of cardiomyocyte apoptosis

In past studies, detection and quantification of myocytes undergoing apoptosis has been based on morphological analysis with light or electron microscopy and the counting of nuclei with DNA fragmentation visualized by in situ nick end-labeling of strand breaks with dUTP (TUNEL) or by the electrophoretic detection of typical DNA "ladders" [6, 9, 11]. However, detection and quantification of myocytes undergoing or committed for apoptosis remains difficult as (i) morphological analysis consists mainly of distinguishing apoptotic from necrotic cells; (ii) apoptosis is not always accompanied by DNA fragmentation in cardiac myocytes and DNA fragmentation evidenced positively by TUNEL can also be observed during cell necrosis [9]. Altogether, these limitations could contribute to the discrepancies observed among the studies aimed to quantify myocyte apoptosis during various cardiac disorders. Moreover, these techniques study late phase apoptosis rather than early stage apoptosis [6, 9-12].

In the early stages of apoptosis, changes occur at the cell surface, which until recently have remained difficult to recognize. One of these plasma membrane alterations is the translocation of the phospholipid phosphatidylserine from the inner side of the plasma membrane to the external surface of the cell [6, 9-12]. Once exposed outside, phosphatidylserine acts as a membrane "flag" on apoptotic cells resulting in the recognition and uptake of these cells by phagocytes [6, 10]. This occurs in the early phases of apoptotic cell death during which the cell membrane itself remains intact [12]. A recently discovered family of proteins, the annexins, has been found to have high affinity for aminophospholipids in the presence of Ca^{2+} ions [6, 10, 12]. A member of this family, annexin V has been shown by several groups to bind preferentially to

phosphatidylserine [6, 9-12]. Thus, this protein has been used as a sensitive probe for phosphatidylserine exposure upon the cell membrane. Translocation of phosphatidylserine to the external surface is not unique to apoptosis, but also occurs during cell necrosis [12]. The difference between these two forms of cell death is that during the initial stages of apoptosis the cell membrane remains intact, while at the moment that necrosis occurs the cell membrane loses integrity and becomes leaky [12]. Therefore, the measurement of annexin V binding to the cell surface as indicative for apoptosis has been performed in conjunction with a dye exclusion test to establish integrity of the cell membrane. Detection of necrosis relies mainly on the use of assays that demonstrate cell membrane damage [7], such as uptake of a tracer dye (i.e. propidium iodide) or leakage of intracellular enzymes (i.e. lactate dehydrogenase) (Figure 5.1) [13].

5.1.4 Project under study

In Chapter 3 and 4, both iron-based oxygen free radical generation and mitochondrial damage were evident in doxorubicin-treated cardiac myocytes and prevented by the iron-chelating drug dexrazoxane. The dose-dependent cardiomyopathy and heart failure due to doxorubicin have been shown to be due to increased oxidative stress and the ongoing loss of cardiac myocytes [1, 10-14, 17]. An emerging view is that mitochondria are the critical step in commitment to both apoptotic and necrotic cell death (Figure 5.2) [2, 15-24].

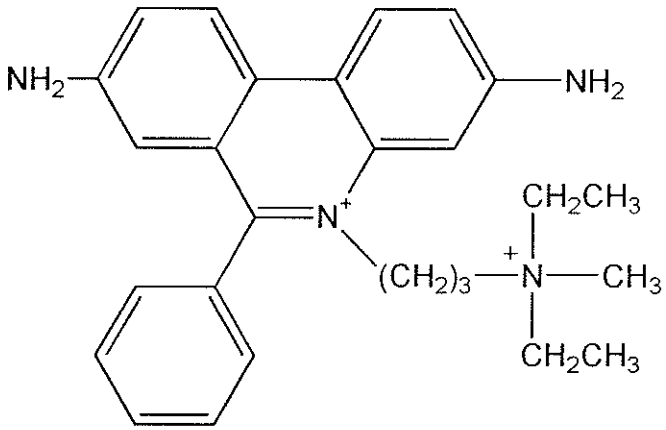

Figure 5.1 The chemical structure of the cell impermeant propidium iodide. Propidium iodide is a phenanthridinium derivative that intercalates between DNA base pairs and yields red fluorescence.

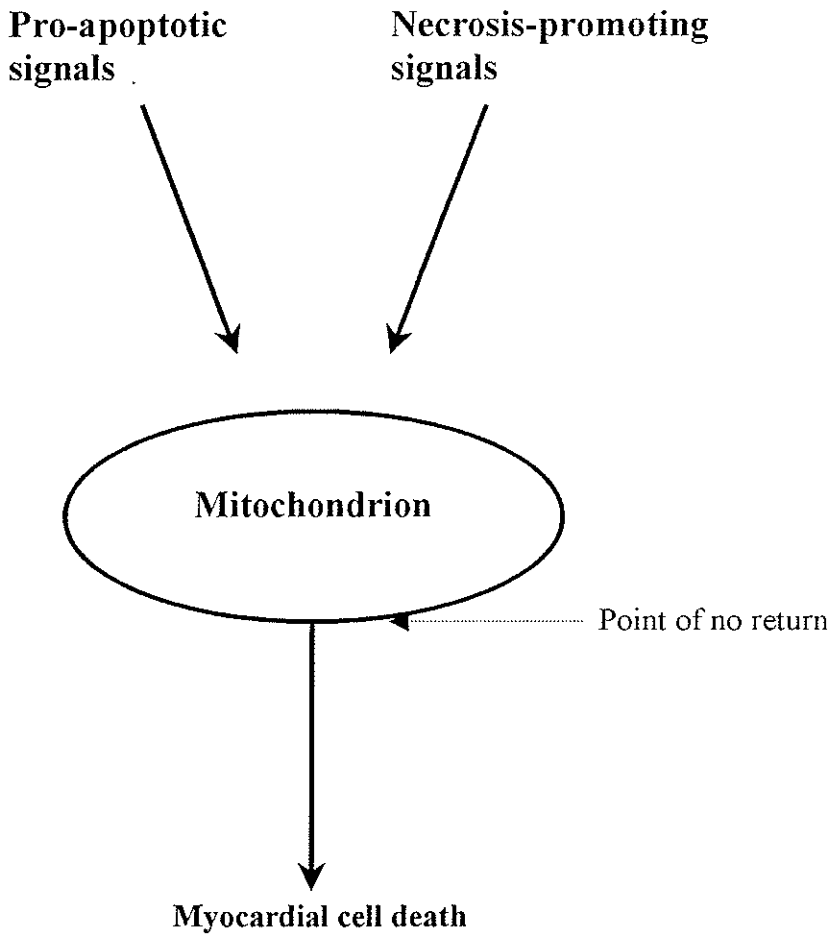

Figure 5.2 Regulatory role of the mitochondrion in myocardial cell death. Mitochondria are the final common pathway on which death signals converge. Once the mitochondrial membrane potential is dissipated, the cell is committed to die by apoptosis or necrosis, depending upon the severity of the insult.

Given that doxorubicin can generate reactive oxygen species, damage mitochondria and induce apoptotic and necrotic death, it was of interest to try to protect the heart at an early stage before a functional deficit in the myocardium was initiated. In this study, we investigated the time frame for apoptosis and necrosis in cardiac myocytes exposed to pharmacological concentrations of doxorubicin using the annexin V/propidium iodide assay with epifluorescence microscopy and an assay for lactate dehydrogenase (LDH). The ultimate goal was to determine whether dexrazoxane could protect cardiac myocytes from doxorubicin-induced apoptotic and necrotic cell death. Assay conditions for neonatal rat cardiomyocytes and drug concentrations and exposure times were optimized and may be used to study dexrazoxane cardioprotective effects. Unfortunately, there was insufficient time to complete the cardioprotective study.

5.2 Materials

Doxorubicin hydrochloride was a gift from Adria-SP Inc. (Columbus, OH). Annexin V-FITC, propidium iodide and binding buffer came together in the ApoAlert Annexin V-FITC Apoptosis Kit ordered from Clontech Laboratories Inc. (cat No. K2025-1, Palo Alto, CA). Poly-l-lysine hydrochloride (cat No. P-2658), trypan blue dye (cat No. T-6146), β-NADH (disodium salt, cat No. N-8129), pyruvic acid (sodium salt, cat No. P-8574) and HEPES (cell culture grade, cat No. H-9136) were purchased from Sigma Chemical Co. (St. Louis, MO). Sodium bicarbonate ($NaHCO_3$, cat. No. BP328-079), Tris (crystallized free base, molecular biology grade, cat No. BP152-1), pre-cleaned microscope slides (cat No. 12-550A), preferred glass cover slips (cat. No. 12-545-85) and magnesium sulfate ($MgSO_4$) were obtained from Fisher Scientific (Fairlawn, NJ). Dulbecco's phosphate buffered saline (PBS, cat No. D-5652), Dulbecco's modified Eagle

medium/F12 (DMEM/F-12, cat No. 12500-062), penicillin-streptomycin (cat No. 25200-072), fetal calf serum (FCS, cat No. 26140-079), horse serum (cat No. 16050-122) and Hank's buffered salt solution (HBSS, without Ca^{2+} or Mg^{2+}, cat No. H-4891) were ordered from Gibco-BRL Life Technologies Inc. (Burlington, ON). D-glucose was supplied by Anala R (Toronto, ON) while calcium chloride ($CaCl_2$, cat No. AC-1946) and potassium chloride (KCl, cat No. AC-7600) were obtained from Anachemia Ltd. (Montreal, QB). Five molar HCl (cat No. LC15360-2) was purchased from LabChem Inc. (Pittsburgh, PA). Six-well flat bottom tissue culture plates (cat No. 83.1839), adhesive, 24-well tissue culture plates (cat No. 83.1836.300) and 0.2 μm acetate syringe filters (cat No. 83.1826.001) were ordered from Sarstedt Inc. (St. Leonard, PQ). Falcon 3025 tissue culture plates and 40 μm cell strainers were obtained from Becton Dickensson (Lincoln Park, NJ). Deoxyribonuclease I (DNAse, cat No. 2139), trypsin (cat No. 3703) and collagenase (cat No. 4176) were obtained from Worthington Biochemical Corporation (Lakewood, NJ). Cell culture media and buffers were prepared in reverse osmosis distilled water and cardiomyocyte cultures were grown in a 37°C incubator in an atmosphere of 5% (v/v) CO_2 in air. Microscopy studies were carried out with a Zeiss epifluorescence microscope (Roper Scientific, Trenton, NJ) equipped with a high resolution, cooled color digital (CCD) camera, a camera coupler (Diagnostic Instruments Inc., Sterling Hts., MI) and fluorescein and rhodamine filter sets (XF-115, Omega Optical, Brattleboro, Vermont). Images were acquired with Photometrics Cool Snap acquisition software (Version 1.2, Roper Scientific, Trenton, NJ) and were analyzed with Scion Image imaging software (Version 4.02, Scion Corporation, Frederick, Maryland).

5.3 Methods

5.3.1 Cell Culture

As described in Section 3.3.2.2, a primary culture of neonatal rat cardiomyocytes was prepared and used as the model for doxorubicin cardiotoxicity studies. Cell viability and cell density was calculated as described in Section 3.3.2.3.

For the epifluorescence microscopy experiment, cells were seeded in sterile, 6-well plates containing poly-l-lysine treated glass cover slips at a density of 200,000 cells per well in 2 ml of plating medium. Details of the seeding process are outlined in Section 3.3.2.4. Forty-eight hours following seeding, cells were transferred from plating medium (7.5% (v/v) horse serum/7.5% (v/v) FCS in DMEMF-12) into culturing medium (DF-10, 10% (v/v) FCS in DMEMF-12) and were grown in an atmosphere of 5% (v/v) CO_2 in air at 37°C. The experiment was commenced on the third day following isolation at which point 80% of the cardiomyocytes were beating.

For the lactate dehydrogenase (LDH) release experiment, cells were seeded in sterile, adhesive, 24-well plates at a density of 500,000 cells per well in 750 µl of plating medium. The cells were seeded with a sterile 1-ml pipette to maintain cell viability and the cell suspension was rocked gently throughout the seeding process to prevent cell aggregation and settlement. The cell density chosen for this experiment allowed for optimum cell viability and a 95% confluent culture the day the experiment was commenced. Forty-eight hours following seeding, cells were transferred from plating medium into a low serum, culturing medium (DF-2, 2% FCS in DMEM F-12) and were grown in an atmosphere of 5% (v/v) CO_2 in air at 37°C for 24 h. A low serum, culturing medium was used because serum contains LDH, which could interfere with the assay for

LDH release. During the 24 h equilibrating period, the beating rate of the cardiomyocytes dropped, although the myocytes were well attached and retained their initial healthy morphology. After the cells adjusted to their new environment, they were treated with doxorubicin as discussed in the next section.

5.3.2 Doxorubicin treatment

The doxorubicin stock was prepared as detailed in Section 3.3.3. Controls for doxorubicin fluorescence in the green (520 nm) and red (590 nm) range were included. For the epifluorescence microscopy experiment, cardiac myocytes were exposed to 0.2 and 1.0 μM doxorubicin for 3 h at 37°C in an atmosphere of 5% (v/v) CO_2 in air. Following treatment with doxorubicin, the cells were washed three times with culture medium (DF-10, 10% FCS in DMEM F-12) to remove any remaining drug. Cells were allowed to grow at 37°C in an atmosphere of 5% (v/v) CO_2 in air for 48 h, stained with annexin V-FITC and propidium iodide (1/5 μg/ml) and imaged with the epifluorescence microscope.

For the LDH release experiment, cells were exposed to 0.3 μM doxorubicin for 24, 48 and 72 h. A well with DF-2 alone was also included to determine the LDH activity in the serum. At each time point, a sample of the supernatant was collected for the LDH assay. The procedure for sampling the supernatant is discussed in section 5.3.5.

5.3.3 Staining with annexin V-FITC and propidium iodide

To study the effect of doxorubicin on cardiomyocyte apoptosis and necrosis, cardiomyocytes were stained with annexin V-FITC and propidium iodide. A 1 μg/ml annexin V-FITC/5 μg/ml propidium iodide solution was prepared daily in binding buffer using the annexin V-FITC and propidium iodide stock solutions provided in the ApoAlert

annexin V-FITC apoptosis kit. The staining solution was wrapped in aluminum foil to prevent photobleaching. Before staining, the cells were equilibrated to room temperature in 2 ml of binding buffer. Cardiomyocytes were stained in the dark at room temperature by applying 500 µl of the staining solution to all areas of the cover slip. After 10 min, cells were washed three times with Ca^{2+}/Mg^{2+} (1.3/0.8 mM)-containing Hank's buffer (pH 7.4) to remove any remaining extracellular probe. Stained cells were imaged by epifluorescence microscopy as discussed in the next section.

5.3.4 Epifluorescent microscope imaging and analysis of doxorubicin-treated cardiac myocytes

Procedures for mounting cover slips and imaging were previously outlined in section 3.3.5. Before the cells were imaged, a camera calibration was completed. Any camera dark noise was accounted for during camera calibration and was subtracted off of the other images. Cells were observed at 16X objective with a Zeiss epifluorescence microscope equipped with a cooled color digital (CCD) camera. Bright field images were acquired first with an exposure time of 0.5 s. Excitation of annexin V-FITC was achieved by selecting the appropriate band of light from the mercury lamp beam with the fluorescein filter set while propidium iodide excitation was achieved with the rhodamine filter set. Fluorescent images were acquired with an exposure time of 1 s. Imaging was done quickly in the dark and the shutter was kept closed between images to limit any photobleaching of the dyes. For each treatment, 4 images were taken. Each field contained approximately 40 cells.

Images of annexin V-FITC- and propidium iodide-stained cardiomyocytes were analyzed using Scion Image imaging software. The total number of cells was determined by counting all the cells in the bright field image. Annexin-stained cell counts

corresponded to the number of apoptotic cells while propidium iodide-stained cell counts corresponded to the number of necrotic cells. Dual-stained cells accounted for less than 1% of the total count and were not included in the analysis. The percentage of apoptotic and necrotic cells was calculated by dividing the number of apoptotic or necrotic cells over the total number of cells counted and multiplying by 100%. On average, a total of 150 cells were counted for each treatment. Some cell loss was apparent in the doxorubicin treatments.

5.3.5 Sampling supernatant for the enzyme lactate dehydrogenase

Before sampling the supernatant from the wells, plates were gently swirled ten times clockwise and ten times counterclockwise to create a homogenous LDH supernatant. LDH is released into the cells immediate surrounding environment and diffuses very slowly. An 80 µl sample of supernatant was removed from the center of each well, placed in a sterile microcentrifuge tube and centrifuged for 5 min at 500 g. After the cells were spun down, 70 µl of the supernatant was saved in a sterile microcentrifuge tube and stored in the – 80°C freezer until ready to assay for LDH activity. All samples were measured for LDH activity within a week of freezing on the same day, as lactate dehydrogenase activity declines over time and during the thawing/refreezing process.

5.3.6 Lactate dehydrogenase (LDH) release assay

5.3.6.1 Preparation of buffer and reagents

The Tris/KCl buffer (50/150 mM) was prepared by dissolving 3.028 g of Tris and 5.592 g of KCl in 500 ml of H_2O. The buffer was titrated to pH 7.4 with 5 M HCl and stored at 4°C in the refrigerator. The 2.5 mM (w/v) NADH disodium salt solution was

prepared fresh on the day of analysis in Tris/KCl buffer, as the NADH solution is unstable and oxidizes to NAD^+ over time. The 25 mM (w/v) pyruvate solution was also prepared fresh on the day of analysis by dissolving pyruvic acid in Tris/KCl buffer. The substrate for the lactate dehydrogenase reaction was made by mixing 10% (v/v) NADH and 10% (v/v) pyruvate in Tris/KCl buffer. The substrate was equilibrated to 25°C in a water bath.

5.3.6.2 Lactate dehydrogenase (LDH) release assay

Damage to the myocytes was evaluated by measuring the amount of LDH released into the medium. Samples of supernatant where thawed, kept on ice and vortexed before analysis. The amount of LDH in the supernatant was assayed with a Cary WIN UV spectrophotometer (Varian Canada Inc., Australia) maintained at 25°C by following the loss of NADH absorbance in its reaction with pyruvate over time at 340 nm (Equation 1).

$$\text{Pyruvate} + \underset{\text{(absorbing species)}}{\text{NADH}} + H^+ \xrightarrow[\text{LDH}]{} \text{Lactate} + \underset{\text{(non-absorbing species)}}{NAD^+} \quad (1)$$

Clean, quartz cuvettes were loaded into the cells and zeroed on air. To each cuvette was added 800 µl of substrate. A 20 µl aliquot of the LDH-containing supernatant was added to each cuvette and the contents mixed gently up and down three times with the stirring rods. The rate of decrease in measured absorbance was measured over ten minutes. The negative slope determined for the serum in the medium was subtracted from the other slopes. Each sample was assayed three times and average slopes and standard

errors were calculated. Levels of significance were determined with SigmaStat statistical software (Version 2.0, Jandel Scientific, San Rafael, CA) using the Student's *t*-test. A *P* value below 0.05 was considered significant.

5.4 Results

5.4.1 Time frame for dose-dependent induction of cardiomyocyte apoptosis and necrosis by doxorubicin

The time frame for doxorubicin-induced cardiomyocyte apoptosis and necrosis was evaluated in annexin V-FITC/propidium iodide stained neonatal rat cardiomyocytes by epifluorescence microscopy. An increase in the percentage of apoptotic cells was observed when cardiomyocytes were grown for 48 h at 37°C following 3 h exposure to 0.2 and 1.0 μM doxorubicin (Figures 5.3 and 5.4). A greater percentage of necrotic cells were also apparent when cardiomyocytes were exposed to 1.0 μM doxorubicin. Moreover, the induction of apoptosis and necrosis by doxorubicin was dose-dependent.

5.4.2 Time frame for lactate dehydrogenase release from doxorubicin-treated cardiomyocytes

The time frame for lactate dehydrogenase release from doxorubicin-treated cardiomyocytes was assessed spectrophotometrically with an LDH release assay. A significant increase in LDH activity was observed when cardiomyocytes were continuously exposed to 0.3 μM doxorubicin for 48 and 72 h (Figure 5.5).

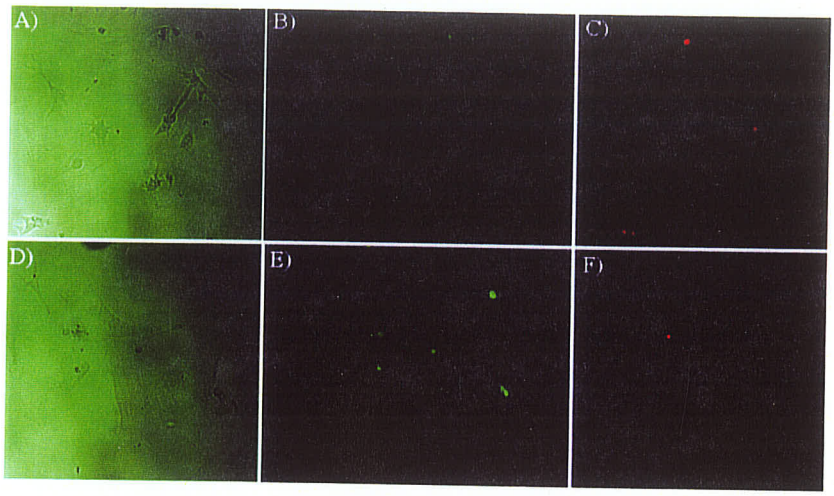

Figure 5.3 Epifluorescence photomicrographs of annexin V-FITC and propidium iodide stained cardiomyocytes grown for 48 h following 3 h exposure with or without 0.2 μM doxorubicin. Cardiomyocytes were stained with 1/5 μg/ml annexin V/propidium iodide for 10 min and imaged with a 16X objective with the epifluorescence microscope. A) – C) control (no added doxorubicin); D) – F) 0.2 μM doxorubicin Apoptotic cells stained with annexin fluoresce green and necrotic cells stained with propidium iodide fluoresce red.

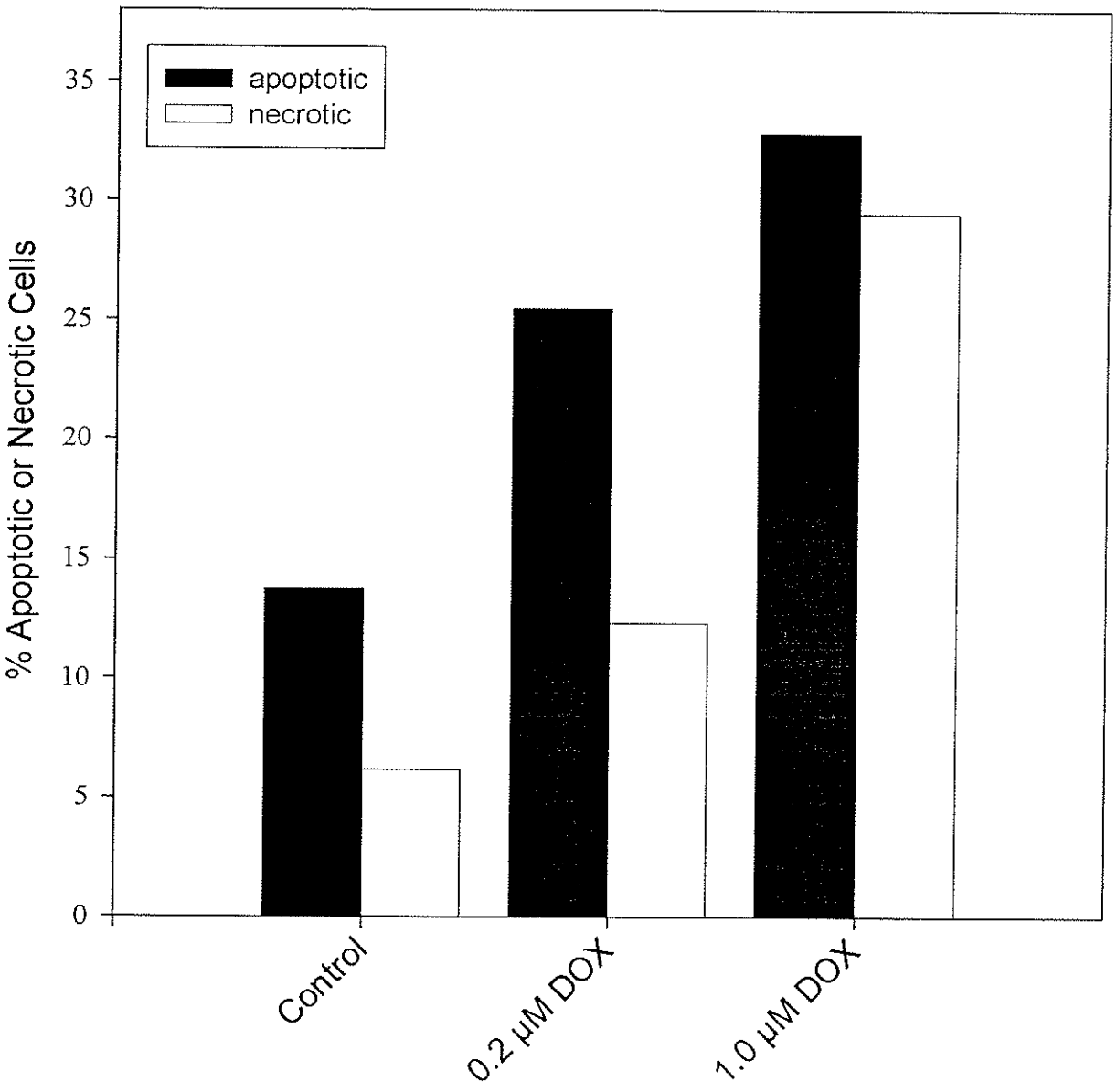

Figure 5.4 Time frame for dose-dependent induction of cardiomyocyte apoptosis and necrosis by doxorubicin. Cardiomyocytes were seeded in 6-well plates containing poly-l-lysine treated glass coverslips at a density of 200,000 cells per well in 2 ml of plating medium. After 48 h, the cells were transferred into culturing medium (DF-10, 10% (v/v) FCS in DMEM/F-12). Three days following isolation, the cardiomyocytes were exposed to 0.2 and 1.0 µM doxorubicin for 3 h at 37°C and washed three times with culturing medium (DF-10) to wash off the remaining drug. Cells were grown at 37°C in an atmosphere of 5% (v/v) CO_2 for 48 h, stained with 1/5 µg/ml annexin V-FITC/ propidium iodide for 10 min and imaged by epifluorescence microscopy. The cells used in this experiment came from one preparation that was > 90% viable. Approximately 150 cells in total were counted for each treatment.

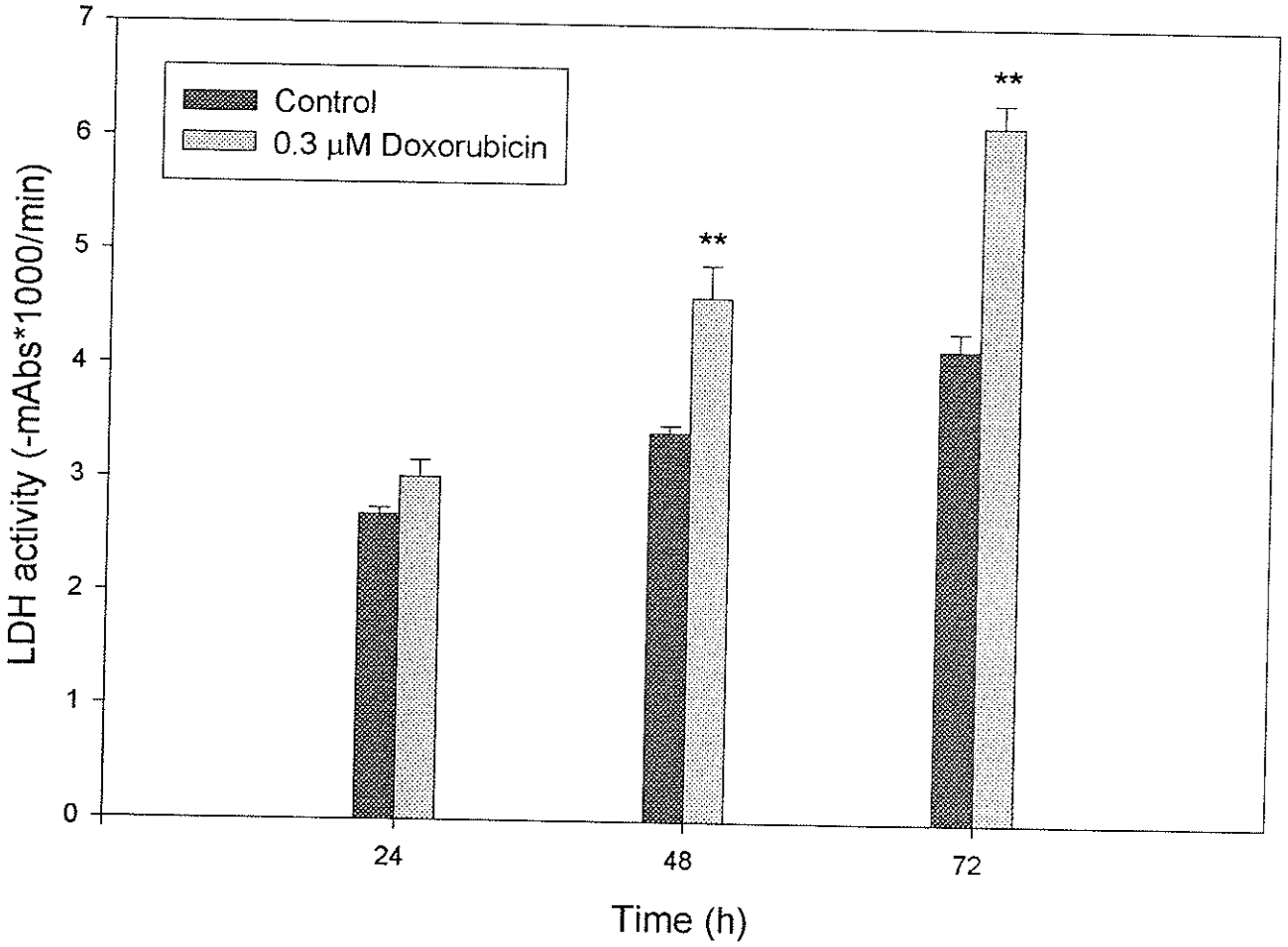

Figure 5.5 Time-frame for lactate dehydrogenase release from doxorubicin-treated cardiomyocytes. Cardiomyocytes were seeded on 24-well plates at a density of 500,000 cells per well in 750 µl of plating medium. After 48 hr, the cells were transferred into low serum-containing culturing medium (DF-2, 2% (v/v) FCS in DMEM/F-12) for 1 day. After equilibration to the culturing medium, the cells were exposed to 0.3 µM doxorubicin for 24, 48 and 72 hr. Damage to the cardiomyocytes was evaluated by measuring the amount of lactat dehydrogenase release into the medium, by following the loss of NADH absorbance in its reaction with pyruvate at 340 nm. The cells used in this experiment came from one preparation and were 90% viable. Three replicates were performed for each treatment and the error bars represent standard errors. ** $P \leq 0.01$ compared to the untreated cardiomyocyte preparation

5.5 Discussion and conclusions

The mechanism by which doxorubicin causes cardiotoxicity has been a subject of much investigation and debate. The data presented in this study suggest that permanent loss in contractile function may occur, in part, through doxorubicin initiation of apoptosis and necrosis of cardiac myocytes. The concentrations of doxorubicin used were clinically relevant [14, 27] and the study suggests that doxorubicin-induced apoptosis and necrosis are dose-dependent. Phosphatidylserine translocation was evident when cardiomyocytes were allowed to grow for 48 h following 3 h exposure to 0.2 and 1.0 μM doxorubicin (Figures 5.3 and 5.4). Translocation of phosphatidylserine to the surface of the cell is an early apoptotic event [10], suggesting that 0.2 and 1.0 μM doxorubicin induced apoptosis within 48 h following a 3 h doxorubicin treatment. Loss of cell membrane integrity, a characteristic of necrotic cells, was first apparent in the LDH release assay after 48 h exposure to 0.3 μM doxorubicin (Figures 5.5). An increase in the percentage of necrotic cells was also observed when cardiomyocytes were grown for 48 h following 3 h treatment with 1.0 μM doxorubicin. In our study, there was also a switch from myocyte apoptosis to myocyte necrosis at 1.0 μM doxorubicin (Figures 5.3 and 5.4). Several other studies have found similar results in adult ventricular myocytes [25, 26]. Reports on DNA fragmentation studies in cardiomyoctes exposed to anthracyclines also suggest the appearance of apoptotic cells after 24 - 48 h [14, 25-27]. In view of these considerations, a cardioprotectant would have to be administered before 24 h in order to preserve cardiomyocyte function of cells exposed to pharmacological doxorubicin concentrations. Moreover, cardioprotection may be less efficient or not present in cardiomyocytes exposed to elevated doxorubicin concentrations. Our studies have set the stage for future

cardioprotective studies with cardioprotectants such as dexrazoxane and demonstrate that the annexin V-FITC/propidium iodide assay in conjunction with epifluorescence microscopy is an efficient method for distinguishing cardiomyocyte apoptosis from cardiomyocyte necrosis.

5.6 Summary of doxorubicin cardiotoxicity studies with dexrazoxane

The doxorubicin cardiotoxicity studies in Chapters 3, 4 and 5 together provide great insight into the mechanisms of doxorubicin cardiotoxicity and dexrazoxane cardioprotective effects. These studies suggest that doxorubicin cardiotoxicity is attributed to its ability to generate reactive oxygen species, depolarize and damage the mitochondrial membrane and induce cardiomyocyte apoptosis and necrosis. Ultimately, these interconnected mechanisms for doxorubicin cardiotoxicity lead to the final common pathway: cell death and loss of cardiomyocyte function.

Several studies suggest that reactive oxygen species are capable of depolarizing and damaging the mitochondrial membrane [16, 20, 21, 23, 28]. It is now recognized that mitochondria contain a latent non-specific protein known as the mitochondrial permeability transition pore in their inner membrane that, when activated, causes an increase in membrane permeability [2, 3, 15, 17]. The mitochondrial permeability transition pore opens when mitochondria are depleted of ATP and exposed to oxidants or high calcium concentrations and studies have shown that oxidative stress greatly enhances the calcium sensitivity of the mitochondrial permeability transition pore [2, 3, 15, 17]. Impaired calcium fluxes and ATP depletion have been observed in doxorubicin-induced cardiac injury [29-31]. Furthermore, pore opening has been associated with reactive oxygen species mediated oxidation of dithiols in the pore complex [3, 31].

Moreover, doxorubicin has a particularly high affinity for the inner mitochondrial membrane, which is the mitochondrial permeability transition pore site [29]. Opening of the mitochondrial permeability transition pore causes swelling and uncoupling of mitochondria, which was evident in our mitochondria morphological studies with JC-1 (Figure 3.18) [17]. In our DCF studies, generation of reactive oxygen species by doxorubicin was demonstrated to be iron-based with hydrogen peroxide involvement. The iron chelator dexrazoxane was shown to prevent mitochondrial depolarization and damage (Figures 3.15, 3.16, 3.17 and 3.18) as well as hydrogen peroxide and doxorubicin-induced reactive oxygen species generation (Figures 4.4, 4.7 and 4.8). Thus, we propose that dexrazoxane prevents doxorubicin cardiotoxicity at the level of the mitochondria possibly through the ability of its metal-chelating hydrolysis product, ADR-925, to either displace iron from iron-doxorubicin-complexes or chelate loosely bound or free iron, thereby reducing iron-based oxygen free radical damage to mitochondria and other cellular components.

Our studies and reports from other researchers also support an involvement of both reactive oxygen species and mitochondria in doxorubicin-induced cardiomyocyte apoptosis and necrosis [24-27, 29-31]. Reactive oxygen species can initiate cardiomyocyte apoptosis and necrosis through the mitochondria indirectly by damaging DNA or directly by damaging the mitochondrion (Figure 5.6) [2, 17, 32]. Following oxidative damage to DNA, the cell cycle, checkpoint, and nuclear protein p53 induces synthesis of the death promoting protein Bax. Bax can open the mitochondrial permeability transition pore and depolarize and injure mitochondria. Whether reactive oxygen species or Bax initiated, depolarization and swelling of mitochondria promotes

intramitochondrial release of various pro-apoptotic proteins (i.e. cytochrome *c* (cyt-*c*), apoptosis inducing factor (AIF), procaspases) that activate caspases and endonucleases, which finally cleave DNA [1-3, 15, 32]. DNA fragmentation is the hallmark of apoptosis [7]. Necrosis does not involve caspases yet if reactive oxygen species generation and ATP depletion is extensive, then cell necrosis is inevitable [2].

Our time and dose-dependent studies with doxorubicin seem to complement the cell death pathway scheme. Both reactive oxygen species generation and dissipation of the membrane potential were observed early on within the first hour of doxorubicin treatment (Figures 3.9, 4.3 and 4.4). When higher doses of doxorubicin were administered reactive oxygen species generation was higher and cell necrosis was present (Figures 4.5 and 5.4). In our cell morphology and cell density microscope observation studies on doxorubicin-treated myocytes (Chapter 3), the cardiomyocytes started to round up and shrink in size after 24 h in a dose-dependent manner. A reduction in myocyte area was also observed when myocytes were exposed to 10 and 50 μM doxorubicin (Figure 4.5). Our mitochondrial morphology studies with JC-1 also showed signs of decreased cell size in cardiomyocytes exposed to 2.0 μM doxorubicin (Figure 3.18D). Cell shrinkage is a hallmark of apoptosis and in fact, phosphatidylserine, a marker of apoptotic cells, was translocated to the cell surface within 48 h (Figures 5.3 and 5.4) [7]. After 48 h, mitochondria started to swell (Figure 3.18), the cardiomyocyte plasma membrane became leaky (Figure 5.5) and both cardiomyocyte apoptosis and necrosis were profound (Figure 5.4).

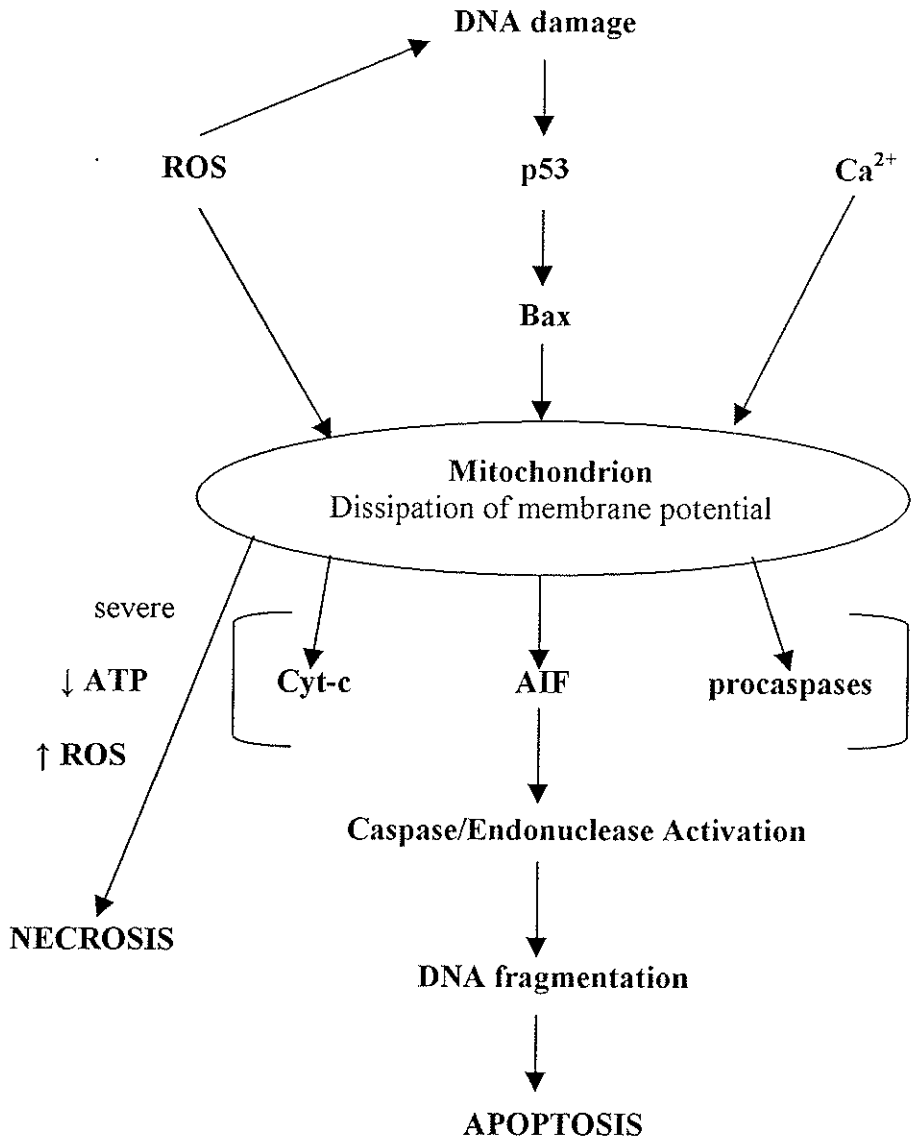

Figure 5.6 Cell death triggers and role of mitochondria in cardiomyocyte apoptosis and necrosis [2], pg 1310.

As for dexrazoxane cardioprotection, it was very efficient at preventing mitochondrial depolarization and mitochondrial damage induced by pharmacological concentrations of doxorubicin over long periods of time but less efficient at preventing reactive oxygen species generation at higher doxorubicin concentrations. To further investigate chronic doxorubicin cardiotoxicity, future studies should examine reactive oxygen species production by low doses of doxorubicin over longer periods of time. The effect of dexrazoxane on doxorubicin-induced cardiomyocyte apoptosis and necrosis should also be investigated along with the relationship between cardiomyocyte loss and cardiomyocyte function. Ultimately such studies could provide insight into improving treatment regimens for anthracycline cardiotoxicity, heart failure and ischemia-reperfusion injury to the heart.

5.7 References

1. Bishopric N, Andreka P, Slepak T, Webster K. 2001. Molecular mechanisms of apoptosis in the cardiac myocyte. *Curr Opin Pharmacol* 1:141-150.

2. Green DR, Reed JC. 1998. Mitochondria and apoptosis. *Science* 281:1309-12.

3. Lemasters JJ, Nieminen AL, Qian T, Trost LC, Elmore SP, Nishimura Y, Crowe RA, Cascio WE, Bradham CA, Brenner DA, Herman B. 1998. The mitochondrial permeability transition in cell death: a common mechanism in necrosis, apoptosis and autophagy. *Biochim Biophys Acta* 1366:177-96.

4. Sabbah HN. 2000. Apoptotic cell death in heart failure. *Cardiovasc Res* 45:704-12.

5. Raff M. 1998. Cell suicide for beginners. *Nature* 396:119-22.

6. van Heerde WL, Robert-Offerman S, Dumont E, Hofstra L, Doevendans PA, Smits JF, Daemen MJ, Reutelingsperger CP. 2000. Markers of apoptosis in cardiovascular tissues: focus on Annexin V. *Cardiovasc Res* 45:549-59.

7. Saraste A, Pulkki K. 2000. Morphologic and biochemical hallmarks of apoptosis. *Cardiovasc Res* 45:528-37.

8. Haunstetter A, Izumo S. 2000. Future perspectives and potential implications of cardiac myocyte apoptosis. *Cardiovasc Res* 45:795-801.

9. Rucker-Martin C, Henaff M, Hatem SN, Delpy E, Mercadier JJ. 1999. Early redistribution of plasma membrane phosphatidylserine during apoptosis of adult rat ventricular myocytes in vitro. *Basic Res Cardiol* 94:171-9.

10. Martin SJ, Reutelingsperger CP, McGahon AJ, Rader JA, van Schie RC, LaFace DM, Green DR. 1995. Early redistribution of plasma membrane phosphatidylserine is a general feature of apoptosis regardless of the initiating stimulus: inhibition by overexpression of Bcl-2 and Abl. *J Exp Med* 182:1545-56.

11. van Engeland M, Ramaekers FC, Schutte B, Reutelingsperger CP. 1996. A novel assay to measure loss of plasma membrane asymmetry during apoptosis of adherent cells in culture. *Cytometry* 24:131-9.

12. Vermes I, Haanen C, Steffens-Nakken H, Reutelingsperger C. 1995. A novel assay for apoptosis. Flow cytometric detection of phosphatidylserine expression on early apoptotic cells using fluorescein labelled Annexin V. *J Immunol Methods* 184:39-51.

13. Haugland R: Handbook of Fluorescent Probes and Research Chemicals. Eugene, Oregon, Molecular Probes, 1996.

14. Sawyer DB, Fukazawa R, Arstall MA, Kelly RA. 1999. Daunorubicin-induced apoptosis in rat cardiac myocytes is inhibited by dexrazoxane. *Circ Res* 84:257-65.

15. Bernardi P, Petronilli V, Di Lisa F, Forte M. 2001. A mitochondrial perspective on cell death. *Trends Biochem Sci* 26:112-7.

16. Cossarizza A, Franceschi C, Monti D, Salvioli S, Bellesia E, Rivabene R, Biondo L, Rainaldi G, Tinari A, Malorni W. 1995. Protective effect of N-acetylcysteine in tumor necrosis factor-alpha- induced apoptosis in U937 cells: the role of mitochondria. *Exp Cell Res* 220:232-40.

17. Halestrap AP, Doran E, Gillespie JP, O'Toole A. 2000. Mitochondria and cell death. *Biochem Soc Trans* 28:170-7.

18. Heerdt BG, Houston MA, Anthony GM, Augenlicht LH. 1998. Mitochondrial membrane potential (delta psi(mt)) in the coordination of p53-independent proliferation and apoptosis pathways in human colonic carcinoma cells. *Cancer Res* 58:2869-75.

19. Heerdt BG, Houston MA, Mariadason JM, Augenlicht LH. 2000. Dissociation of staurosporine-induced apoptosis from G2-M arrest in SW620 human colonic carcinoma cells: initiation of the apoptotic cascade is associated with elevation of the mitochondrial membrane potential (deltapsim). *Cancer Res* 60:6704-13.

20. Roberg K, Johansson U, Ollinger K. 1999. Lysosomal release of cathepsin D precedes relocation of cytochrome c and loss of mitochondrial transmembrane potential during apoptosis induced by oxidative stress. *Free Radic Biol Med* 27:1228-37.

21. Shenker BJ, Guo TL, O I, Shapiro IM. 1999. Induction of apoptosis in human T-cells by methyl mercury: temporal relationship between mitochondrial dysfunction and loss of reductive reserve. *Toxicol Appl Pharmacol* 157:23-35.

22. Tatton WG, Olanow CW. 1999. Apoptosis in neurodegenerative diseases: the role of mitochondria. *Biochim Biophys Acta* 1410:195-213.

23. Virag L, Salzman AL, Szabo C. 1998. Poly(ADP-ribose) synthetase activation mediates mitochondrial injury during oxidant-induced cell death. *J Immunol* 161:3753-9.

24. Wang L, Ma W, Markovich R, Chen JW, Wang PH. 1998. Regulation of cardiomyocyte apoptotic signaling by insulin-like growth factor I. *Circ Res* 83:516-22.

25. Arola OJ, Saraste A, Pulkki K, Kallajoki M, Parvinen M, Voipio-Pulkki LM. 2000. Acute doxorubicin cardiotoxicity involves cardiomyocyte apoptosis. *Cancer Res* 60:1789-92.

26. Kumar D, Kirshenbaum L, Li T, Danelisen I, Singal P. 1999. Apoptosis in isolated adult cardiomyocytes exposed to adriamycin. *Ann N Y Acad Sci* 874:156-68.

27. Kang YJ, Zhou ZX, Wang GW, Buridi A, Klein JB. 2000. Suppression by metallothionein of doxorubicin-induced cardiomyocyte apoptosis through inhibition of p38 mitogen-activated protein kinases. *J Biol Chem* 275:13690-8.

28. Scanlon JM, Reynolds IJ. 1998. Effects of oxidants and glutamate receptor activation on mitochondrial membrane potential in rat forebrain neurons. *J Neurochem* 71:2392-400.

29. Hershko C, Pinson A, Link G. 1996. Prevention of anthracycline cardiotoxicity by iron chelation. *Acta Haematol* 95:87-92.

30. Konorev EA, Kennedy MC, Kalyanaraman B. 1999. Cell-permeable superoxide dismutase and glutathione peroxidase mimetics afford superior protection against doxorubicin-induced cardiotoxicity: the role of reactive oxygen and nitrogen intermediates. *Arch Biochem Biophys* 368:421-8.

31. Miura T, Muraoka S, Ogiso T. 1995. Adriamycin-Fe3+-induced mitochondrial protein damage with lipid peroxidation. *Biol Pharm Bull* 18:514-7.

32. Evan G, Littlewood T. 1998. A matter of life and cell death. *Science* 281:1317-22.

Chapter 6 Preliminary herceptin cardiotoxicity studies in neonatal rat cardiomyocytes with the antineoplastic mouse 7.16.4 antibody

6.1 Introduction

Herceptin® (trastuzumab) is the recombinant, humanized version of the 4D5 murine monoclonal antibody and has recently been approved by the Food and Drug Administration for the treatment of metastatic breast cancer [1-3]. Herceptin selectively targets the extracellular domain of the human epidermal growth factor receptor 2 protein (HER2) [3-7] and has been shown, in both *in vitro* assays and in animals, to inhibit the proliferation of human tumor cells that overexpress HER2 [1, 8, 9]. Overexpression of the HER2 protein has been reported in 25-30% of breast cancer patients [5, 10, 11]. Although superior antitumor efficacy was reported in clinical trials where herceptin was administered in combination with anthracyclines, cardiac toxicity was an unexpected side effect of herceptin treatment in the clinical trials that led to its approval [2, 12]. A substantial number of women treated with herceptin developed ventricular dysfunction and congestive heart failure [2]. The incidence and severity of such cardiac dysfunction was highly dependent on prior or concurrent anthracycline exposure. For patients with prior anthracycline exposure, the risk of cardiac dysfunction was 7% for herceptin monotherapy [2]. For patients treated with herceptin concurrently with anthracyclines, the risk of cardiac dysfunction was 29% [2]. The mechanism for herceptin-associated cardiac dysfunction is unknown, although its dependence on concurrent or prior anthracycline exposure suggests a common pathophysiological basis with anthracycline-induced myocardial injury. A number of clinical trials are in progress to evaluate the efficacy and safety of herceptin in patients with early stage breast cancer and other cancers, which will investigate novel strategies to circumvent this serious cardiac toxicity [13]. Thus, in view

of the rapid rise in herceptin use and the significance of the heart failure side effect, it is imperative that more be learned about herceptin cardiotoxicity in a timely fashion to ensure that patients do not trade one lethal disease for another. Unfortunately no prospective studies have assessed herceptin-induced cardiotoxicity alone or in combination with anthracyclines.

The mouse monoclonal antibody 7.16.4 shares structurally similar binding epitopes as herceptin and elicits cell growth inhibitory effects when bound to rat or human HER2 [7, 8, 14]. The objective of our study was to determine whether 7.16.4 cardiotoxicity was HER2-mediated and whether it was synergistic with doxorubicin. Using our previously developed neonatal rat cardiomyocyte model, we investigated the effect of 7.16.4, alone and in combination with doxorubicin, on cardiomyocyte plasma membrane integrity and cardiomyocyte growth using an LDH release assay and a MTT cytotoxicity assay.

6.2 Materials

Doxorubicin hydrochloride was a gift from Adria-SP Inc. (Columbus, Ohio) and the mouse 7.16.4 monoclonal antibody was a gift from Mark Greene (University of Pennsylvania). MTT (cat No. M-5655), trypan blue dye (cat No. T-6146), β-NADH (disodium salt, cat No. N-8129), pyruvic acid (sodium salt, cat No. P-8574) and HEPES (cell culture grade, cat No. H-9136) were purchased from Sigma Chemical Co. (St. Louis, MO). Sodium bicarbonate ($NaHCO_3$, cat. No. BP328-079) and Tris (crystallized free base, molecular biology grade, cat No. BP152-1) were obtained from Fisher Scientific (Fairlawn, NJ). Dulbecco's phosphate buffered saline (PBS, cat No. D-5652), Dulbecco's modified Eagle medium/F12 (DMEM/F-12, cat No. 12500-062), penicillin-streptomycin (cat No. 25200-072), fetal calf serum (FCS, cat No. 26140-079) and horse serum (cat No.

16050-122) were ordered from Gibco-BRL Life Technologies Inc. (Burlington, ON). D-glucose was supplied by Anala R (Toronto, ON) while potassium chloride (KCl, cat No. AC-7600) was obtained from Anachemia Ltd. (Montreal, QB). Five molar HCl (cat No. LC15360-2) was purchased from LabChem Inc. (Pittsburgh, PA) while sterile, 0.45 μm cellulose acetate syringe filters were obtained from Nalgene (Rochester, NY). Sterile, adhesive 96-well and 24-well tissue culture plates were ordered from Sarstedt Inc. (St. Leonard, PQ). Falcon 3025 tissue culture plates and 40 μm cell strainers were obtained from Becton Dickensson (Lincoln Park, NJ). Deoxyribonuclease I (DNAse, cat No. 2139), trypsin (cat No. 3703) and collagenase (cat No. 4176) were obtained from Worthington Biochemical Corporation (Lakewood, NJ). Cell culture media and buffers were prepared in reverse osmosis distilled water and cardiomyocyte cultures were grown in a 37°C incubator in an atmosphere of 5% (v/v) CO_2 in air.

6.3 Methods

6.3.1 Cell culture

Because the mouse 7.16.4 antibody has been shown to bind to rodent and human growth factor receptors [7] and our goal was to determine whether the antibody was growth inhibitory, we decided to obtain our primary cardiomyocyte culture from the excised hearts of 1-day-old neonatal rats rather than 2-3 day old neonates. Several studies suggest that myocyte proliferation is greatest during the first few days of life [15] and we previously had observed that the greatest cell proliferation occurred immediately after isolation over the 48 h plating and recovery time. The primary culture of neonatal rat cardiomyocytes was prepared as discussed in Section 3.3.2.2 and was used as our model

for 7.16.4 and doxorubicin cardiotoxicity. Cell viability and cell density was calculated as described in Section 3.3.2.3.

For the lactate dehydrogenase (LDH) release experiment, cells were seeded in sterile, 24-well plates at a density of 500,000 cells per well in 750 µl of plating medium. The cells were seeded with a sterile 1-ml pipette to maintain cell viability and the cell suspension was rocked gently throughout the seeding process to prevent cell aggregation and settlement. The cell density chosen for this experiment allowed for optimum cell viability and a 95% confluent culture the day the experiment commenced. Twenty-four hours following seeding, cells were transferred from plating medium into a 2% (v/v) low fetal calf serum-containing culturing medium in DMEM-F12. A low serum, culturing medium was used because the serum contains LDH, which could interfere with the LDH release assay. Only a 1 h equilibration period to the low serum culturing medium was provided to the cells, as it was necessary to commence drug treatment before the cardiomyocyte cell proliferation rate of our preparation decreased.

For the MTT cytotoxicity assay experiment, cells were seeded in sterile, 96-well plates at a density of 50,000 cells per well in 200 µl of plating medium. The cells were seeded with sterile, cut opened end blue pipette tips to maintain cell viability and the cell suspension was rocked gently throughout the seeding process to prevent cell aggregation and settlement. The cell density chosen for this experiment allowed for optimum cell viability, a 95% confluent culture and an adequate number of cells to metabolize MTT and provide a high enough absorbance reading. Twenty-four hours following seeding, the cells were transferred from plating medium (7.5% (v/v) horse serum/7.5% (v/v) FCS in DMEM/F-12) into culturing medium (DF-10, 10% (v/v) FCS in DMEM/F-12). Only a 1

h equilibration period to the culturing medium was provided to the cells, as it was necessary to commence drug treatment before the cardiomyocyte cell proliferation rate of the preparation decreased.

6.3.2 Drug delivery

The 7.16.4 antibody that we received from Dr. Mark Greene (University of Pennsylvania) was provided to us in solution at a stock concentration of 2.4 μg/ml. This solution was stored in the 4°C refrigerator, diluted with cell culture medium to give the desired 7.16.4 concentrations and filter sterilized through a 0.45 μm cellulose acetate syringe filter. Doxorubicin was dissolved in water to give a stock concentration of 1 mM. A 0.6 μM doxorubicin control was included in the LDH experiment such that its effect on LDH release could be compared to combinations of doxorubicin and 7.16.4. A DF-2 control well without cells was also included in the LDH experiment to correct for the LDH activity contributed by the serum.

The range of 7.16.4 concentrations used in the experiments was determined based upon the approximate number of HER2 receptors per cell (10,000) and the binding affinity of 7.16.4 for the HER2 receptor (K_d ~1 nM) [7, 16-18]. Using these approximate values, the highest concentration predicted to provide receptor saturated conditions was approximately 10 ng/ml. A concentration of 0.6 μM doxorubicin was chosen such that the concentration remaining after dilution of the wells through supernatant sampling would still be cardiotoxic. Before the cells were treated with 7.16.4, an 80 μl sample of supernatant was removed from each well and replaced with an equivalent volume of DF-2. The procedure for sampling and storage of supernatant is discussed in Section 5.3.5.

In the LDH experiment, two wells were treated with 1, 5 and 9 ng/ml 7.16.4 antibody following the 1 h equilibration period to the low serum-culturing medium. After 19 h, an 80 µl sample of supernatant was removed and 0.6 µM doxorubicin was added to the appropriate wells. Following 43, 67, 91 and 115 h exposure time to 7.16.4, 80 µl samples of supernatant were removed and replaced with DF-2. After the last time point was sampled, the cells were lysed with Triton-X -100 as discussed in Section 6.3.5.

In the MTT experiment, six replicates were performed at each 7.16.4 concentration. After the 1 h equilibration period in culturing medium (DF-10, 10% (v/v) in DMEM-F-12), cells were exposed to a range of 7.16.4 concentrations (0 – 10 ng/ml). The 7.16.4 antibody was delivered at 20 µl/well to give a final volume of 200 µl. The first column on each plate was filled with 200 µl of PBS for spectrophotometer blanking. Each plate was wrapped with Saran wrap to reduce evaporation and allowed to grow for 72 h at 37°C in an atmosphere of 5% (v/v) CO_2 in air.

6.3.3 Determination of cell growth inhibition using the MTT cytotoxicity assay

The tetrazolium salt MTT (3-(4,5-dimethylthiazol-2-yl)-2,5-diphenyltetrazolium bromide) solution was prepared by dissolving 0.25 g of MTT in 50 ml of PBS and 50 ml of water. Because the MTT solution is photosensitive, it was wrapped in aluminum foil and stored in the refrigerator.

After 72 h of growth in the presence of 7.16.4 antibody, cell survival was measured by the MTT assay. MTT is a yellow tetrazolium salt, which is converted into the water-insoluble blue formazan crystals by mitochondrial dehydrogenases [19]. The amount of formazan produced is directly proportional to the number of metabolically active cells. Into the wells of each plate was added 20 µl of 0.25% (wt/v) MTT solution.

After 4 h incubation at 37°C in an atmosphere of 5% (v/v) CO_2 in air, the cell culture medium was aspirated and 100 µl of DMSO was added to dissolve the crystals. A Thermomax 96-well plate reader (Molecular Devices, Menlo Park, CA) was used to measure the absorbance at 550 nm. The absorbance was corrected by subtracting the absorbance at 650 nm from the absorbance at 550 nm to minimize non-specific, scattered light.

6.3.5 Lysing cells with Triton-X-100 for measurement of total LDH

A 1% (v/v) Triton-X-100 solution in PBS containing 0.1 M potassium phosphate buffer (pH 7.4) and 2 mM EDTA was prepared and stored in the refrigerator. The cells were lysed by aspirating the media from the wells and replacing it with 250 µl of 1% (v/v) Triton-X-100 solution. The plate was left at room temperature for 20 min after which dim, gray, shadows of lysed cells were visible with the microscope. After the cells were lysed, the contents in each well were mixed up and down with a pipette and aliquoted (200 µl/tube) into sterile microcentrifuge tubes. The tubes were centrifuged at 500 g to remove the cells and the supernatant was removed and diluted 1 in 10 with PBS. Supernatant samples were stored in the -80°C freezer and were assayed within a week of sampling on the same day. Damage to the cardiomyocytes was evaluated by measuring the amount of LDH released into the medium. The procedure for measuring LDH release is discussed in Section 5.3.6.2.

6.3.6 Calculations and statistical analysis

After correcting all the data for LDH activity contributed by the serum, the percentage of LDH released was calculated by taking the ratio of LDH released by the cells in each treatment over the total LDH in each well (LDH released + LDH from lysed

cells). This ratio was multiplied by 100 and a 7.16.4 exposure time vs. % LDH release graph was plotted with errors represented as standard deviations. For the MTT experiment, a concentration-absorbance graph was plotted with the errors represented as standard errors. The data points were fit to a linear least square equation to obtain the slope and intercept values. Where indicated, levels of statistical significance were determined with SigmaStat statistical software (Version 2.0, Jandel Scientific, San Rafael, CA) using the Student's *t*-test. A P value below 0.05 was considered significant.

6.4 Results

6.41 Cardiomyocyte growth inhibition by 7.16.4, as measured by MTT cytotoxicity assay

The range of 7.16.4 antibody concentrations (0 – 10 ng/ml) administered to the cardiomyocytes for 72 h had no effect on cell growth, as measured by MTT cytotoxicity assay (Figure 6.1).

6.4.2 Concentration and time-dependent effect of 7.16.4 on doxorubicin-induced LDH release from neonatal rat cardiomyocytes

Doxorubicin- and 7.16.4-induced cardiomyocyte damage was evaluated by measuring the percentage of LDH released into the medium. After 19 h, 7.16.4 at concentrations of 1, 5 and 9 ng/ml did not affect LDH release from cardiomyocytes (Figure 6.2). However, when the cardiomyocytes were exposed to 7.16.4 and doxorubicin concurrently, a dose- and time-dependent reduction in LDH release was observed compared to the percentage of LDH released from cardiomyocytes exposed to 0.6 μM doxorubicin alone (Figure 6.2). The reduction in LDH release was significant ($P < 0.05$) when cardiomyocytes were pre-exposed to 9 ng/ml 7.16.4 antibody for 19 h followed by

concurrent exposure to 0.6 μM doxorubicin and 9 ng/ml 7.16.4 antibody for 72 h and 96 h (Figure 6.2).

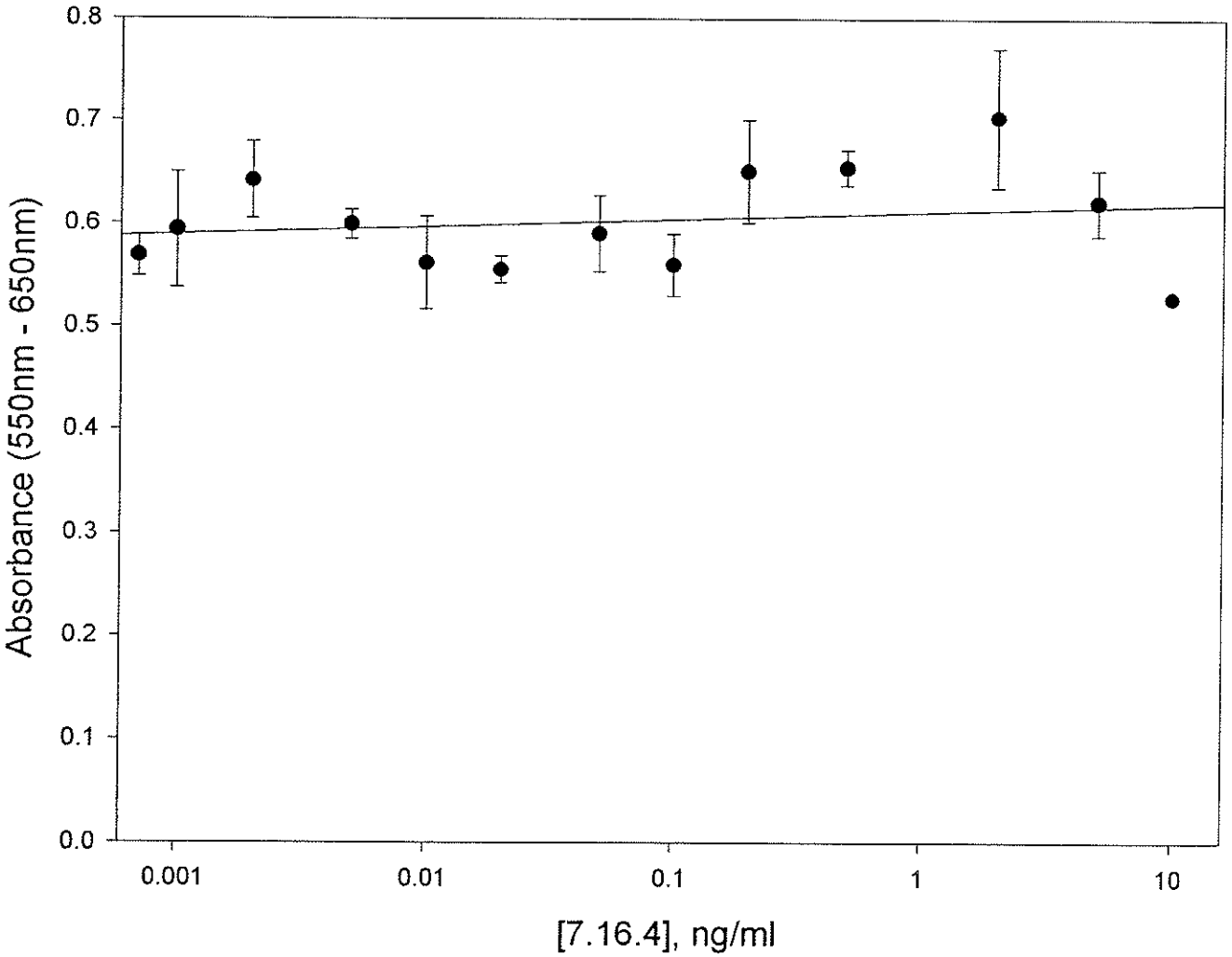

Figure 6.1 Cardiomyocyte growth inhibition by 7.16.4, as measured by MTT cytotoxicity assay. Cardiomyocytes were seeded in sterile, 96-well plates at a density of 50,000 cells per well in 200 μl of plating medium. After 24 hr, the cells were transferred from plating medium (7.5% (v/v) horse serum/7.5% (v/v) FCS in DMEM/F-12) into culturing medium (10% (v/v) FCS in DMEM/F-12). Following a 1 hr equilibration period, the cells were treated with a range of 7.16.4 antibody concentrations (0 - 10 ng/ml) for 72 hr at 37°C in an atmosphere of 5% (v/v) CO_2. The antibody was added at a volume of 20 μl/well such that the final volume of the well was 200 μl. After 72 hr, the cells were exposed to 20 μl of 0.25% (wt/v) MTT solution in PBS for 4 hr at 37°C in an atmosphere of 5% (v/v) CO_2. Following the 4 hr incubation, the cell culture medium was aspirated, 100 μl of DMSO was added to dissolve the blue formazan crystals and the absorbance at 550 nm was measured. The cardiomyocytes used this experiment came from one preparation that was 86% viable. The data points were fit to a linear least square equation. Six replicates were performed at each concentration and the errors represent standard errors. The lowest concentration plotted is the zero value.

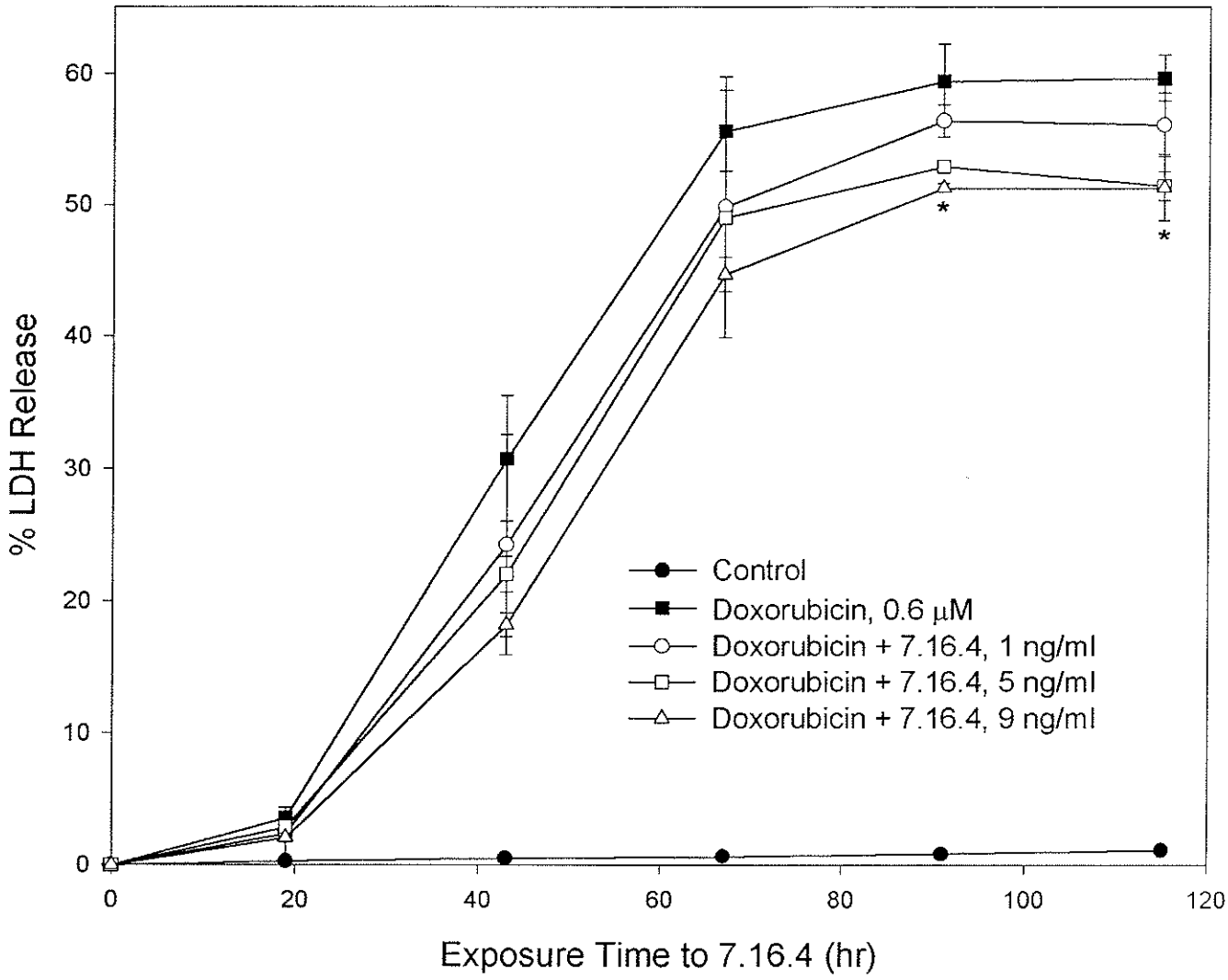

Figure 6.2 Concentration- and time-dependent effect of 7.16.4 on doxorubicin-induced LDH release from neonatal rat cardiomyocytes. Cardiomyocytes were seeded in sterile 24-well tissue culture plates at a density of 500,000 cells per well in 750 μl of plating medium. After 24 hr, the cells were transferred from plating medium (7.5% (v/v) horse serum/7.5% (v/v) FCS in DMEM/F-12) into culturing medium (DF-2, 2% (v/v) FCS in DMEM/F-12). Following a 1 hr equilibration period, the cells were treated with 1, 5 and 9 ng/ml 7.16.4 antibody for 19 hr. After 19 hr, samples of supernatant were removed and 0.6 μM doxorubicin was added to the appropriate wells. Following 43, 67, 91 and 155 hr exposure time to 7.16.4, samples of supernatant were removed and replaced with DF-2. After the last sampling time point, the cells were lysed with 1% (v/v) Triton-X-100 for 20 min at room temperature. The supernatant was saved for LDH analysis. Damage to the myocytes was measured spectrophotometrically by following the loss in NADH absorbance at 340 nm. The cardiomyocytes used in this experiment came from one preparation that was 86% viable. The data represents the average of two trials and the errors represent standard errors of three replicate LDH measurements per treatment. * $P < 0.05$ compared to the doxorubicin treatment alone

6.5 Discussion and conclusions

The mechanism by which 7.16.4 causes cardiotoxicity has not been investigated. The synergistic antitumor and cardiotoxic effect of herceptin and doxorubicin combination therapy observed in breast cancer clinical trials suggests a common pathological basis with anthracycline-induced myocardial injury [2, 12]. In our study, 7.16.4 and doxorubicin cardiotoxicity alone and in combination was examined with an MTT cytotoxicity assay and a LDH release assay. The cardiotoxicity data presented in this study provides preliminary information for the design of subsequent cardiotoxicity studies with 7.16.4 and doxorubicin.

The 7.16.4 antibody did not affect plasma membrane integrity or cardiomyocyte growth when administered alone to cardiomyocytes for 19 and 72 h (Figures 6.1 and 6.2). Several studies have shown that 7.16.4 binds with high affinity to the rat HER2 receptor and that its binding elicits a cell growth inhibitory response in tumor cells [1, 3-6, 8, 9]. HER2 receptors and HER ligands are expressed in the heart and their activation creates a hypertrophic response and promotes cell survival and growth [2]. HER2 blockade and the subsequent inhibition of downstream myocardial signaling should have effects on the heart. There are several possibilities that could explain the negative growth inhibitory result. Since the highest 7.16.4 antibody concentration started to show a decrease in absorbance, it is possible that the concentrations used were not high enough. A second possibility could be that the growth inhibitory effect was masked by the presence of growth factors in the serum. Finally, there is a chance that the cardiotoxic effect of 7.16.4 is elicited by a HER2 independent mechanism.

The 7.16.4 antibody reduced doxorubicin-induced release of LDH from cardiomyocytes in a dose- and time-dependent manner. From this study, it is evident that the 7.16.4 antibody has an effect on cardiomyocytes in the presence of doxorubicin. It is hypothesized that the low serum-containing culture medium permitted us to observe an effect that could have been masked by growth factors or other components in the serum. The main finding of our study was that 7.16.4 is probably cardioprotective in neonatal rat cardiomyocytes, which is opposite to the outcome that was seen in early human clinical trials. Thus, the neonatal rat cardiomyocyte model may not be the best model for 7.16.4 cardiotoxicity. Future studies should examine the effect of 7.16.4 alone and in combination with doxorubicin on cardiomyocyte growth and LDH release with higher concentrations of 7.16.4 in a serum free medium. It would also be interesting to examine the effects over a longer period of time and with prior doxorubicin exposure. One should also consider performing these studies with adult cardiomyocytes that are terminally differentiated like the heart cells of human cancer patients. Our preliminary cardiotoxicity study with 7.16.4 and doxorubicin has set the stage for further investigation of 7.16.4 cardiotoxicity.

6.6 References

1. Baselga J, Norton L, Albanell J, Kim YM, Mendelsohn J. 1998. Recombinant humanized anti-HER2 antibody (Herceptin) enhances the antitumor activity of paclitaxel and doxorubicin against HER2/neu overexpressing human breast cancer xenografts. *Cancer Res* 58:2825-31.

2. Feldman AM, Lorell BH, Reis SE. 2000. Trastuzumab in the treatment of metastatic breast cancer : anticancer therapy versus cardiotoxicity. *Circulation* 102:272-4.

3. Goldenberg MM. 1999. Trastuzumab, a recombinant DNA-derived humanized monoclonal antibody, a novel agent for the treatment of metastatic breast cancer. *Clin Ther* 21:309-18.

4. Hung M, Lau Y. 1999. Basic science of HER2/neu:A review. *Semin Oncol* 26:51-59.

5. Schaller G, Bangemann N, Becker C, Buhler H, Opri F, Weitzel HK. 1999. Therapy of metastatic breast cancer with humanized antibodies against the HER2 receptor protein. *J Cancer Res Clin Oncol* 125:520-4.

6. Sliwkowski MX, Lofgren JA, Lewis GD, Hotaling TE, Fendly BM, Fox JA. 1999. Nonclinical studies addressing the mechanism of action of trastuzumab (Herceptin). *Semin Oncol* 26:60-70.

7. Zhang H, Wang Q, Montone KT, Peavey JE, Drebin JA, Greene MI, Murali R. 1999. Shared antigenic epitopes and pathobiological functions of anti-p185(her2/neu) monoclonal antibodies. *Exp Mol Pathol* 67:15-25.

8. Drebin JA, Link VC, Greene MI. 1988. Monoclonal antibodies reactive with distinct domains of the neu oncogene-encoded p185 molecule exert synergistic anti-tumor effects in vivo. *Oncogene* 2:273-7.

9. Park BW, Zhang HT, Wu C, Berezov A, Zhang X, Dua R, Wang Q, Kao G, O'Rourke DM, Greene MI, Murali R. 2000. Rationally designed anti-HER2/neu peptide mimetic disables P185HER2/neu tyrosine kinases in vitro and in vivo. *Nat Biotechnol* 18:194-8.

10. Reese DM, Slamon DJ. 1997. HER-2/neu signal transduction in human breast and ovarian cancer. *Stem Cells* 15:1-8.

11. van de Vijver MJ, Peterse JL, Mooi WJ, Wisman P, Lomans J, Dalesio O, Nusse R. 1988. Neu-protein overexpression in breast cancer. Association with comedo-type ductal carcinoma in situ and limited prognostic value in stage II breast cancer. *N Engl J Med* 319:1239-45.

12. Ewer MS, Gibbs HR, Swafford J, Benjamin RS. 1999. Cardiotoxicity in patients receiving transtuzumab (Herceptin): primary toxicity, synergistic or sequential stress, or surveillance artifact? *Semin Oncol* 26:96-101.

13. Shak S. 1999. Overview of the trastuzumab (Herceptin) anti-HER2 monoclonal antibody clinical program in HER2-overexpressing metastatic breast cancer. Herceptin Multinational Investigator Study Group. *Semin Oncol* 26:71-7.

14. Peterson NC, Greene MI. 1998. Bacterial expression and characterization of recombinant biologically active anti-tyrosine kinase receptor antibody forms. *DNA Cell Biol* 17:1031-40.

15. Anversa P, Kajstura J. 1998. Ventricular myocytes are not terminally differentiated in the adult mammalian heart. *Circ Res* 83:1-14.

16. Kokai Y, Myers JN, Wada T, Brown VI, LeVea CM, Davis JG, Dobashi K, Greene MI. 1989. Synergistic interaction of p185c-neu and the EGF receptor leads to transformation of rodent fibroblasts. *Cell* 58:287-92.

17. Kokai Y, Cohen JA, Drebin JA, Greene MI. 1987. Stage- and tissue-specific expression of the neu oncogene in rat development. *Proc Natl Acad Sci U S A* 84:8498-501.

18. Samanta A, LeVea CM, Dougall WC, Qian X, Greene MI. 1994. Ligand and p185c-neu density govern receptor interactions and tyrosine kinase activation. *Proc Natl Acad Sci U S A* 91:1711-5.

19. Vistica D, Skehan P, Scudiero D, Monks A, Pittman A, Boyd M. 1991. Tetrazolium-based assays for cellular viability:a critical examination of selected parameters affecting formazan production. *Cancer Res* 51:2515-2520.